



LAWRENCE
LIVERMORE
NATIONAL
LABORATORY

UCRL-TR-204713

Upscaling Radionuclide Retardation—Linking the Surface Complexation and Ion Exchange Mechanistic Approach to a Linear K_d Approach

Mavrik Zavarin, Steven F. Carle, and Reed M. Maxwell

May 2004

Disclaimer

This document was prepared as an account of work sponsored by an agency of the United States Government. Neither the United States Government nor the University of California nor any of their employees, makes any warranty, express or implied, or assumes any legal liability or responsibility for the accuracy, completeness, or usefulness of any information, apparatus, product, or process disclosed, or represents that its use would not infringe privately owned rights. Reference herein to any specific commercial product, process, or service by trade name, trademark, manufacturer, or otherwise, does not necessarily constitute or imply its endorsement, recommendation, or favoring by the United States Government or the University of California. The views and opinions of authors expressed herein do not necessarily state or reflect those of the United States Government or the University of California, and shall not be used for advertising or product endorsement purposes.

Auspices Statement

This work was performed under the auspices of the U.S. Department of Energy by University of California, Lawrence Livermore National Laboratory under Contract W-7405-Eng-48.

This report has been reproduced
directly from the best available copy.

Available to DOE and DOE contractors from the
Office of Scientific and Technical Information
P.O. Box 62, Oak Ridge, TN 37831
Prices available from (423) 576-8401
<http://apollo.osti.gov/bridge>

Available to the public from the
National Technical Information Service
U.S. Department of Commerce
5285 Port Royal Rd,
Springfield, VA 22161
<http://www.ntis.gov/>

OR

Lawrence Livermore National Laboratory
Technical Information Department's Digital Library
<http://www.llnl.gov/library/>

Upscaling Radionuclide Retardation—Linking the Surface Complexation and Ion Exchange Mechanistic Approach to a Linear K_d Approach

Mavrik Zavarin, Steven F. Carle, and Reed M. Maxwell

Lawrence Livermore National Laboratory

Livermore, California

Prepared for the Underground Test Area Project

U.S. Department of Energy

National Nuclear Security Administration

Nevada Site Office

May 2004

TABLE OF CONTENTS

1. Introduction	1
2. Basis for Simplification of the Mechanistic Approach to the K_d Approach.....	2
3. Radionuclides and Sorbing Minerals Included in the Mechanistic Approach and Discussed in This Report	4
4. Component Additivity Methodology.....	5
4.1 Component additivity in the K_d model under porous flow	5
4.2 Component additivity in the K_d model under fracture flow	6
4.3 Accounting for colloid effects in the component additivity K_d model.....	9
5. Evaluation of Upscaling in Porous Flow	10
5.1 Radionuclide–mineral K_d s in Frenchman Flat alluvium groundwater	10
5.2 Average radionuclide K_d s based on CAMBRIC HST model alluvium mineralogy	13
5.3 Comparison of CAMBRIC HST model alluvium mineralogy radionuclide K_d s to measured data	15
5.4 Heterogeneous distribution of radionuclide K_d s in Frenchman Flat alluvium.....	16
5.5 Effects of heterogeneously distributed radionuclide K_d s on CAU-scale reactive transport.....	24
6. Evaluation of Upscaling in the Fracture-Flow Case.....	31
6.1 Radionuclide–mineral K_d s in Pahute Mesa groundwater	32
6.2 Average radionuclide R_s based on CHESHIRE site mineralogy	33
6.2.1 Calculating radionuclide R_s – Americium example	33
6.2.2 Summary of average radionuclide R_s	37
6.2.3 Heterogeneous distribution of radionuclide R_s at the CHESHIRE site.....	39
6.3 Average radionuclide R_s based on Pahute Mesa hydrostratigraphic unit mineralogies	41
6.3.1 Morphology and mineralogy of 6 hydrostratigraphic units	41
6.3.2 Average radionuclide R_s of 6 hydrostratigraphic units.....	44
6.4 Comparison of Tuff Cone hydrostratigraphic unit and CHESHIRE site radionuclide R_s	47

6.5 Heterogeneous distribution of radionuclide R_s at the sub-hydrostratigraphic unit scale	49
6.5.1 Heterogeneous distribution of radionuclide R_s in the matrix of the Tuff Cone hydrostratigraphic unit	49
6.5.2 Heterogeneous distribution of radionuclide R_s in the fractures of the Tuff Cone hydrostratigraphic unit	58
7. Conclusions	68
8. Recommendations	69
9. Acknowledgements.....	70
10. References	70
Appendix A. The Mechanistic Sorption Model.....	77
A.1 Sorption reactions included in the sorption model	77
A.2 Defining surface complexation reactions	79
A.3 Defining ion exchange reactions.....	80
A.4 Surface complexation and ion exchange reaction constants	81
A.5 Implementation of surface complexation and ion exchange reactions.....	84
A.6 Aqueous complexation data	86
Appendix B. The Gaussian Random Field Approach	89
Appendix C. Mineral Abundance and Distribution Coefficient Data for Frenchman Flat Alluvium	93
Appendix D. Mineral Abundance and Predicted Radionuclide Retardation Data for Pahute Mesa Matrix Flow Zones.....	105
Appendix E. Mineral Abundance and Predicted Radionuclide Retardation Data for Pahute Mesa Fracture Flow Zones	125

LIST OF FIGURES

Figure 1. A plot of the parallel plate fracture model used to develop the methodology for upscaling retardation in a fracture flow environment.	8
Figure 2. Comparison of water chemistry reported in Rose (2001) (black) with average water chemistry reported in IT (1999) (red). Error bars represent one standard deviation.	11
Figure 3. Predicted radionuclide K_d s based on sorptive mineral abundances. A–G: average (black circle) and standard deviation based on mineral abundance, median (red) and bars (minimum and maximum). G: Minimum and maximum measured K_d s of Wolfsberg (1978) (green), Zavarin et al. (2002) batch (yellow), and Zavarin et al. (2002) flowthrough (pink). H: Average (black circle) and standard deviation based on mechanistic model uncertainty.	21
Figure 4. Gaussian random field realizations of spatial variability of K_d for Am, Ca, Cs, Eu, and Np.	25
Figure 5. Gaussian random field realizations of spatial variability of K_d for Pu ($O_2(g)$ fugacity = 10^{-5} bars), Pu ($O_2(g)$ fugacity = 10^{-10} bars), Pu ($O_2(g)$ fugacity = 10^{-15} bars), Sm, Sr, and U.	26
Figure 6. Breakthrough of tracer (TR) and Ca negatively, positively, and uncorrelated to the flow field permeability.	27
Figure 7. Breakthrough of tracer (TR) and Sr negatively, positively, and uncorrelated to the flow field permeability.	28
Figure 8. Breakthrough of tracer (TR) and Np negatively, positively, and uncorrelated to the flow field permeability.	28
Figure 9. Breakthrough of tracer (TR) and Pu at 10^{-5} bars $O_2(g)$ negatively, positively, and uncorrelated to the flow field permeability.	29
Figure 10. Breakthrough of tracer (TR) and Pu at 10^{-10} bars $O_2(g)$ negatively, positively, and uncorrelated to the flow field permeability.	29
Figure 11. Breakthrough of tracer (TR) and Pu at 10^{-15} bars $O_2(g)$ negatively, positively, and uncorrelated to the flow field permeability.	30
Figure 12. Breakthrough of tracer (TR) and U negatively, positively, and uncorrelated to the flow field permeability.	30

Figure 13. Comparison of particle model median peak breakthrough for radionuclides with average retardation assuming homogeneous mineralization. Thick black line represents ideal relationship assuming tracer breakthrough peak at 1 year with no test-related heat. Thin gray lines bracket range of uncertainty of peak tracer breakthrough with no test-related heat. Dashed line represents ideal relationship assuming tracer breakthrough peak at 2 years, as inferred from particle model median tracer breakthrough with test-related heat. Thin black line indicates ideal relationship assuming average flow velocity for high permeability hydrofacies (from Pawloski et al., 2001).	40
Figure 14. Am, Eu, and Sm matrix Log R as a function of depth based on mineral abundance data from well J-13.	51
Figure 15. Ca, Cs, and Sr matrix Log R as a function of depth based on mineral abundance data from well J-13.	51
Figure 16. Np, U, and Pu matrix Log R as a function of depth based on mineral abundance data from well J-13.	52
Figure 17. Am, Eu, and Sm matrix Log R as a function of depth based on mineral abundance data from drillhole UE-25.	52
Figure 18. Ca, Cs, and Sr matrix Log R as a function of depth based on mineral abundance data from drillhole UE-25.	53
Figure 19. Np, U, and Pu matrix Log R as a function of depth based on mineral abundance data from drillhole UE-25.	53
Figure 20. Am, Eu, and Sm matrix Log R as a function of depth based on mineral abundance data from drillhole USW-G1.....	54
Figure 21. Ca, Cs, and Sr matrix Log R as a function of depth based on mineral abundance data from drillhole USW-G1.....	54
Figure 22. Np, U, and Pu matrix Log R as a function of depth based on mineral abundance data from drillhole UE-25.	55
Figure 23. Am, Eu, and Sm matrix Log R as a function of depth based on mineral abundance data from drillhole USW-G2.....	55
Figure 24. Ca, Cs, and Sr matrix Log R as a function of depth based on mineral abundance data from drillhole USW-G2.....	56
Figure 25. Np, U, and Pu matrix Log R as a function of depth based on mineral abundance data from drillhole UE-25.	56
Figure 26. Predicted matrix radionuclide R_s based on mineral abundances. Average (black circle) and standard deviation based on mineral abundance, median (red) and bars (minimum and maximum).....	57
Figure 27. Am, Eu, and Sm fracture Log R as a function of depth based on mineral abundance data from drillhole UE-25.	59

Figure 28. Ca, Cs, and Sr fracture Log R as a function of depth based on mineral abundance data from drillhole UE-25	60
Figure 29. Np, U, and Pu fracture Log R as a function of depth based on mineral abundance data from drillhole UE-25	60
Figure 30. Am, Eu, and Sm fracture Log R as a function of depth based on mineral abundance data from drillhole USW-G1.....	61
Figure 31. Ca, Cs, and Sr fracture Log R as a function of depth based on mineral abundance data from drillhole USW-G1.....	61
Figure 32. Np, U, and Pu fracture Log R as a function of depth based on mineral abundance data from drillhole USW-G1.....	62
Figure 33. Am, Eu, and Sm fracture Log R as a function of depth based on mineral abundance data from drillhole USW-G2.....	62
Figure 34. Ca, Cs, and Sr fracture Log R as a function of depth based on mineral abundance data from drillhole USW-G2.....	63
Figure 35. Np, U, and Pu fracture Log R as a function of depth based on mineral abundance data from drillhole USW-G2.....	63
Figure 36. Am, Eu, and Sm fracture Log R as a function of depth based on mineral abundance data from drillhole USW-G3.....	64
Figure 37. Ca, Cs, and Sr fracture Log R as a function of depth based on mineral abundance data from drillhole USW-G3.....	64
Figure 38. Np, U, and Pu fracture Log R as a function of depth based on mineral abundance data from drillhole USW-G3.....	65
Figure 39. Am, Eu, and Sm fracture Log R as a function of depth based on mineral abundance data from drillhole USW-G4.....	65
Figure 40. Ca, Cs, and Sr fracture Log R as a function of depth based on mineral abundance data from drillhole USW-G4.....	66
Figure 41. Np, U, and Pu fracture Log R as a function of depth based on mineral abundance data from drillhole USW-G4.....	66
Figure 42. Predicted fracture flow zone radionuclide R_s based on mineral abundances. Average (black circle) and standard deviation based on mineral abundance, median (red) and bars (minimum and maximum)	67

LIST OF TABLES

Table 1. Ambient Frenchman Flat water chemistry used to predict radionuclide distribution coefficients (K_d s).....	11
Table 2. Radionuclide distribution coefficients (K_d s) calculated using water chemistry of Table 1 and mineral reactivities of Appendix A.....	12
Table 3. Porous media volume fractions defined in CAMBRIC HST simulations of Tompson et al. (1999).	13
Table 4. Predicted radionuclide distribution coefficients (K_d s) for Frenchman Flat alluvium and comparison with earlier values.....	14
Table 5. Reported mineralogic information (by XRD) for Frenchman Flat alluvium.....	17
Table 6. Predicted average radionuclide distribution coefficients (K_d s) using reported radionuclide sorbing mineral abundances.....	20
Table 7. Water chemistry used in the CHESHIRE HST model of Pawloski et al. (2001).	33
Table 8. Radionuclide distribution coefficients (K_d s) calculated using water chemistry of Table 7 and mineral reactivities of Appendix A.....	33
Table 9. Average fracture lining and matrix mineral abundances used in the CHESHIRE HST model (Pawloski et al., 2001).....	34
Table 10. Parameters used in conceptualization of high permeability fracture flow zones in the CHESHIRE HST model (Pawloski et al., 2001).	34
Table 11. Predicted radionuclide distribution coefficients (K_d s) for smectite colloids.	37
Table 12. Predicted radionuclide retardation factors (R_s) at the CHESHIRE site.....	38
Table 13. Parameters used to define radionuclide K_d s and R_s for selected hydrostratigraphic units at Pahute Mesa.	42
Table 14. Predicted retardation factors (R_s) for selected hydrostratigraphic units assuming Fe/MnOx dominated by iron oxide.....	46
Table 15. Predicted retardation factors (R_s) for selected hydrostratigraphic unit fracture flow zones assuming Fe/MnOx dominated by manganese oxides.	47
Table A1. Radionuclide–mineral interaction described by non-electrostatic surface complexation.	78
Table A2. Radionuclide–mineral interaction described by Vanselow ion exchange.....	78
Table A3. Surface complexation reaction for iron oxides using the NEM.....	82

Table A4. Surface complexation reactions for calcite using the NEM.....	82
Table A5. Surface complexation reactions for aluminosilicates using the NEM.....	83
Table A6. Vanselow ion exchange reactions for smectite, mica, and clinoptilolite.....	84
Table A7. Mineral characteristics used to define reactions on mineral surfaces.....	85
Table A8. Basis species used in thermodynamic data base.	86
Table A9. Parameters in extended Debye–Hückel activity coefficient model as a function of temperature (°C).	87
Table A10. Logarithm of equilibrium constants (K) of aqueous reactions used in thermodynamic data base. Most Pu data not shown pending approval for publication by the Nuclear Energy Agency.....	87
Table B1. Parameters for vertical variogram models of $\log_{10}[K_d]$ for radionuclides Ca, Cs, Sr, Am, Eu, Sm, Np, U, and Pu.	90
Table B2. Parameters for lateral variogram models of $\log_{10}[K_d]$ for radionuclides Ca, Cs, Sr, Am, Eu, Sm, Np, U, and Pu.	90
Table B3. Measured cell-to-cell correlation between realizations of \log_{10} permeability and $\log_{10}[K_d]$ for cases of “positive,” “zero,” and “negative” correlation.....	92
Table C1. Radionuclide sorbing mineral abundances and predicted K_d s for Frenchman Flat alluvium samples.	95
Table D1. Radionuclide sorbing mineral abundances and predicted K_d s for Tuff Cone hydrostratigraphic unit matrix flow zones.....	107
Table D2. Sample stratigraphic units and predicted retardation factors for Tuff Cone hydrostratigraphic unit matrix flow zones.....	115
Table E1. Radionuclide sorbing mineral abundances and predicted retardation factors for Tuff Cone hydrostratigraphic unit fracture flow zones.....	129
Table E2. Radionuclide sorbing mineral abundances and predicted retardation factors for Tuff Cone hydrostratigraphic unit fracture flow zones.....	141

1. Introduction

The LLNL near-field hydrologic source term (HST) model is based on a mechanistic approach to radionuclide retardation—that is, a thermodynamic description of chemical processes governing retardation in the near field, such as aqueous speciation, surface complexation, ion exchange, and precipitation (Pawloski et al., 2000; Pawloski et al., 2001; Tompson et al., 1999). The mechanistic approach allows for radionuclide retardation to vary both in space and time as a function of the complex reaction chemistry of the medium. This level of complexity is necessary for near-field HST transport modeling because of the non-linear reaction chemistry expected close to the radiologic source. Large-scale Corrective Action Unit (CAU) models—into which the near-field HST model results feed—require that the complexity of the mechanistic approach be reduced to a more manageable form (e.g. Linear, Langmuir, or Freundlich sorption isotherms, etc).¹ The linear sorption isotherm (or K_d) approach is likely the most simple approach for large-scale CAU models. It may also be the most appropriate since the reaction chemistry away from the near field is expected to be less complex and relatively steady state. However, if the radionuclide retardation approaches in near-field HST and large-scale CAU models are different, they must be proved consistent. In this report, we develop a method to link the near-field HST and large-scale CAU model radionuclide retardation approaches.

The mechanistic approach to radionuclide retardation modeling is more technically defensible than the K_d approach because it is based on a thermodynamic description of chemical processes. Furthermore, unlike the K_d approach, the thermodynamic basis of the mechanistic approach is not affected by data transferability issues. Linking the K_d approach (to be used in large-scale CAU models) to the near-field HST mechanistic approach provides defensibility for the K_d approach and consistency between near-field HST and large-scale CAU models. Nevertheless, it must be noted that the mechanistic approach, like the K_d approach, requires validation to be successful. This report provides a partially validated mechanistic approach for the porous flow reactive transport case. The approach proposed for the fracture flow reactive transport case has not been validated. Thus, the methodology described herein requires significant additional evaluation and validation before implementation. Nevertheless, the approach, in its present partially validated form, provides significant insight into the variability and scale of radionuclide retardation in a number of Nevada Test Site (NTS) stratigraphic units.

In this report, we summarize the process of upscaling the near-field HST model mechanistic radionuclide retardation approach to a simplified large-scale CAU K_d approach. Our proposed method for upscaling radionuclide retardation from the near-field HST mechanistic model to a CAU-scale K_d model requires several steps:

1. A mechanistic sorption model must be developed based on highly controlled single-mineral/single-radionuclide experiments. The experimental data must span a

¹ The large-scale corrective action unit (CAU) models can include spatially variable radionuclide retardation (within the model resolution) but not the complex chemistry applied in near-field models.

large range of solution conditions such that a mechanistic description of each radionuclide–mineral interaction is well constrained. A mechanistic sorption model was initially developed for the CAMBRIC HST simulations (Tompson et al., 1999), has been significantly updated (Zavarin and Bruton, 2000a; Zavarin and Bruton, 2000b; Zavarin et al., 2002) and was most recently implemented in the CHESHIRE HST simulations (Pawloski et al., 2001).

2. The mechanistic model that describes radionuclide–mineral interaction must be simplified to a K_d model. This requires justifiable simplifying assumptions (described in Section 2).
3. Radionuclide sorption to individual minerals must be combined to describe sorption in a medium containing a number of minerals (e.g. alluvium). This is described as component additivity (Davis et al., 1998). Component additivity can be incorporated into mechanistic or K_d models. Component additivity based on a mechanistic model was used in the CHESHIRE HST simulations (Pawloski et al., 2001).
4. Finally, the impacts of spatially variable (heterogeneous) flow and radionuclide sorbing mineral distribution need to be evaluated. This is an explicit transport model scaling issue which relates to effects of model resolution on transport. The effect is dependent on the degree and scale of reactive mineral variability (e.g., Leblanc et al., 1991; Tompson and Jackson, 1996) which may lead to modified dispersion behavior for each radionuclide (e.g., Garabedian et al., 1988).

The development of a mechanistic sorption model has been discussed previously in detail (Zavarin and Bruton, 2000a; Zavarin and Bruton, 2000b); a synopsis is given in Appendix A. The focus of this report is primarily the simplification of the mechanistic to the K_d approach and the use of component additivity. The impacts of sorbing mineral heterogeneity are discussed in context of Frenchman Flat alluvium and several Pahute Mesa hydrostratigraphic units. Some comparisons of predicted K_d s to published batch sorption data (Frenchman Flat alluvium only) are reported. For Frenchman Flat alluvium, we also review earlier HST model simulations (Pawloski et al., 2000; Tompson et al., 2001) and put them into context with newer mineral heterogeneity information (Carle et al., 2002) and transport models. For Pahute Mesa, we use the CHESHIRE site data (Pawloski et al., 2001) in combination with CAU scale and high spatial resolution mineralogy data to examine heterogeneity effects on transport.

2. Basis for Simplification of the Mechanistic Approach to the K_d Approach

Radionuclide retardation in the environment is controlled by a number of processes (aqueous speciation, surface complexation, ion exchange, precipitation, and co-precipitation). A mechanistic approach is required to explicitly account for these processes. Radionuclide retardation based on a mechanistic approach is highly defensible since it is grounded in thermodynamics. The mechanistic approach allows one to predict the behavior of radionuclides under dynamic environmental conditions (such as those

found in the immediate vicinity of underground nuclear tests) because it explicitly accounts for the many factors that will affect radionuclide retardation. However, the mechanistic approach is computationally very costly. While the computational cost can be afforded in near-field HST simulations, this approach is neither feasible nor justifiable for large-scale CAU models (the reaction chemistry away from the near field is expected to be less complex and relatively steady state).

Under certain conditions, the complex mechanistic approach may be simplified to a linear sorption isotherm (or K_d) approach. The conditions required for this simplification are:

- Time-invariant solution conditions (groundwater chemistry)²
- Time-invariant radionuclide sorbing mineral abundances²
- Radionuclide concentrations well below the point at which sorption sites may become saturated (sorption sites are pertinent to surface complexation and ion exchange processes)
- Radionuclide concentrations well below the respective mineral precipitate saturations
- Solution conditions in which radionuclide co-precipitation will not occur.

These required conditions are met for most of the Nevada Test Site (NTS).

While most areas of the NTS should exhibit approximately constant groundwater chemistry, mineralogy, and flow conditions, significant transience in the near field of underground nuclear tests is likely. This is particularly true at times when test-related high temperatures may result in high rates of glass dissolution and mineral alteration, as well as heat-driven flow. Glass dissolution could, for example, increase or decrease aqueous Na^+ , K^+ , Ca^{2+} , and Mg^{2+} concentrations. This would, in turn, affect radionuclide sorption to ion exchange sites. Glass dissolution could affect the groundwater pH which would, in turn, affect protonation of surface complexation sites (Pawloski et al., 2001). Glass dissolution could also affect the redox state of near-field groundwater and severely alter the transport behavior of redox sensitive elements such as Pu and U. Precipitation of secondary minerals could change the radionuclide sorbing mineral abundances. Precipitation of secondary minerals could also affect the permeability of the medium which would, in turn, alter flow conditions.

While some transience in water chemistry is expected in the near field, the mineral composition of NTS rocks will act to buffer the composition of these waters. Thus, the groundwater chemistry should return to its ambient state at some point downstream. Transience in radionuclide sorbing mineral abundance will also be isolated to the near field and should not affect transport outside the cavity. Detailed geochemical modeling of the near field allows for evaluation of the transient near-field effects. CAU scale models are expected to use the near-field HST model results to capture this transient behavior and do not need to account for these effects directly in their model. We base our radionuclide retardation upscaling on far-field (CAU scale) conditions that meet the requirements for simplification of a mechanistic approach to a K_d approach.

² Invariant with respect to time but not necessarily space

While the K_d approach requires that the assumptions listed above be met, the K_d approach can account for spatially variable (but constant) conditions. For example, the water chemistry of the carbonate aquifer is significantly different from the water in the fractured tuffs of Pahute Mesa. Radionuclide retardation (and K_d s) should, therefore, vary spatially as a result of water chemistry. Radionuclide K_d s will also be spatially variable as a result of differences in sorptive mineralogy and dominant flow mechanisms (fracture flow/porous flow). These spatial variations can be accounted for by developing a K_d approach based on categories of sorptive mineralogy, water chemistry, and flow conditions at the NTS.

3. Radionuclides and Sorbing Minerals Included in the Mechanistic Approach and Discussed in This Report

The predicted K_d data presented in this report are based on non-electrostatic surface complexation and Vanselow ion exchange mechanistic models developed for near-field HST modeling. The mechanistic models account for the interaction of radionuclides with the surfaces of iron oxides, carbonates, and aluminosilicates. For detailed information regarding the mechanistic model see Zavarin and Bruton (2000a; 2000b) and Zavarin et al. (2002). The reaction constants used by our model are tabulated in Appendix A. The model was recently partially validated using batch and flow-through experiments with Frenchman Flat and Yucca Flat alluvium (Zavarin et al., 2002).³

Some minerals that may significantly retard radionuclides are not addressed by our model due to lack of published data or time constraints. For example, although manganese oxides comprise a large fraction of the fracture-lining mineralogy in certain locations at Pahute Mesa and other sites, limitations in surface complexation data did not allow for their incorporation into our model. The absence of manganese oxides in our model results in a more conservative simulation of radionuclide transport because these minerals are not available to sorb radionuclides. However, the sorbing minerals included in our model are expected to already comprise a large fraction of the radionuclide retardation capacity of NTS rocks. Nevertheless, the effects of manganese oxides should be addressed in the future to more accurately represent in-situ conditions and improve model defensibility. This can be done by incorporating manganese oxides into our surface complexation/ion exchange model or by providing detailed experimental evidence for their negligible role in radionuclide transport.

The choice of radionuclides discussed in this report is based on a combination of available unclassified radiologic source term (RST) radionuclide information (Smith, 2001; Bowen et al., 2001), available published sorption data, and surface complexation/ion exchange reactions developed to date. Sorbing radionuclides discussed in this report include the following: Ca, Cs, Sr, Am, Eu, Sm, Np, Pu, and U.⁴ For each of these elements, at least one isotope was included in recently published unclassified RSTs

³ Validation under fracture flow conditions has not been examined to date.

⁴ This same set of radionuclides was used in Pawloski et al. (2001).

(Smith, 2001; Bowen, 2001).⁵ Many more radionuclides are included than unclassified RSTs examined here. While some of these radionuclides are likely to behave as tracers (³H, ³⁶Cl, ⁹⁹Tc, etc.), the behavior of other radionuclides can be predicted by analogy to elements investigated here (e.g. Ho should behave similar to Eu). Still other RST radionuclides could not be modeled effectively with our mechanistic model because of data limitations or because surface complexation/ion exchange reactions have not been developed to date. Further discussion with respect to implementing retardation of RST radionuclides can be found in Tompson et al. (2001).

4. Component Additivity Methodology

If conditions for simplifying the mechanistic to the K_d approach have been met, we can calculate a distribution coefficient (K_d) for every radionuclide–mineral pair in our surface complexation/ion exchange database at a particular groundwater chemistry of interest.⁶ In the following two sections, we describe how the individual radionuclide–mineral K_d s, developed for a particular groundwater chemistry condition, can be combined (component additivity) into a K_d for each radionuclide and each mineralogically distinct domain.⁷ In this manner, we establish a method for simplifying the mechanistic approach used in near-field HST models to a K_d approach that can be used in large-scale CAU models.

4.1 Component additivity in the K_d model under porous flow

Component additivity relies on the principle that the sorption of a radionuclide in a particular medium can be determined based on the additive radionuclide sorption effect from the individual minerals contained in that medium:⁸

$$K_d = \frac{mol_{sorb}/g_{tot}}{mol_{aq}/mL} = \sum_{i=1}^n K_{d,i} \phi_{m,i} \quad (1)$$

where K_d is the radionuclide distribution coefficient (mL/g) for a particular medium under specified groundwater chemistry conditions, mol_{sorb}/g_{tot} is the molar quantity of a radionuclide sorbed per gram medium, mol_{aq}/mL is the molar quantity of a radionuclide in solution per mL solution, $K_{d,i}$ is the radionuclide distribution coefficient (mL/g) for the

⁵ We assume here that all isotopes of an element behave geochemically in the same manner. Recently published RST radionuclides include the following elements: H, C, Al, Cl, Ar, K, Ca, Ni, Kr, Sr, Zr, Nb, Tc, Pd, Cd, Sn, I, Cs, Sm, Eu, Ho, Th, U, Np, Pu, Am, and Cm.

⁶ The accuracy of the calculated K_d will depend on a number of factors, including the uncertainty in surface complexation reaction constants, ion exchange constants, aqueous speciation constants, redox condition, mineral surface area, mineral abundance, etc. A few of these uncertainties are reported in Appendix A while most are difficult to estimate. They are not addressed in this report, though they play a critical role in our ability to predict radionuclide transport behavior.

⁷ We develop this model as an ideal case in which mineral surfaces are entirely accessible to the aqueous radionuclides.

⁸ The retardation behavior of each mineral will be dependent on the groundwater chemistry. Thus, distinct radionuclide retardation factors must be evaluated for each distinct groundwater chemistry.

individual mineral i under specified groundwater chemistry conditions, and ϕ_m is the mass fraction of mineral i with respect to the total bulk medium.

The K_d of a radionuclide in a particular medium can be converted to a unitless retardation factor, R , by the following:

$$R = 1 + \frac{mol_{sorb}/mL}{mol_{aq}/mL} = 1 + \frac{K_d \rho_b}{\theta} = 1 + \frac{\rho_b}{\theta} \sum_{i=1}^n K_{d,i} \phi_{m,i} \quad (2)$$

where θ is the porosity and ρ_b is the bulk density of the medium.

4.2 Component additivity in the K_d model under fracture flow

As in the porous-flow case, a K_d approach can be developed for the fracture-flow case using a mechanistic model and based on the simplifying conditions established in Section 2. However, due to the significantly more complex geometry of fracture flow, additional steps must be taken to combine individual radionuclide–mineral K_d s into a single radionuclide K_d for a fractured medium.

Figure 1 is a plot of a simple parallel-plate fracture model. In general, porosities based on a parallel-plate fracture density and aperture model provide a lower limit to the effective porosity of a fractured medium (Shaw, 2003). The difference between parallel-plate model and measured effective porosities, in part, results from the complex morphology of real fractures (compared to the parallel-plate model fracture morphology). Flow in a real fracture may be tortuous, significantly increasing the fluid path length (and effective porosity). A real fracture surface may also include surface roughness which would provide some flow turbulence. This could result in a greater effective porosity and would allow for some small amount of flow in the matrix. A flowing “matrix reactive zone” was conceptualized in CHESHIRE HST simulations to link the parallel-plate fracture model to effective porosities established from field data (Pawloski et al., 2001).⁹ Since the calculated porosities based on the parallel-plate model were significantly lower than the effective porosities determined field data, inclusion of a “matrix reactive zone” was used to adjust the parallel-plate model effective porosity.

This conceptualization of a “matrix reactive zone” was based on a need to merge the parallel-plate fracture model with field observations in CHESHIRE HST simulations and not on a realistic conceptualization of physical flow. While fracture tortuosity or turbulent flow may be used to qualitatively justify the need to incorporate some flow in the matrix, we do not provide any validation for this conceptualization. However, the

⁹ This conceptualization relies on flow in the matrix being allowed in only a very narrow zone alongside the fracture. Allowing flow in a very narrow fraction of matrix can be justified by comparing the rate of diffusion with the fluid residence time. Based on an effective diffusion coefficient of 10^{-6} cm²/sec, several millimeters of matrix will be accessed over 24 hours. Since this rate is very fast when compared to residence times of fluids in large-scale models, it can be considered instantaneous. Nevertheless, it is important to remember that diffusion into the remaining matrix needs to be accounted for by the more traditional treatment of matrix diffusion.

effect of including a small “matrix reactive zone” on simulated fracture transport results was investigated recently and shown to have little effect (Zavarin, 2002). This was, in part, because radionuclides were able to quickly diffuse into the very thin “matrix reactive zone”. Nevertheless, the repercussions of this conceptualization need to be further evaluated under a variety of flow conditions (the use of a “matrix reactive zone” is discussed further in Pawloski et al. (2001), Chapter 6). Furthermore, if the effective porosities and fracture porosities are consistent, there is no need to conceptualize a “matrix flow zone” (i.e. C=0 in the upscaling approach described below).

Matrix diffusion needs to be addressed both at the near-field and CAU scales and is likely to play an important role in radionuclide transport in fracture media. In this report, we provide an approach for calculating radionuclide retardation in the matrix¹⁰ and the fracture zones but do not discuss methods for implementing the diffusion (or exchange) between these two continua. The implementation of matrix diffusion exchange functions in transport models is not discussed in this report.

Based on the parallel-plate model described above, we can determine the effective porosity (θ_{eff}) and the fracture flow zone porosity (θ_{fz}) (see Figure 1) by the following:

$$\theta_{eff} = 2\rho_{fract.}(A + \theta_{fl}B + \theta_mC) \quad (3)$$

and

$$\theta_{fz} = \frac{A + \theta_{fl}B + \theta_mC}{A + B + C} \quad (4)$$

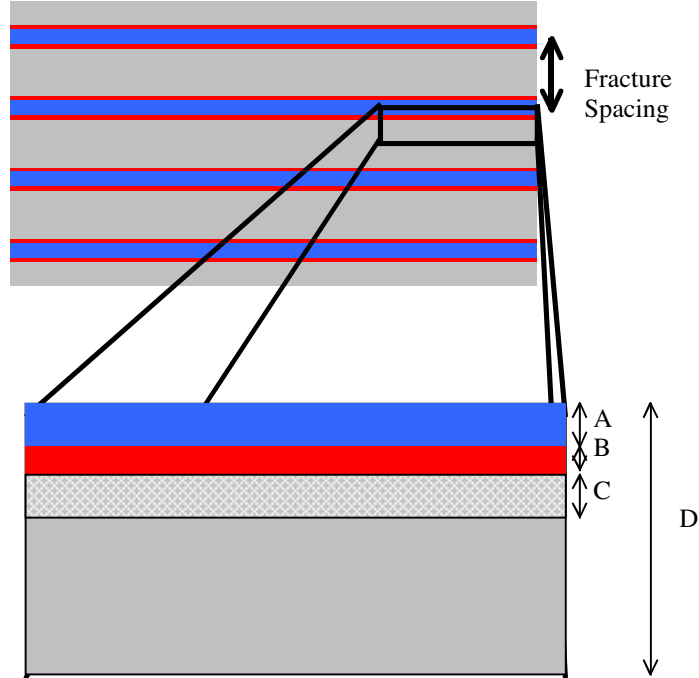
where ρ_{fract} is the fracture density (m^{-1}), θ_{fl} is the fracture-lining porosity, θ_m is the matrix porosity, and A, B, and C are defined in Figure 1 in units of meters. Here, the radionuclide distribution coefficient of the fracture flow zone, $K_{d,fz}$, will be:

$$K_{d,fz} = \frac{mol_{sorb}/g_{fz}}{mol_{aq}/mL} = \sum_{i=1}^n K_{d,i}\phi'_{fz,m,i} \quad (5)$$

where mol_{sorb}/g_{fz} is the molar quantity of a radionuclide sorbed per gram fracture flow zone medium and $\phi'_{fz,m,i}$ is an adjusted fracture flow zone mass fraction that accounts for the fracture lining and matrix reactive zone mineral abundances:

$$\phi'_{fz,m,i} = \frac{\rho_{b,FL}B\phi_{m,i,FL} + \rho_{b,M}C\phi_{m,i,M}}{\rho_{b,M}C + \rho_{b,FL}B} \quad (6)$$

¹⁰ Note that radionuclide retardation in the matrix can be calculated in the same manner as in the porous flow condition described in Section 4.1.



- A = Fracture half-aperture
- B = Fracture lining thickness
- C = Matrix reactive zone
- D = Half fracture distance
- A + B + C = Fracture flow zone

Figure 1. A plot of the parallel plate fracture model used to develop the methodology for upscaling retardation in a fracture flow environment.

where M and FL relate to matrix and fracture-lining parameters, respectively. Note that if no flow is allowed in the matrix reactive zone, the equation is simplified to one resembling porous flow. To determine the radionuclide retardation factor of the fracture flow zone, R_{fz} , we use the following equation:

$$R_{fz} = 1 + \frac{mol_{sorb}/mL}{mol_{aq}/mL} = 1 + \frac{K_{d,fz}\rho'_{b,fz}}{\theta_{fz}} = 1 + \frac{\rho'_{b,fz}}{\theta_{fz}} \sum_{i=1}^n K_{d,i}\phi'_{fz,m,i} \quad (7)$$

where the bulk density of the fracture flow zone is calculated by the following equation:

$$\rho'_{b,fz} = \frac{\rho_{b,FL}B + \rho_{b,M}C}{A + B + C}. \quad (8)$$

4.3 Accounting for colloid effects in the component additivity K_d model

Colloids can significantly affect the net retardation of some radionuclides. Under simplified conditions, the effect of colloids can be taken into account using our K_d approach. The model below assumes that radionuclide desorption kinetics and complex colloid transport effects such as colloid filtration are not significant. This oversimplifies colloid-mediated radionuclide transport significantly but allows one to evaluate colloid effects in a rudimentary way. While this simplification is not likely to adequately treat the process of colloid-facilitated transport at the near-field or CAU scales, it provides a way to compare the effect that colloids have on each radionuclide and how radionuclide transport can be exacerbated by such colloid-facilitated transport.

If we use an equilibrium model, one can determine a distribution coefficient for a radionuclide sorbed to colloids, $K_{d,col}$, using Equation (1). Assuming a constant colloid load in solution, a retardation factor for a radionuclide sorbed to colloids, R_{col} , can be calculated by the following:

$$R_{col} = 1 + \frac{mol_{col}/mL}{mol_{aq}/mL} = 1 + K_{d,col} C_{col} \quad (9)$$

where C_{col} is the colloid load in solution (g/mL) and mol_{col}/mL and mol_{aq}/mL are the molar quantities of a particular radionuclide per mL associated with colloids and as a free ion in solution, respectively.¹¹ The adjusted radionuclide retardation factor in the fracture flow zone (R'_{fz}) which accounts for colloid effects will then be:

$$R'_{fz} = 1 + \frac{\frac{mol_{sorb}}{mL}}{\frac{mol_{aq}}{mL} + \frac{mol_{col}}{mL}} = 1 + \frac{(R_{fz} - 1) \frac{mol_{aq}}{mL}}{\frac{mol_{aq}}{mL} + (R_{col} - 1) \frac{mol_{aq}}{mL}} = 1 + \frac{R_{fz} - 1}{R_{col}} \quad (10)$$

and the respective distribution coefficient ($K'_{d,fz}$) will be:

$$K'_{d,fz} = \frac{\theta_{fz}(R'_{fz} - 1)}{\rho'_{b,fz}}. \quad (11)$$

A similar adjusted radionuclide retardation factor and distribution coefficient can be calculated for porous flow.¹² However, as stated earlier, this adjusted retardation factor is only useful for comparative purposes and is likely to oversimplify colloid effects at the near-field and CAU scales.

¹¹ Note that we are not excluding colloids from the fracture lining or the matrix reactive zone. It is a result of the simplified fracture–flow conceptualization used here.

¹² However, for all predicted K_d s and R s reported here for porous flow, we assume that colloid do not play a significant role.

5. Evaluation of Upscaling in Porous Flow

In this section, we predict radionuclide-mineral K_d s based on Frenchman Flat groundwater conditions. The component additivity approach is then applied to the CAMBRIC near-field HST model mineralogy of Tompson et al. (1999). The mineralogy and water chemistry¹³ used here and in Tompson et al. (1999), Pawloski et al. (2000), and Tompson et al. (2001) is equivalent but the mechanistic sorption model differs. The differences are the result of continued improvements to the mechanistic model parameters. Comparison of our present-day mechanistic model results with the earlier modeling efforts provides some perspective on these changes. We also compare the predicted K_d s to measured K_d s reported for Frenchman Flat alluvium. Finally, we examine predicted K_d spatial variability in Frenchman Flat alluvium using a large number of published mineral abundance data and evaluate this spatial variability in terms of possible upscaling effects.

5.1 Radionuclide–mineral K_d s in Frenchman Flat alluvium groundwater

The K_d for each radionuclide–mineral pair is determined by (1) groundwater chemistry, (2) mineral characteristics (mineral surface area, reactive site density, reactive site types, protonation/deprotonation constants, cation exchange capacities) and (3) the mechanistic models (non-electrostatic surface complexation and Vanselow ion exchange models) used to describe sorption. For all predicted radionuclide K_d s presented in this report, mineral characteristics (2) and the mechanistic models (3) are held constant. Thus, the predicted K_d s listed in this report for each radionuclide–mineral pair are solely a function of groundwater chemistry. The mineral characteristics and surface complexation/ion exchange models are reported in Appendix A.

For the Frenchman Flat alluvium case, the water chemistry used to calculate the individual radionuclide–mineral K_d s was based on water analyses reported by Rose (2001) from a variety of Frenchman Flat wells (Table 1). These water analyses are consistent with those reported in the Frenchman Flat CAU Documentation Package (IT, 1999) (Figure 2). The low ionic strength sodium bicarbonate type waters are typical of much of the NTS.

Given the water chemistry of Table 1 and the mineral reactivities established in Appendix A, K_d s for each radionuclide–mineral pair can be calculated (Table 2). Included in Table 2 are K_d uncertainties for each radionuclide–mineral pair. These uncertainties are based on the surface complexation constant uncertainties in our mechanistic model (listed in Appendix A).¹⁴ The uncertainty in the ion exchange constants could not be readily estimated because the ion exchange constants were taken directly from published data

¹³ Water chemistry used here differs slightly from earlier models but not enough to cause a significant change in predicted radionuclide retardation.

¹⁴ For those surface complexation reactions that do not have standard deviations listed in Appendix A, a Log K standard deviation of 0.5 was used. Note that Log K is not equivalent to Log K_d ; see Appendix A for details.

Table 1. Ambient Frenchman Flat water chemistry used to predict radionuclide distribution coefficients (K_{ds}).

	Concentration [†]
pH	8.4±0.3 [§]
F ⁻	mg/kg
Na ⁺	1.1±0.3
K ⁺	79±26
Mg ²⁺	6.7±1.0
Ca ²⁺	2.8±1.7
Cl ⁻	12.0±4.7
HCO ₃ ⁻	13.2±3.5
SO ₄ ²⁻	190±62
SiO ₂	34.8±8.7
SiO ₂	56±21 [¶]

[†] Data from Rose (2001).

[§] Uncertainty ($\pm 1\text{SD}$) determined from analyses of a number of groundwater samples.

[¶] Data regarding Si was not reported; value of IT (1999) was used.

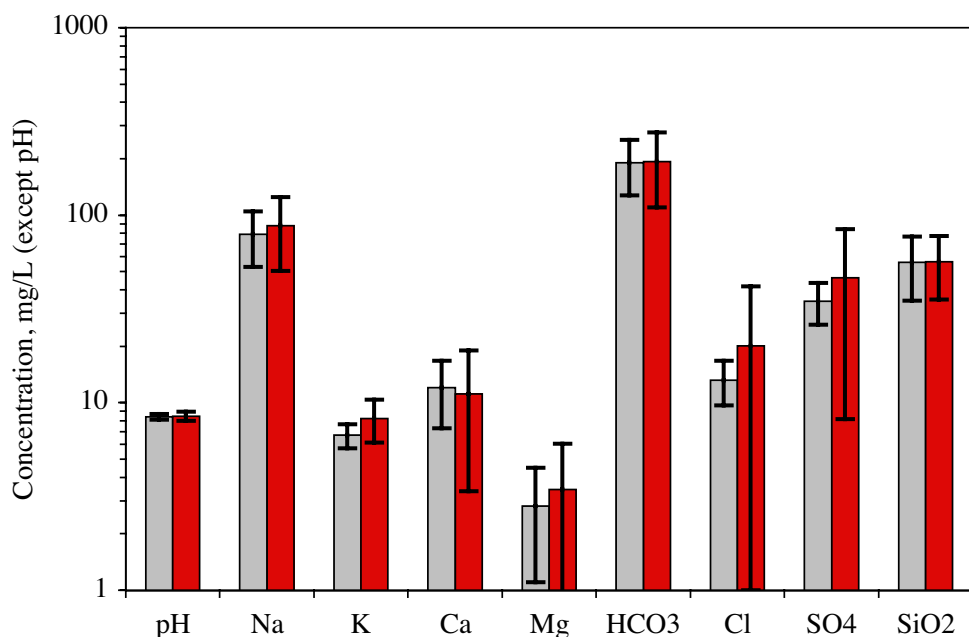


Figure 2. Comparison of water chemistry reported in Rose (2001) (black) with average water chemistry reported in IT (1999) (red). Error bars represent one standard deviation.

and did not include uncertainty estimates. An attempt was made to establish reasonable lower-limit ion exchange constants in the case of Cs. The lower-limit ion exchange constants for Cs were assumed to be equivalent to K ion exchange constants for zeolite, smectite, and basal plane illite. Ion exchange constants for the two illite edge sites were reduced by a Log K of 1. The lower limit ion exchange constants for Cs are not based on measured uncertainties and are, thus, only useful to demonstrate the sensitivity of radionuclide transport to ion exchange constants. Lower limits for Sr and Ca ion exchange constants were not estimated.

Table 2 presents K_d s for Pu at three $O_2(g)$ fugacities: 10^{-5} , 10^{-10} , and 10^{-15} bars. Evidence from Pu solubility experiments in Yucca Mountain waters (Nitsche et al., 1993; Nitsche et al., 1994) suggest that Pu(V) should be the dominant Pu redox state in NTS-type waters. A range of 10^{-5} to 10^{-15} bars was suggested in Zavarin (2002) to bracket the range of possible Pu oxidation states; over this range, Pu(V) dominates but the contribution of Pu(IV) and Pu(VI) varies widely.¹⁵

Table 2. Radionuclide distribution coefficients (K_d s) calculated using water chemistry of Table 1 and mineral reactivities of Appendix A.

	Calcite	Zeolite (clinoptilolite)	Iron Oxide	Mica/illite ^Y	Smectite
	Log (K_d)				
Ca	0.44	3.51		2.33	2.67
Cs		3.47 (2.86) [§]		5.45 (4.45)	2.80 (1.31)
Sr	-1.31±0.5	0.629	-0.02±0.32	2.32	2.27
Am	4.30±0.5		3.23±0.39		4.72±0.30
Eu	4.02±0.5		2.92±0.67		4.09±0.46
Sm	4.56±0.5		3.08±0.67		4.09±0.42
Np	1.58±0.5		1.95±0.47		1.23±0.27
U	-3.07±0.5		1.83±0.43		0.79±0.39
Pu ($O_2 = 10^{-5}$) [§]	1.20±0.5		1.99±0.5		1.77±0.5
Pu ($O_2 = 10^{-10}$)	1.69±0.5		2.48±0.5		2.15±0.5
Pu ($O_2 = 10^{-15}$)	2.30±0.5		3.07±0.5		2.60±0.5

[§] Pu K_d s determined at three $O_2(g)$ fugacities : 10^{-5} , 10^{-10} , and 10^{-15} bars. The range of $O_2(g)$ fugacities was suggested in Zavarin et al. (2002) to evaluate the effect of Pu redox state on transport.

^Y Mechanistic sorption model is based on illite. However, XRD analysis did not distinguish between illite and mica. We assume in our model that these two minerals behave similarly.

[¶] Values in parentheses are estimated K_d lower limits based on lower limits for the respective reaction constants.

¹⁵ It is important to note that the oxidation state of Pu in solution is thought to be kinetically controlled (non-equilibrium). Fixing the $O_2(g)$ fugacity is a simple way to achieve a ratio of Pu oxidation states consistent with experimental data but is not based on observed $O_2(aq)$ concentrations in NTS waters.

5.2 Average radionuclide K_d s based on CAMBRIC HST model alluvium mineralogy

The CAMBRIC near-field HST model mineralogy reported in Tompson et al. (1999) is presented in Table 3. It was based on average radionuclide sorbing mineral abundances reported for wells RNM-1 and UE-5n. This mineralogy was used in the CAMBRIC HST simulations (Tompson et al., 1999), the classified Frenchman Flat HST simulations (Pawloski et al., 2000), and the simplified Frenchman Flat HST simulations (Tompson et al., 2001).

Table 3. Porous media volume fractions defined in CAMBRIC HST simulations of Tompson et al. (1999).

Component	Density [‡] g/cm ³	Volume Fraction %	Mass Fraction %
Inert Matrix	2.5	47	77.3
Clinoptilolite–Ca (zeolite)	2.13	5	7.0
Beidellite–Ca (smectite)	2.83	5	9.3
Calcite	2.71	1	1.8
Muscovite (illite/mica)	2.83	1	1.9
Iron oxide	4.27	1	2.8
Porosity	–	40	–

[‡] Densities from Johnson and Lundeen (1997).

Frenchman Flat alluvium radionuclide K_d s can be predicted using Equation (1) and data from Tables 2 and 3. Table 4 presents the resulting K_d s as well as K_d s reported in two other sources. The “high” and “low” values in were calculated based on one standard deviation or the lower-limit sorption constant (for Cs) for all minerals in combination (i.e. the uncertainty was estimated simply as a linear combination of uncertainties in the single mineral K_d s).¹⁶ As in Table 2, K_d s for Pu were predicted over a range of redox conditions. In general, Pu sorbs more strongly as the solution conditions are more reducing owing to the increased contribution of strongly sorbing Pu(IV).

It is useful to compare the K_d s calculated in this report (Table 4) with CAMBRIC near-field HST radionuclide retardations reported in Tompson et al. (1999).¹⁷ Based on their homogeneous mineral distribution model, a K_d of $10^{2.9}$ mL/g was reported for Cs (see Figure 152 of Tompson et al., 1999) compared to $10^{3.7}$ mL/g reported here. The increase in predicted K_d results from mechanistic model improvements reported in Zavarin et al. (2002). The data in Zavarin et al. (2002) suggest that Cs sorption to illite is stronger than

¹⁶ Uncertainties listed in Tompson et al. (2001) were reported as ± 2 standard deviations. These values were replaced by ± 1 standard deviation in Table 4 to simplify comparisons with K_d s reported here.

¹⁷ Footnote in Tompson reported R_s . We converted to K_d s assuming a porosity of 40% and an average mineral density of 2.5 g/cm³.

Table 4. Predicted radionuclide distribution coefficients (K_d s) for Frenchman Flat alluvium and comparison with earlier values.

Radionuclide	K_d (high,low)	Tompson et al. (1999)	Tompson et al. (2001)
	Log (mL/g)	K_d	K_d (high,low)
Ca	2.4		2.4
Cs	3.7 (3.7,2.7)	2.9	3.0 (3.0, 2.1)
Sr	2.2	2.8	2.5 (2.5, 2.4)
Am	3.7 (4.1,3.4)		4.2 (4.7, 3.7)
Eu	3.1 (3.6,2.7)		3.9 (4.4, 3.4)
Sm	3.4 (3.8,2.9)		4.4 (4.9, 3.9)
Np	0.7 (1.1,0.3)		1.5 (2.0, 1.1)
U	0.4 (0.8,-0.03)		1.7 (2.2, 1.3)
Pu ($O_2 = 0.2$) [†]		2.1	0.8 (1.3, 0.3)
Pu ($O_2 = 10^{-5}$)	0.9 (1.4,0.4)		
Pu ($O_2 = 10^{-10}$)	1.3 (1.8,0.8)		2.0 (2.5, 1.5)
Pu ($O_2 = 10^{-15}$)	1.9 (2.3,1.4)		

[†] O_2 value indicates $O_2(g)$ fugacity (equilibrium redox state) in bars.

previously estimated. Nevertheless, the earlier value falls in the range of estimated K_d uncertainty.¹⁸ In the case of Sr, a K_d of $10^{2.8}$ mL/g was reported in Tompson et al. (1999) as compared to $10^{2.2}$ mL/g calculated here. The decrease in K_d results from several mechanistic model adjustments recommended in Zavarin et al. (2002) including a reduction in the affinity of Sr for smectite and a significant reduction in the reactive surface area of iron oxide (600 m²/g reduced to 0.25 m²/g).¹⁹ While a range of uncertainty is not reported here for Sr, it is important to recognize that the difference between the Sr K_d of Tompson et al. (1999) and that reported here is 0.6 log units. This difference is similar to the range of uncertainty reported for most other radionuclides in Table 4. In the case of Pu, a K_d of $10^{2.1}$ was reported in Tompson et al. (1999) as compared to $10^{0.9 \text{ to } 1.9}$ reported here for $O_2(g)$ fugacities of 10^{-5} to 10^{-15} bars. The difference in K_d results from combined adjustments to the reactive surface area of iron oxide and $O_2(g)$ fugacity. In the case of Pu, the earlier value reported in Tompson et al. (1999) falls within the range of uncertainty reported here (at 10^{-15} bars $O_2(g)$). In general, while the K_d s based on the updated mechanistic model of Zavarin et al. (2002) are more thoroughly validated, the values reported in Tompson et al. (1999) for Cs, Sr, and Pu fall within the expected range of uncertainty in the predicted values reported here.²⁰

The K_d s predicted in this report can also be compared to a recent report on a simplified source term for use in large-scale modeling of radionuclide transport at Frenchman Flat

¹⁸ The uncertainties discussed here are related only to uncertainties in surface complexation and ion exchange reaction constants. Uncertainties in other parameters (reactive surface area, solution chemistry, redox state, and others) will also affect the overall uncertainty in predicted K_d s but have not been estimated here.

¹⁹ The value of 600 m²/g was based on hydrous ferric oxide which is an amorphous iron oxide with an extremely high surface area. The value of 0.25 m²/g is based on results from flow through experiments; it is consistent with lower surface area iron oxides such as hematite and may also reflect the fact that only a fraction of the iron oxide in the alluvium may be accessible to migrating fluids.

²⁰ Tompson et al. (1999) addressed radionuclide retardation for Cs, Sr, and Pu only.

(Tompson et al., 2001). In that report, the groundwater chemistry and alluvium mineralogy were based on data in Tompson et al. (1999) while the mechanistic sorption model was based on data in Zavarin and Bruton (2000a; 2000b). The model in Tompson et al. (2001) did not include recent improvements to the mechanistic model and alluvium reactivity reported in Zavarin et al. (2002). Am, Eu, Np, Pu, Sm, and U K_d s predicted here (Table 4, column 2) are distinctly lower than those in Tompson et al. (2001) (Table 4, column 4). This results primarily from a reduction in the effective reactive surface area of calcite and iron oxide recommended in Zavarin et al. (2002). The Cs K_d is significantly higher than in Tompson et al. (2001) because the Cs affinity for illite was increased. The Ca K_d is identical to that in Tompson et al. (2001). The Sr K_d is slightly lower than in Tompson et al. (2001) as a result of adjustments to the cation exchange capacity of smectite and several Sr reaction constants. Nevertheless, when the reported K_d uncertainties are taken into account, the values reported in Tompson et al. (2001) and here are not altogether very different. In general, radionuclide K_d s differences are within one standard deviation. It, therefore, appears that the most recent predicted radionuclide K_d s improve upon but do not contradict earlier predicted K_d s.

5.3 Comparison of CAMBRIC HST model alluvium mineralogy radionuclide K_d s to measured data

Wolfsberg (1978) reported on several batch sorption experiments using Frenchman Flat alluvium.²¹ Recommended Frenchman Flat alluvium K_d s for Sr, Cs, and Eu were 217 ± 45 ($10^{2.3}$), 7000 ± 1600 ($10^{3.8}$), and >20000 ($>10^{4.3}$) mL/g, respectively. Sorptive mineral abundances and water chemistry of each batch sorption experiment was not reported.²² Thus, we could not attempt to match these K_d results using the specific mineralogy and water chemistry data. However, K_d s estimated by our model using the CAMBRIC HST model alluvium mineralogy and Frenchman Flat groundwater chemistry are in reasonable agreement with the data of Wolfsberg (1978). Predicted K_d s for Sr and Cs ($10^{2.2}$ and $10^{3.7}$ mL/g, respectively) are quite close to batch sorption data. The predicted Eu K_d ($10^{3.1}$ mL/g) is significantly lower than the measured average value. However, given the range of K_d s reported in Wolfsberg (1978) ($10^{3.9}$ to $>10^{5.0}$ mL/g), the uncertainty in our predicted value (two standard deviation range of $10^{2.3}$ to $10^{4.1}$ mL/g), and the limitations of this comparison, the predicted value is in the appropriate range. Wolfsberg (1978) also reported on a small number of uranium sorption experiments. We calculated an average K_d of $10^{1.2}$ mL/g from 5 reported values. The model predicted K_d ($10^{0.4}$ mL/g) is, again, lower than the measured value. However, the variability in measured K_d was quite large, with a Log K_d standard deviation of 0.5. Thus, the predicted K_d is within two standard deviations of experimental data for U. The K_d component additivity approach based on our mechanistic model, combined with our choice of water chemistry and sorptive mineral abundances, results in predicted radionuclide K_d s in reasonable agreement with measured Frenchman Flat alluvium data of Wolfsberg (1978).

²¹ Most alluvium used in these experiments was from RNM-1, 256 meter depth, but some experiments were performed using alluvium from other locations.

²² The initial composition of the water used in these experiments was reported but the composition of waters during batch sorption experiments was not.

Additional model validation information was reported in Zavarin and Bruton (2000a; 2000b) and will not be repeated here. More recently, a large number of Frenchman Flat and Yucca Flat alluvium radionuclide K_d data (both batch sorption and flow through data) was reported in Zavarin et al. (2002) and used to validate our model. Comparisons of measured and predicted radionuclide retardation in both batch and flowthrough experiments and improvements to model parameters have significantly improved our confidence in the mechanistic model approach. The reader is encouraged to review Zavarin et al. (2002) for further details.

While the comparisons between predicted and measured radionuclide K_d reported here and in Zavarin and Bruton (2000a; 2000b) and Zavarin et al. (2002) provide confidence in the ability of the mechanistic model to predict radionuclide retardation in the porous flow case, it is important to remember that a number of uncertainties associated with predicting K_d s must be accounted for in any predictive modeling effort. The uncertainties described here apply only to the uncertainty in surface complexation and ion exchange reaction constants. Uncertainties in mineral abundance, solution composition, solution speciation, reactive surface area, mineral accessibility to fluids, as well as other properties also exist and should be acknowledged. The uncertainty analysis presented in this report should, therefore, not be viewed as a complete uncertainty analysis of the mechanistic model described herein.

5.4 Heterogeneous distribution of radionuclide K_d s in Frenchman Flat alluvium

While relatively little data is available to compare measured and predicted radionuclide K_d s in Frenchman Flat alluvium, there is significant quantitative information on the mineralogy of that alluvium. In Sections 5.1 to 5.3, we evaluated radionuclide–mineral K_d s based on a Frenchman Flat groundwater, compared our updated mechanistic sorption model component additivity results to previously reported radionuclide retardation models, and compared these K_d s to a small number previously published batch sorption data (Wolfsberg, 1978). In the following section, we examine the range of predicted K_d s based on published mineral abundance data for Frenchman Flat alluvium.

A large number of mineral abundance data have been reported for Frenchman Flat alluvium (Table 5). The range of reported radionuclide sorbing mineral abundances will yield a range of predicted radionuclide K_d s. This spatial heterogeneity in radionuclide K_d s can affect radionuclide transport. Near-field HST models have attempted to resolve spatially heterogeneous radionuclide sorption at a relatively fine spatial scale (2 meters in the CAMBRIC HST model of Tompson et al. (1999)). Tompson et al. (1999) showed that, in some cases, the spatially heterogeneous distribution of radionuclide sorbing minerals will have large effects on radionuclide transport. If large-scale CAU models assign uniform properties to Frenchman Flat alluvium (including radionuclide sorption properties), they may not accurately predict radionuclide transport. Spatial heterogeneity needs to be examined both at the near-field HST and large-scale CAU model scales. Below, we examine the range of K_d s that might be expected in Frenchman Flat alluvium as a result of spatially heterogeneous sorbing mineral abundances. This is the first step in

evaluating the effects of spatially heterogeneous radionuclide K_d s. In Section 5.5, we further examine the effects of spatially heterogeneous radionuclide K_d s using 2D reactive transport simulations.

Table 5. Reported mineralogic information (by XRD) for Frenchman Flat alluvium.

	Drill Hole	# of samples	Depth Range meters	Sorptive Minerals	Comments
Ramspott and McArthur (1977) and Beiriger (1977)	UE-5n	47	91–476	All [‡]	Hunt Sidewall 5 wt % detection limit
Warren et al. (2002)	UE-5n	21	213–476	All	Hunt Sidewall ~0.2 wt % detection limit
Jones (1982)	U-11g-1	26	160–329	Zeolite, calcite, clay [†]	< 1mm fraction 5 wt % detection limit
Warren et al. (2002)	U-11g-1	3	306–329	All	< 1mm fraction ~0.2 wt % detection limit
Daniels and Thompson (1984)	RNM-1	8	189–320	All	Core? 1–5 wt % detection limit
Warren et al. (2002)	ER-5-3	10	204–610	All	Cuttings ~0.2 wt % detection limit
Warren et al. (2002)	ER-5-4	94	192–1134	All	Percussion Sidewall and Cuttings ~0.2 wt % detection limit

[†] Oriented mounts of clay fraction suggest clay is smectite dominated.

[‡] “All” sorptive minerals refers to all sorptive minerals included in our mechanistic model (calcite, smectite, zeolite (clinoptilolite), illite/mica, and iron oxide).

Table 5 lists the various sources of mineralogy information on Frenchman Flat alluvium used here to predict radionuclide K_d s. For each reported set of sorbing mineral abundance data, some limitations to the data exist. The XRD data detection limit of Ramspott and McArthur (1977) and Beiriger (1977) for UE-5n alluvium samples was 5 wt %. Iron oxides were found in these alluvium samples only at <5 wt % (i.e. trace levels). Other minerals such as micas were also found to be <5 wt % (labeled as “trace”).²³ Since most sorbing minerals were found at trace quantities, they were poorly quantified. This poor quantification results in significant uncertainty in our predicted K_d s. Recent and more accurate XRD analyses of alluvium samples from UE-5n over a similar depth range revealed iron oxide, mica, and calcite concentrations of 0.5, 2.9, and 1.6 wt % (Warren et al., 2002). These mineral concentrations would all be considered “trace” or non-detectable if the detection limit were 5 wt %. Thus, the high detection limit for mineral abundance data of Ramspott and McArthur (1977) and Beiriger (1977) results in greater uncertainty in predicted K_d s. The effect of XRD detection limits on the predicted K_d s can be examined by comparing the predicted K_d s based on data of Ramspott and McArthur (1977) and Beiriger (1977) to the more recent data of Warren et al. (2002). This comparison will be discussed below.

²³ In predicting radionuclide K_d s based on these data, minerals listed as “trace” were given a nominal value of 2.5 wt %.

Jones (1982) reported mineral abundances for only three of the five radionuclide sorbing minerals included in our mechanistic sorption model. Detection limits were also high (5 wt %). Furthermore, the data were based on the <1mm fraction of the alluvium. Predicted K_d s based on these data may under-predict the true sorptive capacity of the alluvium as a result of missing sorbing minerals and high detection limits. However, K_d s may also be over-predicted because the <1mm fraction was isolated for XRD analysis; this fraction of the alluvium is likely to contain a greater abundance of sorbing minerals than the bulk. Limitations of these data can be evaluated by comparing them with more recent data of Warren et al. (2002) for the same samples (see discussion that follows).

Daniels and Thompson (1984) achieved a lower detection limit by size fractionating alluvium samples for XRD analysis. Unlike Jones (1982), they back-calculated mineral abundances for the bulk alluvium based on their size fractionated data (thus, achieving a mineral abundance detection limit of ~1 wt % for the bulk alluvium). Nevertheless, iron oxide was detected in only one of the ten samples. This may have resulted from a genuine low abundance of iron oxide in the sampled alluvium or as a result of detection limits.

Recent efforts (Warren et al., 2002) were designed to improve detection limits and better quantify minerals present in trace amounts. This has significantly improved the quantification of trace sorbing minerals such as iron oxides. Analysis of ER-5-4 samples revealed a range of 0 to 1.5 wt % iron oxide with an average of 0.5 ± 0.2 wt %. Similarly, micas and other minerals that contribute to the sorptive capacity of the alluvium were better quantified.

Predicted radionuclide K_d s based on the sorptive mineral abundances reported in Ramspott and McArthur (1977), Beiriger (1977), Jones (1982), Daniels and Thompson (1984), and Warren et al. (2002) are reported in Table 6 and Figure 3. The predicted K_d for each individual sample and each radionuclide is reported in Appendix C. To predict radionuclide K_d s, the same K_d component additivity approach described in Sections 5.1 and 5.2 was used. Reactive mineral characteristics and the mechanistic model (Appendix A) do not vary throughout this report. The water chemistry used to predict K_d s here was the same as that used in Section 5.1. Thus, K_d s for radionuclide–mineral pairs are the same as reported in Section 5.1 and listed in Table 2.

Table 6 lists the Log normal K_d standard deviations for each set of data listed in Table 5. These standard deviations (Table 6) are unlike those listed in Table 5. In Table 5, we presented radionuclide K_d standard deviations based on uncertainties in our *mechanistic model sorption constants*. In Table 6, we present radionuclide K_d standard deviations resulting from the *heterogeneous distribution of radionuclide sorbing minerals* in Frenchman Flat alluvium. Similarly, the range of predicted radionuclide K_d s reported in Figure 3 is the result of spatial variability of sorptive mineral abundances.

The standard deviations listed in Table 6 suggest that the heterogeneous distribution of sorptive minerals can significantly affect the transport of radionuclides in Frenchman Flat alluvium. However, it is important to note that this mineral abundance data was not

evaluated in the context of alluvium depth, or depositional environment. The data in Table 6 simply relate to the ranges of radionuclide K_d s that might be expected in Frenchman Flat alluvium given the sorptive mineral abundance data available. The spatial distribution of minerals was discussed in a recent report (Carle et al., 2002) and will not be repeated here. However, the *spatial* analysis of Carle et al. (2002) is used in the following section to evaluate the effects of heterogeneous mineral distribution on flow and transport.

Irrespective of the detection limit, sampling method, sampling interval, sampling area, and other differences between the mineralogic data sets, the average predicted K_d for each radionuclide in each data set is surprisingly similar (Table 6). For example, the average K_d for Ca varies by less than one order of magnitude ($\log K_d = 2.2$ to 2.9). Furthermore, the observed K_d differences between data sets can often be explained by the limitations of certain data sets. For example, the sorbing mineral abundances reported in Jones (1982) result in the highest K_d s for all radionuclides except U and Cs. The reported mineralogy was based on the <1mm fraction of alluvium and, therefore, biased the mineralogic composition towards the clay fraction of the alluvium. It is, therefore, not surprising that this would result in higher K_d s. However, since iron oxide was not reported and U sorbs primarily to iron oxides, the K_d for U is nearly the lowest of all data sets. The Cs K_d is much lower than in other data sets principally because the abundance of mica (the dominant Cs sorber) was not reported.

Regardless of the differences *between* data sets, all data sets suggest that heterogeneous distribution of sorbing minerals results in a large range of K_d s in Frenchman Flat alluvium. When taking all data into account, K_d variability results in a log normal standard deviation of 0.30 to 0.47. Based on a two standard deviation range, spatial variability in K_d results in a K_d range of 1.20 to 1.88 orders of magnitude.

Trends regarding the sorption of the various radionuclides are the following:

- Trivalent radionuclides (Am, Eu, and Sm) behave very similarly and have very high K_d s.
- Cs sorbs as strongly as the trivalent radionuclides as a result of strong sorption to illite/mica.
- Ca and Sr behave nearly identically due to their similar sorption characteristics with respect to smectite, zeolite, and illite/mica.
- Pu sorption at a $O_2(g)$ fugacity of 10^{-10} bars is slightly greater than Np owing to the contribution of Pu(IV) sorption.
- U sorption is weakest.

Table 6. Predicted average radionuclide distribution coefficients (K_d s) using reported radionuclide sorbing mineral abundances.

	Ramspott and McArthur (1977) and Beiriger (1977)	Warren et al. (2002)	Jones (1982)	Warren et al. (2002)	Daniels and Thompson (1984)	Warren et al. (2002)	Warren et al. (2002)	Sum of All Data
Drill Hole		Log K_d						
	UE-5n	UE-5n	U-11g-1	U-11g-1	RNM-1	ER-5-3	ER-5-4	All Drill Holes
Ca	2.74±0.57 [§]	2.28±0.28	2.93±0.24	2.94±0.05	2.18±0.47	2.79±0.26	2.28±0.31	2.54±0.45
Cs	3.93±0.12	3.91±0.12	2.91±0.22	3.86±0.04	3.56±0.22	3.80±0.27	4.03±0.21	3.82±0.39
Sr	2.52±0.58	2.01±0.30	2.70±0.25	2.71±0.06	1.93±0.48	2.56±0.28	2.00±0.34	2.29±0.47
Am	3.39±0.22	3.84±0.09	4.02±0.18	3.79±0.04	3.45±0.35	3.79±0.23	3.91±0.22	3.78±0.30
Eu	2.83±0.23	2.23±0.09	3.52±0.19	3.24±0.07	2.88±0.34	3.27±0.23	3.32±0.23	3.22±0.30
Sm	3.14±0.25	3.45±0.09	3.89±0.21	3.54±0.15	3.16±0.33	3.62±0.25	3.56±0.26	3.50±0.33
Np	0.18±0.30	0.51±0.08	0.90±0.22	0.61±0.13	0.21±0.36	0.65±0.23	0.61±0.24	0.54±0.32
U	-0.52±0.39	0.06±0.07	-0.07±0.19	0.03±0.12	-0.42±0.48	-0.14±0.21	0.09±0.16	-0.11±0.33
Pu ($O_2 = 10^{-5}$)	0.44±0.25	0.91±0.08	1.02±0.18	0.86±0.06	0.52±0.37	0.82±0.22	0.97±0.20	0.83±0.30
Pu ($O_2 = 10^{-10}$)	0.84±0.26	1.30±0.08	1.43±0.18	1.26±0.06	0.92±0.37	1.23±0.21	1.37±0.20	1.23±0.30
Pu ($O_2 = 10^{-15}$)	1.33±0.27	1.77±0.08	1.93±0.18	1.76±0.06	1.40±0.38	1.73±0.20	1.84±0.20	1.71±0.30

[§] Average and standard deviation determined assuming log normal distribution.

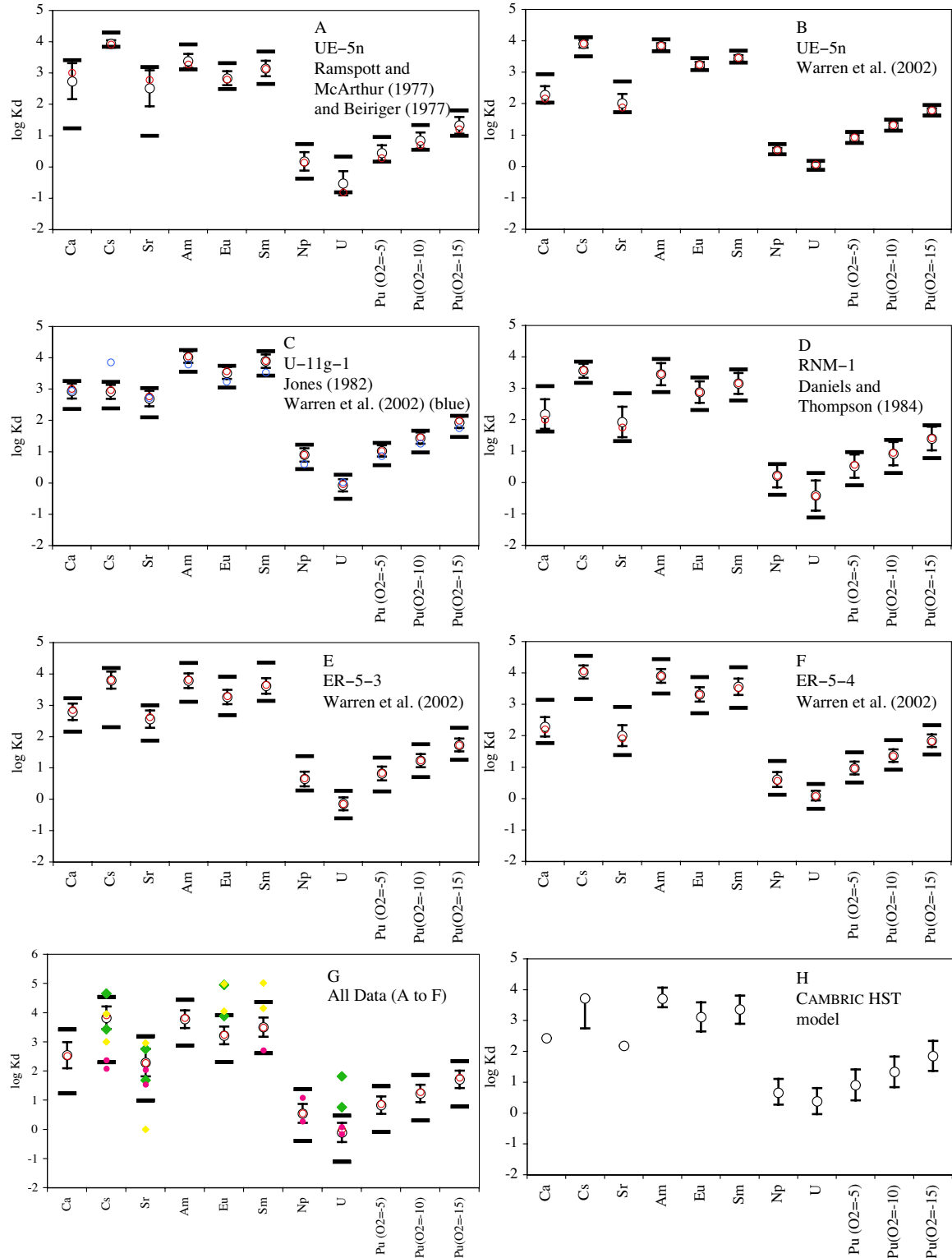


Figure 3. Predicted radionuclide K_d s based on sorptive mineral abundances. A–G: average (black circle) and standard deviation based on mineral abundance, median (red) and bars (minimum and maximum). G: Minimum and maximum measured K_d s of Wolfsberg (1978) (green), Zavarin et al. (2002) batch (yellow), and Zavarin et al. (2002) flowthrough (pink). **H:** Average (black circle) and standard deviation based on mechanistic model uncertainty.

Interestingly, the variability in predicted K_d resulting from heterogeneous mineral distribution is similar in scale to the uncertainty in predicted Am, Eu, Sm, Np, Pu, and U K_d s resulting from uncertainty in our mechanistic model reaction constants (compare Table 5 K_d uncertainties resulting from reaction constant uncertainty to Table 6 K_d uncertainties resulting from reactive mineral variability).²⁴ Since the uncertainty in K_d resulting from the mechanistic model reaction constants is at the same scale as the uncertainty resulting from mineral distribution, it is likely that *both uncertainties need to be taken into account in transport models.*

In Figure 3, the predicted K_d s for each individual mineral abundance data set and the composite data set are plotted alongside the K_d s predicted using mineral abundances from the CAMBRIC HST simulations (i.e. Table 4). Interestingly, Log K_d s predicted using the CAMBRIC HST mineralogy are very similar to average Log K_d s predicted using the composite mineral abundance data (Ca (2.4 vs. 2.5), Cs (3.7 vs. 3.8), Sr (2.2 vs. 2.3), Am (3.7 vs. 3.8), Eu (3.1 vs. 3.2), Sm (3.4 vs. 3.4), Np (0.7 vs. 0.5), and Pu (1.3 vs. 1.2 at $O_2(g)=10^{-10}$ bars, respectively)²⁵ even though mineral abundances are not the same. The mass fraction of smectite, mica, zeolite, calcite, and iron oxide in the CAMBRIC HST simulations is 9.3, 1.9, 7.0, 1.8, and 2.8, respectively, as compared to 11.9, 2.9, 15.8, 5.7, and 0.37, respectively, for the average composite data set (data reported in Appendix C). For the radionuclides listed above, the difference in radionuclide sorbing mineral abundance does not significantly affect the predicted K_d s. However, U Log K_d s are relatively different (0.4 vs. -0.1, respectively). This difference in K_d can be traced to a significant difference in iron oxide abundances (a factor of 8 difference).

Another way to measure the average retardation behavior of Frenchman Flat alluvium is to integrate the available mineral abundance data over depth. If we use the data from ER-5-4 which includes the largest interval of alluvium and the highest sampling density, the depth integrated mass fractions of smectite, mica, zeolite, calcite, and hematite for are 19.0, 3.6, 5.0, 5.8, and 0.47%, respectively. The resulting Log K_d s for Ca, Cs, Sr, Am, Eu, Sm, Np, U, and Pu are 2.4, 4.0, 2.2, 4.1, 3.5, 3.7, 0.8, 0.2, and 1.5 (at $O_2(g)=10^{-10}$ bars), respectively (Appendix C). While these mineral abundance values are somewhat different than the composite mineral abundance reported above, the resulting K_d s are nearly the same (particularly when considering the uncertainty in the predicted values themselves).

It is useful to compare the K_d variability results based on mineral abundance data to the CAMBRIC HST simulations performed by Tompson et al. (1999). Tompson et al. (1999) reported on three models of radionuclide sorbing mineral distribution. In the first, minerals were distributed homogeneously throughout the model domain. In the second, no sorbing minerals were included. These two model were considered the extreme cases of mineral distribution. In the third case, sorbing minerals were included in only those

²⁴ Ca, Cs, and Sr sorption is dominated by ion exchange for which reaction constant uncertainty estimates were not available (see discussion in Section 5.1).

²⁵ All K_d values presented here are in units of mL/g

grid cells whose hydraulic conductivity belonged to the lowest 10% of the entire hydraulic conductivity range. Outside of the lower 10% conductivity grid cells, a K_d of 0 mL/g was assigned. The isolation of sorbing minerals in the low conductivity zones was based on the concept that the sorbing minerals may be preferentially distributed with the lower permeability materials (Tompson and Jackson, 1996; Tompson et al., 1996). This third case can be compared to the observed variability in predicted K_d based on mineral abundance data (i.e. Figure 3). Unlike the third case of Tompson et al. (1999), the overwhelming majority of measured Frenchman Flat mineral abundance data results in predicted radionuclide K_d s greater than 1 mL/g. Only a few Np and Pu (at O₂(g) fugacity of 10⁻⁵ bars) predicted K_d s are less than 1 mL/g. A significant number of data with predicted K_d s less than 1 mL/g appear only in the case of U whose average K_d is quite low (0.8 mL/g). This result suggests that zones in Frenchman Flat alluvium that have no radionuclide retardation are highly unlikely. This, in turn, suggests that the heterogeneous mineral distribution model used in the CAMBRIC near-field HST simulations of Tompson et al. (1999) most likely overestimated the scale of heterogeneity and its effect on radionuclide migration. The mineral abundance data collected in Frenchman Flat and the resulting predicted K_d data suggest that, with the exception of U, alluvium zones in which radionuclide retardation does not occur are rare. The lowest predicted K_d s for Ca, Cs, Sr, Am, Eu, Sm, Np, U, and Pu are 17, 200, 9.9, 750, 210, 410, 0.4, 0.1, and 0.8 mL/g, respectively. In the case of Pu, the lowest value is predicted at an O₂(g) fugacity of 10⁻⁵ bars. At an O₂(g) fugacity of 10⁻¹⁰ bars, the lowest predicted K_d is 2.0 mL/g. These lowest predicted K_d s may be the most appropriate *conservative* estimates of radionuclide retardation in Frenchman Flat alluvium.

Figure 3G includes the ranges of radionuclide K_d s measured by Wolfsberg (1978) and Zavarin et al. (2002). In general, K_d s for each radionuclide range over one to two orders of magnitude, consistent with the predicted K_d variability. However, the range of measured and predicted K_d does not always coincide. For example, Sm and Eu measured K_d s tend to be higher than predicted K_d s. This comparison suggests that the mechanistic model may have limitation in its ability to predict K_d s. However, the comparison cannot be made without some knowledge of the experiment details. For example, K_d data of Wolfsberg (1978) was collected mostly on 100-200 mesh size sieved sediment. This would skew the data to K_d s higher than those expected for the whole sediment (which includes larger and less sorbing particles). Zavarin et al. (2002) batch sorption experiments were performed over a wide range of solution conditions using a single sediment collected from the U-1a tunnel system of Yucca Flat.²⁶ Thus, we cannot strictly compare predicted K_d variability that results from a range of alluvium mineral compositions to a range of measured K_d that results from changes in solution composition using a single sediment. Finally, flowthrough experiments of Zavarin et al. (2002) were performed on only two sediments and a total of four column experiments. The measured range of K_d s may, therefore, not be representative of average Frenchman Flat alluvium mineralogy. Despite the difficulties in comparing the available measured K_d s with predicted radionuclide K_d s, it appears that the mechanistic model predicts the scale and

²⁶ Yucca Flat alluvium sample mineralogy was similar to that of Frenchman Flat alluvium and expected to behave similarly.

magnitude of K_d variability in Frenchman Flat alluvium reasonably well. The application of this predictive model at near-field or CAU scales requires a thorough understanding of its limitations.

5.5 Effects of heterogeneously distributed radionuclide K_d s on CAU-scale reactive transport

To examine the effect of mineral variability on CAU-scale reactive transport, we developed a heterogeneous permeability and K_d field for use in reactive transport simulations. The K_d field for each radionuclide was developed using a Gaussian Random Field approach based on mineralogic data reported in Carle et al. (2002). The 3D K_d fields used here in reactive transport simulations have identical distribution patterns as the 2D K_d fields described in Carle et al. (2002); plots of these 2D K_d fields are reproduced here in Figures 4 and 5. The heterogeneous permeability field was developed based on the Gaussian Random Field approach as well (described in detail in Appendix B). In the simulations presented here, the permeability field was correlated to the Sr K_d field. The Sr K_d field was used because Sr will sorb strongly to clays and zeolites which tend to correlate negatively with permeability. However, this relationship was not based on field data from Frenchman Flat and should be regarded as hypothetical; flow-through results must, therefore, be interpreted with caution. All other radionuclide K_d fields were correlated to the Sr-based permeability field while honoring the original radionuclide K_d distribution patterns developed in Carle et al. (2002). To evaluate the effects of the heterogeneous radionuclide K_d and permeability fields on transport, three scenarios were simulated for each radionuclide: A) negative correlation between K_d field and Sr-based permeability, B) positive correlation between K_d field and Sr-based permeability, and C) no correlation between K_d field and Sr-based permeability. Model details are described in Appendix B.

Flow was simulated over a block of alluvium $18 \times 6 \times 1.5$ km in size. An ambient hydraulic gradient of 0.001 [m/m] was imposed along the x-direction of the domain (consistent with Tompson et al., 1999) and no flow was assumed for all other faces. The domain was discretized onto a 100 m grid longitudinally and 10 m grid vertically. The flow field was determined using the NUFT code; a particle transport model was used to simulate radionuclide transport. Both these codes were used in recent CHESHIRE HST simulations (Pawloski et al., 2001) and are described therein. Radionuclide decay was not included in simulations; simulations presented here are meant only to illustrate effects of heterogeneity. Simulations were run for 20,000 years to provide enough time for most radionuclides to break through. A large (.5 \times 1 \times .5 km) instantaneous, rectangular unit source of contaminant was initially centrally located 1 km from the origin of the x-axis. This large contaminant source was simulated in an effort to provide an ergodic source that sampled a large quantity of both the physical and chemical heterogeneity. The mass flux of contaminant was tracked at three breakthrough planes located 1000, 2500 and 3500 m downgradient from the source edge. All breakthrough data reported here result from the plane at 1000 m.

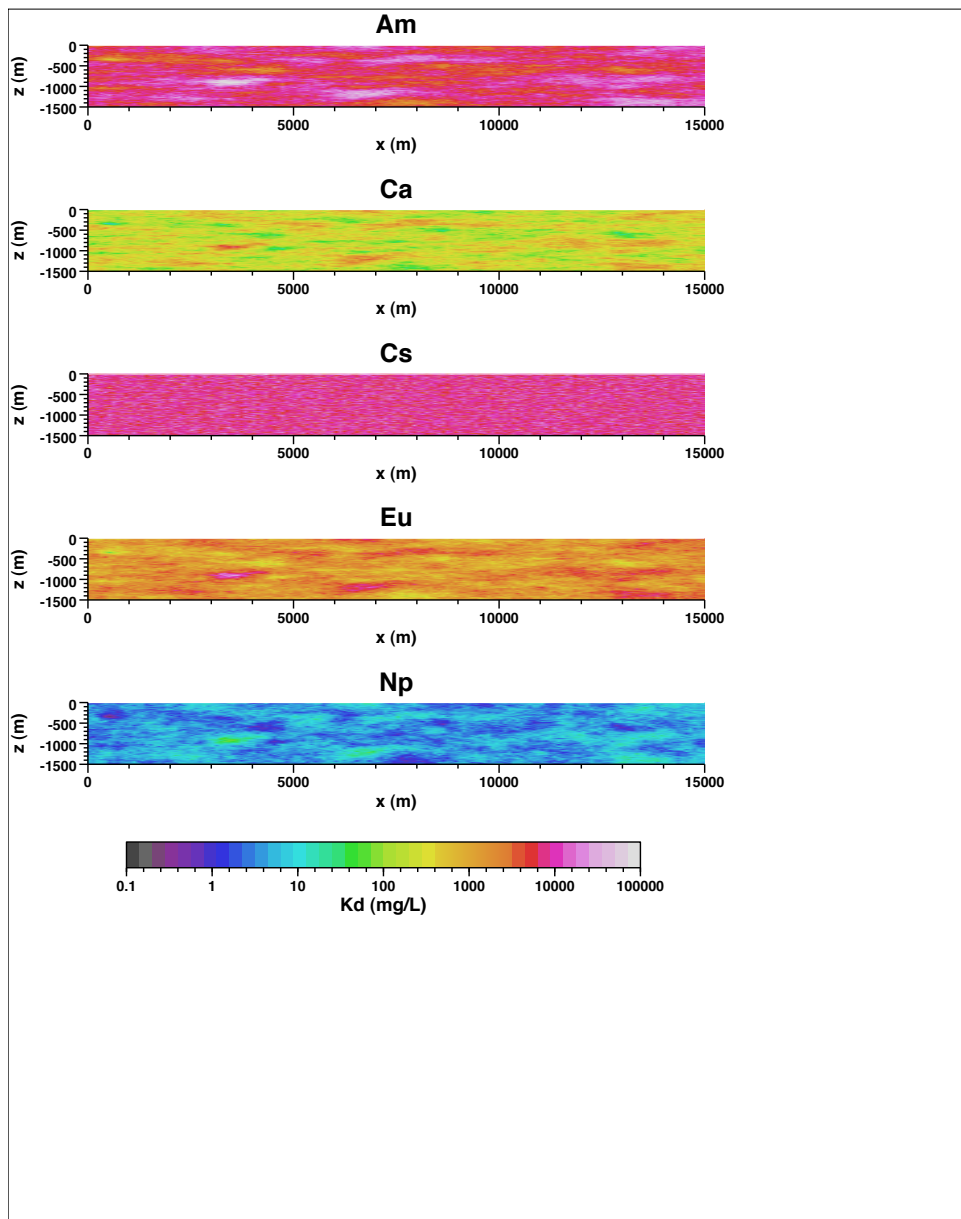


Figure 4. Gaussian random field realizations of spatial variability of K_d for Am, Ca, Cs, Eu, and Np.

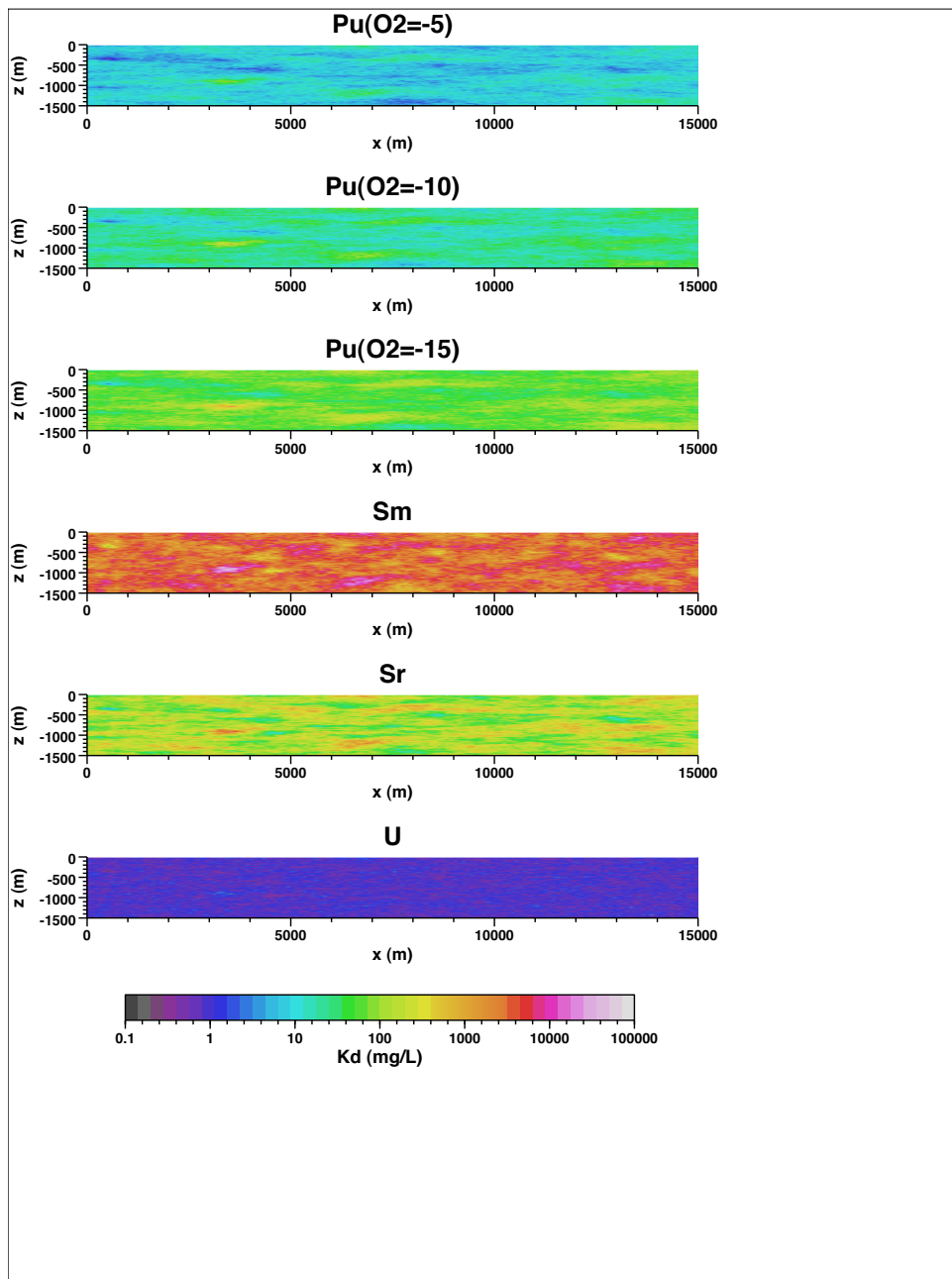


Figure 5. Gaussian random field realizations of spatial variability of K_d for Pu ($O_2(g)$ fugacity = 10^{-5} bars), Pu ($O_2(g)$ fugacity = 10^{-10} bars), Pu ($O_2(g)$ fugacity = 10^{-15} bars), Sm, Sr, and U.

Simulation results for all radionuclides and the three flow field scenarios are plotted in Figures 6 through 11. Am, Eu, Sm, and Cs data are not shown because their breakthrough was not observed over the entire 20,000 year simulation period at the 1000 m breakthrough plane. Indeed, these results suggest that significant transport of these radionuclides through Frenchman Flat alluvium is unlikely. However, a calibrated flow field combined with site specific hydrologic and geologic information would be necessary to confirm this result. Note that the tracer peak breakthrough occurs at 30 years; this is equivalent to a groundwater velocity of 33 m/year.

Ca initial breakthrough is predicted to occur only at ~10,000 years (Figure 6). Nevertheless, these simulations suggest that Ca may migrate as far as 1 km in 10,000 years.²⁷ Also, though subtle, the effects of the flow field correlation with K_d can be observed with the negative correlation resulting in the earliest Ca breakthrough. Since in the negative correlation, lower K_d s are predominantly found in the high permeability zones, this results in faster breakthrough. However, the effect is small, owing largely to the fact that even the low Ca K_d s are, in fact, quite high. Thus, significant retardation occurs even in the high permeability zones.

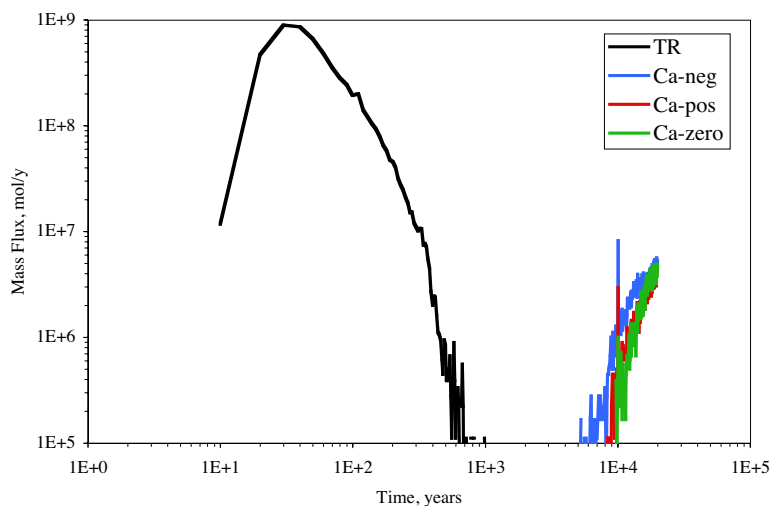


Figure 6. Breakthrough of tracer (TR) and Ca negatively, positively, and uncorrelated to the flow field permeability.

The effect of negatively correlating K_d and permeability is most clearly seen in the case of Sr (Figure 7). Nevertheless, the effect is rather slight for similar reasons as the Ca simulation: Sr K_d s do not vary spatially very much and they are relatively high in all cases.

²⁷ Radionuclide decay was not included in these simulations. Radionuclide decay may further reduce the migration of radionuclides whose half-life is relatively short.

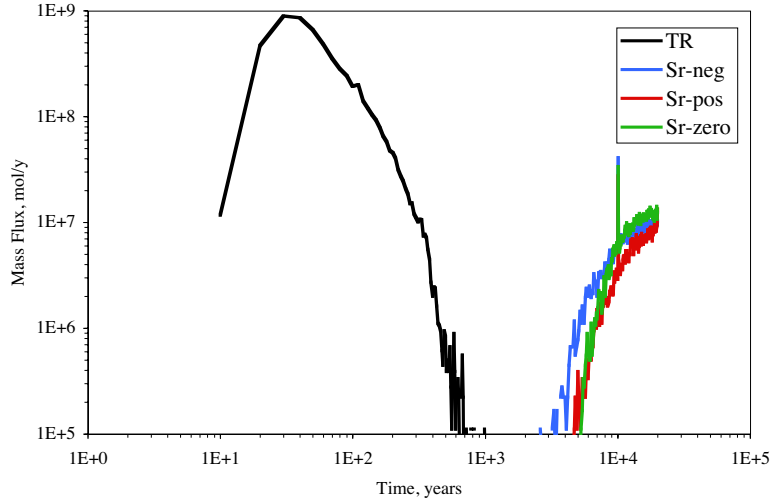


Figure 7. Breakthrough of tracer (TR) and Sr negatively, positively, and uncorrelated to the flow field permeability.

Figure 8 presents the Np breakthrough. For this radionuclide, significant breakthrough is predicted to occur, consistent with the relative weak sorption of Np to most mineral surfaces. Also, the negatively and positively correlated scenarios result in nearly equivalent breakthrough. Because the spatial distribution of Np K_d s is significantly different from that of Sr, and because Np K_d s are quite low throughout the flow field, permeability correlation with the K_d field of Sr has little impact on Np transport. Regardless, Np is predicted to move relatively quickly when compared to Am, Eu, Sm, Cs, Ca, or Sr.

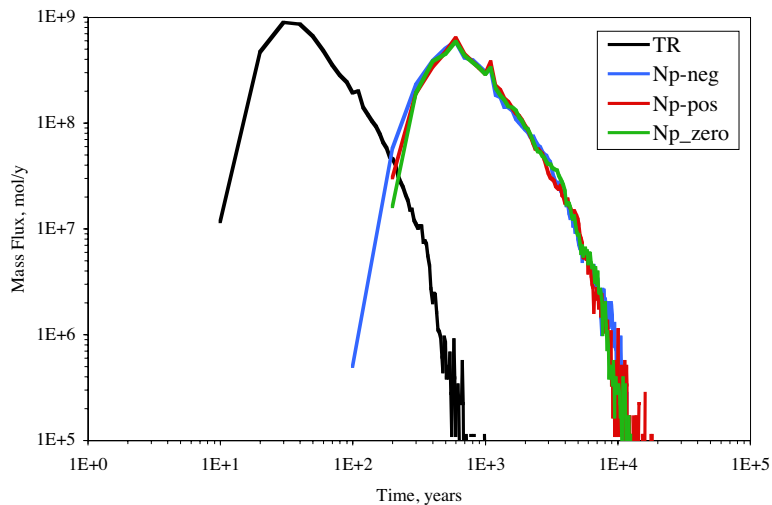


Figure 8. Breakthrough of tracer (TR) and Np negatively, positively, and uncorrelated to the flow field permeability.

As in all K_d s reported here, Pu transport is simulated at three different $O_2(g)$ fugacities. The range of $O_2(g)$ fugacity relates to the range of conditions in which Pu(V) dominates in the aqueous phase. Results are plotted in Figures 9 to 11. At an $O_2(g)$ fugacity of 10^{-5} bars, sorption to mineral surface is dominated by Pu(V) sorption. It should, therefore, not be surprising that its transport behavior is predicted to be nearly identical to that of Np(V). Since Np(V) and Pu(V) aqueous speciation as well as sorption are similar, their similar behavior should be expected. As the fraction of Pu(IV) in solution increases ($O_2(g)$ fugacity decreases), sorption (and retardation) is predicted to increase.

Nevertheless, some migration of Pu is predicted at all $O_2(g)$ fugacities examined here.

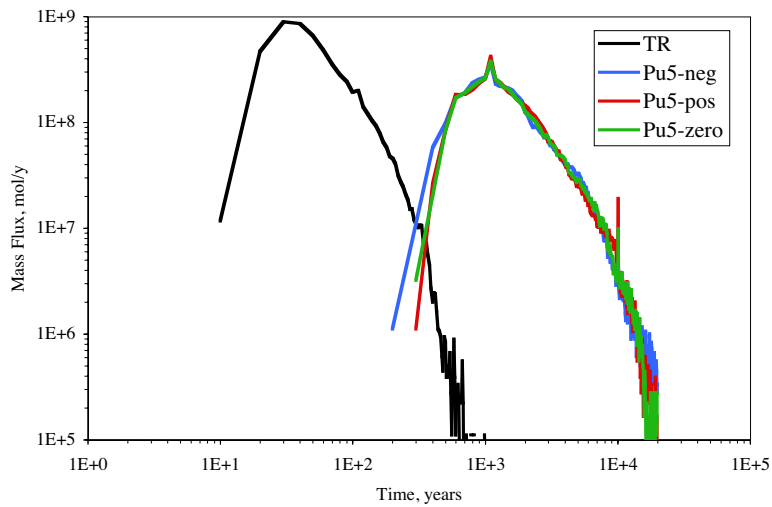


Figure 9. Breakthrough of tracer (TR) and Pu at 10^{-5} bars $O_2(g)$ negatively, positively, and uncorrelated to the flow field permeability.

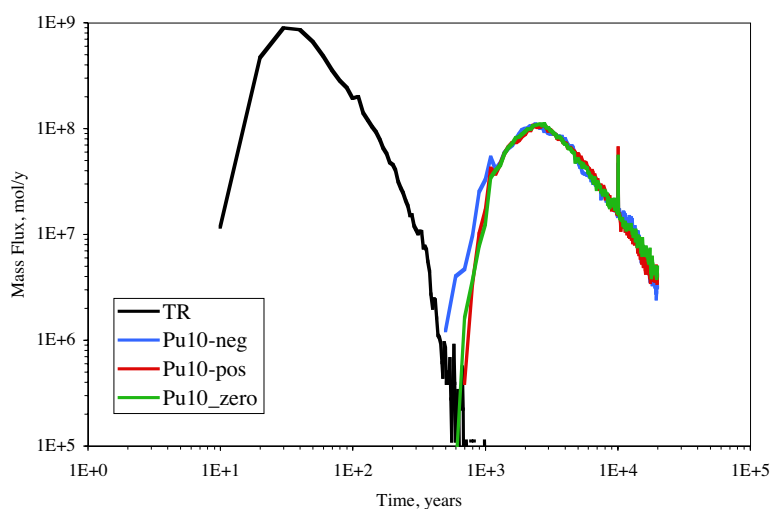


Figure 10. Breakthrough of tracer (TR) and Pu at 10^{-10} bars $O_2(g)$ negatively, positively, and uncorrelated to the flow field permeability.

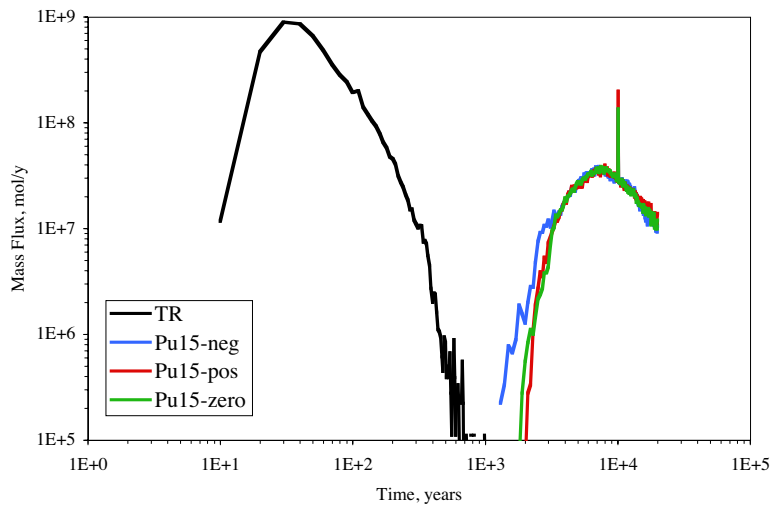


Figure 11. Breakthrough of tracer (TR) and Pu at 10^{-15} bars $O_2(g)$ negatively, positively, and uncorrelated to the flow field permeability.

The migration of U is predicted to be the fastest of all sorbing radionuclides examined here. Typically, U sorbs rather weakly to all mineral except iron oxide. Iron oxide concentrations in Frenchman Flat sediments are low. Furthermore, we have found that the *effective* reactive surface area of iron oxides is also quite low ($0.25\text{ m}^2/\text{g}$, Zavarin et al., 2002) which suggests that a large fraction of the iron oxide is inaccessible (possibly occluded). The low abundance and low effective surface area of iron oxide (the dominant U sorbing mineral) results in very low predicted U retardation in Frenchman Flat sediments.

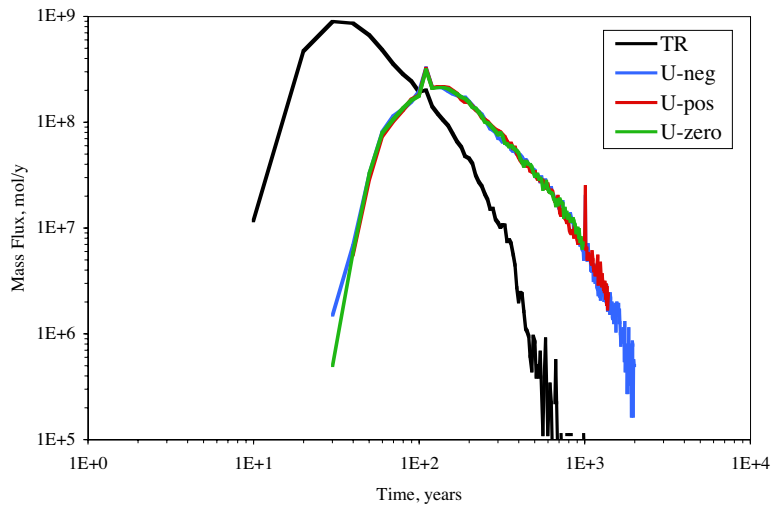


Figure 12. Breakthrough of tracer (TR) and U negatively, positively, and uncorrelated to the flow field permeability.

It is interesting to compare radionuclide retardation in the transport simulations to the average K_d s predicted using all available Frenchman Flat mineral abundance data (Table 6). With a porosity of 40% and a bulk density of 1.5 g/cm³, average Rs for Ca, Cs, Sr, Am, Eu, Sm, Np, U, and Pu using predicted K_d data of Table 6 (column 9, all data) are 1300, 25000, 730, 23000, 6200, 12000, 14, 4.0, and 26/65/193, respectively (three Pu values are reported for O₂(g) fugacities of 10⁻⁵, 10⁻¹⁰, and 10⁻¹⁵ bars). Rs for this same list of radionuclides based on the transport model peak arrival times are >670, >670, >670, >670, >670, >670, 18, 4.3, 37/80/270, respectively.²⁸ It appears that the heterogeneous distribution of radionuclide sorbing minerals and the heterogeneous permeability field used in these simulations do not significantly affect the average transport behavior of these radionuclides at this scale. However, the effect of heterogeneous permeability and radionuclide retardation does have a large effect on dispersion. For example, while the peak breakthrough of Np occurs at 600 years, Np is initially observed 1000 m from the source 500 years earlier.

Based on the predicted radionuclide retardations and the results from reactive transport simulations, we can conclude that:²⁹

- Ca, Cs, Sr, Am, Eu, and Sm appear to be greatly retarded and are not likely to migrate greater than 1 km in 10,000 years *under the conditions examined with these reactive transport simulations*.
- Np, U, Pu, and all non-sorbing radionuclides may travel a significant distance.
- The heterogeneous distribution of radionuclide sorbing minerals in Frenchman Flat alluvium does not seem to significantly affect the average radionuclide retardation *under the conditions examined with these reactive transport simulations*.
- The heterogeneous distribution of permeability and radionuclide retardation may have a very large effect on dispersion which leads to significantly faster initial breakthrough of radionuclides downstream.

6. Evaluation of Upscaling in the Fracture-Flow Case

The methodology for developing a radionuclide R for a fracture flow environment based on single mineral radionuclide K_d s was described in Section 4.2 of this report.³⁰ In this section of the report, we predict radionuclide–mineral K_d s for average Pahute Mesa groundwater (Section 6.1), calculate average radionuclide Rs at the CHESHIRE site

²⁸ Since the simulations were run out to only 20,000 years, we estimate that radionuclides whose peak breakthrough was not observed have retardation factor greater than 670.

²⁹ Note that radionuclide decay was not accounted for in the reactive transport simulations presented in this report. ²⁴¹Pu decay and ²⁴¹Am ingrowth have been shown to significantly affect the spatial distribution of ²⁴¹Am with time (Pawloski et al., 2001); these effects were not accounted for in this report.

³⁰ In the fracture flow case, it is simpler to evaluate radionuclide sorption using the unitless retardation factor (R) instead of the retardation coefficient (Kd). The relationship between Kd and R in both the porous–flow and fracture–flow cases is described in Section 4. Nevertheless, both R and Kd data are reported in Appendix E.

(Section 6.2) and for six hydrostratigraphic units³¹ defined in Drellack et al. (1997) (Section 6.3), and evaluate spatial heterogeneity of R_s at a number of scales (at the near-field scale (Section 6.2), between hydrostratigraphic units (Section 6.3), within hydrostratigraphic units (Sections 6.4 and 6.5)).

6.1 Radionuclide–mineral K_d s in Pahute Mesa groundwater

As in the case of porous flow, radionuclide K_d s in fracture flow systems are based on the mechanistic sorption model described in Appendix A. If conditions defined in Section 2 are held, the mechanistic model can be simplified to the K_d model. To predict a K_d for each radionuclide–mineral pair, the solution composition, mineral characteristics, and mechanistic models must be defined. The mineral characteristics and mechanistic models are developed in Appendix A and are held constant throughout this report. The solution composition at Pahute Mesa is described below.

The solution composition used in the CHESHIRE HST model (Pawloski et al., 2001) is reported in Table 7. This water composition was an average of Area 19 and 20 water data reported in Smith et al. (1998), Smith et al. (1999), Rose et al. (1997), and IT (1999). For modeling purposes, we used an $O_2(g)$ fugacity range of 10^{-5} to 10^{-15} bars. This range of $O_2(g)$ fugacity was suggested in Zavarin (2002) to span the range of redox conditions under which Pu(V) dominates in solution. The dominance of Pu(V) in Pahute Mesa–type waters is suggested from experimental measurements of Pu redox state in waters of similar composition from the NTS ((Nitsche et al., 1993; Nitsche et al., 1994). Analysis of Pu sorption over this entire range can be used to evaluate the sensitivity of Pu transport to redox.

Using the water chemistry in Table 7, K_d s were calculated for the five radionuclide sorbing minerals and the nine radionuclides included in our mechanistic model. The radionuclide K_d s are listed in Table 8. Uncertainties listed in Table 8 are based on real and estimated standard deviations resulting from uncertainties in the sorption constants of our mechanistic model, as described earlier.

The K_d for each radionuclide–mineral pair is quite similar in Frenchman Flat and Area 19 and 20 waters (compare Table 2 with Table 8). The small changes result from the subtle changes in water chemistry between Frenchman Flat alluvium waters (Table 1) and Area 19 and 20 waters (Table 7). Nevertheless, both waters are low ionic strength sodium bicarbonate type waters with pH~8 which results in similar radionuclide–mineral K_d s.

³¹ HSU's used in Drellack (1997) were based on the designations used in the regional model of IT (1997). These HSU's were used here because documentation on fracture densities, fracture apertures, effective porosities, fracture lining mineralogy, matrix mineralogy, matrix porosity were all available, published, or could be derived/averaged. These data had not been reported at a finer scale. As a result we chose to examine RN retardation at this scale. However, this document was written as an approach and not a solution. Data and methods are documented in detail such that RN retardation values can be recalculated if HSU and their properties are revised. All necessary mineralologic, K_d , and R data is included in Appendices to allow for K_d calculations.

Table 7. Water chemistry used in the CHESHIRE HST model of Pawloski et al. (2001).

Constituent	CHESHIRE Water Concentration, mg/L (except pH)
pH	8.2
Na	65
K	3.4
Ca	10.4
Mg	0.5
HCO ₃	107
Cl	12
SO ₄	35
SiO ₂	56
O ₂ (aq)	†

† O₂(aq) concentrations controlled by O₂(g) fugacities of 10⁻⁵, 10⁻¹⁰, and 10⁻¹⁵ bars.

Table 8. Radionuclide distribution coefficients (K_d s) calculated using water chemistry of Table 7 and mineral reactivities of Appendix A.[†]

	Calcite	Zeolite (clinoptilolite)	Iron Oxide	Mica/illite [‡]	Smectite
				Log (K_d)	—
Am	4.49±0.5		3.40±0.41		4.98±0.38
Ca	0.52	3.60		2.51	2.85
Cs		3.50 (2.90)		5.56(4.56)	2.89 (1.39)
Eu	4.37±0.5		3.48±0.67		4.51±0.46
Np	1.84±0.5		1.81±0.44		1.27±0.28
Pu (O ₂ = 10 ⁻⁵) [§]	1.71±0.5		2.10±0.5		1.93±0.5
Pu (O ₂ = 10 ⁻¹⁰)	2.10±0.5		2.57±0.5		2.27±0.49
Pu (O ₂ = 10 ⁻¹⁵)	2.85±0.5		3.37±0.5		2.96±0.47
Sm	4.67±0.5		3.64±0.67		4.67±0.42
Sr	-1.24±0.5	3.37	-0.20±0.30	2.51	2.45
U	-1.80±0.5		2.66±0.43		1.63±0.38

[§] Pu K_d s determined at three O₂(g) fugacities : 10⁻⁵, 10⁻¹⁰, and 10⁻¹⁵ bars. The range of O₂(g) fugacities was suggested in Zavarin et al. (2002) to evaluate the effect of Pu redox state on transport.

[‡] Mechanistic sorption model is based on illite. However, XRD analysis did not distinguish between illite and mica. We assume in our model that these two mineral behave similarly.

[†] Uncertainties reported here represent the uncertainty in the mechanistic model reaction constants. When a value in parentheses is listed, it represents a lower limit Kd value (upper limit not assigned).

6.2 Average radionuclide R_s based on CHESHIRE site mineralogy

6.2.1 Calculating radionuclide R_s – Americium example

Using the radionuclide-mineral K_d s of Table 8, radionuclide retardation in fractures with Table 7 water compositions can be estimated using the component additivity approach outlined in Section 4.2. The *average* mineralogy of the fracture linings and matrix developed in the CHESHIRE HST model (Pawloski et al., 2001) is listed in Table 9. The

fracture-lining mineralogy was based on an average fracture lining mineral abundance for devitrified tuffs below the water table at Yucca Mountain (data of Carlos et al., 1995). The matrix mineralogy was based on a combination of XRD and petrographic measurements for the devitrified mafic poor Calico Hills lava at the CHESHIRE site. Additional parameters developed in the conceptualization of the high permeability fracture flow zones at the CHESHIRE site are listed in Table 10. These are the parameters required to predict R_s at the CHESHIRE site using the radionuclide-mineral K_d s listed in Table 8 and component additivity described in Section 4.2.

Table 9. Average fracture lining and matrix mineral abundances used in the CHESHIRE HST model (Pawloski et al., 2001).[¶]

Mineral	Density g/cm ³	Volume %	Mass %
Fracture Lining[†]			
Inert Matrix	2.5	61.7	71.3
Iron Oxide (hematite)	5.27	1.1	2.7
Mica	2.83	0	0
Smectite	2.83	8.0	10.5
Calcite	2.71	5.9	7.4
Zeolite (clinoptilolite)	2.13	8.3	8.2
Matrix[‡]			
Inert Matrix	2.5	84.69	99.56
Iron Oxide (hematite)	5.27	0.02	0.050
Mica	2.83	0.04	0.053
Smectite	2.83	0.25	0.33
Calcite	2.71	0	0
Zeolite (clinoptilolite)	2.13	0	0

[¶] Small errors in fracture-lining mineral abundances were found in the CHESHIRE HST model of Pawloski et al. (2001); these are corrected here.

[†] Fracture lining defined by 8 fractures/meter, 100 micrometer coating with 15% porosity. Fracture linings also contain 19.7 vol. % manganese oxides but their reaction with radionuclides was not considered due to lack of data. From the mineral density and volume fractions, the fracture lining bulk density is 2.16 g/cm³.

[‡] Matrix porosity is 15%. From the mineral density and volume fractions, the matrix bulk density is 2.13 g/cm³.

Table 10. Parameters used in conceptualization of high permeability fracture flow zones in the CHESHIRE HST model (Pawloski et al., 2001).

Fracture density	m ⁻¹	8 (= (2D) ⁻¹) [†]
Fracture aperture	m	5×10 ⁻⁴ (= 2A)
Fracture lining thickness	m	1×10 ⁻⁴ (= B)
Matrix reactive zone thickness	m	2.5×10 ⁻³ (= C)
Colloid concentration	g/mL	1.17×10 ⁻⁴

[†] A, B, C, and D are employed in the radionuclide retardation calculations. They are shown in Figure 1.

As an example, we calculate the Am R under the fracture flow conditions defined by Tables 9 and 10. Calculations are based on radionuclide–mineral K_d s presented in Table 8. The conceptualization of the fracture flow medium is described in Section 4.2 and Figure 1.

The effective porosity of the medium is calculated using Equation (3):

$$\theta_{eff} = 2 \times 8(2.5 \times 10^{-4} + 0.15 \times 10^{-4} + 0.15 \times 2.5 \times 10^{-3}) = 0.01024. \quad (12)$$

This effective porosity includes the porosity from the fracture aperture, the porosity of the fracture lining, and the porosity of the “matrix reactive zone”. In the CHESHIRE HST model (Pawloski et al., 2001), flow was assumed to occur in all these zones. The simulations were conceptualized in this manner to link the calibrated flow model and the mechanistic sorption model. The need arrived from the fact that calibration of the flow field at the CHESHIRE site resulted in an estimated effective porosity of the fractured medium of ~1%. This effective porosity could not be accounted for simply from fracture aperture related porosity unless fracture densities and apertures were increased to unrealistic values. Instead, fracture densities and apertures were taken from field observations and the effective porosity was accounted for by allowing some flow in the matrix along the fractures (called the “matrix reactive zone” in this report). This conceptualization was discussed in Zavarin (2002), Pawloski et al. (2001), and in Section 4.2 of this report. Additional discussion can also be found in Appendix E.

To determine R_s , the porosity of the fracture flow zone (θ_{fz}) must also be calculated. The fracture flow zone porosity is defined as the combined porosity of the fracture, fracture lining, and matrix reactive zone. It is calculated using Equation (4):

$$\theta_{fz} = \frac{2.5 \times 10^{-4} + 0.15 \times 10^{-4} + 0.15 \times 2.5 \times 10^{-3}}{2.5 \times 10^{-4} + 10^{-4} + 2.5 \times 10^{-3}} = 0.225 \quad (13)$$

To calculate the Am K_d of the fracture flow zone ($K_{d,fz}$), the mass fraction of each mineral must be determined. Since the fracture flow zone encompasses both the fracture lining and matrix reactive zones, average mineral mass fractions in the fracture flow zone must be determined. Using Equation (6), the mass fractions of illite, zeolite, smectite, calcite, hematite, and inert matrix are 5.03×10^{-4} , 3.21×10^{-3} , 7.25×10^{-3} , 2.89×10^{-3} , 1.49×10^{-3} , and 0.969, respectively. The Am $K_{d,fz}$ can then be calculated using Equation (5):

$$K_{d,fz} = 10^{4.98} \times 7.25 \times 10^{-3} + 10^{4.49} \times 2.89 \times 10^{-3} + 10^{3.40} \times 1.49 \times 10^{-3} = 785 \quad (14)$$

Once the Am $K_{d,fz}$ is known, the Am R of the fracture flow zone (R_{fz}) is calculated using Equations (7) and (8) to yield:

$$R_{fz} = 1 + \frac{785 \times 1.94}{0.225} = 6.77 \times 10^3 \quad (15)$$

In Equation (15), the Am R_{fz} is calculated in the absence of colloids. However, colloids effects on Am migration should be significant and similar to those observed for Eu migration (Kersting et al., 1999). In an equilibrium model, the Am R_{fz} can be adjusted by the R related to Am sorption to colloids (R_{col}). Radionuclide distribution coefficients for smectite colloids ($K_{d,col}$) used in the CHESHIRE HST model are listed in Table 11. The Am R_{col} is determined using Equation (9):

$$R_{col} = 1 + \left(10^{5.92} \times 1.17 \times 10^{-4} \right) = 98 \quad (16)$$

The adjusted Am R in the fracture flow zone which accounts for colloid effects (R'_{fz}) is determined using Equation (10):

$$R'_{fz} = 1 + \left(\frac{(6.77 \times 10^3) - 1}{98} \right) = 70 \quad (17)$$

Thus, sorption to colloids decreases the Am R by nearly two orders of magnitude.

As described in Section 4.3, we have made some significant simplifications to the transport behavior of colloids. First, colloid loads in the fractures are assumed to be constant. Second, colloids are not subjected to filtration processes. Third, radionuclide sorption to colloids is assumed to be an equilibrium process. And, fourth, colloids travel within the entire fracture flow zone and are not restricted to the fracture. Comparative simulations in which colloids were homogeneously distributed in the fracture flow zone or isolated to the fracture did not result in any difference in breakthrough (Zavarin, 2002). This occurred because of the relatively fast diffusive exchange of ions between the fracture and the very narrow fracture lining (100 μm) and matrix reactive zones (2.5 mm) and the lack of any slow sorption/desorption kinetics in our model. However, the lack of colloid filtration and radionuclide sorption kinetics in this simplified model severely limits its applicability. While this simplified colloid model is not likely to adequately treat the process of colloid-facilitated transport at the near-field or CAU scales, it does provide a way to compare the effect that colloids have on each radionuclide and how radionuclide transport can be exacerbated by colloid-facilitated transport.

An important aspect of the fracture flow case is the diffusion between the fracture and the matrix. Radionuclide retardation in the matrix, combined with matrix diffusion increases the effect of matrix diffusion on transport. While matrix diffusion needs to be accounted for, this aspect of fracture transport is not discussed here. Furthermore, since radionuclide retardation in the matrix is calculated in the same manner as the porous flow case, it is not discussed in this section unless warranted.

Table 11. Predicted radionuclide distribution coefficients (K_d s) for smectite colloids†.

Radionuclide	Smectite Colloids (high,low) ^a Log (mL/g)
Ca(II)	-
Cs(I)	-¶
Sr(II)	-
Am(III)	5.92 (6.31, 5.62)
Eu(III)	5.45 (5.91, 5.05)
Sm(III)	5.61 (6.07, 5.16)
Np(V)	2.21 (2.50, 1.93)
Pu ($O_2 = 10^{-5}$) [§]	2.87 (3.39, 2.39)
Pu ($O_2 = 10^{-10}$)	3.19 (3.68, 2.74)
Pu ($O_2 = 10^{-15}$)	3.88 (4.37, 3.43)
U(VI)	2.58 (2.99, 2.25)

† Colloid reactivity was based on the reactivity of smectite using a 1:1 ratio of >AlOH and >SiOH reactive sites. However, the reactive site concentrations were based on particle size measurements and colloid concentrations reported by Kersting and Brachman (1998) (7.86×10^{10} particles/mL and 80.8 nm average particle diameter). A reactive site density of 2.31 sites/nm² was used.

¶ If illite/mica colloids were included, the Cs colloid Log K_d would be 5.56 (Table 8 data).

§ Pu K_d s determined at three $O_2(g)$ fugacities : 10^{-5} , 10^{-10} , and 10^{-15} bars. The range of $O_2(g)$ fugacities was suggested in Zavarin et al. (2002) to evaluate the effect of Pu redox state on transport.

^a High and low values represent the uncertainty associated with the mechanistic model reaction constants.

6.2.2 Summary of average radionuclide Rs

Table 12 lists the Rs for all radionuclides examined here and for both the fracture flow zone and the matrix.³² These radionuclide Rs were calculated using the surface complexation and ion exchange reactions and sorbing mineral properties reported in Zavarin et al. (2002). It is interesting to compare these values to the radionuclide retardation ratios presented in Table K.9 of Pawloski et al. (2001) and reproduced here in Table 12.³³ The differences in radionuclide Rs are related to mechanistic sorption model adjustments suggested in Zavarin et al. (2002). For example, we predict here that the Cs fracture flow R is $10^{3.24}$ while in the CHESHIRE HST simulations (Pawloski et al., 2001), an R of $10^{2.63}$ was reported. The difference is related primarily to an increase in the affinity of Cs for mica/illite suggested by our recent sorption experiments (Zavarin et al., 2002). Sr Rs are lower because the cation exchange capacity of smectite and the affinity

³² While uncertainties associated with the mechanistic model reaction constant are reported throughout this report, the uncertainties are similar in the case of porous flow and fracture flow. They are, therefore, not discussed in this section unless warranted.

³³ Note that in Pawloski et al. (2001) Table K.9, retardation ratios are reported. Retardation ratios are defined as the ratio of sorbed to aqueous moles of a radionuclide. Here, we present retardation factors which are equal to “retardation ratio”+1. This difference in units is only significant in cases where sorption is extremely low.

of Sr for smectite and zeolite were lowered. Am, Eu, Sm, Np, U, and Pu R_s s are significantly lower in the fractures as a result of decreased calcite and iron oxide surface areas. However, this effect is minimized in the matrix since no calcite and very little iron oxide exists in the matrix.

Adjustments to the reactive surface areas of calcite and iron oxide were based on *alluvium* porous flow experiments (Zavarin et al., 2002). However, the reactive surface area of these minerals may not necessarily be the same in a fracture flow environment (it may, in fact, be rather site specific). We chose to use the mineral reactivities reported in Zavarin et al. (2002) for consistency and because these values provide more conservative estimates of transport for most radionuclides. Without a significant validation effort, it is not possible to evaluate the accuracy of the mechanistic model or this upscaling approach in the fracture flow case. Radionuclide R_s s calculated in this report for the fracture flow case should be interpreted with these limitations in mind.

Kersting et al. (1999) found that most aqueous Cs was associated with colloids in water from ER-20-5. Based on a smectite-dominated colloid model, we predict that Cs would not be strongly associated with colloids, resulting in a large R for Cs in the fracture flow zone ($10^{3.24}$). Since Kersting et al. (1999) reported that illite was also part of the colloid mineralogy, we propose an alternate Cs R based, conservatively, on an illite-dominated colloid mineralogy. In this case, the fracture flow zone R for Cs is $10^{1.60}$, significantly lower than the earlier value. Based on the observations of Kersting et al. (1999), it is likely that this may be more reasonable (and conservative) R for colloid-mediated Cs fracture transport conditions.

Table 12. Predicted radionuclide retardation factors (R_s) at the CHESHIRE site.

	Fracture flow zone	Matrix	CHESHIRE HST model
			(Pawloski et al., 2001)
	Average (Low, High) ^a	Average (Low, High) ^a	Fracture/Matrix
		Log R	Average
Ca	2.19	1.56	2.30/1.77
Cs	3.24 (2.26) [†]	3.44 (2.44)	2.63/2.72
Sr	1.93	1.22	2.37/1.77
Am	1.84 (1.87, 1.79)	3.64 (3.35, 4.00)	2.38/3.68
Eu	1.89 (1.81, 1.92)	3.18 (2.72, 3.64)	2.77/3.08
Sm	2.01 (1.97, 2.04)	3.34 (2.88, 3.81)	3.11/3.24
Np	0.68 (0.41, 1.04)	0.37 (0.23, 0.61)	1.72/0.84
U	0.97 (0.65, 1.33)	0.79 (0.50, 1.17)	1.84/1.39
Pu ($O_2 = 10^{-5}$) [§]	0.94 (0.56, 1.33)	0.77 (0.41, 1.21)	1.87/1.29*
Pu ($O_2 = 10^{-10}$)	1.25 (0.85, 1.60)	1.09 (0.67, 1.55)	
Pu ($O_2 = 10^{-15}$)	1.75 (1.44, 1.94)	1.78 (1.31, 2.25)	

[†] If colloids assumed to be dominantly mica/illite, R_s for fracture flow zone would be $10^{1.61}$.

* R measured at $O_2(g)$ fugacity of 10^{-7} .

[§] Pu K_{dS} determined at three $O_2(g)$ fugacities : 10^{-5} , 10^{-10} , and 10^{-15} bars. The range of $O_2(g)$ fugacities was suggested in Zavarin (2002) to evaluate the effect of Pu redox state on transport.

^a High and low values represent the uncertainty associated with the mechanistic model reaction constants. When only one value is listed, it represents the lower limit value (an upper limit was not assigned).

6.2.3 Heterogeneous distribution of radionuclide Rs at the CHESHIRE site

To evaluate heterogeneity and scaling issues at the near-field scale, the average fracture radionuclide Rs were related in Chapter 8 of Pawloski et al. (2001) to initial breakthrough of radionuclides at the downstream boundary of the CHESHIRE HST model.³⁴ The results are reproduced here in Figure 13 which presents the time of median peak breakthrough at the downstream boundary of the near-field HST model as a function of fracture R .³⁵ Several 1:1 correlation lines are plotted to illustrate the relationship between tracer peak breakthrough arrival time, retarded radionuclide arrival time, and R . For example, in the simulations which included heat-related transient flow in the near field, peak tracer breakthrough occurs at 2 years (i.e. $R = 1$ at 2 years). Based on tracer breakthrough at 2 years, the 1:1 correlation line, which relates effective R to peak breakthrough arrival time, does not intersect the data for the retarded radionuclides. This suggests that the average predicted fracture Rs for the sorbing radionuclides would overestimate peak arrival times of retarded radionuclides. Interestingly, based on the mean flow velocity of high permeability zones, peak tracer breakthrough is predicted at 0.4 years. With this tracer breakthrough time, median peak breakthroughs for the sorbing radionuclides correlate quite well with the predicted average Rs of the fracture flow zone. This suggests that the predicted transport of sorbing radionuclides in a heterogeneous and transient near-field HST model may still be related to the average predicted Rs along the dominant flow path (the high permeability fracture flow zones). The results suggest that near-field scale flow field and radionuclide retardation heterogeneities may possibly be regarded as dispersion effects and that the near-field scale radionuclide retardation can be qualitatively related to average Rs of the high permeability fracture flow zones.

It is critical to note that the average Rs were not, in this case, average Rs for the entire CHESHIRE HST model domain. In fact, average Rs for only the high permeability fracture flow zones can be related to average near-field radionuclide transport. This issue is further complicated in large-scale models since hydrologic characteristics of the domain are known at a scale much larger than the high permeability zone scale observed at the CHESHIRE site (high permeability zones are at the scale of tens of meters). The question thus becomes: what is the most appropriate mineralogic conceptual model for the small high permeability zones that are likely to account for most of the flow in large-scale models? In the following sections of this report, we provide data at the scales for which mineralogic data are available. Some discussion of how these data may be used in large-scale models are suggested but further refinement of these scaling issues is undoubtedly necessary.

³⁴ Dispersion effects are not discussed in this report. However, discussion of upscaling effects in a fracture–flow environment as they relate to hydrodynamic dispersion can be found in Chapter 8 of Pawloski et al. (2001).

³⁵ This plot can be used to compare the simulated retardation of radionuclides to their respective predicted average Rs . For example, if tracer peak breakthrough occurs at one year and is plotted at $R=1$, all retarded radionuclides should fall along the 1:1 correlation line that intersect the tracer. Thus, if $R = 100$, the peak breakthrough time should be 100 years.

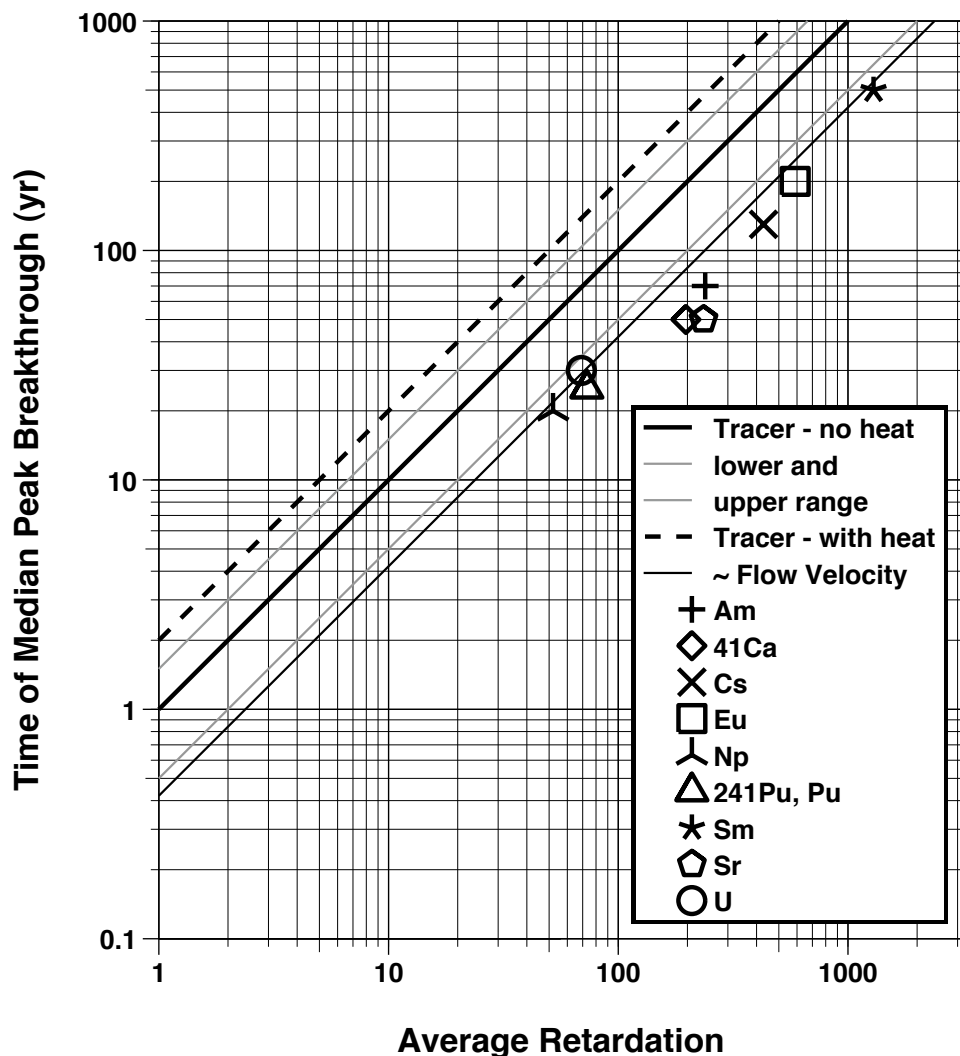


Figure 13. Comparison of particle model median peak breakthrough for radionuclides with average retardation assuming homogeneous mineralization.
 Thick black line represents ideal relationship assuming tracer breakthrough peak at 1 year with no test-related heat. Thin gray lines bracket range of uncertainty of peak tracer breakthrough with no test-related heat. Dashed line represents ideal relationship assuming tracer breakthrough peak at 2 years, as inferred from particle model median tracer breakthrough with test-related heat. Thin black line indicates ideal relationship assuming average flow velocity for high permeability hydrofacies (from Pawloski et al., 2001).

6.3 Average radionuclide Rs based on Pahute Mesa hydrostratigraphic unit mineralogies

In Section 6.2, average radionuclide Rs at the CHESHIRE site were reported and the effects of heterogeneity at that scale were evaluated. Below, we predict average radionuclide Rs for six hydrostratigraphic units whose scale is significantly larger. The resulting radionuclide Rs are compared to determine whether significant differences in radionuclide Rs are predicted at the scale of hydrostratigraphic unit.

6.3.1 Morphology and mineralogy of 6 hydrostratigraphic units

In Table 13, data regarding six hydrostratigraphic units (Timber Mountain Aquifer, Tuff Cone, Bullfrog Confining Unit, Belted Range Aquifer, Basal Confining Unit, and Basal Aquifer) are summarized. The CHESHIRE HST model domain lies within the Tuff Cone (TC) hydrostratigraphic unit as defined in Drellack et al. (1997).³⁶ The data in Table 13 were collected from a variety of sources; the origins of the data are described in the following text.

Information regarding fractures was gathered from Drellack et al. (1997). This data set represents one of the most comprehensive examinations of fracture densities and mineralogies on Pahute Mesa. The *fracture density* listed in Table 13 is the density of open fractures. A significant number of closed fractures also exist but it was assumed that these would not contribute to fracture flow. Also, the fracture density was originally measured as fractures per vertical foot. Because the majority of these fractures were high angle, the fracture density, when corrected for the dip, is significantly greater. The fracture density presented in Table 13 was calculated assuming an average fracture dip of ~75 degrees. The *percent open fracture* relates to the fact that significant fracture infilling as a result of fracture-lining secondary mineral formation reduces actual fracture aperture compared to the ideal reported *fracture aperture*. A range of fracture openness was reported for each hydrostratigraphic unit. In general, these values suggest fracture-lining mineral thicknesses on the order of 40 to 350 micrometers, consistent with observations in IT (1998) and what was applied in the CHESHIRE HST model (100 μm).

³⁶ Assignments of stratigraphic units to hydrostratigraphic units have changed with time (more recently, Shaw (2003) placed the mafic poor Calico Hills Lavas near CHESHIRE into the Calico Hills zeolitized composite unit (CHSCM)). However, we continue our evaluation using the assignments in Drellack et al. (1997) and IT (1997) to retain consistency with the fracture and matrix parameters/assignments listed in these reports.

Table 13. Parameters used to define radionuclide K_d s and R_s for selected hydrostratigraphic units at Pahute Mesa.

Hydrostratigraphic Unit † (HSU)	Timber Mountain Aquifer (TMA)	Tuff Cone (TC)	Bullfrog Confining Unit (TCB)	Belted Range Aquifer (TBA)	Basal Confining Unit (BCU)	Basal Aquifer (BAQ)						
Fracture Density, m^{-1} ‡	0.38	2.16	0	2.79	0	7.61						
Fracture Aperture, mm	0.72	0.53	–	0.08	–	0.3						
% Open Fracture	10 – 100	1 – 50	–	1 – 10	–	1 – 10						
Effective Porosity §	0.0013 (0.00051 – 0.0035)	0.0013 (0.00051 – 0.0035)	–	0.0013 (0.00051 – 0.0035)	–	0.0013 (0.00051 – 0.0035)						
Matrix Porosity §	0.08 – 0.50	0.12 – 0.45	0.07 – 0.47	0.19 – 0.39	0.33 – 0.45	0.09 – 0.27						
----- FRACTURE LINING SORBING MINERAL ABUNDANCES¶, wt % -----												
Calcite	13	3 (5.2)§	–	0	–	50						
Zeolite	7	30 (32.5)	–	24	–	50						
Smectite	15	11 (13.3)	–	12	–	0						
Fe/MnOx	5	20 (1.1, 6.3)	–	60	–	0						
----- MATRIX SORBING MINERAL PROBABILITY AND ABUNDANCE (log wt %)ª -----												
Calcite	0.09	0.23 ± 0.86	0.14	0.09 ± 0.65	0.07	-0.20 ± 0.17	0.55	0.37 ± 0.55	0.73	0.41 ± 0.55	0.71	0.58 ± 0.58
Zeolite	0.44	1.41 ± 0.64	0.41	1.34 ± 0.62	0.45	1.50 ± 0.51	0.28	0.98 ± 0.72	0.37	0.98 ± 0.69	0.60	1.24 ± 0.65
Smectite	0.60	0.50 ± 0.57	0.81	0.50 ± 0.54	0.84	-0.28 ± 0.52	0.95	0.85 ± 0.53	0.97	1.04 ± 0.35	0.92	1.05 ± 0.33
Iron oxide	0.54	-0.21 ± 0.24	0.48	-0.15 ± 0.29	0.55	-0.16 ± 0.18	0.37	-0.08 ± 0.34	0.28	-0.08 ± 0.22	0.33	$0.00 \pm ?$
Mica	0.50	0.03 ± 0.40	0.65	0.07 ± 0.42	0.82	0.03 ± 0.42	0.76	0.18 ± 0.55	0.59	0.29 ± 0.56	0.29	0.58 ± 0.23

† Stratigraphic units that comprise these hydrostratigraphic units are defined in IT (1997).

‡ Fracture density, fracture aperture, % of fracture aperture that is open, and the fracture-lining mineral composition were taken from Drellack et al. (1997). Fracture density was corrected for fracture orientation by assuming all fractures dip at ~75 degrees.

§ Effective porosities and bulk matrix porosities were taken from IT (1997) Phase I Data Analysis Task Volume 7, Table 5–1. Values in parentheses for effective porosities are the range of porosities for a 2 standard deviation Log normal range. Matrix porosity values represent the lower and upper bounds of porosity.

¶ Average and standard deviations of matrix sorbing mineral concentrations were calculated from an analysis of all XRD data available in Warren et al. (2000) for the hydrostratigraphic units of interest.

§ Wt % in parentheses based on data from Carlos et al. (1995).

ª The probability is a measure of how often the particular mineral was observed. The abundance is a measure of the average quantity of the particular mineral observed in only those samples where the particular mineral was observed. Thus, to calculate the true average abundance, one must multiply the reported abundance by the probability.

TC fracture apertures were reported to be 0.5 mm, consistent with the CHESHIRE HST model (Pawloski et al., 2001). However, fracture densities reported in Drellack et al. (1997) are lower than those used in the CHESHIRE HST model. The fracture density used in the CHESHIRE HST model high permeability zones was 8 per meter as compared to an average of 2 per meter for the TC unit reported in Drellack et al. (1997). Observations of Blankennagel and Weir (1973) suggest that fracture densities in the high permeability zones at the CHESHIRE site could be as high as 14 per meter but the open fracture fraction was not reported. Erikson (1991) observed fracture densities in the range of 3 per meter in high permeability fracture flow zones in a drill hole near CHESHIRE (UE-20n #1). Prothro and Drellack (1997) observed fracture densities of 8.5 per meter in high permeability fracture flow zones 2 km north of CHESHIRE (ER-20-6 #1). The relatively low fracture densities reported in Drellack et al. (1997) as compared to observations of Blankennagel and Weir (1973) and others may be largely the result of scaling. The individual hydrostratigraphic units reported in Drellack et al. (1997) comprise high and low permeability zones, the average of which may be significantly lower than the narrow regions of high fracture density zones reported by Blankennagel and Weir (1973) and others.

The *effective porosities* reported in IT (1997) are not consistent with fracture porosities calculated using fracture densities and apertures of Drellack et al. (1997). For example, fracture densities and apertures for the TMA suggest that the fracture porosity should be 0.00027 if flow is contained within parallel fractures. This porosity is a factor of five lower than the effective porosity in IT (1997). The inconsistency between effective porosity and fracture porosity was also encountered during development of the CHESHIRE HST model. In the CHESHIRE HST model, the effective porosity was linked to physical measurements of fracture densities and porosities by conceptualizing a “matrix flow zone” (Pawloski et al., 2001). The larger effective porosity is accounted for by allowing flow within the matrix along the fracture boundary (see Figure 1 and Sections 4.2 and 6.1). A recent report examined the effect of using this conceptualization on radionuclide breakthrough (Zavarin, 2002) and found that the effect of adding flow to a small zone of matrix that borders a fracture does not significantly alter radionuclide breakthrough (as long as this matrix zone is small enough to be accessed by diffusion at a time scale much shorter than the fluid travel times in the domain).

The *fracture-lining sorbing mineral abundances* reported in Drellack et al. (1997) were determined by counting the number of times a particular fracture-lining mineral was observed. This observational probability cannot be directly related to the quantitative abundances of the various minerals in the various hydrostratigraphic units. However, we found that the quantitative abundances of fracture-lining minerals (based on data from Carlos et al., 1995) were similar to the observational probabilities reported by Drellack et al. (1997) for the TC hydrostratigraphic unit. For modeling purposes, we assume that the observational probabilities are equivalent to average abundances of radionuclide sorbing fracture-lining minerals. In Section 6.5.3, we report on mineral abundances and resulting Rs of the TC hydrostratigraphic unit based on the fracture mineral abundance data of Carlos et al. (1995). The comparison of mineral data from Drellack et al. (1997) and Carlos et al. (1995) is discussed there.

Fracture-lining iron and manganese oxide minerals were not distinguished in the analysis of Drellack et al. (1997). However, the reactivity of iron and manganese oxides can be quite different. In the simulations presented below, we present two cases: (1) Fe/MnOx reported values are dominated by iron oxides and (2) Fe/MnOx reported values are dominated by manganese oxides for which sorption constants are not known. Evaluation of the sorptive capacity and distribution of manganese oxides is necessary to effectively distinguish their radionuclide retardation effects from those of iron oxides.

The *matrix sorbing mineral abundances* in the various hydrostratigraphic units were calculated by averaging the available XRD data contained in Warren et al. (2000) for the stratigraphic units that comprise each hydrostratigraphic unit. The average abundances reported in Table 13 are the average abundances for each mineral *in cases where it is observed*. The associated mineral observational probability indicates the degree to which the particular mineral is distributed throughout the hydrostratigraphic unit. The standard deviations reported in Table 13 are a clear indication of the strongly variable abundance of minerals. The probabilities suggest that minerals are distributed heterogeneously (calcite, in particular) which may significantly affect the radionuclide transport in these units.

6.3.2 Average radionuclide Rs of 6 hydrostratigraphic units

Below, we present radionuclide *Rs* for six hydrostratigraphic units located on Pahute Mesa. The K_d s for each radionuclide–mineral pair were based on the water chemistry for Pahute Mesa listed in Table 7. It was assumed that the water chemistry in all six hydrostratigraphic units was the same and equivalent to the water chemistry used in the CHESHIRE HST model (based on an average groundwater composition from Area 19 and 20 wells). Thus, K_d s for each radionuclide–mineral pair are equivalent to those used in Section 6.1.

Combined with the component additivity approach outlined in Section 4.2 and the morphology and mineralogy data described in Section 6.3, radionuclide *Rs* can be assigned to each of the six hydrostratigraphic units. Tables 14 and 15 list the *Rs* determined for six hydrostratigraphic units and nine radionuclides. In Table 14, fracture flow zone *Rs* are reported for the iron oxide dominating case.³⁷ In Table 15, fracture flow zone *Rs* are reported for the manganese oxides dominating case. Additional details regarding the calculation performed to compute the predicted *Rs* can be found in Appendix E. This appendix also contains the associated K_d data.

Several assumptions were made in calculating radionuclide *Rs*. Fracture densities and apertures were taken from Table 13 but the percent open was ignored; for simplicity it was assumed that the fractures are entirely open. A nominal fracture-lining thickness of 100 micrometers was used throughout. The thickness of the matrix reactive zone was adjusted so that the average effective porosity listed in Table 13 was consistent with the

³⁷ The two reported cases are defined in Section 6.3.1.

fracture conceptualized effective porosity. For the TMA, TC, and TBA, the matrix reactive zone thicknesses were: 4.6, 0.05, and 0.62 mm. For the BAQ, the high fracture density and aperture resulted in an effective porosity of 0.0029, significantly larger than the average effective porosity listed in Table 13. No matrix reactive zone was included for this hydrostratigraphic unit but the fracture density and aperture was not adjusted to the effective porosity listed in Table 13. For all simulations, the matrix porosity was taken to be the average of the range reported in Table 13. Although significant variability in the matrix mineral abundances is reported, we evaluate the average mineral abundance case here. The product of mineral abundance and probability (Table 13) defined the average mineral abundance. For all fracture flow zone R_s , the effect of colloids on radionuclide retardation was based on the simplistic approach described in this report and colloid $K_d s$ from Table 11. The case in which illite colloids are present is also reported for Cs (see footnote to Table 11).

Differences in radionuclide R_s between the four hydrostratigraphic units in the case of fracture flow and between the six hydrostratigraphic units in the case of matrix flow are on the order of 0.4 to 2.3 Log R . The source of these differences is the differences in sorbing mineral abundances and fracture/matrix morphologies (i.e. Table 13 data) of these units. The results suggest that radionuclide retardation in the various hydrostratigraphic units will differ significantly. However, it is important to note that the uncertainties in R_s (based on the mechanistic model uncertainties) are, in some cases, significantly larger than the differences between the various hydrostratigraphic units. In those cases, uncertainty in radionuclide retardation constants may have a greater effect on model uncertainty than the retardation differences between hydrostratigraphic units.

The R uncertainties reported in Tables 15 and 16 relate to uncertainties in our mechanistic sorption model. In general, the uncertainties in Am, Eu, and Sm retardation are very small in fracture flow zones but large in the matrix. In the fracture case, sorption to fracture-lining minerals is buffered by sorption to colloids. Thus, the uncertainty in the colloid sorption counteracts the uncertainty in the fracture-lining mineral sorption. The net effect is that retardation uncertainty is small. This buffering effect is not observed in matrix case because colloids are absent. For these radionuclides (Am, Eu, and Sm), the greater uncertainty in the fracture-flow R_s comes from the estimate of colloid loads and reactive site densities. These uncertainties were not included in our analysis, in part, because it is not clear how these uncertainties should be approached. Uncertainty in Np, Pu, and U R_s is large in both the fracture and matrix cases. Under conditions specified in Table 7, U and Np are not expected to sorb strongly to colloids (see Table 11). The effect of colloids on Pu retardation is a function of its redox state. At an $O_2(g)$ fugacity of 10^{-5} bars, Pu(IV) concentrations in solution are very low which results in a weak association of Pu with colloids. At an $O_2(g)$ fugacity of 10^{-15} bars, Pu(IV) concentrations in solution are significantly higher resulting in a stronger colloid effect. This stronger colloid effect also results in a reduction in the R uncertainty in fracture flow zone data with decreasing $O_2(g)$ fugacity (see Tables 16 and 17). For U in BAQ, sorption is weak enough that uncertainty in retardation becomes irrelevant.

Table 14. Predicted retardation factors (Rs) for selected hydrostratigraphic units assuming Fe/MnOx dominated by iron oxide.

	TMA		TC		TCB		TBA		BCU		BAQ	
	Fracture	Matrix	Fracture	Matrix	Matrix	Fracture	Matrix	Matrix	Fracture	Matrix	Fracture	Matrix
Log R (low, high) ^a												
Ca	3.34	3.44	2.95	3.37	3.57	3.24	2.99	2.94	3.36	3.74		
Cs	4.04 (3.13) ^j	4.15 (3.24)	3.19 (2.40)	4.28 (3.34)	4.38 (3.46)	4.30 (3.34)	4.43 (3.44)	4.24 (3.25)	3.27 (2.66)	4.70 (3.74)		
Sr	3.12	3.22	2.72	3.14	3.35	2.99	2.73	2.67	3.14	3.50		
Am	2.03 (2.06,1.99)	4.05 (3.77,4.40)	1.92 (1.94,1.88)	4.19 (3.90,4.54)	3.47 (3.18,3.81)	2.64 (2.65,2.61)	4.62 (4.35,4.96)	4.62 (4.35,4.97)	2.26 (2.50,1.94)	5.08 (4.81,5.42)		
Eu	2.06 (1.98,2.08)	3.60 (3.14,4.06)	1.98 (1.89,2.03)	3.73 (3.27,4.20)	3.04 (2.56,3.52)	2.69 (2.59,2.73)	4.18 (3.72,4.65)	4.18 (3.72,4.65)	2.60 (2.49,2.65)	4.65 (4.19,5.12)		
Sm	2.14 (2.11,2.16)	3.79 (3.32,4.26)	2.06 (2.02,2.11)	3.92 (3.46,4.39)	3.23 (2.76,3.72)	2.74 (2.70,2.78)	4.41 (3.94,4.89)	4.41 (3.94,4.88)	2.98 (2.92,3.02)	4.90 (4.43,5.38)		
Np	0.80 (0.57,1.13)	0.77 (0.57,1.07)	1.08 (0.74,1.49)	0.83 (0.62,1.14)	0.64 (0.48,0.93)	1.72 (1.35,2.15)	1.21 (0.91,1.58)	1.18 (0.89,1.54)	1.61 (1.15,2.09)	1.69 (1.37,2.08)		
U	1.18 (0.85,1.54)	1.20 (0.87,1.59)	1.77 (1.37,2.17)	1.26 (0.93,1.65)	1.17 (0.84,1.56)	2.46 (2.05,2.86)	1.45 (1.11,1.85)	1.37 (1.05,1.77)	0.19 (0.20,0.19)	1.85 (1.51,2.25)		
Pu ($O_2 = 10^{-5}$)	1.12 (0.74,1.51)	1.16 (0.77,1.62)	1.36 (0.93,1.77)	1.27 (0.85,1.74)	0.89 (0.59,1.31)	2.04 (1.57,2.46)	1.64 (1.17,2.12)	1.62 (1.16,2.11)	1.46 (1.03,1.87)	2.09 (1.62,2.58)		
Pu ($O_2 = 10^{-10}$)	1.43 (1.03,1.79)	1.50 (1.06,1.98)	1.74 (1.31,2.11)	1.61 (1.16,2.09)	1.24 (0.84,1.70)	2.43 (1.98,2.80)	1.98 (1.51,2.47)	1.97 (1.49,2.45)	1.81 (1.37,2.18)	2.44 (1.96,2.93)		
Pu ($O_2 = 10^{-15}$)	1.94 (1.62,2.12)	2.21 (1.73,2.69)	2.31 (1.97,2.50)	2.31 (1.84,2.79)	1.96 (1.49,2.44)	3.00 (2.66,3.20)	2.68 (2.21,3.16)	2.66 (2.19,3.14)	2.34 (2.00,2.54)	3.14 (2.66,3.62)		

^a High and low values represent the uncertainty associated with the mechanistic model reaction constants. When only one value is listed, it represents the lower limit value (an upper limit was not assigned)..

^j In the case where illite colloids exist, Cs Log Rs would be reduced to 2.40, 1.56, 2.67, and 1.64 for TMA, TC, TBA, and BAQ, respectively.

Table 15. Predicted retardation factors (Rs) for selected hydrostratigraphic unit fracture flow zones assuming Fe/MnOx dominated by manganese oxides.

	TMA	TC	TBA	BAQ
			Log R (low, high) ^a	
Sr	3.12	2.68	2.90	3.14
Am	2.03	1.86	2.59	2.26
	(2.05,1.99) [†]	(1.88,1.82)	(2.60,2.55)	(2.50,1.94)
Eu	2.06	1.89	2.60	2.60
	(1.98,2.08)	(1.81,1.91)	(2.53,2.62)	(2.49,2.65)
Sm	2.13	1.98	2.66	2.98
	(2.10,2.15)	(1.95,2.00)	(2.63,2.68)	(2.92,3.02)
Np	0.77	0.57	1.13	1.61
	(0.55,1.10)	(0.37,0.88)	(0.86,1.48)	(1.15,2.09)
U	1.10	0.65	1.37	0.19
	(0.79,1.46)	(0.44,0.96)	(1.05,1.74)	(0.20,0.19)
Pu ($f(O_{2(g)}) = 10^{-5}$)	1.10	0.88	1.55	1.46
	(0.72,1.49)	(0.53,1.25)	(1.12,1.97)	(1.03,1.87)
Pu ($f(O_{2(g)}) = 10^{-10}$)	1.40	1.15	1.86	1.81
	(1.00,1.75)	(0.77,1.50)	(1.44,2.22)	(1.37,2.18)
Pu ($f(O_{2(g)}) = 10^{-15}$)	1.90	1.63	2.35	2.34
	(1.58,2.08)	(1.32,1.80)	(2.04,2.53)	(2.00,2.54)

[†] Average Log R is followed by the Log R range (in parentheses) determined from uncertainties in surface complexation and ion exchange constants.

^a High and low values represent the uncertainty associated with the mechanistic model reaction constants. When values are not listed, lower/upper limits were not assigned.

The radionuclide R data presented in Tables 15 and 16 represent the first attempt to base large-scale hydrostratigraphic unit radionuclide Rs for a fracture flow environment on the detailed mechanistic approach developed for near-field HST models. This linking of the mechanistic model to a simpler radionuclide R model may provide a seamless methodology for upscaling retardation and a defensible mechanistic basis for assigning Rs .³⁸ In the following section, we discuss heterogeneity issues first by comparing CHESHIRE site and TC hydrostratigraphic unit radionuclide retardation and second, by examining the heterogeneous mineral distribution in the fractures and matrix of the TC hydrostratigraphic unit.

6.4 Comparison of Tuff Cone hydrostratigraphic unit and CHESHIRE site radionuclide Rs

The CHESHIRE site falls within one of the hydrostratigraphic units (TC) described in Section 6.3. By comparing radionuclide Rs of the TC hydrostratigraphic unit with those of the CHESHIRE site, we can illustrate the significant spatial heterogeneity of radionuclide Rs observed at the sub-hydrostratigraphic unit scale.

³⁸ It is important to remember that the methods described here for the fracture flow case have not been validated or tested against laboratory fracture flow experiments. Thus, they are largely theoretical and require a significant validation effort before implementation.

Comparison of radionuclide Rs at the CHESHIRE site and the TC hydrostratigraphic unit reveals some important issues. At CHESHIRE, *fracture* Ca, Cs, Sr, Am, Eu, Sm, Np, U, and Pu predicted Log Rs are 2.2, 3.2, 1.9, 1.8, 1.9, 2.0, 0.7, 1.0, and 0.9/1.3/1.8, respectively (Table 12; note that three values for Pu are related to the three O₂(g) fugacities examined). In the TC unit, predicted *fracture* Log Rs are 3.0, 3.2, 2.7, 1.9, 2.0, 2.1, 1.1, 1.8, and 1.4/1.7/2.3, respectively in the iron oxide dominated case (Table 14) and 3.0, 3.2, 2.7, 1.9, 1.9, 2.0, 0.6, 0.7, 0.9/1.2/1.6, respectively in the manganese oxide dominated case (Table 15). In the case of Ca and Sr, the TC Rs are significantly higher than the CHESHIRE site values because of the greater abundance of zeolite in the average TC unit. In contrast, Cs, which sorbs primarily to illite/mica, and Am, Eu, and Sm, which sorb strongly to smectite, iron oxide, calcite, and colloids, appear to have similar Rs at the CHESHIRE site and the average TC unit. As will be discussed in Section 6.5, radionuclide sorbing mineral abundances vary spatially across the TC hydrostratigraphic unit. As a result, radionuclide retardation at the CHESHIRE site is not representative of the entire TC unit.

In the case of Np, U, and Pu, the predicted TC unit Rs based on the iron oxide dominating case (Table 14) are significantly higher than for the CHESHIRE site Rs . Conversely, average TC unit Rs based on the manganese oxide dominating case (Table 15) are similar to or slightly lower than the CHESHIRE site Rs . Since the TC unit data in Drellack et al. (1997) does not distinguish between iron and manganese oxides, and our mechanistic model does not, at present, include sorption to manganese oxides, the manganese oxide dominating case is the more conservative. If radionuclide sorption to manganese oxides was included in our model, the CHESHIRE site and TC unit predicted Rs for those radionuclides that sorb strongly to this oxide would likely be significantly higher.

The difference between the CHESHIRE site and the TC *matrix* Log Rs for all radionuclides is quite large (up to 2 order of magnitude difference in R). The difference in radionuclide matrix Rs results from the difference in average sorbing mineral abundance in the matrix. As mentioned in Section 6.3.1 and will be shown in the following section, the distribution of radionuclide sorbing minerals in the matrix is very heterogeneous at the scale of the TC unit. Within the TC unit, zeolitized, devitrified and vitric tuffs and lavas all exist and their mineralogy can be quite distinct. For example, the CHESHIRE site is dominated by devitrified lavas which contain little or no zeolite and only small quantities of iron oxide, smectite, and mica. As a result of the low abundance of sorbing minerals, Rs are relatively low. Other parts of the TC unit are largely zeolitized or have high quantities of smectite, which would result in much higher Rs .

In Section 6.3.2, we reported on heterogeneity at the hydrostratigraphic unit scale. Comparison of the CHESHIRE site and TC unit suggests that spatial heterogeneity may play an important role in radionuclide transport at the sub-hydrostratigraphic unit scale as well. CHESHIRE site average radionuclide Rs (Section 7.3) were developed using sorbing mineral abundance data specific to the CHESHIRE site located entirely within one stratigraphic unit (mafic-poor Calico Hills, a sub-unit of the Volcanics of Area 20). In the TC case, radionuclide Rs were based on average sorbing mineral abundance data for several stratigraphic units that comprise the TC hydrostratigraphic unit (Paintbrush

group, Volcanics of Area 20, and Crater Flat Group). Spatial heterogeneity of sorbing minerals at the sub-hydrostratigraphic unit scale accounts for the difference in Rs for the TC and CHESHIRE site cases.

It is also important to note that spatial heterogeneity of both flow and sorbing mineral abundance was predicted even at the sub-CHESHIRE HST model scale (Pawloski et al., 2001). Spatial heterogeneity at this scale was shown to have an effect on radionuclide transport as well. However, the results suggest that small near-field scale flow field and R heterogeneities may be regarded as dispersion effects and that the near-field scale radionuclide retardation can be semi-quantitatively related to average Rs of the high permeability fracture flow zones (Section 6.2.2). The impact of these different scales of heterogeneity need to be evaluated to justify radionuclide retardation upscaling approaches. Furthermore, the integration of heterogeneous flow with radionuclide retardation needs to be evaluated, particularly in the highly heterogeneous fracture flow regime. The integration of heterogeneous flow and radionuclide retardation was evaluated in this report for the Frenchman Flat alluvium case (Section 5) but will not be evaluated for the fracture-flow case. However, in the following section, we illustrate heterogeneous radionuclide retardation in the fracture flow domain based on data at the sub-hydrostratigraphic unit (TC unit). Integration of these data with a heterogeneous flow model would allow for an evaluation of heterogeneity scales and their effect on large-scale transport.

6.5 Heterogeneous distribution of radionuclide Rs at the sub-hydrostratigraphic unit scale

The comparison of CHESHIRE site and TC unit radionuclide Rs suggests that radionuclide retardation at the sub-hydrostratigraphic unit scale will be heterogeneously distributed. To further examine this scale of heterogeneity, we evaluated the heterogeneous distribution of predicted Rs as a function of depth for a number of wells located on Pahute Mesa and Yucca Mountain. Only samples that are part of the TC unit were examined, revealing heterogeneity at the *sub-hydrostratigraphic scale*. The water chemistry, fracture density, fracture aperture, porosity, and other parameters were held constant and based on the average TC unit parameters listed in Table 13. Thus, we evaluated only the effects of heterogeneous mineral distribution and not other parameters. These Rs were calculated using the same methods as those described in Section 6.3 for the average hydrostratigraphic unit case. Details regarding the calculations performed and all mineralogy, K_d , and R data are reported in Appendices D and E.

6.5.1 Heterogeneous distribution of radionuclide Rs in the matrix of the Tuff Cone hydrostratigraphic unit

The distribution of Rs as a function of depth in the matrix of the TC unit are shown in Figures 14 through 25. The matrix mineralogy data were collected from Warren et al. (2000). The data presented here are a subset of those used to determine matrix mineral abundance averages listed in Table 13. The subset includes data from a select number of wells with a relatively high density of reported mineral abundance data. Sorbing mineral

abundances and predicted radionuclide Rs (and K_dS) for data point reported here are listed in Appendix D.

In the four drill holes (J-13, UE-25, USW-G1, USW-G2) examined, tremendous heterogeneity in R appears for all radionuclides examined. Furthermore, some structure is observable, indicating that a number of layers within the TC hydrostratigraphic unit have distinctly different retardation behavior. For example, a zone of high Cs retardation occurs near a depth of 750 feet in the J-13 well. This may be related to a distinct stratigraphic unit. Similarly, a zone ranging from 250 and 1000 feet in UE-25 shows distinct Rs for Am, Eu, Sm, Ca, and Sr.³⁹ Below 1500 feet, the variability in R for most radionuclides in UE-25 is large but distinct zones cannot be distinguished. It may be that zones of distinct R are on the scale of 100 feet which would be too small to observe with these data. Nevertheless, the data suggest that the distribution of Rs in the matrix of the TC unit will be much more complex than in the Frenchman Flat alluvium. It is likely that heterogeneous distribution of radionuclide sorbing minerals in the TC unit will have a significant effect on transport. The differences between the average CHESHIRE site and the average TC unit predicted Rs result from the heterogeneous distribution of radionuclide sorbing minerals.

Figure 26 summarizes the data in Figures 14 to 25 in a similar manner as shown for Frenchman Flat alluvium in Figure 3. The heterogeneous distribution of radionuclide sorbing minerals is significantly greater when compared to the Frenchman Flat alluvium radionuclide K_dS . The summary of all data suggests that the minimum R for all radionuclides is 1 (i.e. unretarded transport) while the standard deviation to the average is greater than 1 log R for the majority of sorbing radionuclides.

³⁹ Note that a distinction between vadose zone and saturated zone was not made here.

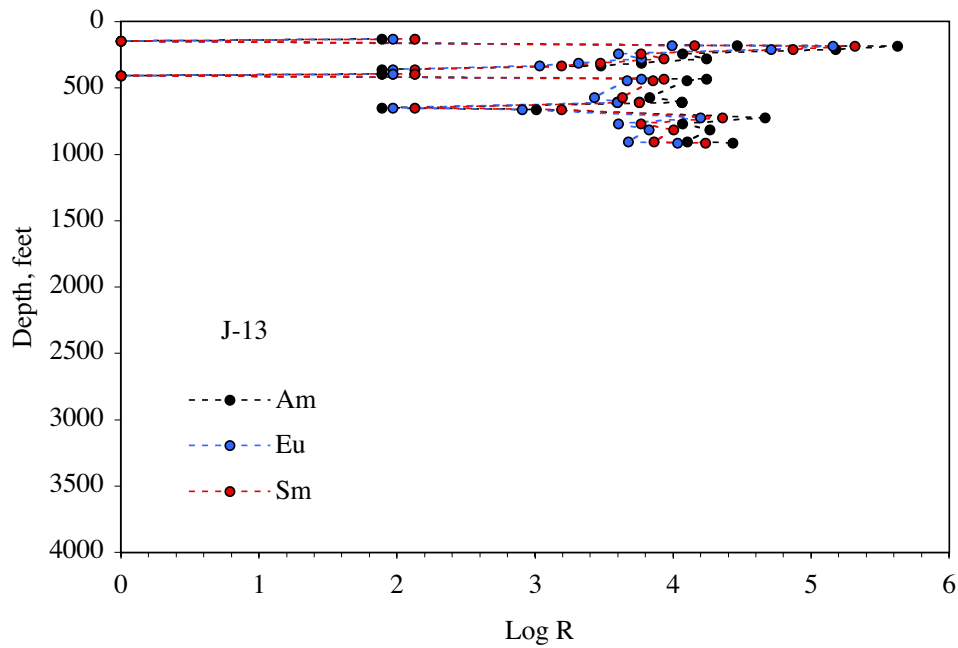


Figure 14. Am, Eu, and Sm matrix Log R as a function of depth based on mineral abundance data from well J-13.

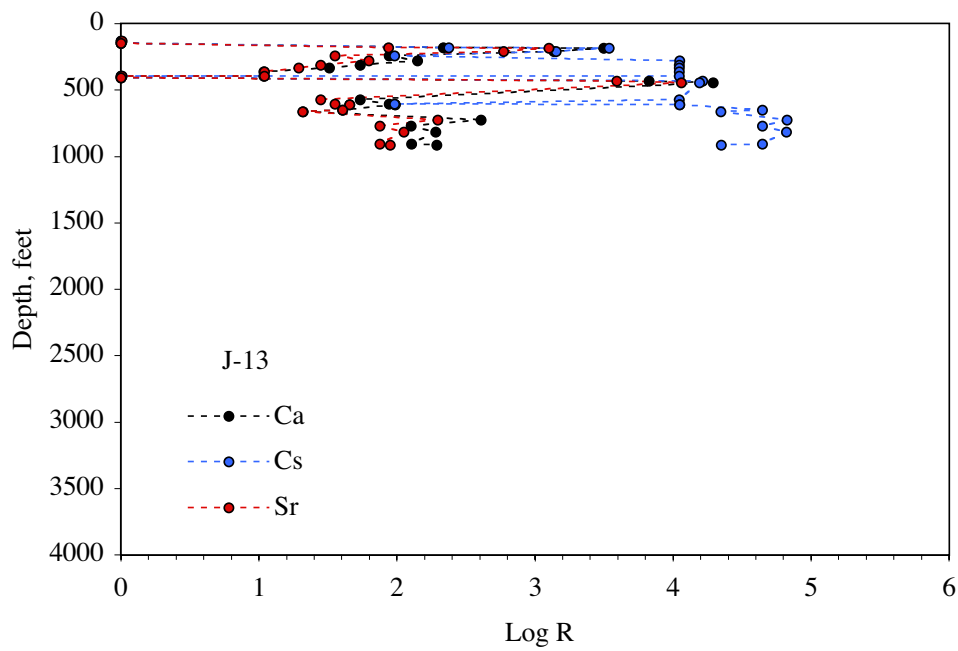


Figure 15. Ca, Cs, and Sr matrix Log R as a function of depth based on mineral abundance data from well J-13.

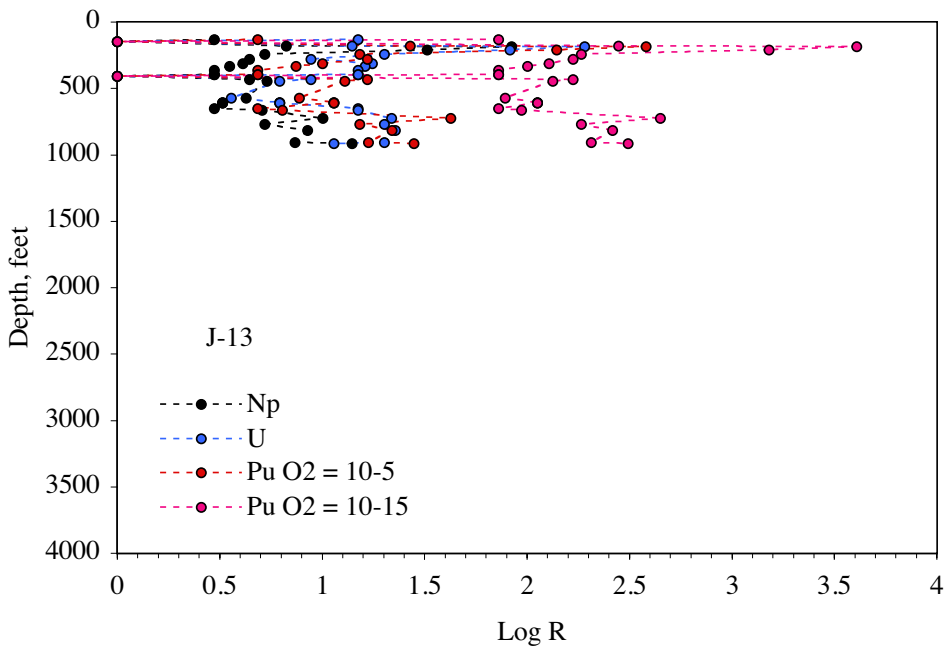


Figure 16. Np, U, and Pu matrix Log R as a function of depth based on mineral abundance data from well J-13.

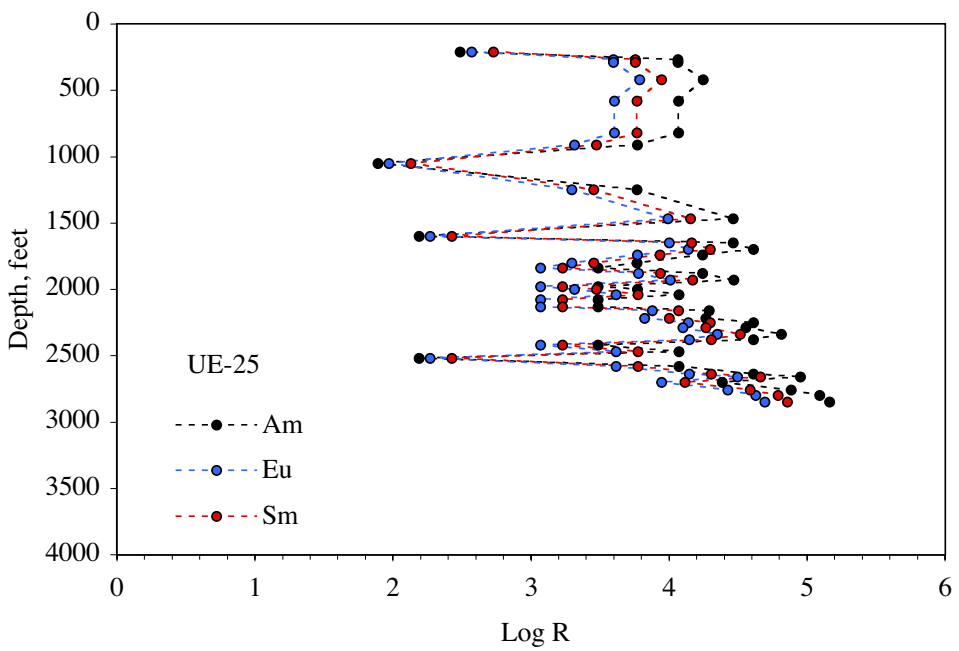


Figure 17. Am, Eu, and Sm matrix Log R as a function of depth based on mineral abundance data from drillhole UE-25.

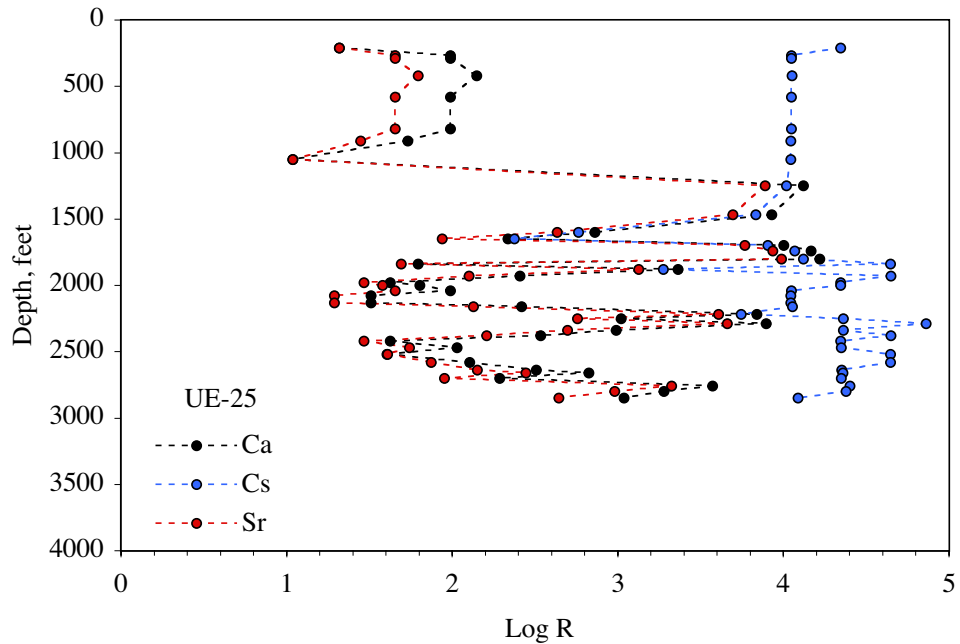


Figure 18. Ca, Cs, and Sr matrix Log R as a function of depth based on mineral abundance data from drillhole UE-25.

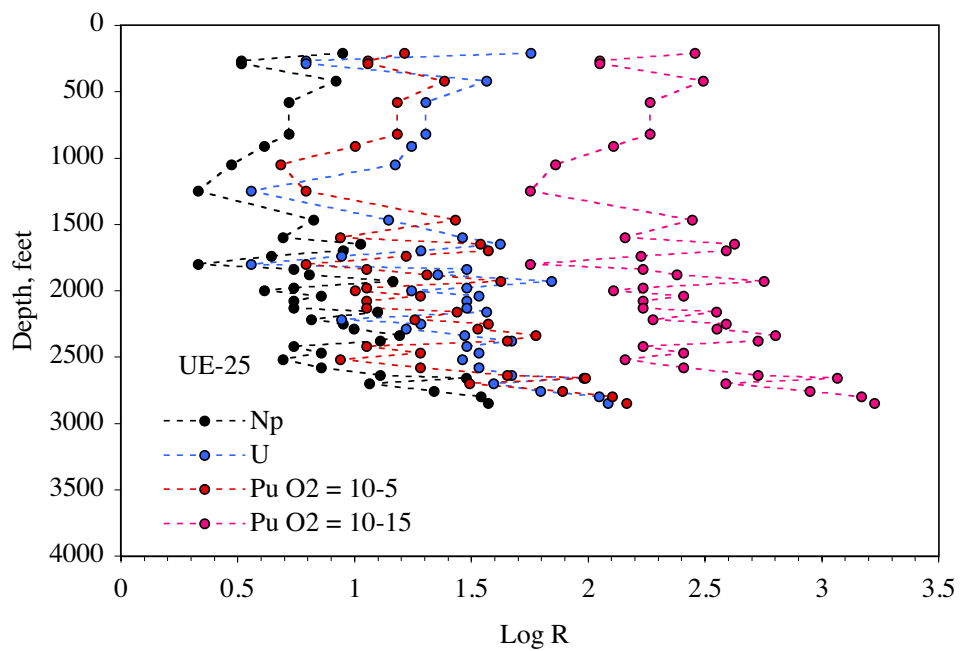


Figure 19. Np, U, and Pu matrix Log R as a function of depth based on mineral abundance data from drillhole UE-25.

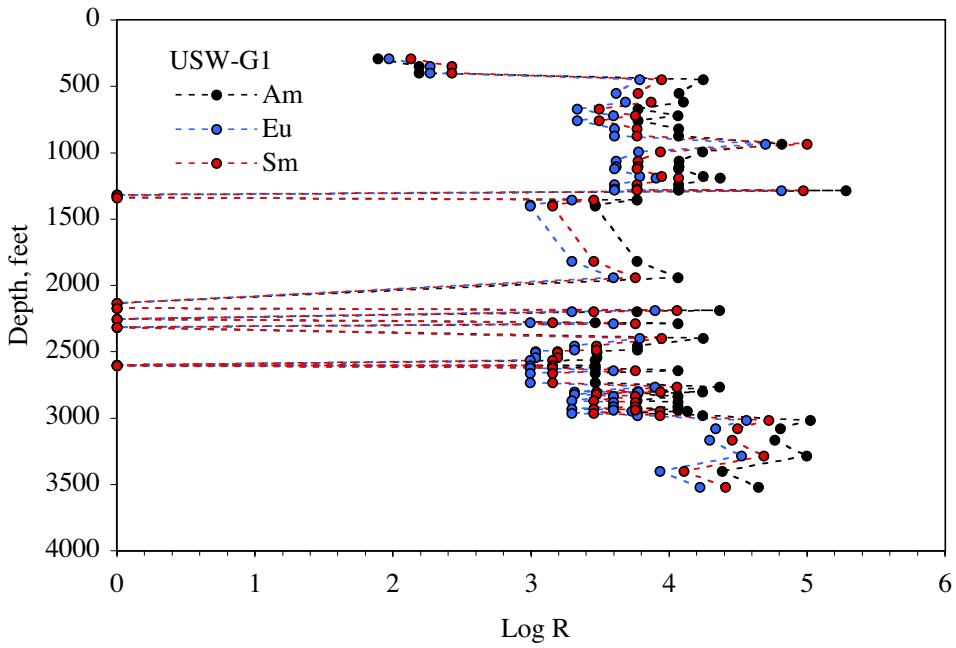


Figure 20. Am, Eu, and Sm matrix Log R as a function of depth based on mineral abundance data from drillhole USW-G1.

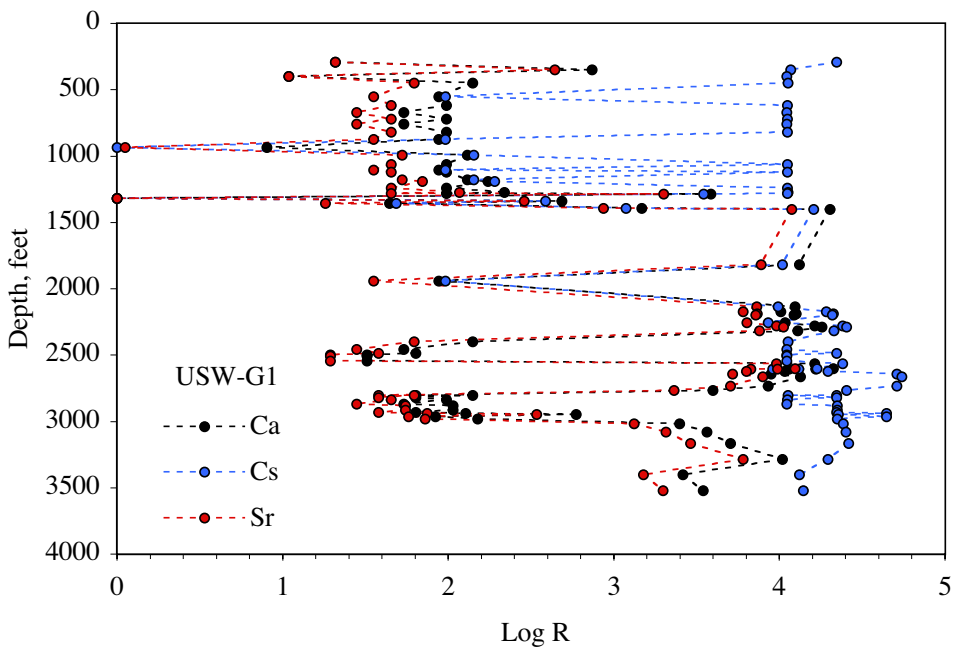


Figure 21. Ca, Cs, and Sr matrix Log R as a function of depth based on mineral abundance data from drillhole USW-G1.

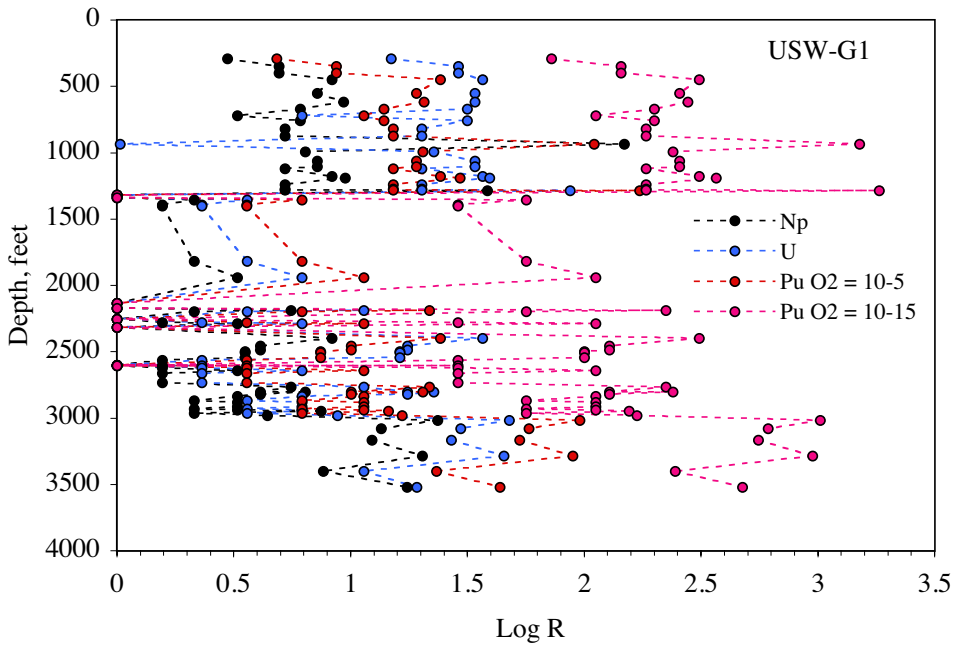


Figure 22. Np, U, and Pu matrix Log *R* as a function of depth based on mineral abundance data from drillhole UE-25.

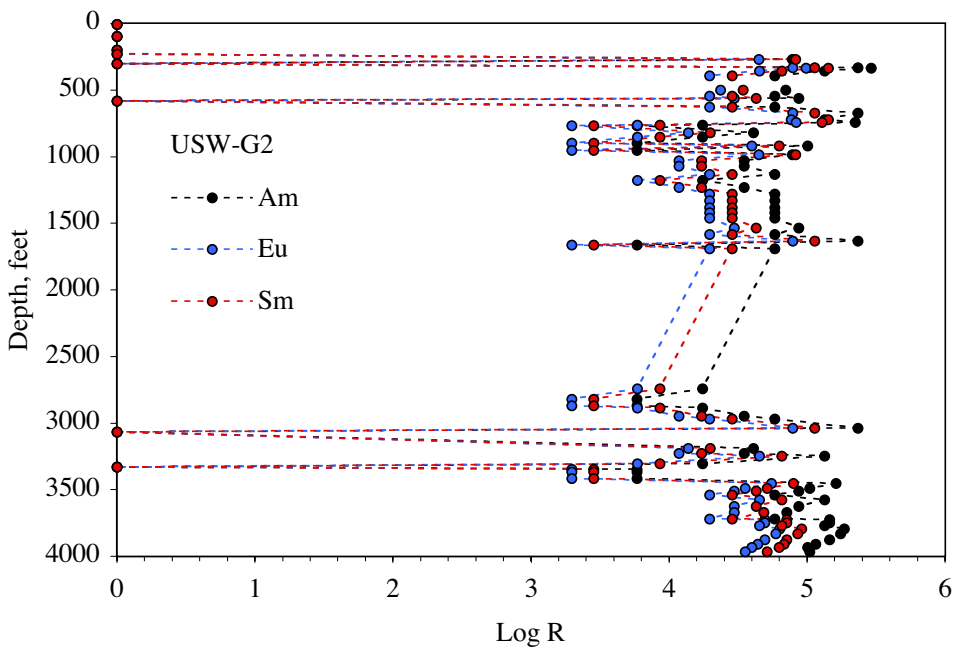


Figure 23. Am, Eu, and Sm matrix Log *R* as a function of depth based on mineral abundance data from drillhole USW-G2.

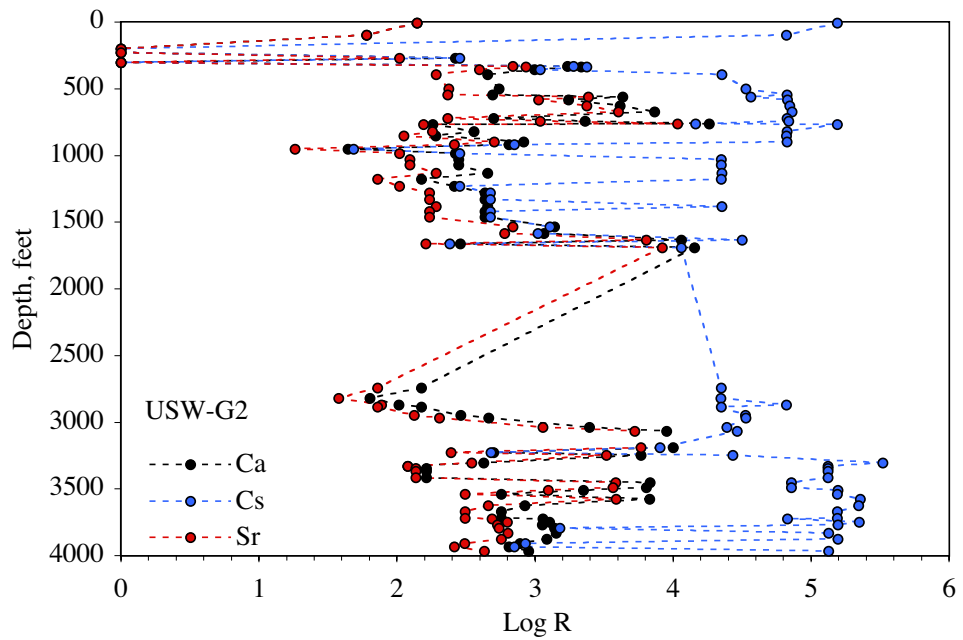


Figure 24. Ca, Cs, and Sr matrix Log R as a function of depth based on mineral abundance data from drillhole USW-G2.

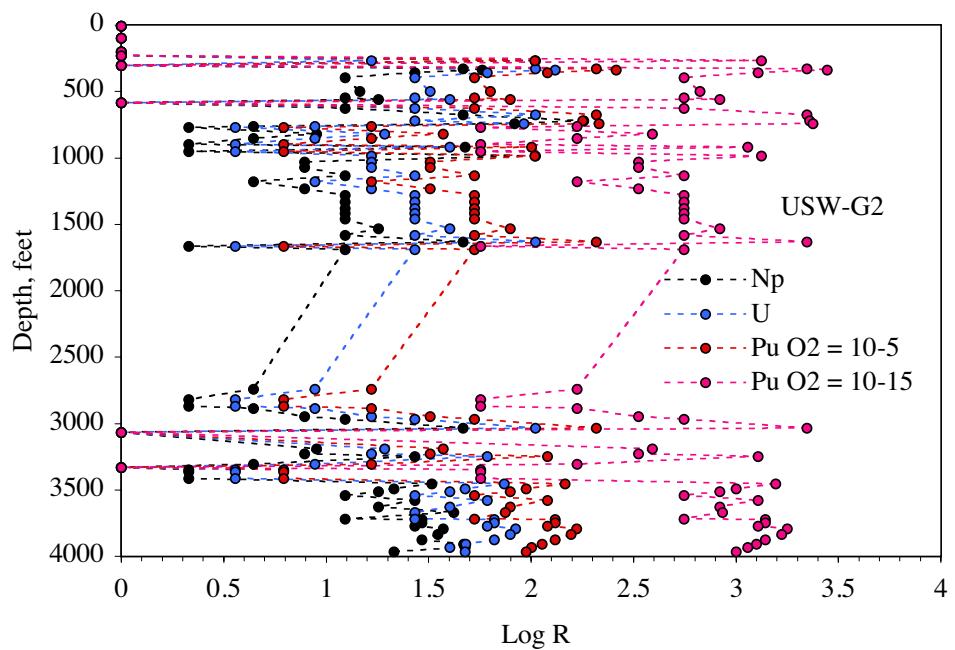


Figure 25. Np, U, and Pu matrix Log R as a function of depth based on mineral abundance data from drillhole UE-25.

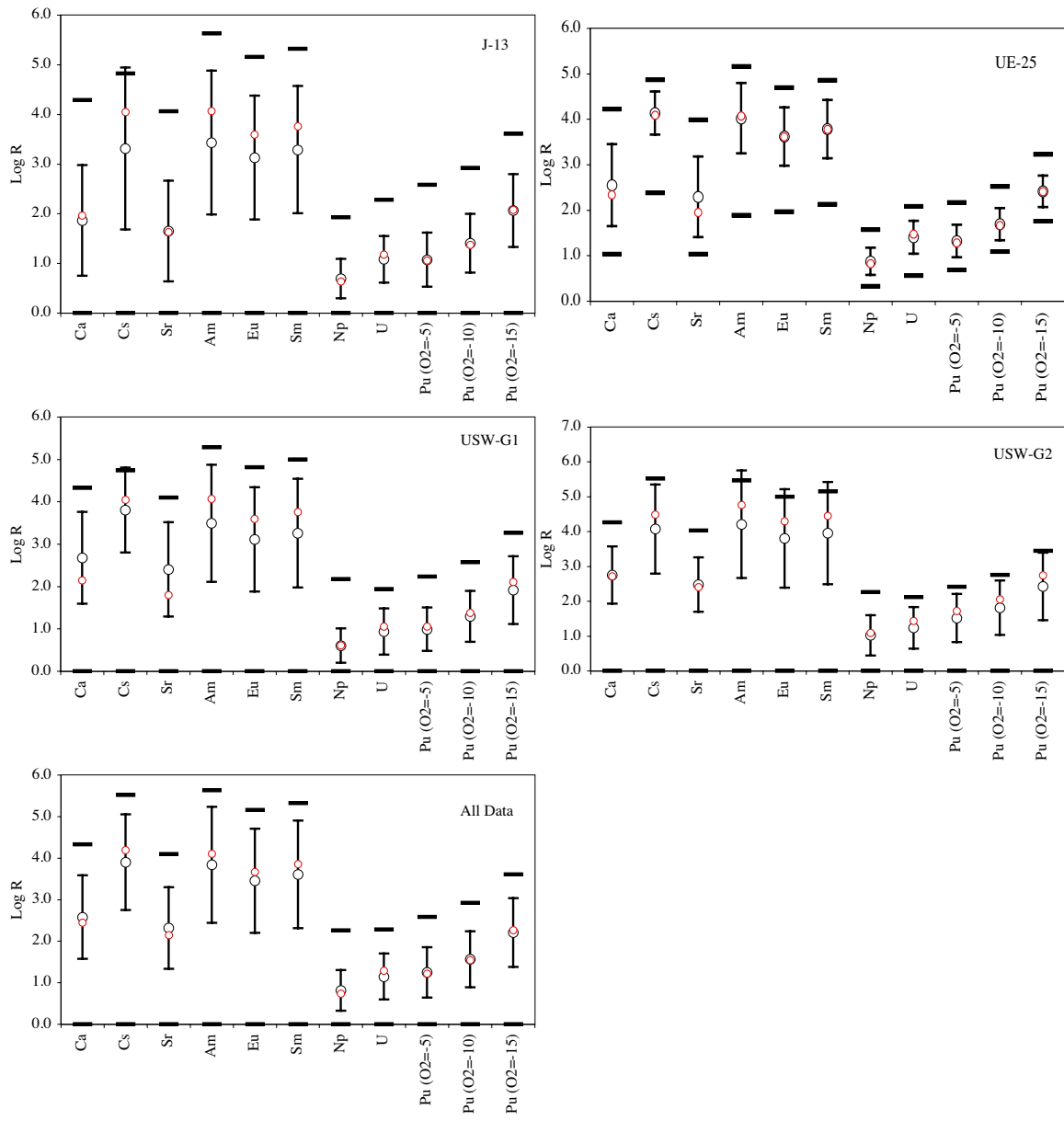


Figure 26. Predicted matrix radionuclide R_s based on mineral abundances. Average (black circle) and standard deviation based on mineral abundance, median (red) and bars (minimum and maximum).

6.5.2 Heterogeneous distribution of radionuclide Rs in the fractures of the Tuff Cone hydrostratigraphic unit

The distribution of Rs as a function of depth in the fracture flow zones of the TC unit are shown in Figures 27 through 41 for UE-25, USW-G1, USAW-G2, USW-G3, and USW-G4. In the case of fracture flow zone mineral abundance data, these Rs are calculated based on a combination of available fracture-lining mineral abundance data and the *average* matrix mineral abundance reported in Table 13 for the TC unit. Thus, the variability of the fracture flow zone mineral abundances are calculated only as the variability relates to fracture-lining minerals and not to the underlying matrix mineralogy. Since the fracture flow zone conceptual model includes sorption effects from a small amount of accessible matrix, applying an average matrix mineralogy reduces the possible scale of R variability. Furthermore, it is assumed that fracture densities, apertures, and other parameters remain constant across the entire TC unit. This is unlikely, especially since significant lithologic changes occur in this unit. Inclusion of information regarding the heterogeneous distribution of parameters other than fracture-lining mineralogy would add additional layers of complexity to our analysis. Analysis of variability of a suite of parameters would help elucidate which parameters have the greatest impact on transport. However, this analysis is beyond the scope of this report. Sorbing mineral abundances and predicted radionuclide Rs (and K_d s) for each data point reported here are listed in Appendix E.

For the case of Cs, the data presented here are reported for the case where illite colloids contribute to the reduction of the Cs R . However, both the illite colloid and smectite colloid case is reported in Appendix E for Cs. The inclusion of illite colloids reduces the variability in Cs R since colloids are assumed to be distributed homogeneously and dampen the observed R variability. This dampening is more severe for Cs than for other colloid-sorbing radionuclides (e.g. Am, Eu, and Sm) because the dominant Cs sorber is illite which is found in the matrix but not in fracture lining. Since average matrix mineralogy is used in this analysis, the resulting Cs R varies less than any other radionuclide. If variability in matrix mineralogy were included, significantly greater variability would be observed (see Cs R data in Figures 15, 18, 21, and 24).

The variability in fracture flow zone R for individual radionuclides is slightly less than in the matrix case. The reduction in R variability, in part, results from our use of an average matrix flow zone mineralogy. The contribution of the average matrix mineral abundances is easily observed for certain radionuclides as a minimum R value. For example, in Figure 27, Am, Eu, and Sm all have minimum R values near 10 ($\log R = 1.0$). If heterogeneous distribution of matrix minerals were included in this analysis, greater variability in R might be observed.

As in the case of radionuclide R distribution in the matrix, zones of distinct retardation can be observed in the fracture flow zone data. For example, a 300 foot thick zone near the 1250 foot depth of USW-G1 has predicted Rs for Am, Eu, and Sm that are over an order of magnitude greater than the surrounding medium. This same zone includes a peak

in Np, Pu, and U Rs . In USW-G2, Ca and Sr Rs are consistently lower at depths below 2500 feet than above 2500 feet.

Figure 42 summarizes the data in Figures 27 to 41 in a similar manner as shown for Frenchman Flat alluvium in Figure 3. Again, the significantly greater heterogeneous distribution of radionuclide sorbing minerals compared to the Frenchman Flat alluvium K_d s is quite obvious. The lower limit R for all radionuclides is controlled by the average mineralogy of the matrix which contributes to the fracture flow zone radionuclide Rs . If matrix mineral variability were included, heterogeneity in R would likely increase. Nevertheless, the standard deviation to the average Rs range from 0.5 to 1 $\log R$ for the majority of sorbing radionuclides. Unlike Frenchman Flat alluvium, it seems likely that heterogeneous distribution of radionuclide sorbing minerals in the TC unit will have a significant effect on transport. Heterogeneity at the sub-hydrostratigraphic unit scale will need to be accounted for in large-scale CAU models.

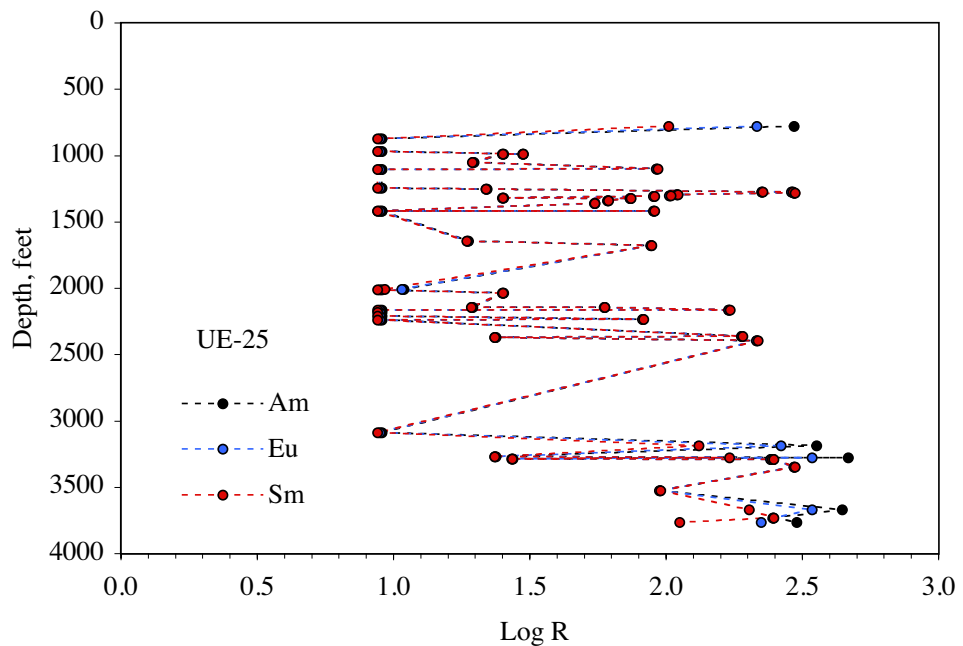


Figure 27. Am, Eu, and Sm fracture Log R as a function of depth based on mineral abundance data from drillhole UE-25.

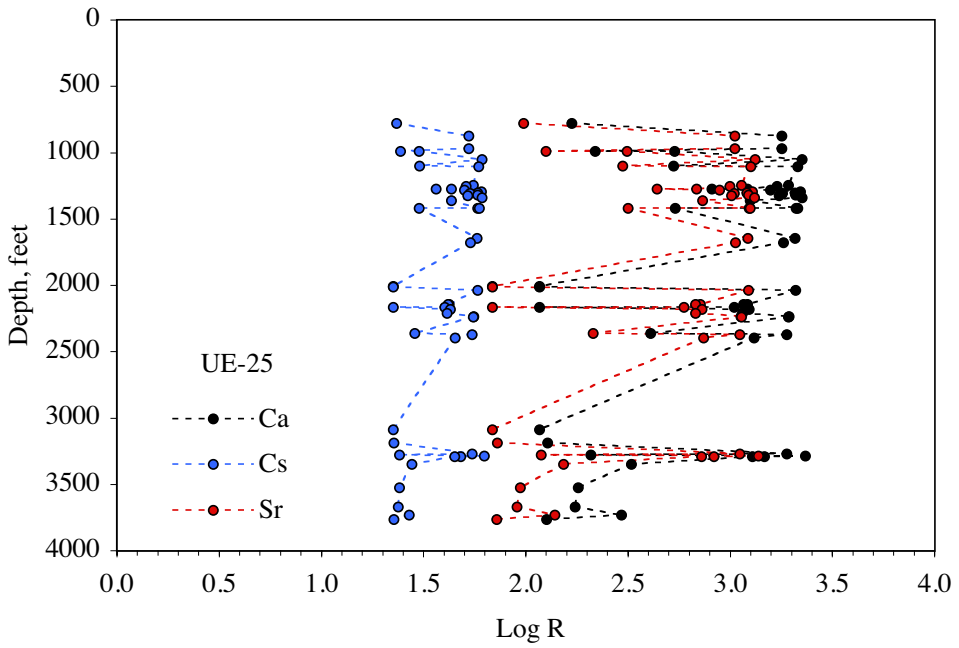


Figure 28. Ca, Cs, and Sr fracture Log R as a function of depth based on mineral abundance data from drillhole UE-25.

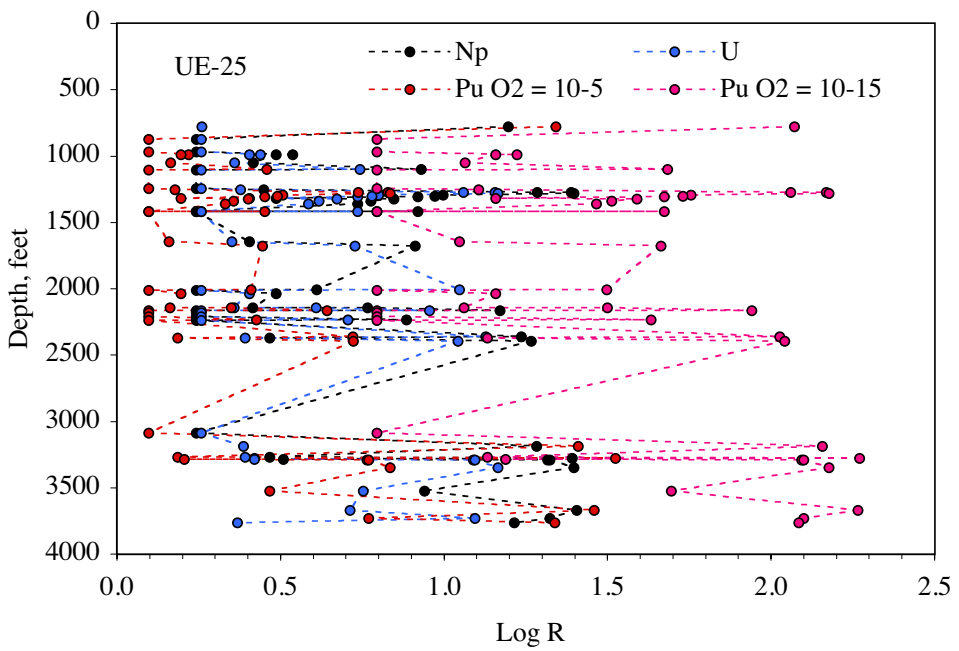


Figure 29. Np, U, and Pu fracture Log R as a function of depth based on mineral abundance data from drillhole UE-25.

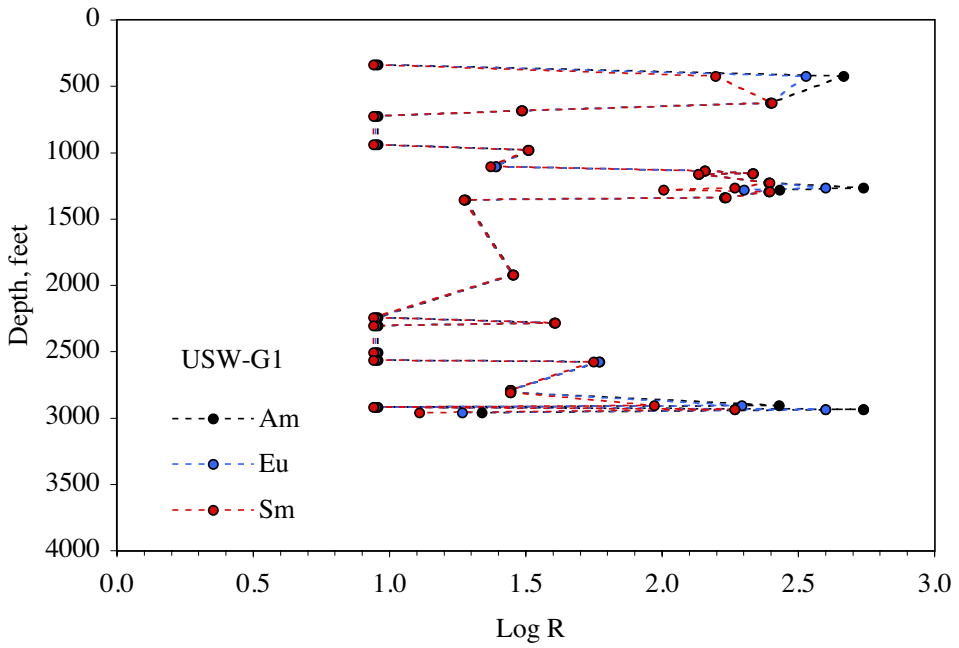


Figure 30. Am, Eu, and Sm fracture Log R as a function of depth based on mineral abundance data from drillhole USW-G1.

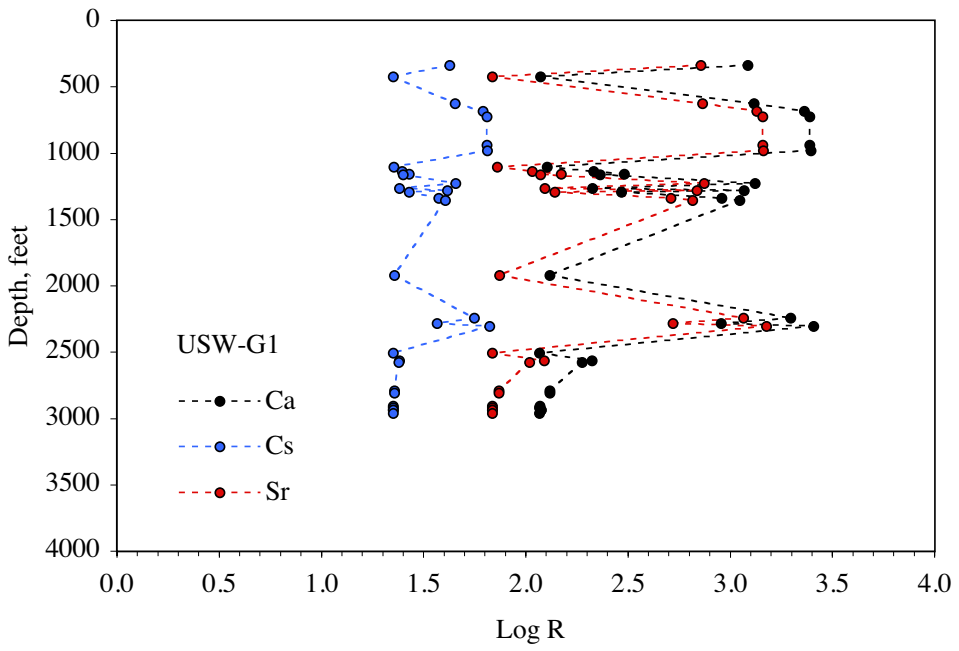


Figure 31. Ca, Cs, and Sr fracture Log R as a function of depth based on mineral abundance data from drillhole USW-G1.

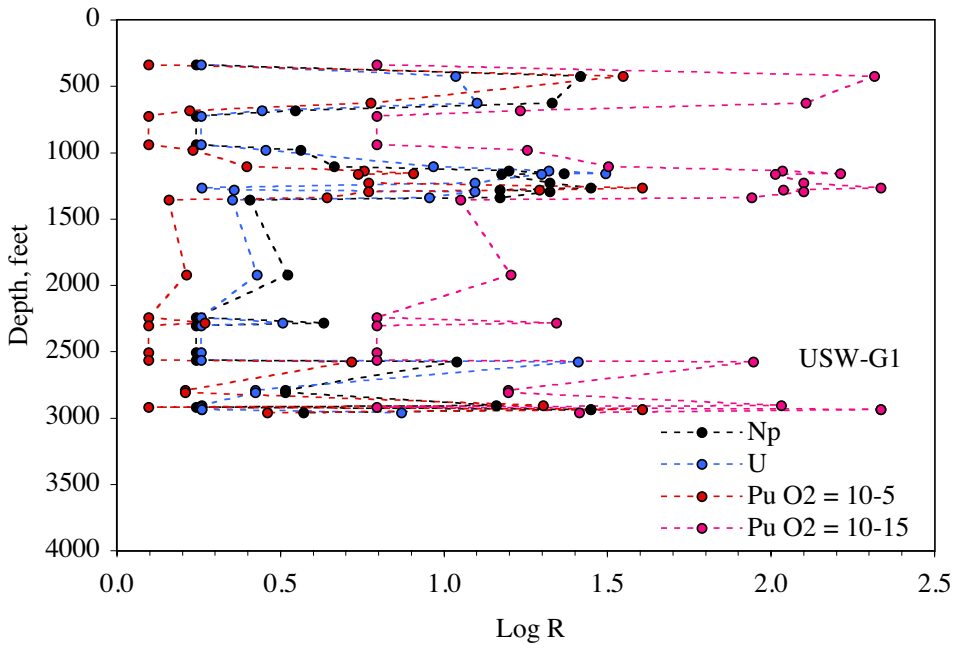


Figure 32. Np, U, and Pu fracture Log R as a function of depth based on mineral abundance data from drillhole USW-G1.

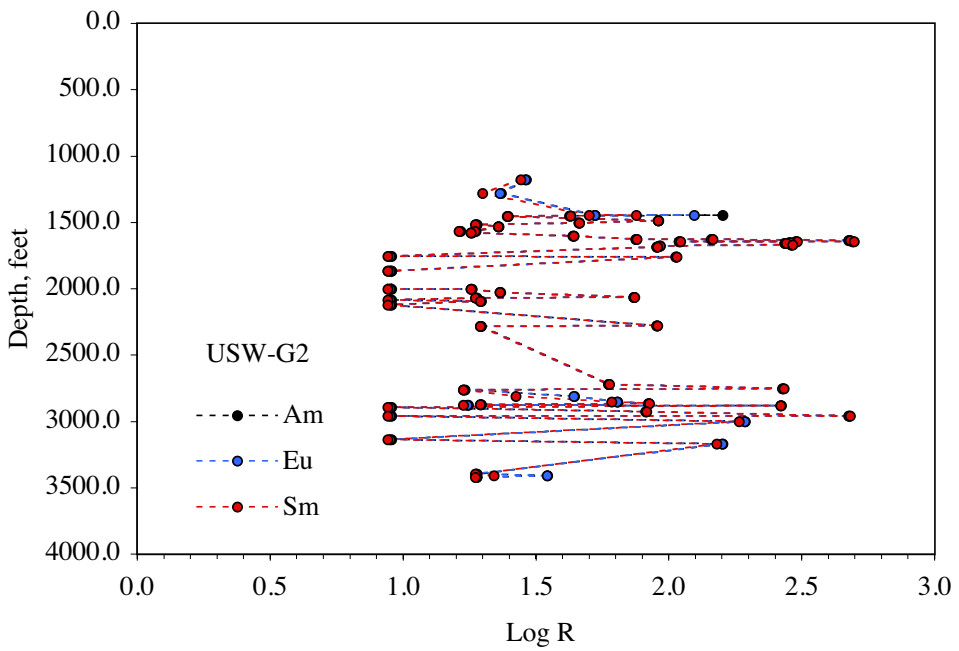


Figure 33. Am, Eu, and Sm fracture Log R as a function of depth based on mineral abundance data from drillhole USW-G2.

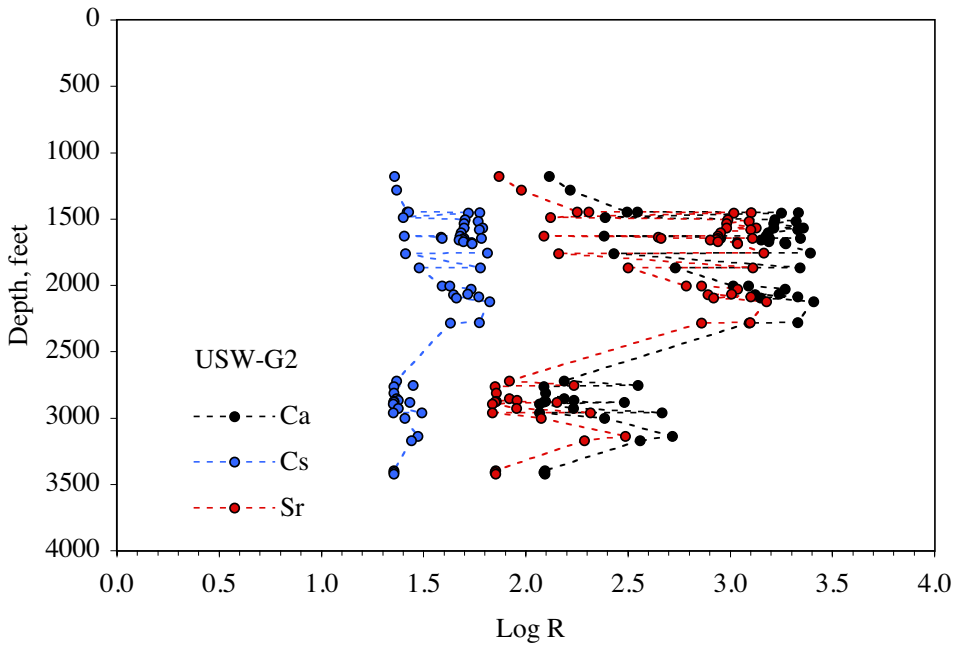


Figure 34. Ca, Cs, and Sr fracture Log R as a function of depth based on mineral abundance data from drillhole USW-G2.

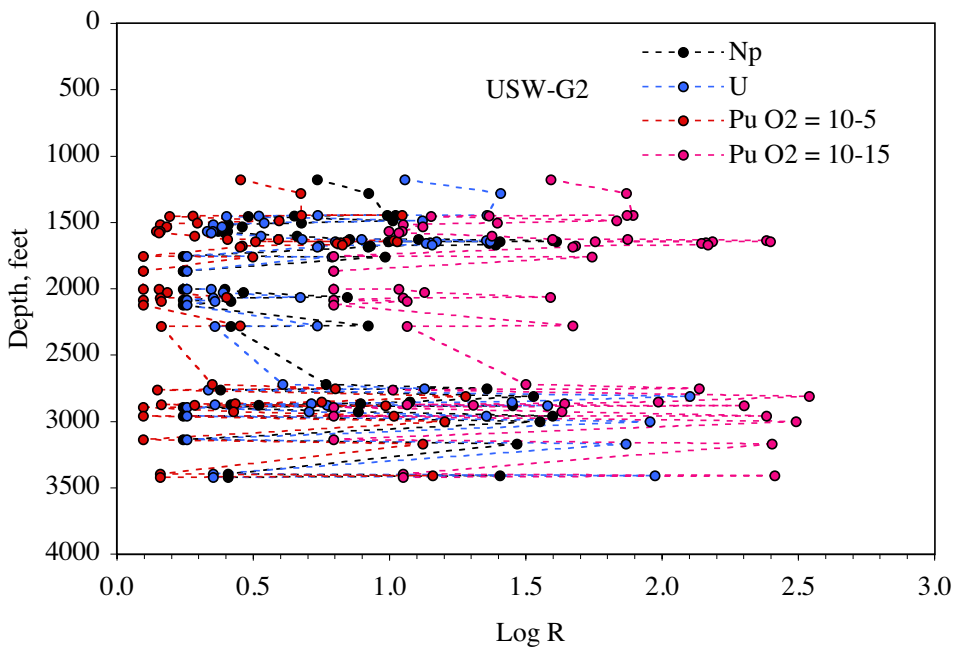


Figure 35. Np, U, and Pu fracture Log R as a function of depth based on mineral abundance data from drillhole USW-G2.

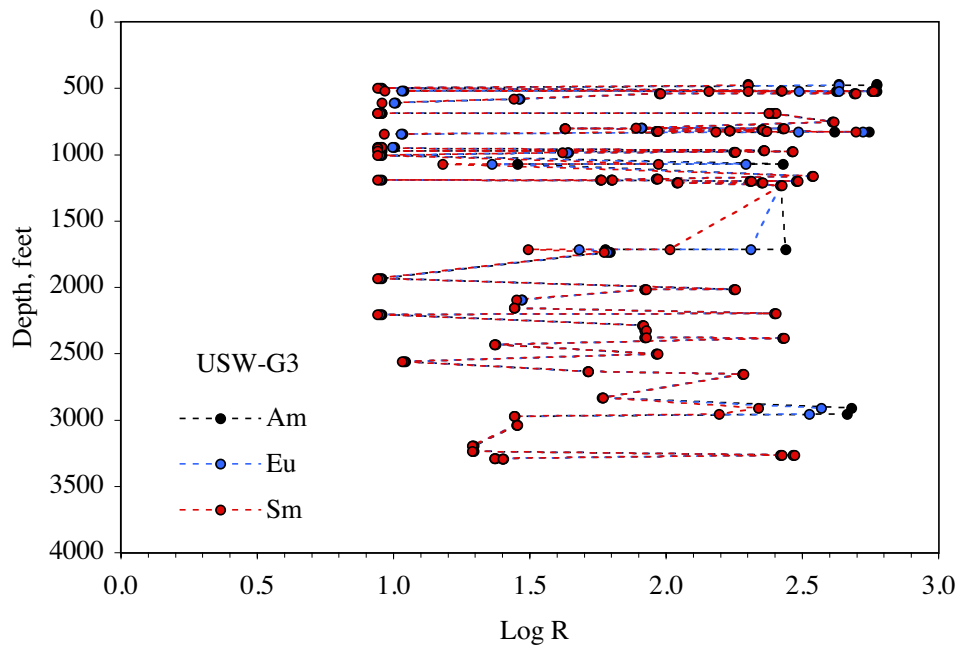


Figure 36. Am, Eu, and Sm fracture Log R as a function of depth based on mineral abundance data from drillhole USW-G3.

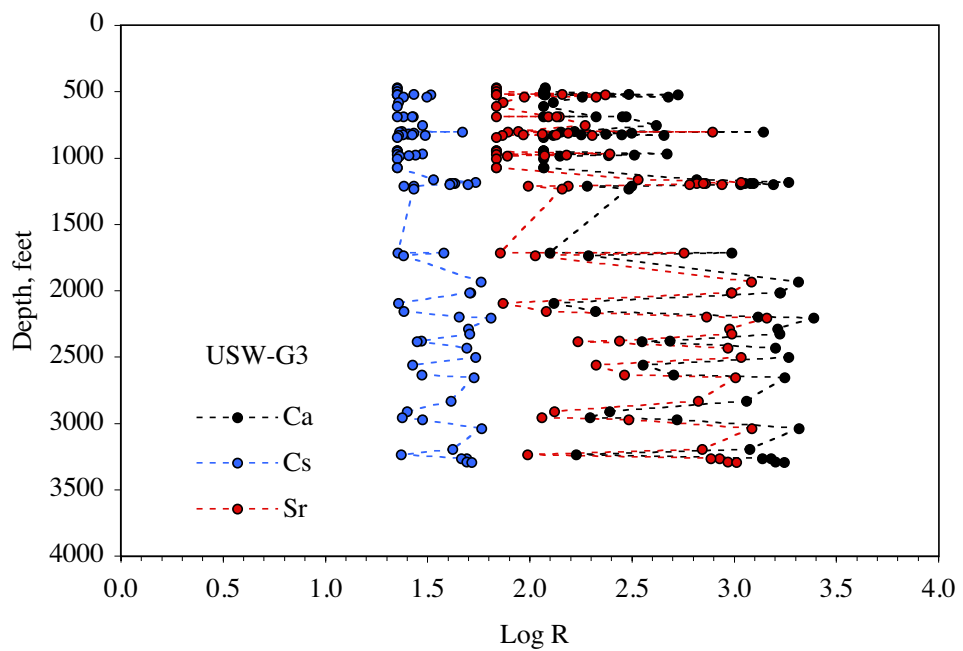


Figure 37. Ca, Cs, and Sr fracture Log R as a function of depth based on mineral abundance data from drillhole USW-G3.

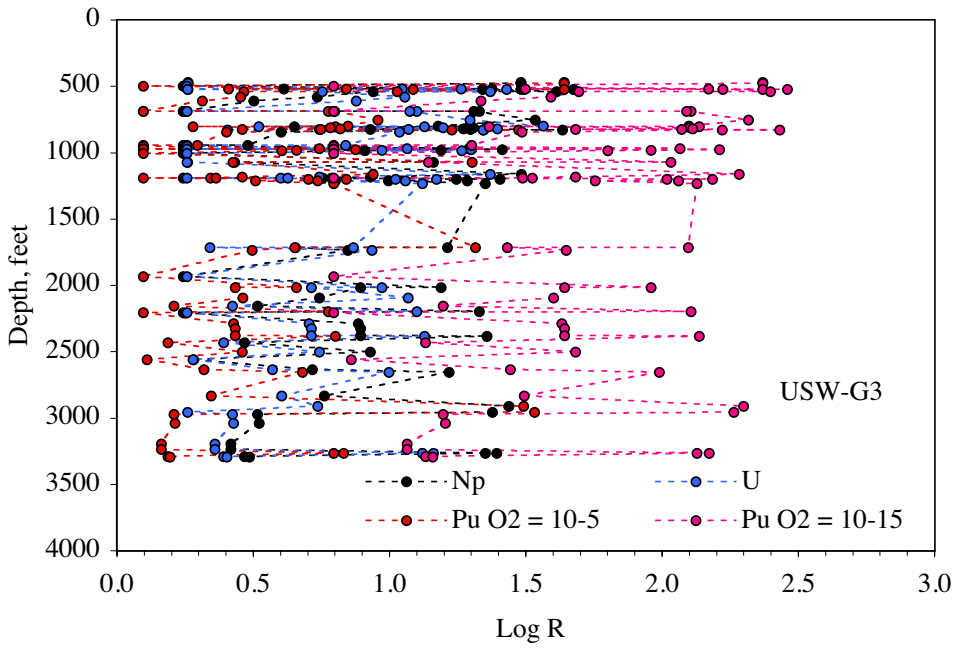


Figure 38. Np, U, and Pu fracture Log R as a function of depth based on mineral abundance data from drillhole USW-G3.

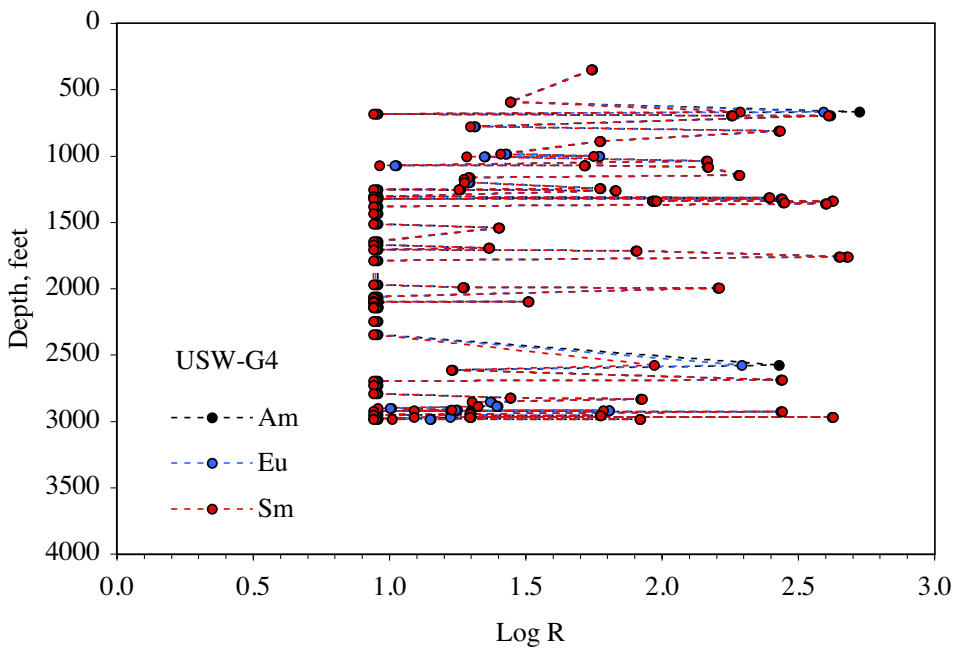


Figure 39. Am, Eu, and Sm fracture Log R as a function of depth based on mineral abundance data from drillhole USW-G4.

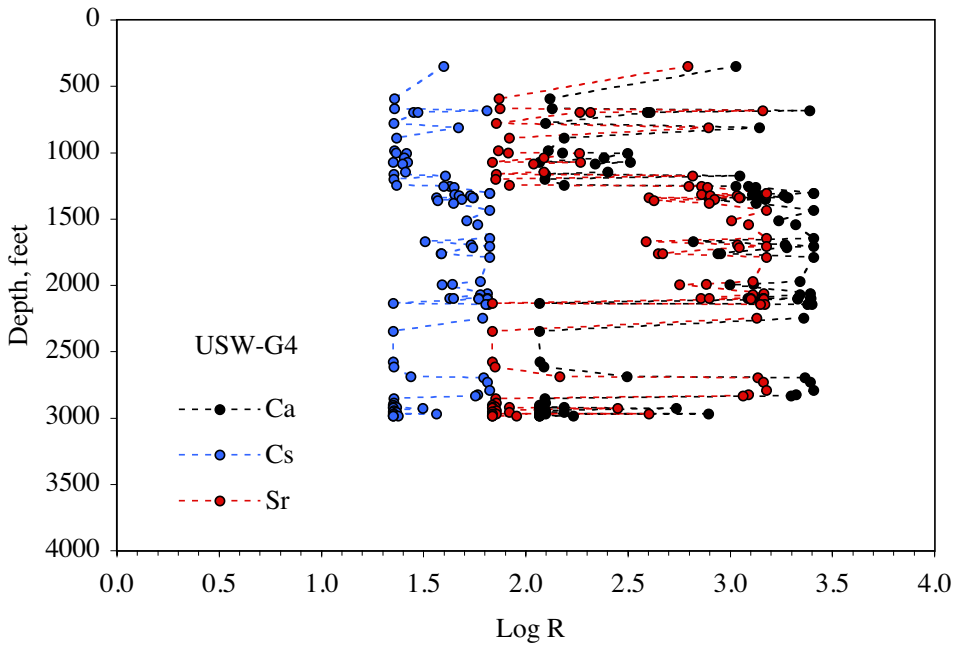


Figure 40. Ca, Cs, and Sr fracture Log R as a function of depth based on mineral abundance data from drillhole USW-G4.

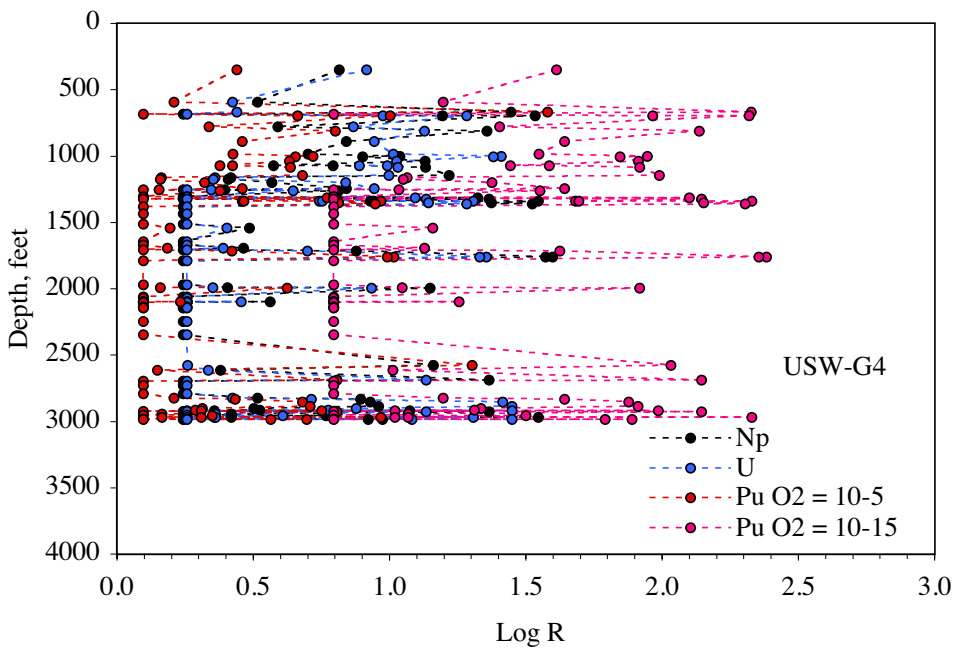


Figure 41. Np, U, and Pu fracture Log R as a function of depth based on mineral abundance data from drillhole USW-G4.

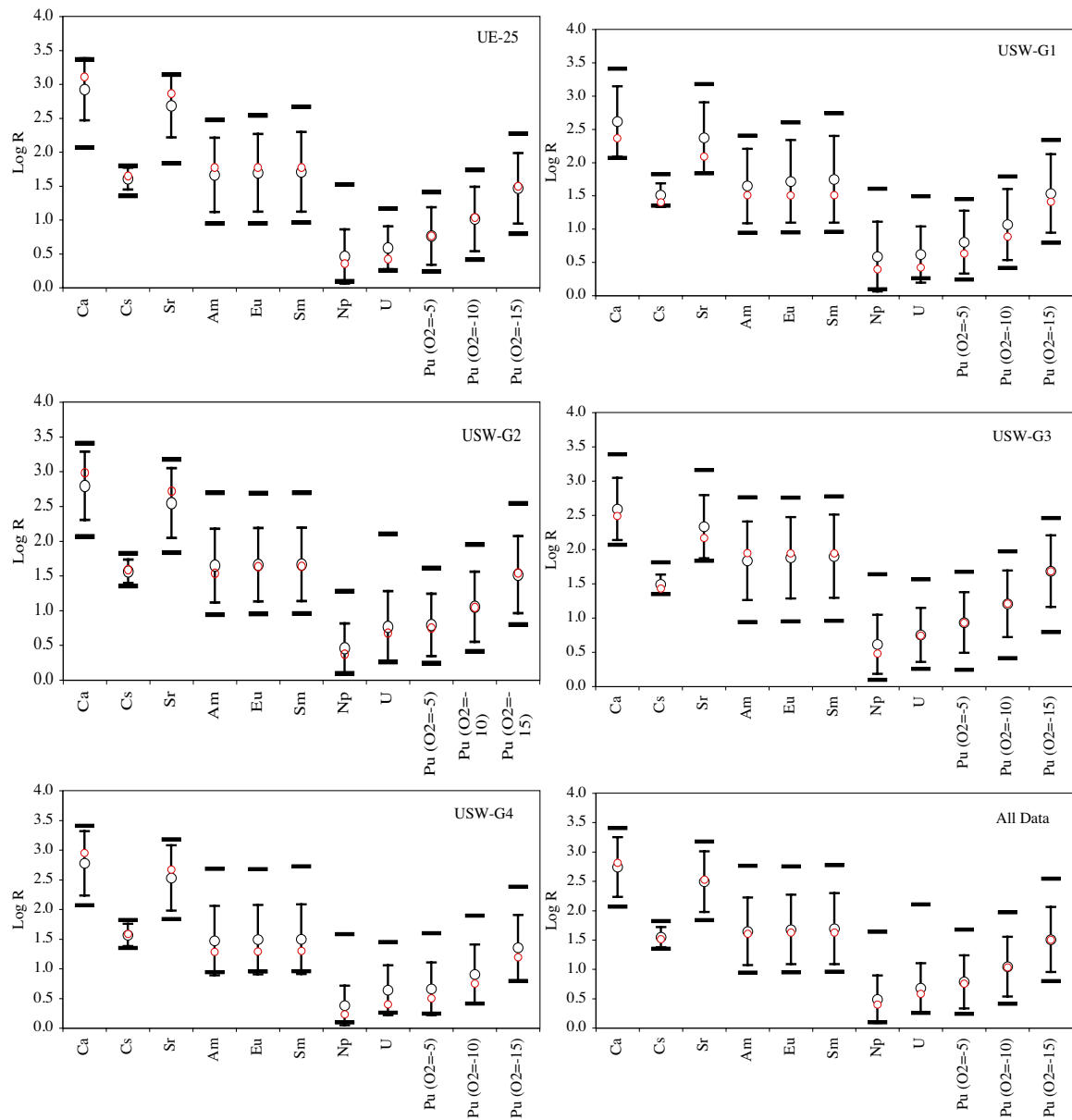


Figure 42. Predicted fracture flow zone radionuclide R_s based on mineral abundances. Average (black circle) and standard deviation based on mineral abundance, median (red) and bars (minimum and maximum).

7. Conclusions

Radionuclide K_d s predicted using the recently updated version of our mechanistic model (Zavarin et al., 2002) combined with the mineralogy and water chemistry from CAMBRIC HST simulations (Tompson et al., 1999) compare well with earlier predicted K_d s reported in Tompson et al. (1999), Pawloski et al. (2000), and Tompson et al. (2001). This suggests that improvements to our sorption model expand our ability to predict K_d s and provide validation to our model but do not contradict earlier predicted K_d data.

A number of reports on Frenchman Flat alluvium mineralogy were used to estimate the variability in predicted radionuclide K_d s resulting from spatially heterogeneous radionuclide sorbing mineral distributions. The range in radionuclide K_d s resulting from variations in sorbing mineral abundances are on the same scale ($\pm 0.5 \log K_d$) as the uncertainties in radionuclide K_d s that result from uncertainties in our mechanistic surface complexation constants. This suggests that both the uncertainty in predicted K_d s and the variability in mineral abundance will affect radionuclide transport predictions.⁴⁰

Based on heterogeneous flow field and heterogeneous K_d distribution simulations, we can conclude that Ca, Cs, Sr, Am, Eu, and Sm appear to be greatly retarded and are not likely to migrate greater than 1 km in 10,000 years *under the Frenchman Flat alluvium conditions examined with these simulations*.⁴¹ However, Np, U, Pu, and all non-sorbing radionuclides are predicted to travel a significant distance. 3D simulations reveal that the heterogeneous distribution of radionuclide sorbing minerals (in conjunction with a heterogeneous permeability field) in Frenchman Flat alluvium does not seem to significantly affect the average radionuclide retardation *under the conditions examined with reactive transport simulations*. Average radionuclide K_d s predict peak breakthrough in 3D simulations accurately even under heterogeneous permeability and K_d distribution conditions. However, dispersion of radionuclides as a result of heterogeneous permeability and K_d distributions is apparent in 3D simulations.

We have demonstrated the methodology by which our mechanistic model can be simplified to a K_d model in a fracture flow environment. R_s were predicted for several radionuclides using the average CHESHIRE site sorbing mineral abundance data and flow conceptualizations used in Pawloski et al. (2001). Based on these data, it appears that the average radionuclide retardation in the *dominant fracture flow zone* at the near-field scale can be related to the overall radionuclide peak breakthrough at that scale. These CHESHIRE site results were compared to radionuclide R_s for six hydrostratigraphic units. The result suggest that (1) heterogeneous sorbing mineral distribution at the hydrostratigraphic unit scale is significant and should be included in CAU models and

⁴⁰ A large number of other uncertainties have not been evaluated in this report (uncertainties in reactive surface area, surface charging behavior, aqueous speciation constants, conceptual model, solution chemistry, mechanistic model validity, Vanselow ion exchange validity, etc.). Our analysis is, by no means, a complete uncertainty analysis. However, uncertainty in mechanistic model reaction constants clearly needs to be accounted for (along with many other uncertainties).

⁴¹ Note that the effect of radionuclide decay was not accounted for in these simulations.

(2) heterogeneous radionuclide sorbing mineral distribution at the sub-hydrostratigraphic unit scale is significant and needs to be included in CAU models. Examination of matrix and fracture radionuclide retardation as a function of well depth for the TC unit reveals significantly greater heterogeneity in radionuclide retardation than observed in Frenchman Flat alluvium. This suggests that heterogeneous radionuclide retardation in the Pahute Mesa hydrostratigraphic units (at least in the case of the TC unit) will have a much greater effect on the transport of sorbing radionuclides than in the Frenchman Flat alluvium case.

8. Recommendations

We make the following recommendations for upscaling retardation in the Frenchman Flat alluvium porous-flow case:

- The methodology described in Section 4 should be used, in conjunction with available measured K_d data, to calculate large-scale CAU model radionuclide K_{ds} in Frenchman Flat alluvium.
- Uncertainties of $\pm 0.5 \log K_d$ represent the uncertainty in upscaled mechanistic model reaction constants.
- Recent ER-5-4 mineral abundance data is extensive and more precise than data used in earlier Frenchman Flat HST models. The depth averaged mineral abundances provide the best estimate of average Frenchman Flat alluvium mineralogy.
- The redox behavior of Pu needs further study. At present, uncertainty in Pu redox behavior can be estimated by sensitivity analyses over a range of $O_2(g)$ fugacities from 10^{-5} to 10^{-15} bars, the range over which Pu(V) is the dominant oxidation state in solution.
- Based on 3D simulations reported here, it appears that the peak breakthrough of radionuclides can be predicted by the average radionuclide K_{ds} in Frenchman Flat alluvium (i.e. heterogeneous distribution of K_d may not need to be included in large-scale models). However, a critical examination of permeability variability in alluvium needs to be examined to confirm this.
- The effect of (K_d and permeability) heterogeneity on dispersion is significant and needs to be examined further.

We make the following recommendation to upscaling retardation for the Pahute Mesa fracture-flow case:

- The methodology described in Section 4.2 can be used to calculate large-scale CAU model R_s in fracture flow environments but needs further validation and testing. Furthermore, a more robust colloid model is likely to be necessary.
- Uncertainties of $\pm 0.5 \log K_d$ represent the uncertainty in upscaled mechanistic model reaction constants.
- Differences in radionuclide retardation between hydrostratigraphic units (HSUs of Drellack, 1997) is significant and should be accounted for in CAU scale models.
- Spatially heterogeneous radionuclide retardation in the fracture linings and matrix at the sub-HSU scale needs to be accounted for in large-scale models. A statistical

representation of heterogeneity such as the one described here for Frenchman Flat alluvium may be appropriate but needs further examination.

- Uncertainty in colloid loads and reactivity must be further investigated as this comprises one of the largest uncertainties in predicting R_s for certain radionuclides in fracture flow conditions.
- Colloid-facilitated Pu transport is highly dependent on the redox behavior of Pu. At present, uncertainty should be estimated by incorporating Pu transport sensitivity analyses at $O_2(g)$ fugacities ranging from 10^{-5} to 10^{-15} bars.

9. Acknowledgements

Funding for this investigation was provided by the Environment Restoration Division's Underground Test Area Project at the U.S. Department of Energy, National Nuclear Security Administration, Nevada Site Office. This work was performed under the auspices of the U.S. Department of Energy by Lawrence Livermore National Laboratory under contract number W-7405-Eng-48.

10. References

- Abulaban A. and Nieber J. L. (2000) Modeling the effects of nonlinear equilibrium sorption on the transport of solute plumes in saturated heterogeneous porous media. *Advances in Water Resources* **23**(8), 893–905.
- Beiriger W. (1977) X-ray Analysis of 36 Samples from Ue5n (ed. L. D. Ramspott).
- Bethke C. M. (1998) The Geochemist's Workbench: Release 3.0. University of Illinois.
- Blankenagel R. K. and Weir J. E., Jr. (1973) Geohydrology of the Eastern Part of Pahute Mesa, Nevada Test Site, Nye County, Nevada. 712-B, U.S. Geological Survey, Washington D.C.
- Bowen S.M., Finnegan D. L., Thompson J. L., Miller C. M., Baca P. L., Olivas L. F., Geoffrion C. G., Smith D. K., Goishi W., Esser B. K., Meadows J. W., Nambookiri N., Wild J. F. (2001) Nevada Test Site Radionuclide Inventory: 1951-1992. LA-13859-MS, Los Alamos National Laboratory, Los Alamos, New Mexico.
- Bradbury M. H. and Baeyens B. (1997) A mechanistic description of Ni and Zn sorption on Na- montmorillonite .2. Modeling. *Journal of Contaminant Hydrology* **27**(3-4), 223–248.
- Carle S. F., Zavarin M., and Pawloski G. A. (2002) Geostatistical Analysis of Spatial Variability of Mineral Abundance and K_d in Frenchman Flat, NTS, Alluvium. Draft, Lawrence Livermore National Laboratory, Livermore, California.

- Carlos B. A., Chipera S. J., and Bish D. L. (1995) Distribution and Chemistry of Fracture–Lining Minerals at Yucca Mountain, Nevada. LA–12977–MS, Los Alamos National Laboratory, Los Alamos.
- Daniels W. R. and Thompson J. L. (1984) Laboratory and Field Studies Related to the Radionuclide Migration Project, October 1, 1982 to September 30, 1983. LA–10121–PR, Lawrence Livermore National Laboratory, Los Alamos, New Mexico.
- Davis J. A., Coston J. A., Kent D. B., and Fuller C. C. (1998) Application of the surface complexation concept to complex mineral assemblages. *Environmental Science & Technology* **32**(19), 2820–2828.
- Deutsch C. V. and Journel A. G. (1998) *Geostatistical Software Library and User's Guide*. Oxford University Press.
- Drellack S. L., Jr., Prothro L. B., Roberson K. E., Schier B. A., Stevens D. B., and Price E. H. (1997) Analysis of Fractures in Volcanic Cores from Pahute Mesa, Nevada Test Site. DOE/NV/11718–160, Bechtel Nevada, Las Vegas.
- Duff M. C. and Amrhein C. (1996) Uranium(VI) adsorption on goethite and soil in carbonate solutions. *Soil Science Society of America Journal* **60**(5), 1393–1400.
- Duff M. C., Hunter D. B., Triay I. R., Bertsch P. M., Reed D. T., Sutton S. R., Shea-Mccarthy G., Kitten J., Eng P., Chipera S. J., and Vaniman D. T. (1999) Mineral associations and average oxidation states of sorbed Pu on tuff. *Environmental Science & Technology* **33**(13), 2163–2169.
- Dzombak D. A. and Morel F. M. M. (1990) *Surface complexation modeling : hydrous ferric oxide*. Wiley.
- Erikson S. J. (1991) Report of Drilling and Radionuclide Migration Investigations at UE20n#1, Pahute Mesa, Nevada Test Site, 1987. DOE/NV/10384–35, Desert Research Institute, University of Nevada System, Las Vegas.
- Garabedian S. P., Gelhar L. W., and Celia M. A. (1988) Large-scale dispersive transport in aquifers: Field experiments and reactive transport theory. Tech. Report 315, R.M. Parsons Laboratory, Department of Civil Engineering, Massachusetts Institute of Technology, Cambridge, MA.
- Helgeson H. C. (1969) Thermodynamics of hydrothermal systems at elevated temperatures and pressures. *American J. Science* **267**, 729–804.
- Hsi C. D. and Langmuir D. (1985) Adsorption of uranyl onto ferric oxyhydroxides; application of the surface complexation site–binding model. *Geochimica et Cosmochimica Acta* **49**(9), 1931–1941.

- IT Corporation. (1997) Regional Groundwater Flow and Tritium Transport Modeling and Risk Assessment of the Underground Test Area, Nevada Test Site. DOE/NV--477; ITLV/10972–181, Prepared for DOE/NV by IT Corporation, Las Vegas, NV.
- IT Corporation. (1998) Summary of Micrographic Analysis of Fracture Coating Phases on Drill Cores from Pahute Mesa, Nevada Test Site. DOE/NV/13052–050, IT Corporation, Las Vegas.
- IT Corporation. (1999) Underground Test Area Project, Corrective Action Unite 98: Frenchman Flat. Volume 2: Groundwater Data Documentation Package. DOE/NV/13052–044–V2 DRAFT, IT Corporation,
- IT Corporation. (1999, Draft) Modeling of Carbon–14 Transport in the Vicinity of Pahute Mesa and Oasis Valley, Nevada. IT Corporation, Las Vegas, NV.
- Johnson J. W. and Lundein S. R. (1997) GEMBOCHS thermodynamic datafiles for use with the EQ3/6 modeling package. Lawrence Livermore National Laboratory, Livermore.
- Jones B. F. (1982) Mineralogy of Fine Grained Alluvium from Borehole U11g, Expl. 1, Northern Frenchman Flat Area, Nevada Test Site. Open–File Report 82–765, U.S. Geological Survey,
- Keeney–Kennicutt W. L. and Morse J. W. (1984) The interaction of Np(V)O_2^+ with common mineral surfaces in dilute aqueous solutions and seawater. *Marine Chemistry* **15**, 133–150.
- Keeney–Kennicutt W. L. and Morse J. W. (1985) The redox chemistry of Pu(V)O_2^+ interaction with common mineral surfaces in dilute solutions and seawater. *Geochimica et Cosmochimica Acta* **49**(12), 2577–2588.
- Kersting A. B. and Brachman A. (1998) Progress Report FY98: Characterization of Groundwater Colloids from ER20–5 Well Cluster. UGTA Internal Report, Lawrence Livermore National Laboratory, Livermore.
- Kersting A. B., Efurd D. W., Finnegan D. L., Rokop D. J., Smith D. K., and Thompson J. L. (1999) Migration of plutonium in ground water at the Nevada Test Site. *Nature* **397**(6714), 56–59.
- Koeppenkastrop D. and Decarlo E. H. (1992) Sorption of Rare–Earth Elements From Seawater Onto Synthetic Mineral Particles – an Experimental Approach. *Chemical Geology* **95**(3–4), 251–263.
- Krishnaswami S., Graustein W. C., Turekian K. K., and Dowd J. F. (1982) Radium, thorium, and radioactive lead isotopes in groundwaters: Application to the in situ

- determination of adsorption–desorption rate constants and retardation factors. *Water Resources Research* **18**(6), 1663–1675.
- Kurbatov M. H., Wood G. B., and Kurbatov J. D. (1951) Isothermal adsorption of cobalt from dilute solutions. *Journal of Physical Chemistry* **55**, 1170–1182.
- Leblanc D. R., Garabedian S. P., Hess K. M., Gelhar L. W., Quadri R. D., Stollenwerk K. G., and Wood W. W. (1991) Large-scale natural gradient tracer test in sand and gravel, Cape Cod, Massachusetts, I. Experiment design and observed tracer movement. *Water Resources Research* **27**(5), 895–910.
- McKinley J. P., Zachara J. M., Smith S. C., and Turner G. D. (1995) The influence of uranyl–hydrolysis and multiple site–binding reaction on adsorption of U(VI) to montmorillonite. *Clays and Clay Minerals* **45**(5), 586–598.
- Miralles-Wilhelm F. and Gelhar L. W. (1996) Stochastic analysis of sorption macrokinetics in heterogeneous aquifers. *Water Resources Research* **32**(6), 1541–1549.
- Moore R. M. and Hunter K. A. (1985) Thorium adsorption in the ocean: Reversibility and distribution amongst particle sizes. *Geochimica et Cosmochimica Acta* **49**, 2253–2257.
- Nitsche H., Gatti R. C., Standifer E. M., Lee S. C., Muller A., Prussin T., Deinhammer R. S., Maurer H., Becraft K., Leung S., and Carpenter S. A. (1993) Measured solubilities and speciations of neptunium, plutonium, and americium in a typical groundwater (J-13) from Yucca Mountain region. LA-12562-MS, Los Alamos National Laboratory, Los Alamos.
- Nitsche H., Roberts K., Prussin T., Muller A., Becraft K., Keeney D., Carpenter S. A., and Gatti R. C. (1994) Measured solubilities and speciations from oversaturated experiments on neptunium, plutonium, and americium in UE-25p #1 well water from the Yucca Mountain region. LA-12563-MS, Los Alamos National Laboratory, Los Alamos.
- Painter S., Cvetkovic V., and Turner D. R. (2001) Effect of heterogeneity on radionuclide retardation in the alluvial aquifer near Yucca Mountain, Nevada. *Ground Water* **39**(3), 326–338.
- Pawloski G. A., Tompson A. F. B., Bruton C. J., and Zavarin M., Eds. (2000) Evaluation of the Hydrologic Source Term from Underground Nuclear Tests in Frenchman Flat and the Nevada Test Site (U). Contributors: W.L. Bourcier, C.J. Bruton, S.F. Carle, B.K. Esser, A.B. Kersting, R.M. Maxwell, G.A. Pawloski, J.A. Rard, D.E. Shumaker, D.K. Smith, A.F.B. Tompson, and M. Zavarin. UCRL-ID-138007, Lawrence Livermore National Laboratory, Livermore, California.

- Pawloski G. A., Tompson A. F. B., and Carle S. F. (2001) Evaluation of the Hydrologic Source Term from Underground Nuclear Tests on Pahute Mesa at the Nevada Test Site: The CHESHIRE Test, Bourcier, W.L., Bruton, C.J., Carle, S.F., Daniels, J.I., Maxwell, R.M., Pawloski, G.A., Shumaker, D.S., Smith, D.K., Tompson, A.F.B., and Zavarin, M., Contributors. UCRL-ID-147023, Lawrence Livermore National Laboratory, Livermore, California.
- Prothro L. B. and Drellack S. L., Jr. (1997) Nature and Extent of Lava-Flow Aquifers Beneath Pahute Mesa, Nevada Test Site. DOE/NV/11718-156, Bechtel Nevada, Las Vegas.
- Rai D., Hess N. J., Felmy A. R., Moore D. A., Yui M., and Vitorge P. (1999) A thermodynamic model for the solubility of PuO₂(am) in the aqueous K⁺-HCO₃⁻-CO₃²⁻-OH-H₂O system. *Radiochimica Acta* **86**(3-4), 89-99.
- Ramspott L. D. and McArthur R. D. (1977) Results of the Exploratory Drill Hole Ue5n, Frenchman Flat, Nevada Test Site. UCID-128000, Lawrence Livermore National Laboratory, Livermore, California.
- Rose T. P. (2001) Water Chemistry of Frenchman Flat.
- Rose T. P., Keneally J. M., Smith D. K., Davisson M. L., Hudson G. B., and Rego J. H. (1997) Chemical and Isotopic Data for Groundwater in Southern Nevada. UCRL-ID-128000, Lawrence Livermore National Laboratory, Livermore, CA.
- Sanchez A. L., Schell W. R., and Sibley T. H. (1981) Distribution coefficients for plutonium and americium on particulates in aquatic environments. *Environmental Migration of Long-Lived Radionuclides*.
- Shaw Environmental, Inc. (2003) Contaminant Transport Parameters for the Groundwater Flow and Contaminant Transport Model of Corrective Action Units 101 and 102: Central and Western Pahute Mesa, Nye County, Nevada, Shaw/13052-201, Revision No.: 0, August, 2003.
- Smith D. K. (2001) Unclassified Radiologic Source Term for Nevada Test Site Areas 19 and 20. Lawrence Livermore National Laboratory, Livermore, CA.
- Smith D. K., Kersting A. B., Rose T. P., Keneally J. M., Hudson G. B., Eaton G. F., and Davisson M. L. (1998) Hydrologic Resources Management Program and Underground Test Area Operable Unit, FY 1997 Progress Report. UCRL-ID-130792, Lawrence Livermore National Laboratory, Livermore.
- Smith D. K., Kersting A. B., Rose T. P., Keneally J. M., Hudson G. B., Eaton G. F., Davisson M. L., Benedict F. C. J., and Criss R. E. (1999) Hydrologic Resources Management Program and Underground Test Area, FY 1998. UCRL-ID-135170, Lawrence Livermore National Laboratory, Livermore, CA.

- Tompson A. F. B. (1993) Numerical simulation of chemical migration in physically and chemically heterogeneous porous media. *Water Resources Research* **29**(11), 3709–3726.
- Tompson A. F. B., Bruton C. J., and Pawloski G. A. (1999) Evaluation of the hydrologic source term from the underground nuclear tests in Frenchman Flat and the Nevada Test Site: The CAMBRIC test. UCRL-ID-132300, Lawrence Livermore National Laboratory, Livermore.
- Tompson A. F. B. and Jackson K. J. (1996) Reactive transport in heterogeneous systems: An overview. In *Reactive Transport in Porous Media*, Vol. 34 (ed. P. C. Lichtner, C. I. Steefel, and E. H. Oelkers), pp. 269–310.
- Tompson A. F. B., Schafer A. L., and Smith R. W. (1996) Impacts of physical and chemical heterogeneity on co-contaminant transport in a sandy porous medium. *Water Resources Research* **32**(4), 801–801.
- Tompson A. F. B., Zavarin M., Bruton C. J., and Pawloski G. A. (2001) Simplified Hydrologic Source Term for Frenchman Flat Sensitivity Studies. Internal Report, Lawrence Livermore National Laboratory, Livermore, California.
- Turner G. D., Zachara J. M., McKinley J. P., and Smith S. C. (1996) Surface charge properties and UO₂⁺ adsorption of a subsurface smectite. *Geochimica et Cosmochimica Acta* **60**(18), 3399–3414.
- Vaniman D., Furlano A., Chipera S., Thompson J., and Triay I. (1995) Microautoradiography in studies of Pu(V) sorption by trace and fracture minerals in tuff. In *Scientific Basis for Nuclear Waste Management XIX*, Vol. 412 (ed. W. M. Murphy and D. A. Knecht), pp. 639–646. Material Research Society.
- Viani B. E. and Bruton C. J. (1992) Modeling fluid–rock interaction at Yucca Mountain, Nevada: A progress report. UCRL-ID-109921, Lawrence Livermore National Laboratory, Livermore, CA.
- Viani B. E. and Bruton C. J. (1996) Assessing the role of cation exchange in controlling groundwater chemistry during fluid mixing in fractured granite at Aspo, Sweden. UCRL-JC-121527, Lawrence Livermore National Laboratory, Livermore, CA.
- Warren R. G., Benedict F. C., Jr., Rose T. P., Smith D. K., Chipera S. J., Kluk E. C., and Raven K. M. (2002) Alluvial Layering and Distribution of Reactive Phases within Drill Holes ER5/4 and UE5n of Frenchman Flat. LA-UR-02-XXXX, Los Alamos National Laboratory, Los Alamos, New Mexico.
- Warren R. G., Sawyer D. A., Byers F. M., Jr., and Cole G. L. (2000) A Petrographic/Geochemical Database and Stratigraphic Framework for the Southwestern Nevada Volcanic Field, Vol. 2000. National Oceanic and Atmospheric Administration.

- Wolfsberg K. (1978) Sorption–desorption studies of Nevada Test Site alluvium and leaching studies of nuclear test debris. LA-7216-MS, Los Alamos National Laboratory, Los Alamos.
- Zachara J. M., Cowan C. E., and Resch C. T. (1993) Metal cation/anion adsorption on calcite carbonate. In *Metals in groundwater* (ed. H. E. Allen, E. M. Perdue, and D. S. Brown), pp. 37–71. Lewis Publishers.
- Zachara J. M., Resch C. T., and Smith S. C. (1994) Influence of humic substances on Co²⁺ sorption by a subsurface mineral separate and its mineralogic components. *Geochimica et Cosmochimica Acta* **58**(2), 553–566.
- Zavarin M. (2002) Matrix Diffusion and Colloid–Facilitated Transport in Fractured Rock: Model and Parameter Validation. UCRL-ID-149817, Lawrence Livermore National Laboratory, Livermore, CA.
- Zavarin M. and Bruton C. J. (2000a) A Non-Electrostatic Surface Complexation Approach to Modeling Radionuclide Migration at the Nevada Test Site: Aluminosilicates. UCRL-ID-141840 DR, Lawrence Livermore National Laboratory, Livermore.
- Zavarin M. and Bruton C. J. (2000b) A Non-Electrostatic Surface Complexation Approach to Modeling Radionuclide Migration at the Nevada Test Site: Iron Oxides and Calcite. UCRL-ID-141841 DR, Lawrence Livermore National Laboratory, Livermore.
- Zavarin M., Roberts S. K., Rose T. P., and Phinney D. L. (2002) Validating Mechanistic Sorption Model Parameters and Processes for Reactive Transport in Alluvium. UCRL-ID-149728, Lawrence Livermore National Laboratory, Livermore, California.
- Zhong S. J. and Mucci A. (1995) Partitioning of rare earth elements (REEs) between calcite and seawater solutions at 25-degrees-C and 1 atm, and high dissolved REE concentrations. *Geochimica et Cosmochimica Acta* **59**(3), 443–453.

Appendix A. The Mechanistic Sorption Model

The data presented below document the information used to calculate the distribution coefficients (K_d s) and retardation factors (R_s) presented in this report. This appendix includes all surface complexation constants, ion exchange constants, mineral surface properties, and aqueous complexation constants used to define radionuclide K_d s/ R_s . The methods used to implement our mechanistic models are also discussed.

A.1 Sorption reactions included in the sorption model

Table A1 lists the radionuclide–mineral surface complexation reactions accounted for in our reactive transport model. Table A2 lists the ion exchange reactions accounted for in our model. In all cases, isotopes of the same element were treated identically. While the radionuclide–mineral reactions used in our near-field HST model represent a large proportion of reactions expected to control radionuclide migration in the near field, several notable reactions are missing. In particular, manganese oxide minerals may play an important role in decreasing radionuclide migration but published sorption data are scarce. Data from Keeney–Kennicutt and Morse (1985) suggest that Pu sorbs more strongly to goethite (an iron oxide) and calcite than δ -MnO₂ (a manganese oxide). Vaniman et al. (1995) found that Pu was most strongly associated with smectite in fracture linings while Pu sorbed strongly to disordered Mn–oxides in the bulk tuff (Duff et al., 1999). Data in Keeney–Kennicutt and Morse (1984) suggests that calcite and goethite sorb Np much more strongly than δ -MnO₂ or Na–montmorillonite (a smectite). Although these data suggest that manganese oxides may not be the primary sorbers, the sorptive capacity of the many different manganese oxide minerals still need to be examined. Additional data regarding the interaction of radionuclides with manganese oxide minerals would likely result in a more accurate description of radionuclide migration; the absence of such data results in a more conservative measure of radionuclide migration.

In addition to the absence of manganese oxide reactions, some radionuclide–mineral interactions were approximated. For Sm(III), data regarding sorption to iron oxides and aluminosilicates was not available in the literature. Thus, surface complexation constants were assumed to be equivalent to those of Eu(III). This is not altogether unreasonable; rare earth elements (REEs) are often assumed to behave similarly, with K_d s decreasing slightly with increased REE Z (see calcite data in Zhong and Mucci (1995) and goethite data in Koeppenkastrop and Decarlo (1992)).

Table A1. Radionuclide–mineral interaction described by non-electrostatic surface complexation.

Element	Iron Oxide	Calcite	Aluminosilicate [†]
Am(III)	✓	✓	✓
⁴¹ Ca(II)	–	✓	‡
Cs(I)	§	§	‡
Eu(III)	✓	✓	✓
Np(V)	✓	✓	✓
Pu(IV)	✓	✓	✓
Pu(V)	✓	✓	✓
Sm(III)	§	✓	§
Sr(II)	✓	✓	‡
U(VI)	✓	✓	✓

[†] Surface complexation to aluminosilicates modeled assuming smectite to be the dominant reactive aluminosilicate.

[‡] Sorption to aluminosilicates via ion exchange

[§] This radionuclide–mineral interaction was not taken into account but is known to be relatively insignificant

[§] Sm(III)–iron oxide and Sm–aluminosilicate interaction was estimated using the reaction constants of Eu(III) because data was not available.

Table A2. Radionuclide–mineral interaction described by Vanselow ion exchange.

Element	smectite	illite/mica [‡]	zeolite (clino–)
Na ⁺	✓	✓	✓
K ⁺	✓	✓	✓
Ca ^{2+§}	✓	✓	✓
Mg ²⁺	✓	✓	§
Cs ⁺	✓	✓	✓
Sr ²⁺	✓	✓	✓
UO ₂ ²⁺	†	†	†

[†] sorption of actinides and REEs to aluminosilicates dominated by surface complexation in most cases.

[‡] 3 site types on illite/mica with varying affinities.

[§] Mg²⁺ does not exchange readily into the inner channels of clinoptilolite (clino–).

[§] Both background (stable) and test-related (⁴¹Ca) isotopes were accounted for and their reactivity was assumed to be equal.

A.2 Defining surface complexation reactions

Surface complexation (SC) reactions involve mineral surface functional groups and aqueous species. A typical surface complexation reaction and associated equilibrium constant can be written in the following manner:



$$K = \frac{(>\text{SiOPu}^{3+})(\text{H}^+)}{(>\text{SiOH})(\text{Pu}^{4+})} \quad (\text{A2})$$

where $>\text{SiOH}$ is a surface functional group (on a silicate mineral), Pu^{4+} is an aqueous Pu species that reacts with the surface (to form $>\text{SiOPu}^{3+}$), and H^+ is released as a result of the reaction. Just as for simple aqueous complexation reactions, the above surface complexation reaction has an equilibrium reaction constant, K , that describes the relative activity of all species at equilibrium.

Factors that influence surface complexation on a particular mineral include:

- Surface area
- pH
- Aqueous complexation
- Ionic strength
- Surface charge

Since sorption reactions occur at the mineral–water interface, sorption will be dependent on the mineral surface area available for reaction. The pH can significantly affect sorption as well. For example, in Equation (A1), as the concentration of H^+ increases, a larger fraction of Pu^{4+} will remain in solution. Surface functional groups (e.g. $>\text{SiOH}$) may also become protonated/deprotonated as a function of pH and affect sorption.

Aqueous complexation will influence the concentration of aqueous species in solution; this may increase or decrease sorption depending on the species involved in the reactions. For example, U sorption decreases as a function of carbonate concentration in solution due to the formation of uranyl carbonate complexes (Duff and Amrhein, 1996). Ionic strength may influence sorption by reducing the effective concentration (i.e. activity) of aqueous species and affect the charging behavior of the surface. Surface complexes as well as surface protonation and deprotonation can also affect the charging of the surface which will, in turn, influence sorption. Unlike K_d s, surface complexation reactions can, ideally, account for all factors that influence the ratio of sorbed to aqueous radionuclide concentrations. Because surface complexation reactions account for changes in environmental conditions, they provide a much more robust basis for simulating radionuclide sorption.

Here, we use the non-electrostatic surface complexation model (NEM). The NEM (Kurbatov et al., 1951) assumes that surface electrical charge does not affect equilibrium surface complexation reactions. Although the NEM over-simplifies the factors affecting surface complexation, several investigators have used this model approach to describe sorption reactions (Bradbury and Baeyens, 1997; Davis et al., 1998; Zachara et al., 1994). Davis et al. (1998) argued that the NEM approach may be the most appropriate for complex environmental applications since the surface charging behavior of non-ideal natural mineral phases is not well known. For additional information regarding the non-electrostatic model and data, see Zavarin and Bruton (2000a; 2000b) and the model update in Zavarin et al. (2002).

A.3 Defining ion exchange reactions

The permanent charge on some clay minerals is the result of non-charge-balanced ion substitution. For example, the substitution of Si^{4+} for Al^{3+} in a clay will result in a permanent negative charge. A permanent negative charge is typically balanced by cations in solution that are attracted to the mineral surface. For example, the aluminosilicate montmorillonite will typically have a permanent negative charge equal to ~800 meq/kg. In soils, the majority of this charge is balanced by the major cations in the waters (Na^+ , K^+ , Ca^{2+} , and Mg^{2+}). When other cations such as Cs^+ are present, they may also become associated with the negatively charged surface via ion exchange. The distribution of cations on surfaces as a result of permanent charge can be described by ion exchange reactions of the following form:



with an associated equilibrium constant :

$$K = \frac{(\text{Cs-X})(\text{Na}^+)}{(\text{Na-X})(\text{Cs}^+)} \quad (\text{A4})$$

where “X” designates a surface association and the four terms in parentheses are the activities of the respective species. For homovalent exchange such as the reaction shown here, the activity of surface-associated species is often assumed to be defined by the relative concentration of each species ($\frac{[\text{Cs-X}]}{[\text{Cs-X}] + [\text{Na-X}]}$ and $\frac{[\text{Na-X}]}{[\text{Cs-X}] + [\text{Na-X}]}$).

Because the denominators for Cs-X and Na-X activity are identical, the activity ratio of surface species can be simplified to the total mol ratio of Cs and Na associated with the mineral surface. The activity of species in solution are determined from speciation and ionic strength activity corrections. The constant, K , describes the relative activity of the various species at equilibrium.

For heterovalent ion exchange, the equilibrium reactions are complicated by the fact that the two exchanging ions balance different amounts of charge on the surface. Heterovalent ion exchange reactions can be written in several forms. By the Vanselow convention, a

heterovalent exchange reaction is written in a form that relates to the relative mol concentration of surface species:



with an associated equilibrium constant of the form:

$$K = \frac{(\text{Ca-X}_2)^{0.5} (\text{Na}^+)}{(\text{Na-X})(\text{Ca}^{2+})^{0.5}} \quad (\text{A6})$$

The two terms in the above equation that relate to surface species activity are determined by:

$$\left(\frac{[\text{Ca-X}_2]}{([\text{Ca-X}_2] + [\text{Na-X}])} \right)^{0.5} \text{ and } \left(\frac{[\text{Na-X}]}{([\text{Ca-X}_2] + [\text{Na-X}])} \right) \quad (\text{A7})$$

where the terms in the brackets relate to mol/L concentrations. For more information regarding the Vanselow and other ion exchange conventions, see Zavarin and Bruton (2000a; 2000b).

A.4 Surface complexation and ion exchange reaction constants

All surface complexation and ion exchange reactions used in our near-field HST model are listed in Tables A3 – A6. The reaction constants were calculated by fitting published or collected sorption data to the NEM and Vanselow models or by using published reaction constants directly. References to the large set of sorption data used are listed in Zavarin and Bruton (2000a; 2000b). When multiple sets of data were evaluated, a standard deviation was calculated for each reaction constant. These values can be used to evaluate the uncertainty in reaction constants and, in turn, radionuclide sorption. An update to the mechanistic model was reported in Zavarin et al. (2002) based on additional batch and flowthrough sorption data. This updated model is used here.

Table A3. Surface complexation reaction for iron oxides using the NEM.

Reaction	# of Curves Evaluated	Log K
$>\text{FeOH} \leftrightarrow \text{FeO}^- + \text{H}^+$		-8.93
$>\text{FeOH} + \text{H}^+ \leftrightarrow \text{FeOH}_2^+$		7.29
$>\text{FeOH} + \text{Am}^{3+} \leftrightarrow >\text{FeOAm}^{2+} + \text{H}^+$	11	1.24 ± 0.43
$>\text{FeOH} + \text{Am}^{3+} + 2\text{H}_2\text{O} \leftrightarrow >\text{FeOAm(OH)}_2 + 3\text{H}^+$		-15.29 ± 0.37
$>\text{FeOH} + \text{Eu}^{3+} \leftrightarrow >\text{FeOEu}^{2+} + \text{H}^+$	11	1.85 ± 0.58
$>\text{FeOH} + \text{NpO}_2^+ \leftrightarrow >\text{FeOHNPo}_2^+$	10	4.32 ± 0.11
$>\text{FeOH} + \text{NpO}_2^+ + \text{H}_2\text{O} \leftrightarrow >\text{FeOHNPo}_3^- + 2\text{H}^+$		-11.26
$>\text{FeOH} + \text{Pu}^{4+} + \text{H}_2\text{O} \leftrightarrow >\text{FeOHPuO}^{2+} + 2\text{H}^+$	2	6.93
$>\text{FeOH} + \text{Pu}^{4+} + 2\text{H}_2\text{O} \leftrightarrow >\text{FeOHPuO}_2 + 4\text{H}^+$		-1.29
$>\text{FeOH} + \text{PuO}_2^+ \leftrightarrow >\text{FeOHPuO}_2^+$	2	4.79
$>\text{FeOH} + \text{PuO}_2^+ + \text{H}_2\text{O} \leftrightarrow >\text{FeOHPuO}_3^- + 2\text{H}^+$		-10.66
$>\text{FeOH} + \text{Sr}^{2+} \leftrightarrow >\text{FeOHSr}^{2+}$	12	2.22 ± 0.13
$>\text{FeOH} + \text{Sr}^{2+} \leftrightarrow >\text{FeOSr}^+ + \text{H}^+$		-5.30 ± 0.31
$>\text{FeOH} + \text{Sr}^{2+} + \text{H}_2\text{O} \leftrightarrow >\text{FeOSrOH} + 2\text{H}^+$		-14.14 ± 0.40
$>\text{FeOH} + \text{UO}_2^{2+} + \text{H}_2\text{O} \leftrightarrow >\text{FeOHUO}_3 + 2\text{H}^+$	17	-3.05 ± 0.43
$>\text{FeOH} + \text{UO}_2^{2+} \leftrightarrow >\text{FeOHUO}_2^{2+}$		6.63 ± 0.54

Table A4. Surface complexation reactions for calcite using the NEM.

Reaction	# of Curves Evaluated	Log K
$>\text{Ca}^{2+} + \text{AmCO}_3^+ \leftrightarrow >\text{AmCO}_3^+ + \text{Ca}^{2+}$	10 ^a	4.13 ± 0.06
$>\text{Ca}^{2+} + \text{EuCO}_3^+ \leftrightarrow >\text{EuCO}_3^+ + \text{Ca}^{2+}$	1	4.14
$>\text{Ca}^{2+} + \text{NpO}_2^+ \leftrightarrow >\text{NpO}_2^+ + \text{Ca}^{2+}$	1	1.46
$>\text{Ca}^{2+} + \text{PuO}_2^+ \leftrightarrow >\text{PuO}_2^+ + \text{Ca}^{2+}$	1	1.63
$>\text{Ca}^{2+} + \text{Pu(OH)}_3^+ \leftrightarrow >\text{Pu(OH)}_3^+ + \text{Ca}^{2+}$	1	7.23
$>\text{Ca}^{2+} + \text{SmCO}_3^+ \leftrightarrow >\text{SmCO}_3^+ + \text{Ca}^{2+}$	1	4.62
$>\text{Ca}^{2+} + \text{Sr}^{2+} \leftrightarrow >\text{Sr}^{2+} + \text{Ca}^{2+}$	1	-1.75
$>\text{Ca}^{2+} + \text{UO}_2^{2+} \leftrightarrow >\text{UO}_2^{2+} + \text{Ca}^{2+}$	17 ^a	5.12

^a Single point data

Table A5. Surface complexation reactions for aluminosilicates using the NEM.

Reaction	# of Curves Evaluated	Log K
$>\text{AlOH} + \text{Am}^{3+} \leftrightarrow >\text{AlOAm}^{2+} + \text{H}^+$	11	2.49 ± 0.26
$>\text{SiOH} + \text{Am}^{3+} \leftrightarrow >\text{SiOAm}^{2+} + \text{H}^+$	4	0.7 ± 0.1
$>\text{SiOH} + \text{Am}^{3+} + \text{H}_2\text{O} \leftrightarrow >\text{SiOAmO} + 3\text{H}^+$		-14.2 ± 0.8
$>\text{AlOH} + \text{Eu}^{3+} \leftrightarrow >\text{AlOEu}^{2+} + \text{H}^+$	5	2.21 ± 0.54
$>\text{SiOH} + \text{Eu}^{3+} \leftrightarrow >\text{SiOEu}^{2+} + \text{H}^+$	4	-0.62
$>\text{SiOH} + \text{Eu}^{3+} + \text{H}_2\text{O} \leftrightarrow >\text{SiOEuO} + 3\text{H}^+$		-15.30
$>\text{AlOH} + \text{NpO}_2^+ \leftrightarrow >\text{AlONpO}_2 + \text{H}^+$	9	-4.67 ± 0.27
$>\text{AlOH} + \text{NpO}_2^+ + \text{H}_2\text{O} \leftrightarrow >\text{AlONpO}_3\text{H}^- + 2\text{H}^+$		-14.26 ± 0.04
$>\text{SiOH} + \text{NpO}_2^+ \leftrightarrow >\text{SiONpO}_2 + \text{H}^+$	6	-3.72 ± 0.15
$>\text{SiOH} + \text{NpO}_2^+ + \text{H}_2\text{O} \leftrightarrow >\text{SiONpO}_3\text{H}^- + 2\text{H}^+$		-12.16
$>\text{AlOH} + \text{Pu}^{4+} + \text{H}_2\text{O} \leftrightarrow >\text{AlOPuO}^+ + 3\text{H}^+$	4	5.95 ± 0.47
$>\text{AlOH} + \text{Pu}^{4+} + 2\text{H}_2\text{O} \leftrightarrow >\text{AlOPuO}_2^- + 5\text{H}^+$		-11.93
$>\text{SiOH} + \text{Pu}^{4+} + \text{H}_2\text{O} \leftrightarrow >\text{SiOPuO}^+ + \text{H}^+$		2.32 ± 0.89
$>\text{AlOH} + \text{PuO}_2^+ \leftrightarrow >\text{AlOPuO}_2 + \text{H}^+$	2	-3.09
$>\text{SiOH} + \text{PuO}_2^+ \leftrightarrow >\text{SiOPuO}_2 + \text{H}^+$	2	-6.43
$>\text{SiOH} + \text{PuO}_2^+ + \text{H}_2\text{O} \leftrightarrow >\text{SiOPuO}_3\text{H}^- + 2\text{H}^+$		-14.80
$>\text{AlOH} + \text{UO}_2^{2+} \leftrightarrow >\text{AlOUO}_2^+ + \text{H}^+$	5	3.13 ± 0.15
$>\text{SiOH} + \text{UO}_2^{2+} + \text{H}_2\text{O} \leftrightarrow >\text{SiOUO}_3\text{H} + 2\text{H}^+$	15	-5.18 ± 0.31
$>\text{SiOH} + \text{UO}_2^{2+} + \text{H}_2\text{O} \leftrightarrow >\text{SiOUO}_3^- + 3\text{H}^+$		-12.35

Table A6. Vanselow ion exchange reactions for smectite, mica, and clinoptilolite.

Exchange Reaction	Log K	Site Type
SMECTITE [†]		
$\text{Na}^+ \rightarrow 0.5 \text{Ca}^{2+}, 0.5 \text{Mg}^{2+}$	0.0	
$\text{Na}^+ \rightarrow 0.5 \text{Sr}^{2+}$	-0.2	
$\text{Na}^+ \rightarrow \text{K}^+$	0.255	
$\text{Na}^+ \rightarrow \text{Cs}^+$	1.75	
$0.5 \text{Ca}^{2+} \rightarrow 0.5 \text{UO}_2^{2+}$	-0.125	
$\text{Na}^+ \rightarrow 0.5 \text{UO}_2^{2+}$	-0.040	
ILLITE/MICA [‡]		
$\text{Na}^+ \rightarrow 0.5 \text{Ca}^{2+}, 0.5 \text{Mg}^{2+}, 0.5 \text{Sr}^{2+}$	-0.375	I
	-0.147	II
	0.000	III
$\text{Na}^+ \rightarrow \text{K}^+$	1.613	I
	1.686	II
	0.894	III
$\text{Na}^+ \rightarrow \text{Cs}^+$	6.718	I
	3.079	II
	1.539	III
CLINOPTIOLITE [§]		
$\text{Na}^+ \rightarrow \text{K}^+$	1.40	
$\text{Na}^+ \rightarrow \text{Cs}^+$	2.01	
$\text{Na}^+ \rightarrow 0.5 \text{Ca}^{2+}$	0.36	
$\text{Na}^+ \rightarrow 0.5 \text{Sr}^{2+}$	0.25	

[†] 0.425 meq/g smectite

[‡] 0.2 meq/g illite/mica total, 0.005 = I, 0.03 = II, 0.965 = III

[§] 2.12 meq/g clinoptilolite

A.5 Implementation of surface complexation and ion exchange reactions

To use the surface complexation and ion exchange data listed above, several additional mineral characteristics parameters need to be established. These are: surface area, reactive site type, reactive site density, and cation exchange capacity for each mineral. These mineral characteristics parameters are listed in Table A7. For iron oxide, the effective surface area used was based on recent fits to flowthrough experiments performed on U-1a and UE-5n alluvium ($0.25 \text{ m}^2/\text{g}$). This value is significantly lower than typically measured for hematite ($2 \text{ m}^2/\text{g}$, (Hsi and Langmuir, 1985) or goethite ($50 \text{ m}^2/\text{g}$) and was attributed to iron oxide accessibility. The site density was taken from a Dzombak and Morel (1990) estimate of site density on hydrous ferric oxide. Unlike Dzombak and Morel (1990), only one site was used in our model (see Zavarin and Bruton (2000a; 2000b) for further discussion). The calcite effective surface area was based on recent fits to flowthrough and batch experiments ($0.2 \text{ m}^2/\text{g}$); the site density was taken

from Zachara et al. (1993). As in the case of iron oxide, only one site was used in our model. Smectite surface area was taken from McKinley et al. (1995). The site density was determined by estimating that 10% of the smectite surface accounts for edge sites and that the site density at those edge sites is 2.31 per nm². The fraction of >SiOH and >AlOH sites on the smectite is consistent with values proposed in McKinley et al. (1995) and Turner et al. (1996). The cation exchange capacities of smectite, clinoptilolite, and illite were taken from Viani and Bruton (1992; 1996) with some adjustments reported in Zavarin et al. (2002). Surface complexation on illite and clinoptilolite was not included in our model. Our surface complexation model is based on the assumption that >AlOH and >SiOH sites on any aluminosilicate will behave identically. This is an expansion of the modeling approach used by Turner et al. (1996) and others. Thus, surface complexation reactions on clinoptilolite and illite will be equivalent to smectite. Since smectite is the most homogeneously distributed, the most abundant, and has a high surface area, we expect that smectite will be the dominant sorbing aluminosilicate mineral. Clinoptilolite and illite will, nevertheless, contribute significantly to radionuclide sorption via ion exchange.

In our model, all surface complexation and ion exchange reactions are based on an equilibrium model. Thus, irreversible sorption and sorption/desorption kinetics are not employed. Published information regarding the reversibility of sorption vary. For example, Sanchez et al. (1981) showed that K_dS measured from desorption experiments are consistently higher than sorption experiments for both Pu and Am. This indicates that some fraction of the sorbed radionuclide may not desorb. Krishnaswami et al. (1982), on the other hand, examined the sorption/desorption kinetics of Ra and Th in the field using U and Th series radionuclides and found that sorption occurred on the scale of minutes while desorption occurred on the scale of a week or less. This would tend to indicate that sorption and desorption is relatively fast (albeit not instant). Moore and Hunter (1985) found that Th is reversibly sorbed onto suspended sediment particles in the ocean with sorption/desorption rates on the scale of hours, consistent with the observations of Krishnaswami et al. (1982). For the case of radionuclide sorption to reactive minerals, the equilibrium model is a more conservative model of radionuclide migration (however, for the case of radionuclide sorption to colloids, the equilibrium model is less conservative).

Table A7. Mineral characteristics used to define reactions on mineral surfaces.

Mineral	Iron Oxide (hematite)	Calcite	Smectite (montmorillonite)	Zeolite (clinoptilolite)	Illite/Mica (illite)
Density, g/cm ³	5.27	2.71	2.83	2.13	2.83
Surface Area, m ² /g	0.25	0.1	30.0	--	--
Site Density, nm ⁻²	2.31	5.0	0.231	--	--
Site Type	>FeOH	>Ca ²⁺	>SiOH (0.5) >AlOH (0.5) (ion exchange)	(ion exchange)	I (0.005) II (0.03) III (0.965)
CEC, meq/g	--	--	0.425	2.12	0.2

A.6 Aqueous complexation data

Thermodynamic data for aqueous species were taken from version DATACOM.V8.R6 of the GEMBOCHS thermodynamic database (Johnson and Lundein, 1997) with revised and updated thermodynamic data as given in Tompson et al. (1999) and noted below. The thermodynamic data is listed in Tables A8 through A10 below. The choice of aqueous species used in the simulations is based on recent simulations of Pahute Mesa and Frenchman Flat groundwaters (Pawloski et al., 2000; Pawloski et al., 2001; Tompson et al., 1999). Additional aqueous species may be required when modeling conditions in the carbonate aquifer and other geologic units in which groundwater chemistry is significantly different.

The extended Debye–Hückel formulation (also known as the B–DOT model) was used for activity coefficients of aqueous species (Bethke, 1998; Helgeson, 1969). This formulation is well suited to describe the groundwaters at NTS, which possess ionic strengths significantly less than 0.1. Values of the ion size parameter (Bethke, 1998; Helgeson, 1969) for aqueous species added to the database were estimated by analogy to aqueous species of similar valence and ligand. Parameters used in the Debye–Hückel activity coefficient model are listed in Tables A8 and A9.

Table A8. Basis species used in thermodynamic data base.

	Ion size Å†	Mol. Wt. g/mol
H ₂ O	3	18.0
Al ³⁺	9	27.0
Am ³⁺	5	243.0
Ca ²⁺	6	40.1
Cl ⁻	3	35.5
Cs ⁺	2.5	132.9
Eu ³⁺	5	152.0
Fe ²⁺	6	55.8
H ⁺	9	1.0
HCO ₃ ⁻	4	61.0
K ⁺	3	39.1
Mg ²⁺	8	24.3
Na ⁺	4	23.0
Np ⁴⁺	5.5	237.0
Pu ⁴⁺	5.5	244.0
SO ₄ ²⁻	4	96.1
SiO ₂ (aq)	3	60.1
Sm ³⁺	9	150.4
Sr ²⁺	5	87.6
UO ₂ ²⁺	4.5	270.0
O ₂ (aq)	3	32.0

† Ion size parameter used in Debye–Hückel activity coefficient model.

Table A9. Parameters in extended Debye–Hückel activity coefficient model as a function of temperature (°C).

Constants	0 °C	25 °C	60 °C	100 °C	150 °C	200 °C	250 °C	300 °C
A	0.4939	0.5114	0.5465	0.5995	0.6855	0.7994	0.9593	1.218
B	0.3253	0.3288	0.3346	0.3421	0.3525	0.3639	0.3766	0.3925
B'	0.0374	0.041	0.044	0.046	0.047	0.047	0.034	—

Table A10. Logarithm of equilibrium constants (K) of aqueous reactions used in thermodynamic data base. Most Pu data not shown pending approval for publication by the Nuclear Energy Agency.

Reaction	Log K	Ion size [†] Å
$\text{H}_2\text{O} = \text{OH}^- + \text{H}^+$	-14.0	3.5
$\text{Al}^{3+} + 2 \text{H}_2\text{O} = \text{AlO}_2^- + 4 \text{H}^+$	-22.2	4
$\text{HCO}_3^- = \text{CO}_3^{2-} + \text{H}^+$	-10.3	4.5
$\text{Fe}^{2+} + 0.25 \text{O}_2(\text{g}) + \text{H}^+ = \text{Fe}^{3+} + 0.5 \text{H}_2\text{O}$	7.8	9
$\text{Fe}^{3+} + 2 \text{H}_2\text{O} = \text{FeO}_2^- + 4 \text{H}^+$	-21.6	4
$\text{Fe}^{3+} + 2 \text{H}_2\text{O} = \text{HFeO}_2^0 + 3 \text{H}^+$	-12.0	3
$\text{SiO}_2(\text{aq}) + \text{H}_2\text{O} = \text{HSiO}_3^- + \text{H}^+$	-9.6	4
$\text{Ca}^{2+} + \text{HCO}_3^- = \text{CaCO}_3^0 + \text{H}^+$	-7.0	3
$\text{O}_2(\text{aq}) = \text{O}_2(\text{g})$	-2.9	—
$\text{Np}^{4+} + 0.25 \text{O}_2(\text{g}) + 1.5 \text{H}_2\text{O} = \text{NpO}_2^+ + 3 \text{H}^+$	-9.9	4
$\text{NpO}_2^+ + \text{HCO}_3^- = \text{NpO}_2\text{CO}_3^- + \text{H}^+$	-5.7	4
$\text{NpO}_2^+ + \text{H}_2\text{O} = \text{NpO}_2\text{OH}^0 + \text{H}^+$	-8.9	3
$\text{Np}^{4+} + 4 \text{H}_2\text{O} = \text{Np(OH)}_4^0 + 4 \text{H}^+$	-9.6	3
$\text{Am}^{3+} + 2 \text{HCO}_3^- = \text{Am}(\text{CO}_3)_2^- + 2 \text{H}^+$	-8.4	4
$\text{Am}^{3+} + 2 \text{H}_2\text{O} = \text{Am(OH)}_2^+ + 2 \text{H}^+$	-4.1	4
$\text{Am}^{3+} + \text{HCO}_3^- = \text{AmCO}_3^+ + \text{H}^+$	-2.5	4
$\text{Am}^{3+} + \text{H}_2\text{O} = \text{AmOH}^{2+} + \text{H}^+$	-6.4	4.5
$\text{Eu}^{3+} + 2 \text{HCO}_3^- = \text{Eu}(\text{CO}_3)_2^- + 2 \text{H}^+$	-7.7	4
$\text{Eu}^{3+} + 2 \text{H}_2\text{O} = \text{Eu(OH)}_2^+ + 2 \text{H}^+$	-14.9	4
$\text{Eu}^{3+} + \text{HCO}_3^- = \text{EuCO}_3^+ + \text{H}^+$	-2.4	4
$\text{Sm}^{3+} + 2 \text{HCO}_3^- = \text{Sm}(\text{CO}_3)_2^- + 2 \text{H}^+$	-7.9	4
$\text{Sm}^{3+} + \text{HCO}_3^- = \text{SmCO}_3^+ + \text{H}^+$	-2.5	4
$\text{UO}_2^{2+} + 2 \text{HCO}_3^- = \text{UO}_2(\text{CO}_3)_2^{2-} + 2 \text{H}^+$	-3.8	4
$\text{UO}_2^{2+} + 3 \text{HCO}_3^- = \text{UO}_2(\text{CO}_3)_3^{4-} + 3 \text{H}^+$	-9.4	4
$\text{UO}_2^{2+} + \text{H}_2\text{O} = \text{UO}_3^0 + 2 \text{H}^+$	-10.3	3
$\text{UO}_2^{2+} + 2 \text{H}^+ = \text{U}^{4+} + 0.5 \text{O}_2(\text{g}) + \text{H}_2\text{O}$	-32.5	5.5
$\text{U}^{4+} + 2 \text{H}_2\text{O} = \text{UO}_2^0 + 4 \text{H}^+$	-4.6	3
$\text{Pu}^{4+} + 2 \text{HCO}_3^- + 2 \text{H}_2\text{O} = \text{Pu}(\text{OH})_2(\text{CO}_3)_2^{2-} + 4 \text{H}^+$	-2.8§	3

† Ion size parameter, used in Debye–Hückel activity coefficient model, for the aqueous complex formed by the basis species.

§ Speciation constant derived from Rai et al. (1999). Other Pu speciation data will be released in a forthcoming comprehensive NEA publication.

INTENTIONALLY LEFT BLANK

Appendix B. The Gaussian Random Field Approach

For this study, the “Gaussian random field” is used as the conceptual model for describing 3D heterogeneity of both permeability and K_d . Under Gaussian random field assumptions, a normal (Gaussian) frequency distribution is assumed. Spatial correlation is described by a covariance (or variogram) model. The Gaussian random field is the most common stochastic conceptual model used for considering spatial variation of permeability and K_d for reactive transport modeling in hydrology (Abulaban and Nieber, 2000; Garabedian et al., 1988; Miralles-Wilhelm and Gelhar, 1996; Painter et al., 2001; Pawloski et al., 2000; Tompson, 1993; Tompson et al., 1996). In particular, a log-normal distribution and exponentially decaying spatial covariance of permeability or K_d is typically assumed. In some cases, a negative cross-correlation between K_d and permeability is assumed.

In Carle et al. (2002), $\log_{10}[K_d]$ was treated as a random variable after converting mineral concentration data from Frenchman Flat to K_d s based on the component additivity approach. A combination of nugget and exponential variogram model structures were found to provide plausible fits to the experimental vertical variograms of $\log_{10}[K_d]$ for all radionuclides (see Table B.1). Based on limited lateral correlation data, anisotropic 2D variogram models were developed (see Table B.2), having lateral:vertical anisotropy ratios ranging from about 4.5:1 to 13:1. Assuming second-order stationarity, these variogram models can be directly converted to exponentially decaying spatial covariance models. Nugget structure is attributed to small or “micro” scale variability that may either be explicitly included in the random field model or folded into the average or effective K_d s.

The realizations of K_d for each radionuclide were generated using the code “sgsim” from the Geostatistical Software Library (Deutsch and Journel, 1998) based on the variogram models specified in Tables B.1 and B.2. Figures 4 and 5 of Section 5 illustrate 2D cross-sections of the resulting spatial variation of $\log_{10}[K_d]$ for each radionuclide. The differences in the spatial structure of K_d for different radionuclides are attributed to differences in variogram model structure. For example, Am shows spatially correlated regions of relatively low or high K_d , whereas Cs shows only random variation. The variogram model for Am has pronounced spatial correlation, whereas the variogram model for Cs is pure nugget without spatial correlation, which yields only small-scale variability.

Table B1. Parameters for vertical variogram models of $\log_{10}[K_d]$ for radionuclides Ca, Cs, Sr, Am, Eu, Sm, Np, U, and Pu.

Radionuclide	Nugget	Sill	Range (m)	Vertical Variogram Model Equation
Ca	0.015	0.105	150	$?(\mathbf{h}_z) = 0.015 + 0.090 \left[1 - \exp\left(-\frac{3\mathbf{h}_z}{150 \text{ m}}\right) \right]$
Cs	0.040	0.040	0	$?(\mathbf{h}_z) = 0.040$
Sr	0.015	0.12	150	$?(\mathbf{h}_z) = 0.015 + 0.105 \left[1 - \exp\left(-\frac{3\mathbf{h}_z}{150 \text{ m}}\right) \right]$
Am	0.016	0.052	300	$?(\mathbf{h}_z) = 0.016 + 0.036 \left[1 - \exp\left(-\frac{3\mathbf{h}_z}{300 \text{ m}}\right) \right]$
Eu	0.020	0.065	300	$?(\mathbf{h}_z) = 0.020 + 0.045 \left[1 - \exp\left(-\frac{3\mathbf{h}_z}{300 \text{ m}}\right) \right]$
Sm	0.028	0.087	300	$?(\mathbf{h}_z) = 0.028 + 0.059 \left[1 - \exp\left(-\frac{3\mathbf{h}_z}{300 \text{ m}}\right) \right]$
Np	0.020	0.065	400	$?(\mathbf{h}_z) = 0.020 + 0.045 \left[1 - \exp\left(-\frac{3\mathbf{h}_z}{400 \text{ m}}\right) \right]$
U	0.023	0.027	300	$?(\mathbf{h}_z) = 0.023 + 0.004 \left[1 - \exp\left(-\frac{3\mathbf{h}_z}{300 \text{ m}}\right) \right]$
Pu(O ₂ =-5)	0.018	0.043	300	$?(\mathbf{h}_z) = 0.018 + 0.043 \left[1 - \exp\left(-\frac{3\mathbf{h}_z}{300 \text{ m}}\right) \right]$
Pu(O ₂ =-10)	0.017	0.042	300	$?(\mathbf{h}_z) = 0.017 + 0.042 \left[1 - \exp\left(-\frac{3\mathbf{h}_z}{300 \text{ m}}\right) \right]$
Pu(O ₂ =-15)	0.016	0.041	300	$?(\mathbf{h}_z) = 0.016 + 0.041 \left[1 - \exp\left(-\frac{3\mathbf{h}_z}{300 \text{ m}}\right) \right]$

Table B2. Parameters for lateral variogram models of $\log_{10}[K_d]$ for radionuclides Ca, Cs, Sr, Am, Eu, Sm, Np, U, and Pu.

Radionuclide	Nugget	Sill	Range (m)	Lateral Variogram Model Equation
Ca	0.015	0.105	1750	$?(\mathbf{h}_x) = 0.015 + 0.090 \left[1 - \exp\left(-\frac{3\mathbf{h}_x}{1750 \text{ m}}\right) \right]$
Cs	0.040	0.040	0	$?(\mathbf{h}_x) = 0.040$
Sr	0.015	0.12	1800	$?(\mathbf{h}_x) = 0.015 + 0.105 \left[1 - \exp\left(-\frac{3\mathbf{h}_x}{1800 \text{ m}}\right) \right]$
Am	0.016	0.052	3500	$?(\mathbf{h}_x) = 0.016 + 0.036 \left[1 - \exp\left(-\frac{3\mathbf{h}_x}{3500 \text{ m}}\right) \right]$
Eu	0.020	0.065	2400	$?(\mathbf{h}_x) = 0.020 + 0.045 \left[1 - \exp\left(-\frac{3\mathbf{h}_x}{2400 \text{ m}}\right) \right]$
Sm	0.028	0.087	1350	$?(\mathbf{h}_x) = 0.028 + 0.059 \left[1 - \exp\left(-\frac{3\mathbf{h}_x}{1350 \text{ m}}\right) \right]$
Np	0.020	0.065	1750	$?(\mathbf{h}_x) = 0.020 + 0.045 \left[1 - \exp\left(-\frac{3\mathbf{h}_x}{1750 \text{ m}}\right) \right]$
U	0.023	0.027	3000	$?(\mathbf{h}_x) = 0.023 + 0.004 \left[1 - \exp\left(-\frac{3\mathbf{h}_x}{3000 \text{ m}}\right) \right]$
Pu(O ₂ =-5)	0.018	0.043	3900	$?(\mathbf{h}_x) = 0.018 + 0.043 \left[1 - \exp\left(-\frac{3\mathbf{h}_x}{3900 \text{ m}}\right) \right]$
Pu(O ₂ =-10)	0.017	0.042	3900	$?(\mathbf{h}_x) = 0.017 + 0.042 \left[1 - \exp\left(-\frac{3\mathbf{h}_x}{3900 \text{ m}}\right) \right]$
Pu(O ₂ =-15)	0.016	0.041	3900	$?(\mathbf{h}_x) = 0.016 + 0.041 \left[1 - \exp\left(-\frac{3\mathbf{h}_x}{3900 \text{ m}}\right) \right]$

For this study, 3D realizations of both permeability and K_d are needed. Unfortunately, sufficient permeability data were not available to analyze 3D spatial correlation of permeability. Alternatively, a random field model for \log_{10} permeability was developed in a two-step approach:

1. Fourteen permeability data obtained from the Frenchman Flat HST model report (Tompson et al., 1999) were used to establish mean and variance of \log_{10} permeability.
2. Considering that permeability and K_d of Sr are strongly related to clay (smectite) content, the spatial correlation model for \log_{10} permeability is scaled directly to that of $\log_{10}[K_d]$ for Sr.

The x:y:z coordinate dimensions of the 3D realizations are 180:60:150 for a total 1,620,000 cells. The x:y:z grid block size is 100 m:100 m:10 m. The resulting 3D realizations measure 18 km: 6 km: 1.5 km in the x:y:z directions.

The 3D stochastic realizations assume that lateral correlation of both \log_{10} permeability and $\log_{10}[K_d]$ is isotropic. Furthermore, it is recognized that \log_{10} permeability and $\log_{10}[K_d]$ may be spatially cross-correlated. To impart either negative, zero, or positive spatial cross-correlation between \log_{10} permeability and $\log_{10}[K_d]$, the following approach was taken:

- For Sr, perfect positive or negative correlation is imparted by linear scaling of \log_{10} permeability to $\log_{10}[K_d]$, or visa versa.
- For all other radionuclides, $\log_{10}[K_d]$ fields are generated using the variogram models specified in Tables B.1 and B.2. Positively correlated $\log_{10}[K_d]$ fields are generated by using the same “seed” value in the sgsim code as for the \log_{10} permeability field. In this case, the resulting positive correlation is not exactly 1.0. This is realistic considering that the spatial correlation models for \log_{10} permeability and $\log_{10}[K_d]$ are not identical. Negatively correlated fields are created by flipping the sign of the deviation of $\log_{10}[K_d]$ from the mean on the positively correlated fields.
- Zero correlation fields are generated by using a different “seed” value in the sgsim code for both \log_{10} permeability and $\log_{10}[K_d]$.

Table B.3 specifies the correlation of \log_{10} permeability and $\log_{10}[K_d]$ fields for the different 3D random fields used in this study. The seed-based approach produces relatively strong cross-correlations. However, much of this cross-correlation occurs at the “micro-scale” (within a 100 m: 100 m: 10 m grid cell) as part of the small scale spatial variation encapsulated in the “nugget” structure of the variogram. Therefore, although the realizations of log-permeability and $\log_{10}[K_d]$ can be strongly cross-correlated between individual cells, the overall *spatial* cross-correlation is not necessarily large in magnitude.

Table B3. Measured cell-to-cell correlation between realizations of \log_{10} permeability and $\log_{10}[K_d]$ for cases of “positive,” “zero,” and “negative” correlation.

Radionuclide	Positive	Zero	Negative
Ca	0.973	-0.003	-0.973
Cs	0.603	0.000	-0.603
Sr	1.000	-0.003	-1.000
Am	0.861	-0.005	-0.861
Eu	0.906	-0.003	-0.906
Sm	0.897	-0.001	-0.897
Np	0.871	-0.003	-0.871
U	0.727	0.001	-0.727
Pu($O_2=-5$)	0.870	-0.005	-0.870
Pu($O_2=-10$)	0.869	-0.005	-0.869
Pu($O_2=-15$)	0.857	-0.005	-0.857

As discussed by Carle et al. (2002), the $\log_{10}[K_d]$ frequency distributions for Ca and Sr appear bi-modal and thus do not closely conform to the Gaussian random field conceptual model. The $\log_{10}[K_d]$ realizations for Ca and Sr were nonetheless constructed under the assumption of a Gaussian random field. The spatial variation of K_d in these realizations exhibits the largest variations in magnitude compared to other radionuclides, reflecting the high sill parameters of the fitted variogram models. A potential problem with using a Gaussian random field model for Ca and Sr is that the realizations produce a normal distribution of $\log_{10}[K_d]$ values, which will contain an excess of intermediate values instead of two modes of low K_d and high K_d s. Carle et al. (2002) have suggested an alternative multi-scale approach that applies separate Gaussian random field models to each of the two modes. However, this approach was not investigated in this study.

Appendix C. Mineral Abundance and Distribution Coefficient Data for Frenchman Flat Alluvium

The tabulated data below lists the abundance of radionuclide sorbing minerals for each sample of Frenchman Flat alluvium reported in Ramspott and McArthur (1977), Beiriger (1977), Jones (1982), Daniels and Thompson (1984), and Warren et al. (2002). We also include all other alluvium mineralogy information discussed in this report (mineralogy used in Tompson et al. (1999), average/standard deviation/minimum/maximum mineral abundances from each source listed above, depth integrated ER-5-4 mineral abundance data, etc.) Only those sorbing minerals included in our mechanistic sorption model are reported. Predicted radionuclide K_d s are reported alongside the mineral abundance data. Porous flow radionuclide K_d s are discussed in Sections 4 and 5 of this report. In general, we report porous flow radionuclide retardation in terms of K_d . The methods for calculating K_d were defined in Section 4.1 of this report. For convenience, the following example calculation provides step-by-step instruction of how K_d s (and R s) are determined.

For a particular alluvium mineralogy, radionuclide Kds are calculated using the component additivity approach (Equation (1)):

$$K_d = \frac{mol_{sorb}/g_{tot}}{mol_{aq}/mL} = \sum_{i=1}^n K_{d,i} \phi_{m,i} . \quad (C1)$$

Thus, we simply need individual radionuclide-mineral K_d s and the mass fractions of minerals to calculate a K_d . As an example, we use the mineral abundance information from first entry in Table C1 (sample from ER-5-3 at 300 feet) to calculate the K_d for Ca. Individual radionuclide-mineral K_d s based on Frenchman Flat water chemistry (Table 1) and mechanistic model reaction constants (Appendix A) are reported in Table 2. For Ca, K_d s are reported for calcite, zeolite, mica/illite, and smectite (iron oxide information is not listed in Table 2 due to lack of mechanistic model data). The K_d is calculated by:

$$K_d = 10^{0.44} \times 0.059 + 10^{3.51} \times 0.045 + 10^{2.33} \times 0.025 + 10^{2.67} \times 0.13 = 10^{2.33}, \quad (C2)$$

which is consistent with the K_d reported in Table C1.

In some cases, a retardation factor (R) is reported. For Frenchman Flat porous flow calculations, R is always based on an average mineral density of 2.5 g/cm³ and a porosity of 40%. Combining Equation (2),

$$R = 1 + \frac{K_d \rho_b}{\theta}, \quad (C3)$$

with the relationship between mineral and bulk density,

$$\rho_b = \rho_m(1 - \theta), \quad (C4)$$

can be used to calculate R :

$$R = 1 + \frac{10^{2.33} \times 2.5 \times (1 - 0.4)}{0.4} = 10^{2.90}. \quad (C5)$$

All K_d s and R s reported in Section 5 of this report and Table C1 were calculated in this manner.

Table C1. Radionuclide sorbing mineral abundances and predicted K_d s for Frenchman Flat alluvium samples.

Sample	Depth feet	smectite	mica	zeolite	hematite	calcite	Ca	Cs	Sr	Am	Eu	Sm	Np	U	Pu -5	Pu -10	Pu -15
		Mass %						Log K_d									
Tompson et al. (1999) [†]	-	9.3	1.9	7.0	2.8	1.8	2.4	3.7 (3.7,2.7)	2.2 (2.2,2.2)	3.7 (4.1,3.4)	3.1 (3.6,2.7)	3.4 (3.8,2.9)	0.7 (1.1,0.3)	0.4 (0.8,-0.03)	0.9 (1.4,0.4)	1.3 (1.8,0.8)	1.9 (2.3,1.4)
Depth Avg ER-5-4	-	19.0	3.6	5.0	0.47	5.8	2.4	4.0	2.2	4.1	3.5	3.7	0.8	0.2	1.1	1.5	2.0
ER-5-3 [§]	300.0	13.0	2.5	4.5	0.4	5.9	2.33	3.86	2.07	3.90	3.35	3.65	0.68	0.03	0.95	1.35	1.83
ER-5-3	360.0	8.7	4.0	8.8	0.4	4.8	2.52	4.06	2.29	3.74	3.20	3.52	0.56	-0.09	0.79	1.20	1.69
ER-5-3	446.0	6.1	4.0	6.1	0.6	3.5	2.37	4.06	2.14	3.59	3.05	3.38	0.46	-0.11	0.67	1.08	1.58
ER-5-3	567.0	7.5	2.4	5.6	0.6	0.9	2.35	3.84	2.11	3.61	3.01	3.23	0.33	-0.06	0.71	1.11	1.59
ER-5-3	648.0	3.5	4.0	9.2	0.7	5.8	2.51	4.06	2.29	3.48	3.02	3.44	0.54	-0.16	0.56	0.99	1.53
ER-5-3	670.0	1.2	1.0	19.3	0.6	3.2	2.80	3.53	2.58	3.11	2.69	3.14	0.29	-0.32	0.25	0.70	1.26
ER-5-3	700.0	1.8	1.0	13.8	0.4	3.8	2.66	3.51	2.44	3.23	2.79	3.23	0.32	-0.42	0.31	0.75	1.29
ER-5-3	740.0	5.7	3.0	34.3	0.0	2.5	3.06	3.97	2.83	3.54	2.98	3.29	0.28	-0.45	0.57	0.97	1.44
ER-5-3	752.0	9.7	1.6	17.7	0.6	4.1	2.79	3.70	2.56	3.77	3.21	3.51	0.57	0.00	0.84	1.24	1.73
ER-5-3	776.0	4.6	2.0	25.7	0.6	2.0	2.93	3.80	2.71	3.45	2.89	3.19	0.32	-0.16	0.56	0.97	1.47
ER-5-3	779.0	11.4	2.0	13.6	0.8	3.1	2.70	3.78	2.46	3.82	3.24	3.50	0.58	0.09	0.90	1.30	1.78
ER-5-3	801.0	9.3	1.5	20.6	1.0	10.3	2.85	3.69	2.62	3.84	3.35	3.73	0.81	0.10	0.90	1.32	1.84
ER-5-3	812.0	23.7	3.1	15.5	0.5	17.8	2.79	3.97	2.55	4.20	3.68	4.03	1.05	0.26	1.23	1.64	2.13
ER-5-3	830.0	10.3	3.0	27.2	0.0	8.3	2.97	3.97	2.74	3.85	3.33	3.69	0.69	-0.20	0.86	1.27	1.76
ER-5-3	850.0	5.0	2.0	23.9	0.6	2.8	2.90	3.80	2.68	3.50	2.96	3.28	0.39	-0.15	0.60	1.01	1.51
ER-5-3	870.0	12.0	2.0	21.0	0.0	4.8	2.87	3.80	2.64	3.86	3.30	3.59	0.59	-0.13	0.89	1.28	1.76
ER-5-3	881.9	16.0	1.1	22.2	0.8	7.1	2.90	3.58	2.67	3.99	3.43	3.74	0.79	0.18	1.05	1.45	1.94
ER-5-3	890.0	11.4	3.0	25.5	0.0	1.3	2.95	3.96	2.72	3.79	3.19	3.40	0.39	-0.15	0.84	1.22	1.68
ER-5-3	900.0	24.4	2.4	9.3	0.5	3.2	2.62	3.85	2.36	4.13	3.52	3.75	0.76	0.27	1.18	1.57	2.04
ER-5-3	932.0	12.3	2.5	35.1	0.0	0.1	3.08	3.91	2.85	3.81	3.18	3.35	0.33	-0.12	0.86	1.24	1.69
ER-5-3	934.0	16.6	5.5	1.7	0.0	6.7	2.16	4.19	1.88	4.00	3.44	3.73	0.73	0.01	1.03	1.42	1.90
ER-5-3	936.0	6.9	2.5	26.0	0.0	19.9	2.94	3.89	2.72	3.88	3.46	3.93	0.94	-0.37	0.85	1.29	1.83
ER-5-3	940.0	20.6	0.0	2.3	0.6	0.0	2.23	2.30	1.92	4.03	3.40	3.57	0.61	0.22	1.10	1.49	1.95
ER-5-3	940.0	11.8	4.2	20.4	0.4	9.5	2.86	4.09	2.63	3.91	3.39	3.75	0.78	0.00	0.94	1.35	1.85
ER-5-3	942.0	4.0	1.3	33.5	0.0	5.9	3.04	3.67	2.82	3.52	3.04	3.46	0.47	-0.61	0.51	0.93	1.44
ER-5-3	944.0	4.8	3.5	25.8	0.0	17.2	2.94	4.02	2.71	3.78	3.38	3.85	0.87	-0.53	0.74	1.18	1.73

Table C1. (continued)

Sample	Depth feet	smectite	mica	zeolite	hematite	calcite	Ca	Cs	Sr	Am	Eu	Sm	Np	U	Pu -5	Pu -10	Pu -15
		Mass %						Log K_d									
ER-5-3	946.0	7.0	1.7	14.9	0.0	18.7	2.72	3.72	2.49	3.87	3.45	3.91	0.92	-0.36	0.85	1.28	1.81
ER-5-3	985.0	9.4	2.3	8.9	0.4	15.9	2.53	3.83	2.29	3.91	3.45	3.87	0.90	-0.07	0.92	1.35	1.87
ER-5-3	1036.0	5.7	2.1	8.9	0.3	9.1	2.50	3.79	2.27	3.68	3.22	3.64	0.67	-0.26	0.70	1.13	1.64
ER-5-3	1050.0	5.7	2.0	29.4	0.3	12.9	2.99	3.81	2.77	3.75	3.31	3.76	0.79	-0.26	0.75	1.18	1.71
ER-5-3	1069.0	4.9	1.8	43.7	0.0	3.0	3.16	3.80	2.93	3.50	2.96	3.29	0.30	-0.52	0.52	0.92	1.40
ER-5-3	1100.0	9.6	2.5	15.9	0.2	13.7	2.75	3.87	2.52	3.89	3.42	3.83	0.85	-0.14	0.90	1.32	1.83
ER-5-3	1122.0	10.9	2.6	28.6	0.0	9.8	2.99	3.91	2.76	3.88	3.37	3.74	0.75	-0.17	0.90	1.30	1.80
ER-5-3	1150.0	17.3	3.2	17.8	0.0	8.2	2.82	3.98	2.58	4.03	3.47	3.79	0.78	0.03	1.06	1.45	1.93
ER-5-3	1154.0	13.3	3.1	50.1	0.0	6.1	3.23	4.01	3.00	3.91	3.36	3.66	0.66	-0.09	0.94	1.34	1.81
ER-5-3	1160.0	6.6	2.0	29.5	0.4	9.1	3.00	3.81	2.77	3.72	3.25	3.65	0.69	-0.17	0.75	1.17	1.69
ER-5-3	1187.0	7.8	1.5	34.7	0.0	11.0	3.07	3.72	2.84	3.80	3.32	3.73	0.74	-0.32	0.80	1.21	1.72
ER-5-3	1240.0	7.2	1.9	14.5	0.0	9.3	2.71	3.76	2.47	3.75	3.27	3.67	0.68	-0.35	0.75	1.17	1.67
ER-5-3	1259.0	11.1	3.0	24.0	0.0	19.9	2.92	3.96	2.69	3.99	3.54	3.96	0.98	-0.16	0.98	1.41	1.92
ER-5-3	1260.0	22.3	1.6	3.7	0.0	52.7	2.36	3.67	2.07	4.35	3.91	4.36	1.38	0.14	1.33	1.76	2.29
ER-5-3	1490.0	15.5	2.0	12.2	0.2	9.2	2.67	3.78	2.43	4.00	3.46	3.79	0.80	0.04	1.03	1.43	1.91
ER-5-3	1680.0	10.8	1.5	18.0	0.0	5.2	2.80	3.68	2.57	3.83	3.27	3.58	0.58	-0.18	0.85	1.25	1.73
ER-5-3	1760.0	10.4	1.5	30.3	0.0	5.5	3.01	3.71	2.79	3.82	3.27	3.59	0.59	-0.19	0.84	1.24	1.72
ER-5-3	1860.0	8.0	1.5	39.4	0.0	5.4	3.12	3.73	2.89	3.72	3.19	3.53	0.53	-0.31	0.74	1.14	1.63
ER-5-3	2000.0	7.9	1.5	40.1	0.0	3.9	3.13	3.73	2.90	3.69	3.14	3.45	0.45	-0.31	0.72	1.11	1.59
Avg	-	-	-	-	-	-	2.79	3.80	2.56	3.79	3.27	3.62	0.65	-0.14	0.82	1.23	1.73
SD	-	-	-	-	-	-	0.26	0.27	0.28	0.23	0.23	0.25	0.23	0.21	0.22	0.21	0.20
Median	-	-	-	-	-	-	2.85	3.81	2.62	3.82	3.30	3.65	0.67	-0.15	0.85	1.24	1.73
Min	-	-	-	-	-	-	2.16	2.30	1.88	3.11	2.69	3.14	0.28	-0.61	0.25	0.70	1.26
Max	-	-	-	-	-	-	3.23	4.19	3.00	4.35	3.91	4.36	1.38	0.27	1.33	1.76	2.29
ER-5-4	630.0	9.2	2.0	2.6	0.4	2.0	2.12	3.76	1.86	3.72	3.13	3.38	0.43	-0.08	0.78	1.18	1.65
ER-5-4	672.0	13.3	1.8	5.3	0.4	6.6	2.38	3.72	2.12	3.92	3.37	3.68	0.71	0.04	0.96	1.36	1.85
ER-5-4	760.0	11.0	4.0	3.8	0.5	1.7	2.26	4.05	2.01	3.79	3.19	3.42	0.47	0.01	0.86	1.25	1.72
ER-5-4	1035.0	7.6	5.9	41.5	0.0	4.6	3.14	4.25	2.92	3.69	3.15	3.48	0.48	-0.33	0.71	1.11	1.59
ER-5-4	1040.0	8.8	5.7	9.3	1.5	1.0	2.55	4.21	2.32	3.68	3.08	3.29	0.51	0.19	0.83	1.24	1.74
ER-5-4	1045.0	11.7	3.1	23.1	0.0	0.0	2.91	3.97	2.68	3.79	3.16	3.33	0.30	-0.14	0.84	1.21	1.67

Table C1. (continued)

Sample	Depth feet	smectite	mica	zeolite	hematite	calcite	Ca	Cs	Sr	Am	Eu	Sm	Np	U	Pu -5	Pu-10	Pu-15
		Mass %					Log K_d										
ER-5-4	1050.0	18.3	3.8	23.3	0.0	0.0	2.93	4.06	2.69	3.98	3.35	3.52	0.49	0.05	1.03	1.41	1.86
ER-5-4	1056.0	9.5	3.6	11.3	0.6	0.0	2.62	4.02	2.39	3.70	3.07	3.24	0.33	0.00	0.79	1.18	1.65
ER-5-4	1060.0	7.3	5.4	20.9	0.5	0.0	2.86	4.20	2.63	3.58	2.96	3.12	0.23	-0.10	0.68	1.07	1.54
ER-5-4	1065.0	7.2	3.5	10.6	0.4	0.0	2.58	4.00	2.35	3.58	2.95	3.12	0.20	-0.15	0.66	1.05	1.52
ER-5-4	1071.0	14.4	12.3	17.6	0.5	5.9	2.82	4.54	2.60	3.94	3.38	3.68	0.71	0.09	0.99	1.39	1.87
ER-5-4	1072.0	8.1	5.7	23.5	0.5	0.0	2.91	4.22	2.68	3.63	3.00	3.17	0.26	-0.08	0.72	1.11	1.58
ER-5-4	1073.0	19.2	3.1	17.3	0.5	1.6	2.82	3.97	2.58	4.02	3.40	3.61	0.64	0.18	1.08	1.47	1.93
ER-5-4	1074.0	10.0	7.0	10.4	0.5	1.3	2.60	4.30	2.37	3.74	3.14	3.36	0.42	-0.02	0.82	1.21	1.68
ER-5-4	1075.0	13.1	8.0	9.4	0.5	6.0	2.58	4.36	2.35	3.91	3.35	3.66	0.70	0.06	0.96	1.36	1.84
ER-5-4	1076.0	13.5	8.0	4.8	0.3	10.3	2.37	4.35	2.13	3.96	3.44	3.79	0.81	0.02	0.99	1.40	1.89
ER-5-4	1078.0	5.5	6.5	13.7	0.3	3.8	2.68	4.27	2.46	3.56	3.03	3.38	0.42	-0.27	0.61	1.02	1.52
ER-5-4	1080.0	5.5	7.0	16.9	0.3	1.1	2.77	4.30	2.55	3.49	2.90	3.14	0.21	-0.27	0.57	0.96	1.44
ER-5-4	1085.0	14.9	8.1	16.8	0.3	1.0	2.80	4.36	2.57	3.90	3.29	3.49	0.50	0.05	0.96	1.35	1.81
ER-5-4	1090.0	4.6	3.7	8.6	0.6	0.0	2.49	4.02	2.26	3.38	2.76	2.92	0.12	-0.16	0.52	0.92	1.40
ER-5-4	1095.0	4.2	5.6	12.9	0.9	0.0	2.65	4.20	2.43	3.34	2.72	2.89	0.18	-0.06	0.52	0.93	1.43
ER-5-4	1114.0	23.4	6.5	16.2	0.9	0.0	2.81	4.27	2.57	4.09	3.46	3.63	0.68	0.31	1.16	1.55	2.01
ER-5-4	1155.0	14.3	3.1	3.9	0.5	3.7	2.30	3.95	2.04	3.92	3.33	3.59	0.63	0.09	0.97	1.37	1.84
ER-5-4	1180.0	11.1	5.3	4.1	0.5	1.0	2.29	4.17	2.05	3.78	3.17	3.38	0.43	0.01	0.85	1.24	1.71
ER-5-4	1210.0	17.3	5.0	1.5	0.5	0.0	2.15	4.15	1.86	3.96	3.33	3.50	0.53	0.15	1.03	1.41	1.87
ER-5-4	1238.0	15.2	4.6	2.2	0.5	0.9	2.18	4.11	1.91	3.91	3.29	3.49	0.53	0.11	0.98	1.37	1.83
ER-5-4	1270.0	12.9	4.4	2.0	0.5	0.0	2.13	4.09	1.86	3.83	3.20	3.37	0.42	0.05	0.91	1.29	1.76
ER-5-4	1300.0	8.8	4.3	1.8	0.5	0.0	2.04	4.08	1.78	3.66	3.04	3.20	0.29	-0.06	0.75	1.14	1.61
ER-5-4	1334.0	12.1	4.3	3.1	0.5	6.3	2.22	4.08	1.96	3.88	3.33	3.65	0.69	0.04	0.93	1.33	1.82
ER-5-4	1350.0	14.5	4.2	3.4	0.5	2.6	2.27	4.08	2.01	3.91	3.31	3.55	0.59	0.09	0.97	1.36	1.84
ER-5-4	1355.0	10.8	4.6	2.2	0.5	2.2	2.12	4.11	1.86	3.79	3.19	3.44	0.49	0.00	0.85	1.25	1.72
ER-5-4	1360.0	15.0	3.1	2.5	0.5	0.5	2.20	3.94	1.92	3.90	3.28	3.46	0.50	0.10	0.97	1.36	1.82
ER-5-4	1363.0	15.8	5.6	2.2	0.6	0.9	2.20	4.20	1.92	3.93	3.31	3.50	0.55	0.14	1.00	1.39	1.85
ER-5-4	1364.0	12.2	6.8	1.9	0.6	1.9	2.12	4.28	1.87	3.83	3.23	3.46	0.52	0.06	0.90	1.30	1.77
ER-5-4	1365.0	8.9	4.2	3.4	0.6	2.3	2.21	4.07	1.96	3.71	3.13	3.39	0.47	-0.02	0.79	1.19	1.67
ER-5-4	1366.0	15.0	4.3	1.1	0.6	2.4	2.06	4.08	1.76	3.92	3.32	3.55	0.60	0.12	0.99	1.38	1.85
ER-5-4	1367.0	8.0	5.8	0.9	0.6	1.9	1.90	4.21	1.65	3.66	3.07	3.33	0.42	-0.05	0.75	1.14	1.63

Table C1. (continued)

sample	Depth feet	smectite	mica	zeolite	hematite	calcite	Ca	Cs	Sr	Am	Eu	Sm	Np	U	Pu -5	Pu-10	Pu-15
		Mass %						Log K_d									
ER-5-4	1370.0	12.9	5.6	1.3	0.6	11.2	2.06	4.20	1.78	3.95	3.44	3.81	0.84	0.08	1.00	1.41	1.91
ER-5-4	1374.0	10.0	6.1	2.9	0.6	2.6	2.19	4.23	1.94	3.76	3.18	3.44	0.51	0.01	0.84	1.23	1.71
ER-5-4	1380.0	10.4	3.2	1.6	0.4	10.3	2.03	3.96	1.76	3.88	3.37	3.75	0.78	-0.04	0.91	1.32	1.82
ER-5-4	1385.0	13.4	4.1	1.8	0.5	0.8	2.11	4.06	1.83	3.86	3.24	3.43	0.48	0.07	0.93	1.32	1.78
ER-5-4	1390.0	11.1	5.4	1.3	0.5	1.0	2.02	4.18	1.76	3.78	3.17	3.38	0.43	0.01	0.85	1.24	1.71
ER-5-4	1395.0	16.8	6.6	2.7	0.7	2.3	2.26	4.27	1.99	3.97	3.36	3.59	0.64	0.18	1.04	1.43	1.90
ER-5-4	1404.0	9.2	4.3	2.8	0.5	0.7	2.15	4.08	1.91	3.70	3.08	3.28	0.36	-0.04	0.78	1.17	1.64
ER-5-4	1405.0	12.3	4.6	1.8	1.0	0.6	2.10	4.11	1.83	3.82	3.20	3.39	0.51	0.16	0.92	1.31	1.79
ER-5-4	1420.0	14.1	3.5	1.9	0.4	1.3	2.13	4.00	1.85	3.88	3.27	3.48	0.51	0.06	0.95	1.33	1.80
ER-5-4	1435.0	10.1	1.9	2.5	0.5	0.3	2.12	3.73	1.85	3.73	3.11	3.29	0.36	-0.02	0.81	1.20	1.67
ER-5-4	1480.0	17.5	3.3	1.7	0.5	1.6	2.16	3.97	1.86	3.98	3.37	3.57	0.61	0.15	1.04	1.43	1.89
ER-5-4	1500.0	12.8	3.1	1.9	0.5	1.3	2.11	3.94	1.83	3.84	3.23	3.45	0.49	0.05	0.91	1.30	1.77
ER-5-4	1540.0	13.4	3.4	3.5	0.8	0.4	2.26	3.99	2.00	3.85	3.23	3.41	0.50	0.14	0.94	1.33	1.80
ER-5-4	1568.0	13.8	4.1	2.0	0.5	6.3	2.14	4.06	1.86	3.93	3.37	3.68	0.72	0.08	0.98	1.38	1.86
ER-5-4	1600.0	9.6	4.0	1.2	1.0	4.2	1.97	4.05	1.69	3.77	3.21	3.51	0.62	0.10	0.86	1.27	1.76
ER-5-4	1620.0	15.7	3.6	1.7	0.5	3.3	2.13	4.01	1.84	3.95	3.36	3.61	0.64	0.12	1.01	1.40	1.87
ER-5-4	1650.0	22.7	2.9	1.4	0.5	13.5	2.20	3.92	1.88	4.16	3.62	3.95	0.97	0.24	1.20	1.60	2.09
ER-5-4	1710.0	18.7	4.3	6.5	0.5	6.4	2.49	4.09	2.23	4.04	3.47	3.76	0.78	0.17	1.09	1.49	1.97
ER-5-4	1760.0	20.2	3.2	7.8	0.3	3.6	2.55	3.97	2.29	4.05	3.46	3.70	0.71	0.16	1.10	1.49	1.96
ER-5-4	1870.0	21.5	2.3	2.8	0.6	4.7	2.29	3.82	2.00	4.09	3.50	3.75	0.78	0.24	1.14	1.53	2.01
ER-5-4	2000.0	20.3	3.7	3.1	0.6	6.4	2.31	4.02	2.02	4.08	3.50	3.78	0.81	0.22	1.13	1.52	2.00
ER-5-4	2016.0	9.9	8.2	5.5	0.4	1.2	2.38	4.36	2.15	3.73	3.13	3.35	0.40	-0.05	0.80	1.20	1.67
ER-5-4	2047.0	11.6	3.8	2.6	0.6	2.7	2.17	4.03	1.90	3.82	3.23	3.49	0.55	0.05	0.89	1.29	1.77
ER-5-4	2105.0	25.7	4.6	0.9	0.6	2.0	2.20	4.11	1.87	4.14	3.53	3.73	0.75	0.30	1.20	1.59	2.05
ER-5-4	2146.0	28.2	2.1	1.4	0.6	2.7	2.26	3.78	1.92	4.18	3.57	3.78	0.80	0.33	1.24	1.63	2.09
ER-5-4	2210.0	17.7	2.1	1.4	0.6	2.6	2.12	3.78	1.81	3.99	3.39	3.62	0.66	0.18	1.05	1.45	1.92
ER-5-4	2252.0	17.0	4.2	1.6	0.6	3.5	2.15	4.07	1.85	3.98	3.39	3.64	0.68	0.16	1.04	1.44	1.91
ER-5-4	2320.0	40.5	2.2	6.4	0.6	21.8	2.60	3.82	2.31	4.41	3.86	4.18	1.20	0.46	1.44	1.84	2.32
ER-5-4	2398.0	27.8	3.1	6.3	0.6	20.5	2.53	3.95	2.26	4.27	3.74	4.10	1.12	0.33	1.30	1.71	2.20
ER-5-4	2454.0	29.0	3.2	1.3	0.6	17.3	2.27	3.96	1.93	4.27	3.73	4.06	1.08	0.34	1.31	1.71	2.19
ER-5-4	2502.0	42.0	3.9	8.3	0.0	17.5	2.68	4.06	2.39	4.41	3.84	4.14	1.14	0.41	1.44	1.83	2.30

Table C1. (continued)

sample	Depth feet	smectite	mica	zeolite	hematite	calcite	Ca	Cs	Sr	Am	Eu	Sm	Np	U	Pu -5	Pu-10	Pu-15
		Mass %						Log K_d									
ER-5-4	2546.0	35.3	2.7	2.2	0.0	16.4	2.39	3.89	2.06	4.34	3.78	4.09	1.09	0.34	1.37	1.76	2.24
ER-5-4	2601.0	38.0	2.3	0.4	0.5	2.7	2.29	3.82	1.92	4.31	3.70	3.89	0.90	0.43	1.36	1.75	2.21
ER-5-4	2657.0	28.9	2.8	2.1	0.0	27.1	2.32	3.91	2.00	4.31	3.80	4.18	1.18	0.25	1.33	1.73	2.23
ER-5-4	2694.0	21.0	2.1	0.9	0.3	2.2	2.12	3.78	1.78	4.06	3.45	3.66	0.67	0.18	1.11	1.50	1.96
ER-5-4	2704.0	11.9	1.2	0.0	0.0	0.4	1.77	3.53	1.39	3.80	3.18	3.36	0.34	-0.13	0.85	1.23	1.68
ER-5-4	2740.0	33.2	3.2	3.2	0.0	23.8	2.43	3.96	2.11	4.35	3.82	4.16	1.17	0.31	1.36	1.77	2.25
ER-5-4	2810.0	19.0	4.5	0.4	0.6	3.1	2.05	4.10	1.72	4.02	3.43	3.66	0.69	0.20	1.09	1.48	1.95
ER-5-4	2860.0	19.8	2.1	0.0	0.0	15.7	1.99	3.78	1.61	4.13	3.61	3.97	0.97	0.09	1.15	1.55	2.04
ER-5-4	2910.0	47.2	4.5	12.3	0.0	14.7	2.80	4.12	2.53	4.44	3.87	4.14	1.13	0.46	1.48	1.87	2.34
ER-5-4	2960.0	12.4	2.6	0.4	0.5	2.9	1.88	3.87	1.56	3.85	3.26	3.52	0.56	0.04	0.91	1.31	1.78
ER-5-4	3000.0	10.4	4.1	0.6	0.5	8.9	1.89	4.06	1.60	3.86	3.34	3.71	0.75	-0.01	0.90	1.31	1.81
ER-5-4	3047.0	34.8	4.2	0.6	0.5	3.9	2.28	4.08	1.93	4.28	3.67	3.89	0.89	0.40	1.33	1.72	2.18
ER-5-4	3115.0	14.8	4.2	0.1	0.5	1.1	1.91	4.07	1.58	3.90	3.29	3.49	0.53	0.10	0.97	1.36	1.82
ER-5-4	3151.0	12.2	2.2	0.1	0.7	2.8	1.81	3.79	1.46	3.84	3.25	3.51	0.58	0.09	0.92	1.31	1.79
ER-5-4	3214.0	15.4	4.3	0.1	0.3	2.1	1.93	4.08	1.60	3.93	3.33	3.55	0.57	0.06	0.98	1.37	1.84
ER-5-4	3250.0	14.9	4.1	0.3	0.7	3.3	1.95	4.06	1.62	3.93	3.34	3.59	0.64	0.14	1.00	1.39	1.87
ER-5-4	3302.0	14.1	4.1	10.5	0.6	1.5	2.62	4.07	2.38	3.89	3.28	3.49	0.54	0.11	0.96	1.35	1.82
ER-5-4	3361.0	8.0	4.1	11.5	0.4	5.2	2.62	4.07	2.39	3.72	3.18	3.52	0.57	-0.12	0.77	1.18	1.67
ER-5-4	3400.0	16.8	2.7	0.3	0.5	4.2	1.97	3.88	1.63	3.98	3.40	3.66	0.69	0.14	1.04	1.43	1.91
ER-5-4	3450.0	25.5	3.8	0.4	0.6	2.3	2.15	4.03	1.80	4.14	3.53	3.74	0.76	0.30	1.20	1.59	2.05
ER-5-4	3502.0	17.7	4.2	0.0	0.6	0.6	1.96	4.07	1.62	3.97	3.35	3.53	0.58	0.18	1.04	1.43	1.89
ER-5-4	3554.0	11.6	3.2	0.4	0.6	2.8	1.87	3.95	1.56	3.82	3.24	3.49	0.55	0.05	0.89	1.29	1.77
ER-5-4	3580.0	14.8	2.7	0.4	0.6	2.8	1.94	3.88	1.61	3.92	3.33	3.57	0.61	0.12	0.99	1.38	1.85
ER-5-4	3620.0	9.8	0.9	0.4	0.6	0.8	1.78	3.41	1.44	3.72	3.11	3.32	0.40	0.00	0.81	1.20	1.68
ER-5-4	3670.0	11.7	1.1	0.9	0.6	1.1	1.94	3.50	1.62	3.80	3.19	3.40	0.47	0.05	0.88	1.27	1.74
ER-5-4	3720.0	11.4	0.5	0.9	0.6	0.7	1.92	3.17	1.60	3.79	3.17	3.37	0.44	0.04	0.87	1.26	1.73
Avg	-	-	-	-	-	-	2.28	4.03	2.00	3.91	3.32	3.56	0.61	0.09	0.97	1.37	1.84
SD	-	-	-	-	-	-	0.31	0.21	0.34	0.22	0.23	0.26	0.24	0.16	0.20	0.20	0.20
Median	-	-	-	-	-	-	2.20	4.06	1.92	3.90	3.31	3.52	0.57	0.08	0.96	1.36	1.82
Min	-	-	-	-	-	-	1.77	3.17	1.39	3.34	2.72	2.89	0.12	-0.33	0.52	0.92	1.40
Max	-	-	-	-	-	-	3.14	4.54	2.92	4.44	3.87	4.18	1.20	0.46	1.48	1.87	2.34

Table C1. (continued)

sample	Depth feet	smectite	mica	zeolite	hematite	calcite	Ca	Cs	Sr	Am	Eu	Sm	Np	U	Pu -5	Pu-10	Pu-15
		Mass %						Log K_d									
RNM-1S	620.1	4.0	0.5	2.5	0.0	2.5	2.00	3.17	1.76	3.41	2.88	3.21	0.21	-0.61	0.44	0.84	1.32
RNM-1S	738.2	2.5	1.0	2.5	0.0	1.0	1.98	3.46	1.74	3.18	2.61	2.91	-0.09	-0.81	0.21	0.60	1.08
RNM-1S	794.0	5.0	1.0	0.5	2.5	1.0	1.62	3.45	1.32	3.46	2.87	3.11	0.54	0.30	0.74	1.18	1.71
RNM-1S	839.9	1.3	2.0	2.5	0.0	0.5	1.96	3.75	1.74	2.88	2.31	2.61	-0.40	-1.11	-0.09	0.30	0.77
RNM-1S	872.7	10.0	2.5	2.5	0.0	3.5	2.12	3.85	1.86	3.77	3.20	3.49	0.48	-0.21	0.81	1.20	1.67
RNM-1S	981.0	6.0	1.0	35.0	0.0	1.0	3.07	3.59	2.84	3.52	2.93	3.16	0.15	-0.43	0.56	0.95	1.41
RNM-1S	1049.9	15.0	1.5	7.5	0.0	3.5	2.50	3.65	2.25	3.93	3.34	3.60	0.59	-0.03	0.97	1.36	1.82
Avg	-	-	-	-	-	-	2.18	3.56	1.93	3.45	2.88	3.16	0.21	-0.42	0.52	0.92	1.40
SD	-	-	-	-	-	-	0.47	0.22	0.48	0.35	0.34	0.33	0.36	0.48	0.37	0.37	0.38
Median	-	-	-	-	-	-	2.00	3.59	1.76	3.46	2.88	3.16	0.21	-0.43	0.56	0.95	1.41
Min	-	-	-	-	-	-	1.62	3.17	1.32	2.88	2.31	2.61	-0.40	-1.11	-0.09	0.30	0.77
Max	-	-	-	-	-	-	3.07	3.85	2.84	3.93	3.34	3.60	0.59	0.30	0.97	1.36	1.82
U-11g-1	526.2	15.0	0.0	10.0	0.0	5.0	2.60	2.59	2.35	3.95	3.37	3.66	0.65	-0.03	0.98	1.37	1.84
U-11g-1	565.0	20.0	0.0	5.0	0.0	15.0	2.41	2.44	2.13	4.13	3.60	3.96	0.96	0.09	1.15	1.55	2.04
U-11g-1	604.0	10.0	0.0	10.0	0.0	10.0	2.57	2.56	2.33	3.86	3.36	3.73	0.74	-0.21	0.87	1.28	1.77
U-11g-1	639.1	15.0	0.0	20.0	0.0	35.0	2.86	2.84	2.62	4.17	3.74	4.19	1.20	-0.03	1.15	1.58	2.11
U-11g-1	649.9	25.0	0.0	30.0	0.0	20.0	3.04	3.02	2.80	4.23	3.71	4.07	1.07	0.19	1.25	1.65	2.14
U-11g-1	654.9	20.0	0.0	20.0	0.0	30.0	2.87	2.86	2.63	4.22	3.75	4.16	1.17	0.09	1.21	1.63	2.14
U-11g-1	680.1	15.0	0.0	5.0	0.0	10.0	2.37	2.39	2.10	3.99	3.46	3.80	0.80	-0.03	1.01	1.41	1.90
U-11g-1	762.8	15.0	0.0	25.0	0.0	25.0	2.94	2.92	2.71	4.11	3.65	4.07	1.08	-0.03	1.10	1.52	2.04
U-11g-1	798.2	25.0	0.0	20.0	0.0	20.0	2.88	2.88	2.64	4.23	3.71	4.07	1.07	0.19	1.25	1.65	2.14
U-11g-1	804.5	10.0	0.0	55.0	0.0	10.0	3.26	3.23	3.04	3.86	3.36	3.73	0.74	-0.21	0.87	1.28	1.77
U-11g-1	831.4	15.0	0.0	30.0	0.0	10.0	3.02	2.99	2.79	3.99	3.46	3.80	0.80	-0.03	1.01	1.41	1.90
U-11g-1	862.5	15.0	0.0	40.0	0.0	10.0	3.14	3.11	2.90	3.99	3.46	3.80	0.80	-0.03	1.01	1.41	1.90
U-11g-1	883.9	10.0	0.0	30.0	0.0	10.0	3.01	2.98	2.78	3.86	3.36	3.73	0.74	-0.21	0.87	1.28	1.77
U-11g-1	904.5	10.0	0.0	40.0	0.0	10.0	3.13	3.10	2.90	3.86	3.36	3.73	0.74	-0.21	0.87	1.28	1.77
U-11g-1	907.2	5.0	0.0	45.0	0.0	5.0	3.17	3.13	2.95	3.56	3.05	3.43	0.44	-0.51	0.57	0.98	1.47
U-11g-1	917.3	10.0	0.0	20.0	0.0	40.0	2.84	2.82	2.61	4.12	3.73	4.21	1.23	-0.21	1.08	1.53	2.08
U-11g-1	932.4	15.0	0.0	35.0	0.0	10.0	3.08	3.05	2.85	3.99	3.46	3.80	0.80	-0.03	1.01	1.41	1.90
U-11g-1	944.9	10.0	0.0	30.0	0.0	30.0	3.01	2.98	2.78	4.05	3.64	4.10	1.12	-0.21	1.02	1.46	2.00

Table C1. (continued)

sample	Depth feet	smectite	mica	zeolite	hematite	calcite	Ca	Cs	Sr	Am	Eu	Sm	Np	U	Pu -5	Pu-10	Pu-15
		Mass %					Log K_d										
U-11g-1	973.1	10.0	0.0	15.0	0.0	30.0	2.73	2.71	2.49	4.05	3.64	4.10	1.12	-0.21	1.02	1.46	2.00
U-11g-1	988.5	20.0	0.0	40.0	0.0	10.0	3.14	3.12	2.91	4.10	3.54	3.86	0.86	0.09	1.12	1.52	2.00
U-11g-1	1003.6	20.0	0.0	45.0	0.0	15.0	3.19	3.16	2.96	4.13	3.60	3.96	0.96	0.09	1.15	1.55	2.04
U-11g-1	1006.6	5.0	0.0	30.0	0.0	5.0	3.00	2.96	2.77	3.56	3.05	3.43	0.44	-0.51	0.57	0.98	1.47
U-11g-1	1030.2	15.0	0.0	35.0	0.0	10.0	3.08	3.05	2.85	3.99	3.46	3.80	0.80	-0.03	1.01	1.41	1.90
U-11g-1	1038.4	10.0	0.0	20.0	0.0	30.0	2.84	2.82	2.61	4.05	3.64	4.10	1.12	-0.21	1.02	1.46	2.00
U-11g-1	1079.4	30.0	0.0	30.0	0.0	10.0	3.05	3.03	2.80	4.25	3.67	3.96	0.95	0.27	1.28	1.67	2.14
U-11g-1	1080.1	20.0	0.0	35.0	0.0	15.0	3.09	3.07	2.85	4.13	3.60	3.96	0.96	0.09	1.15	1.55	2.04
Avg	-	-	-	-	-	-	2.93	2.91	2.70	4.02	3.52	3.89	0.90	-0.07	1.02	1.43	1.93
SD	-	-	-	-	-	-	0.24	0.22	0.25	0.18	0.19	0.21	0.22	0.19	0.18	0.18	0.18
Median	-	-	-	-	-	-	3.01	2.98	2.78	4.05	3.57	3.91	0.90	-0.03	1.02	1.46	2.00
Min	-	-	-	-	-	-	2.37	2.39	2.10	3.56	3.05	3.43	0.44	-0.51	0.57	0.98	1.47
Max	-	-	-	-	-	-	3.26	3.23	3.04	4.25	3.75	4.21	1.23	0.27	1.28	1.67	2.14
U-11g-1*	1003.0	8.1	2.6	26.8	0.4	7.1	2.96	3.91	2.73	3.75	3.24	3.61	0.65	-0.11	0.80	1.21	1.71
U-11g-1*	1038.0	11.1	2.2	21.8	0.8	0.9	2.88	3.84	2.65	3.78	3.17	3.37	0.47	0.09	0.87	1.26	1.74
U-11g-1*	1080.0	10.6	2.1	28.3	0.9	6.8	2.99	3.83	2.76	3.84	3.30	3.64	0.72	0.10	0.91	1.32	1.82
Avg	-	-	-	-	-	-	2.94	3.86	2.71	3.79	3.24	3.54	0.61	0.03	0.86	1.26	1.76
SD	-	-	-	-	-	-	0.05	0.04	0.06	0.04	0.07	0.15	0.13	0.12	0.06	0.06	0.06
UE-5n*	700.0	8.3	2.2	5.1	0.5	1.5	2.32	3.80	2.08	3.67	3.07	3.31	0.39	-0.07	0.75	1.14	1.62
UE-5n*	720.0	13.8	2.3	6.7	0.5	1.7	2.46	3.83	2.21	3.88	3.27	3.49	0.54	0.08	0.95	1.34	1.81
UE-5n*	961.7	19.8	3.9	14.9	0.4	3.7	2.77	4.06	2.52	4.05	3.45	3.69	0.71	0.17	1.10	1.49	1.96
UE-5n*	963.7	9.0	2.3	3.7	0.5	1.4	2.22	3.82	1.97	3.70	3.10	3.33	0.40	-0.05	0.78	1.17	1.65
UE-5n*	1140.0	14.2	4.4	24.3	0.3	2.6	2.94	4.12	2.70	3.90	3.31	3.55	0.56	0.03	0.95	1.34	1.81
UE-5n*	1160.0	9.4	2.2	15.8	0.3	2.6	2.75	3.82	2.52	3.74	3.15	3.42	0.46	-0.11	0.79	1.19	1.66
UE-5n*	1200.0	11.5	3.0	12.0	0.4	0.6	2.65	3.94	2.42	3.79	3.17	3.36	0.40	-0.01	0.86	1.25	1.71
UE-5n*	1240.0	11.2	3.3	6.1	0.6	1.2	2.41	3.98	2.16	3.79	3.18	3.39	0.46	0.04	0.86	1.26	1.73
UE-5n*	1280.0	10.0	1.1	1.8	0.6	0.8	2.03	3.50	1.75	3.73	3.12	3.32	0.41	0.01	0.82	1.21	1.68
UE-5n*	1320.0	11.7	2.7	2.1	1.1	0.7	2.11	3.88	1.83	3.80	3.18	3.38	0.51	0.17	0.90	1.30	1.78
UE-5n*	1360.0	14.2	2.7	1.1	0.7	0.0	2.03	3.88	1.73	3.87	3.24	3.41	0.48	0.13	0.95	1.34	1.81
UE-5n*	1400.0	16.5	3.3	2.9	0.4	3.0	2.25	3.97	1.97	3.97	3.37	3.61	0.63	0.11	1.02	1.41	1.88

Table C1. (continued)

sample	Depth feet	smectit e	mica	zeolite	hematit e	calcite	Ca	Cs	Sr	Am	Eu	Sm	Np	U	Pu -5	Pu-10	Pu-15
	Mass %						Log K_d										
UE-5n*	1420.0	11.9	3.3	2.0	0.6	2.0	2.11	3.97	1.83	3.82	3.22	3.46	0.52	0.06	0.90	1.29	1.76
UE-5n*	1420.0	12.3	2.7	2.0	0.6	1.8	2.11	3.88	1.83	3.83	3.23	3.46	0.52	0.07	0.91	1.30	1.77
UE-5n*	1420.0	11.2	3.5	1.6	0.6	1.8	2.05	3.99	1.77	3.79	3.20	3.43	0.49	0.04	0.87	1.26	1.74
UE-5n*	1500.0	14.7	2.9	2.2	0.6	1.6	2.17	3.92	1.88	3.90	3.30	3.51	0.56	0.12	0.97	1.37	1.84
UE-5n*	1500.0	15.3	3.4	2.2	0.6	1.6	2.18	3.98	1.89	3.92	3.31	3.53	0.57	0.13	0.99	1.38	1.85
UE-5n*	1500.0	14.2	2.6	2.1	0.5	1.1	2.15	3.87	1.86	3.88	3.27	3.47	0.52	0.08	0.95	1.34	1.81
UE-5n*	1560.0	14.1	2.9	1.8	0.5	1.6	2.12	3.92	1.83	3.89	3.28	3.50	0.54	0.08	0.95	1.34	1.81
UE-5n*	1560.0	13.2	2.9	1.2	0.5	1.4	2.03	3.91	1.73	3.86	3.25	3.46	0.51	0.06	0.93	1.32	1.79
UE-5n*	1560.0	12.9	3.2	1.7	0.7	1.4	2.09	3.96	1.80	3.85	3.24	3.45	0.53	0.10	0.93	1.32	1.79
Avg	-	-	-	-	-	-	2.28	3.91	2.01	3.84	3.23	3.45	0.51	0.06	0.91	1.30	1.77
SD	-	-	-	-	-	-	0.28	0.12	0.30	0.09	0.09	0.09	0.08	0.07	0.08	0.08	0.08
Median	-	-	-	-	-	-	2.17	3.92	1.88	3.85	3.24	3.46	0.52	0.07	0.93	1.32	1.79
Min	-	-	-	-	-	-	2.03	3.50	1.73	3.67	3.07	3.31	0.39	-0.11	0.75	1.14	1.62
Max	-	-	-	-	-	-	2.94	4.12	2.70	4.05	3.45	3.69	0.71	0.17	1.10	1.49	1.96
UE-5n	300.0	7.0	7.0	2.5	0.0	2.5	2.11	4.29	1.88	3.62	3.05	3.34	0.33	-0.36	0.65	1.04	1.51
UE-5n	450.0	7.0	7.0	2.5	2.5	2.5	2.11	4.29	1.88	3.62	3.06	3.34	0.64	0.33	0.84	1.27	1.79
UE-5n	600.0	2.5	2.5	2.5	2.5	7.0	1.99	3.85	1.77	3.44	3.02	3.48	0.73	0.27	0.70	1.16	1.72
UE-5n	730.0	2.5	2.5	5.0	0.0	2.0	2.25	3.85	2.03	3.23	2.71	3.07	0.07	-0.81	0.25	0.65	1.14
UE-5n	740.0	2.5	2.5	5.0	0.0	1.0	2.25	3.85	2.03	3.18	2.61	2.91	-0.09	-0.81	0.21	0.60	1.08
UE-5n	760.0	2.5	2.5	5.0	0.0	0.5	2.25	3.85	2.03	3.15	2.56	2.80	-0.21	-0.81	0.19	0.57	1.04
UE-5n	780.0	2.5	2.5	5.0	0.0	2.0	2.25	3.85	2.03	3.23	2.71	3.07	0.07	-0.81	0.25	0.65	1.14
UE-5n	800.0	2.5	2.5	5.0	0.0	1.0	2.25	3.85	2.03	3.18	2.61	2.91	-0.09	-0.81	0.21	0.60	1.08
UE-5n	820.0	2.5	2.5	5.0	0.0	1.0	2.25	3.85	2.03	3.18	2.61	2.91	-0.09	-0.81	0.21	0.60	1.08
UE-5n	840.0	2.5	2.5	5.0	0.0	2.0	2.25	3.85	2.03	3.23	2.71	3.07	0.07	-0.81	0.25	0.65	1.14
UE-5n	860.0	2.5	2.5	2.5	0.0	0.5	1.99	3.85	1.77	3.15	2.56	2.80	-0.21	-0.81	0.19	0.57	1.04
UE-5n	870.0	2.5	2.5	2.5	0.0	2.0	1.99	3.85	1.77	3.23	2.71	3.07	0.07	-0.81	0.25	0.65	1.14
UE-5n	880.0	2.5	2.5	5.0	0.0	3.0	2.25	3.85	2.03	3.28	2.79	3.19	0.19	-0.81	0.29	0.70	1.20
UE-5n	890.0	2.5	2.5	0.0	0.0	3.0	1.23	3.84	1.00	3.28	2.79	3.19	0.19	-0.81	0.29	0.70	1.20
UE-5n	900.0	5.0	2.5	2.5	0.0	1.0	2.04	3.85	1.80	3.45	2.86	3.10	0.09	-0.51	0.49	0.88	1.34
UE-5n	899.9	7.0	2.5	2.5	2.5	1.0	2.08	3.85	1.82	3.59	2.99	3.22	0.58	0.33	0.83	1.25	1.77

Table C1. (continued)

sample	Depth feet	smectite	mica	zeolite	hematite	calcite	Ca	Cs	Sr	Am	Eu	Sm	Np	U	Pu -5	Pu-10	Pu-15
		Mass %						Log K_d									
UE-5n	910.0	2.5	2.5	5.0	0.0	2.0	2.25	3.85	2.03	3.23	2.71	3.07	0.07	-0.81	0.25	0.65	1.14
UE-5n	920.0	2.5	2.5	15.0	0.0	1.0	2.70	3.87	2.48	3.18	2.61	2.91	-0.09	-0.81	0.21	0.60	1.08
UE-5n	930.0	2.5	2.5	15.0	0.0	1.0	2.70	3.87	2.48	3.18	2.61	2.91	-0.09	-0.81	0.21	0.60	1.08
UE-5n	940.0	2.5	2.5	25.0	0.0	0.0	2.92	3.89	2.69	3.12	2.49	2.65	-0.37	-0.81	0.17	0.54	1.00
UE-5n	945.0	5.0	2.5	50.0	0.0	3.0	3.22	3.93	2.99	3.51	2.97	3.30	0.30	-0.51	0.53	0.93	1.41
UE-5n	950.0	15.0	2.5	37.5	0.0	2.0	3.11	3.91	2.88	3.92	3.31	3.54	0.52	-0.03	0.96	1.34	1.80
UE-5n	955.0	7.5	2.5	62.5	0.0	2.0	3.31	3.95	3.09	3.64	3.05	3.32	0.31	-0.33	0.67	1.06	1.53
UE-5n	955.1	7.0	2.5	40.0	0.0	7.0	3.13	3.91	2.90	3.70	3.20	3.58	0.59	-0.36	0.72	1.12	1.62
UE-5n	960.0	2.5	2.5	62.5	0.0	2.0	3.31	3.95	3.09	3.23	2.71	3.07	0.07	-0.81	0.25	0.65	1.14
UE-5n	965.0	2.5	2.5	62.5	0.0	1.0	3.31	3.95	3.09	3.18	2.61	2.91	-0.09	-0.81	0.21	0.60	1.08
UE-5n	970.0	10.0	2.5	50.0	0.0	3.0	3.22	3.93	3.00	3.77	3.19	3.46	0.45	-0.21	0.80	1.19	1.66
UE-5n	970.1	10.0	2.5	30.0	0.0	7.0	3.01	3.90	2.78	3.82	3.29	3.64	0.64	-0.21	0.84	1.24	1.73
UE-5n	975.0	2.5	2.5	75.0	0.0	3.0	3.39	3.96	3.17	3.28	2.79	3.19	0.19	-0.81	0.29	0.70	1.20
UE-5n	980.0	2.5	2.5	50.0	0.0	5.0	3.21	3.93	2.99	3.36	2.92	3.35	0.37	-0.81	0.35	0.78	1.30
UE-5n	980.0	7.0	2.5	40.0	0.0	10.0	3.13	3.91	2.90	3.75	3.28	3.69	0.70	-0.36	0.75	1.17	1.68
UE-5n	985.0	7.5	2.5	75.0	0.0	2.0	3.39	3.97	3.17	3.64	3.05	3.32	0.31	-0.33	0.67	1.06	1.53
UE-5n	990.0	7.5	2.5	75.0	0.0	2.0	3.39	3.97	3.17	3.64	3.05	3.32	0.31	-0.33	0.67	1.06	1.53
UE-5n	1000.0	5.0	2.5	40.0	0.0	0.5	3.12	3.91	2.90	3.43	2.82	3.04	0.02	-0.51	0.48	0.86	1.32
UE-5n	1010.0	5.0	2.5	40.0	0.0	0.5	3.12	3.91	2.90	3.43	2.82	3.04	0.02	-0.51	0.48	0.86	1.32
UE-5n	1020.0	2.5	2.5	37.5	0.0	1.0	3.09	3.91	2.87	3.18	2.61	2.91	-0.09	-0.81	0.21	0.60	1.08
UE-5n	1030.0	2.5	2.5	40.0	0.0	0.5	3.12	3.91	2.90	3.15	2.56	2.80	-0.21	-0.81	0.19	0.57	1.04
UE-5n	1040.0	2.5	2.5	75.0	0.0	3.0	3.39	3.96	3.17	3.28	2.79	3.19	0.19	-0.81	0.29	0.70	1.20
UE-5n	1050.0	2.5	2.5	62.5	0.0	0.3	3.31	3.95	3.09	3.13	2.52	2.73	-0.28	-0.81	0.18	0.56	1.02
UE-5n	1060.0	5.0	2.5	50.0	0.0	2.0	3.22	3.93	2.99	3.48	2.92	3.21	0.21	-0.51	0.51	0.90	1.38
UE-5n	1080.0	5.0	2.5	50.0	0.0	3.0	3.22	3.93	2.99	3.51	2.97	3.30	0.30	-0.51	0.53	0.93	1.41
UE-5n	1100.0	2.5	2.5	80.0	0.0	0.3	3.42	3.97	3.19	3.13	2.52	2.73	-0.28	-0.81	0.18	0.56	1.02
UE-5n	1100.1	2.5	2.5	60.0	0.0	2.5	3.29	3.94	3.07	3.26	2.75	3.13	0.14	-0.81	0.27	0.68	1.17
UE-5n	1120.0	5.0	2.5	75.0	0.0	0.8	3.39	3.96	3.17	3.44	2.84	3.07	0.05	-0.51	0.48	0.87	1.33
UE-5n	1300.0	7.0	7.0	2.5	2.5	2.5	2.11	4.29	1.88	3.62	3.06	3.34	0.64	0.33	0.84	1.27	1.79

Table C1. (continued)

sample	Depth feet	smectite	mica	zeolite	hematite	calcite	Ca	Cs	Sr	Am	Eu	Sm	Np	U	Pu -5	Pu-10	Pu-15
		Mass %						Log K_d									
UE-5n	1460.0	7.0	2.5	15.0	2.5	2.5	2.72	3.87	2.49	3.62	3.06	3.34	0.64	0.33	0.84	1.27	1.79
UE-5n	1560.0	2.5	7.0	2.5	2.5	2.5	2.03	4.29	1.83	3.27	2.77	3.14	0.56	0.27	0.63	1.09	1.64
Avg	-	-	-	-	-	-	2.74	3.93	2.52	3.39	2.83	3.14	0.18	-0.52	0.44	0.84	1.33
SD	-	-	-	-	-	-	0.57	0.12	0.58	0.22	0.23	0.25	0.30	0.39	0.25	0.26	0.27
Median	-	-	-	-	-	-	3.01	3.91	2.78	3.28	2.79	3.13	0.14	-0.81	0.29	0.70	1.20
Min	-	-	-	-	-	-	1.23	3.84	1.00	3.12	2.49	2.65	-0.37	-0.81	0.17	0.54	1.00
Max	-	-	-	-	-	-	3.42	4.29	3.19	3.92	3.31	3.69	0.73	0.33	0.96	1.34	1.80
----- ALL DATA -----																	
Avg	-	-	-	-	-	-	2.54	3.82	2.29	3.78	3.22	3.50	0.54	-0.11	0.83	1.23	2.54
SD	-	-	-	-	-	-	0.45	0.39	0.47	0.30	0.30	0.33	0.32	0.33	0.30	0.30	0.45
Median	-	-	-	-	-	-	2.51	3.91	2.27	3.82	3.24	3.49	0.55	-0.01	0.87	1.28	2.51
Min	-	-	-	-	-	-	1.23	2.30	1.00	2.88	2.31	2.61	-0.40	-1.11	-0.09	0.30	1.23
Max	-	-	-	-	-	-	3.42	4.54	3.19	4.44	3.91	4.36	1.38	0.46	1.48	1.87	3.42

‡ UE-5n data from Ramspeck and McArthur (1977) and Beiriger (1977), UE-5n* data from Warren et al. (2002), U-11g-1* data from Warren et al. (2002), U-11g-1 data from Jones (1982), RNM-1 data from Daniels and Thompson (1984), ER-5-3 data from Warren et al. (2002), ER-5-4 data from Warren et al. (2002).

† Mineral abundances reported in Tompson et al. (1999) were estimated volume fractions assigned to Frenchman Flat alluvium reactive transport simulations. The volume fractions and mineral densities reported in Table 3 of this report were used to convert volume fractions to mass fractions reported here.

Appendix D.

Mineral Abundance and Predicted Radionuclide Retardation Data for Pahute Mesa Matrix Flow Zones

Tables D1 and D2 include all mineralogy/ R/K_d information discussed in this report with regards to radionuclide matrix flow in Pahute Mesa rocks. This includes the mineralogy and radionuclide retardation parameters based on data Pawloski et al. (2001) (Section 6.2). It also includes the mineralogy/ Rs/K_d s for the average hydrostratigraphic units described in Section 6.3. The data in Tables D1 and D2 also includes the abundance of radionuclide sorbing minerals and associated Rs/K_d s for each sample within the Tuff Cone hydrostratigraphic unit reported in Warren et al. (2000) and discussed in Section 6.5.1. In general, sample names in the tabulated data refer to the sample name formulation used in Warren et al. (2000). Only those sorbing minerals included in our mechanistic sorption model are reported here. Predicted radionuclide K_d s are reported alongside the mineral abundance data in Table D1. Table D2 lists the retardation factors for the same samples listed in D1. Table D2 also contains stratigraphic information for each sample as reported in Warren et al. (2000). Radionuclide K_d s and Rs were calculated in the same manner as described in Appendix C for porous flow. The methods for calculating K_d for porous flow conditions were defined in Section 4.1 of this report. For convenience, the following example calculation provides step-by-step instruction of how K_d s (and Rs) were determined.

For a particular matrix flow mineralogy, radionuclide K_d s are calculated using the component additivity approach (Equation (1)):

$$K_d = \frac{mol_{sorb}/g_{tot}}{mol_{aq}/mL} = \sum_{i=1}^n K_{d,i} \phi_{m,i} . \quad (D1)$$

Thus, we simply need (1) individual radionuclide-mineral K_d s and (2) the mass fractions of minerals to calculate K_d . As an example, we use the mineral abundance information from the first entry in Table D1 (CHESHIRE unclassified HST average matrix mineralogy, Table 9) and individual radionuclide-mineral K_d s of Table 8 (based on Pahute Mesa water chemistry (Table 7) and mechanistic model reaction constants (Appendix A)) to calculate the Ca K_d . Ca K_d s in Table 8 are reported for calcite, zeolite, mica/illite, and smectite (iron oxide information is not listed in Table 8 due to lack of mechanistic model data). Using the mineral mass fractions listed in Table D1, the K_d is calculated by:

$$K_d = 10^{0.52} \times 0.0 + 10^{3.60} \times 0.0 + 10^{2.51} \times 0.00053 + 10^{2.85} \times 0.0033 = 10^{0.40} , \quad (D2)$$

which is consistent with the K_d reported in Table D1.

In some cases, Rs are discussed in this report. To calculate Rs in Pahute Mesa porous flow samples, both porosity and matrix bulk density information is needed such that:

$$R = 1 + \frac{K_d \rho_b}{\theta}. \quad (\text{D3})$$

In the case of CHESHIRE near-field calculations, data in Table 9 can be used to calculate a matrix bulk density of 2.13 g/cm³ and a porosity of 15%. Using these values:

$$R = 1 + \frac{10^{0.40} 2.13}{0.15} = 10^{1.56} \quad (\text{D4})$$

as reported in appendix D2 and Table 12.

The porosities and bulk densities used to calculate retardation factors vary depending on the data source. When calculating radionuclide R_s for the 6 hydrostratigraphic units discussed in Section 6.3, the average porosities listed in Table 13 were used. TMA, TC, TCB, TBA, BCU, and BAQ average porosities are 0.29, 0.285, 0.27, 0.29, 0.39, and 0.18, respectively. Bulk densities were estimated assuming an average mineral density of 2.5 g/cm³. From porosities and average mineral density, bulk densities of 1.78, 1.79, 1.83, 1.78, 1.53, and 2.05 g/cm³ were estimated for TMA, TC, TCB, TBA, BCU, and BAQ hydrostratigraphic units, respectively. When calculating R heterogeneity at the sub hydrostratigraphic (sub-TC) unit scale (Section 6.5), the porosity and bulk density of the matrix was held constant and equal to the average TC hydrostratigraphic unit parameters ($\rho_b = 1.79$, $\theta = 0.285$). Colloid effects were never included when predicting K_d/R in porous flow conditions.

Table D1. Radionuclide sorbing mineral abundances and predicted K_d s for Tuff Cone hydrostratigraphic unit matrix flow zones.

Sample	Depth feet	calcite	zeolite	hematite	mica	smectite	Ca	Cs	Sr	Am	Eu	Sm	Np	U	Pu-5	Pu-10	Pu-15
		Mass %						Log K_d									
CHESHIRE ^a	-	0	0	0.02	0.04	0.25	0.4 (0.4,0.4)	2.3 (1.3,2.3)	0.0 (0.0,0.0)	2.5 (2.2,2.9)	2.0 (1.6,2.5)	2.2 (1.7,2.7)	-1.0 (-1.3,-0.7)	-0.4 (-0.8,-0.0)	-0.5 (-1.0,0.0)	-0.1 (-0.6,0.4)	0.6 (0.1,1.1)
TMA ^{a,b}	-	0.2	11.3	0.3	0.5	1.9	2.7 (2.7,2.7)	3.4 (2.5,3.4)	2.4 (2.4,2.4)	3.3 (3.0,3.6)	2.8 (2.4,3.3)	3.0 (2.5,3.5)	-0.1 (-0.3,0.3)	0.4 (0.0,0.8)	0.4 (-0.1,0.8)	0.7 (0.2,1.2)	1.4 (0.9,1.9)
TC ^{a,b}	-	0.2	9.0	0.3	0.8	2.6	2.6 (2.6,2.6)	3.5 (2.5,3.5)	2.3 (2.3,2.3)	3.4 (3.1,3.7)	2.9 (2.5,3.4)	3.1 (2.7,3.6)	0.0 (-0.3,0.3)	0.4 (0.1,0.9)	0.4 (0.0,0.9)	0.8 (0.3,1.3)	1.5 (1.0,2.0)
TCB ^{a,b}	-	0.0	14.2	0.4	0.9	0.4	2.8 (2.8,2.8)	3.6 (2.6,3.6)	2.5 (2.5,2.5)	2.6 (2.4,3.0)	2.2 (1.7,2.7)	2.4 (1.9,2.9)	-0.3 (-0.5,0.1)	0.3 (-0.1,0.7)	0.0 (-0.4,0.5)	0.4 (-0.1,0.9)	1.1 (0.7,1.6)
TBA ^{a,b}	-	1.3	2.7	0.3	1.2	6.7	2.2 (2.2,2.2)	3.6 (2.6,3.6)	1.9 (1.9,1.9)	3.8 (3.6,4.2)	3.4 (2.9,3.9)	3.6 (3.2,4.1)	0.4 (0.1,0.8)	0.6 (0.3,1.1)	0.8 (0.4,1.3)	1.2 (0.7,1.7)	1.9 (1.4,2.4)
BCU ^{a,b}	-	1.9	3.5	0.2	1.2	10.6	2.3 (2.3,2.3)	3.6 (2.7,3.6)	2.1 (2.1,2.1)	4.0 (3.8,4.4)	3.6 (3.1,4.1)	3.8 (3.3,4.3)	0.6 (0.2,0.9)	0.8 (0.4,1.2)	1.0 (0.5,1.5)	1.4 (0.9,1.9)	2.1 (1.6,2.5)
BAQ ^{a,b}	-	2.7	10.4	0.3	1.1	10.3	2.7 (2.7,2.7)	3.6 (2.7,3.6)	2.4 (2.4,2.4)	4.0 (3.8,4.4)	3.6 (3.1,4.1)	3.8 (3.4,4.3)	0.6 (0.3,1.0)	0.8 (0.4,1.2)	1.0 (0.6,1.5)	1.4 (0.9,1.9)	2.1 (1.6,2.6)
J13-130M(1)	130.0	0.0	0.0	0.5	0.0	0.0	log(0) ^d	log(0)	-2.50	1.10	1.18	1.34	-0.49	0.36	-0.20	0.27	1.07
J13-150M(1)	150.0	0.0	0.0	0.0	0.0	0.0	log(0)	log(0)	log(0)	log(0)	log(0)	log(0)	log(0)	log(0)	log(0)	log(0)	log(0)
J13-180M(1)	180.0	0.0	0.0	0.0	0.0	5.0	1.55	1.59	1.15	3.68	3.21	3.37	-0.03	0.33	0.63	0.97	1.66
J13-185M(1)	185.0	0.0	0.0	0.0	0.0	73.0	2.71	2.75	2.31	4.84	4.37	4.53	1.13	1.49	1.79	2.13	2.82
J13-210M(1)	210.0	0.0	1.0	0.5	0.0	26.0	2.35	2.37	1.99	4.40	3.93	4.09	0.71	1.13	1.36	1.70	2.40
J13-244M(1)	244.0	0.0	0.0	0.5	0.0	2.0	1.15	1.19	0.75	3.28	2.82	2.98	-0.16	0.50	0.37	0.75	1.48
J13-282M(1)	282.0	0.0	0.0	0.0	0.5	3.0	1.36	3.26	1.00	3.46	2.99	3.15	-0.25	0.11	0.41	0.75	1.44
J13-315M(1)	315.0	0.0	0.0	0.5	0.5	1.0	0.94	3.26	0.65	2.99	2.53	2.69	-0.29	0.43	0.17	0.57	1.32
J13-336M(1)	336.0	0.0	0.0	0.5	0.5	0.5	0.71	3.26	0.48	2.69	2.25	2.41	-0.38	0.40	0.02	0.45	1.21
J13-364M(1)	364.0	0.0	0.0	0.5	0.5	0.0	0.21	3.26	0.21	1.10	1.18	1.34	-0.49	0.36	-0.20	0.27	1.07
J13-394M(1)	394.0	0.0	0.0	0.5	0.5	0.0	0.21	3.26	0.21	1.10	1.18	1.34	-0.49	0.36	-0.20	0.27	1.07
J13-395M(1)	395.0	0.0	0.0	0.5	0.0	0.0	log(0)	log(0)	-2.50	1.10	1.18	1.34	-0.49	0.36	-0.20	0.27	1.07
J13-410M(1)	410.0	0.0	0.0	0.0	0.0	0.0	log(0)	log(0)	log(0)	log(0)	log(0)	log(0)	log(0)	log(0)	log(0)	log(0)	log(0)
J13-433M(1)	433.0	0.0	27.0	0.0	0.5	3.0	3.04	3.43	2.81	3.46	2.99	3.15	-0.25	0.11	0.41	0.75	1.44
J13-444M(1)	444.0	0.5	80.0	0.0	0.0	2.0	3.51	3.41	3.27	3.31	2.88	3.07	-0.14	-0.07	0.29	0.64	1.34
J13-574M(1)	574.0	0.5	0.0	0.0	0.5	1.0	0.94	3.26	0.65	3.05	2.64	2.85	-0.27	-0.37	0.04	0.40	1.10
J13-608M(1)	608.0	0.0	0.0	0.0	0.0	2.0	1.15	1.19	0.75	3.28	2.81	2.97	-0.43	-0.07	0.23	0.57	1.26
J13-610M(1)	610.0	0.0	0.0	0.0	0.5	2.0	1.20	3.26	0.86	3.28	2.81	2.97	-0.43	-0.07	0.23	0.57	1.26
J13-611M(1)	611.0	0.0	0.0	0.0	0.5	2.0	1.20	3.26	0.86	3.28	2.81	2.97	-0.43	-0.07	0.23	0.57	1.26

Table D1. (Continued)

Sample	Depth feet	calcite	zeolite	hematite	mica	smectite	Ca	Cs	Sr	Am	Eu	Sm	Np	U	Pu-5	Pu-10	Pu-15
		Mass %					Log K_d										
J13-650M(1)	650.0	0.0	0.0	0.5	2.0	0.0	0.81	3.86	0.81	1.10	1.18	1.34	-0.49	0.36	-0.20	0.27	1.07
J13-664M(1)	664.0	0.5	0.0	0.5	1.0	0.0	0.51	3.56	0.51	2.22	2.12	2.41	-0.17	0.36	-0.05	0.40	1.18
J13-726M(1)	726.0	0.0	0.0	0.0	3.0	8.0	1.82	4.04	1.51	3.88	3.41	3.57	0.17	0.53	0.83	1.17	1.86
J13-772M(1)	772.0	0.0	0.0	0.5	2.0	2.0	1.31	3.86	1.08	3.28	2.82	2.98	-0.16	0.50	0.37	0.75	1.48
J13-817M(1)	817.0	0.5	0.0	0.5	3.0	3.0	1.49	4.04	1.26	3.48	3.04	3.22	0.09	0.55	0.54	0.91	1.63
J13-909M(1)	909.0	0.5	0.0	0.5	2.0	2.0	1.31	3.86	1.08	3.32	2.89	3.08	0.02	0.50	0.41	0.79	1.53
J13-914M(1)	914.0	2.0	0.0	0.0	1.0	4.0	1.50	3.56	1.16	3.65	3.25	3.45	0.33	0.23	0.65	1.00	1.70
Avg ^e	-	-	-	-	-	-	1.41	3.13	0.85	2.93	2.60	2.77	-0.14	0.35	0.33	0.72	1.45
SD ^{c,e}	-	-	-	-	-	-	0.85	0.83	1.28	1.08	0.88	0.88	0.40	0.39	0.49	0.45	0.43
Median ^e	-	-	-	-	-	-	1.26	3.26	0.86	3.28	2.82	2.98	-0.25	0.36	0.26	0.60	1.33
Min ^e	-	-	-	-	-	-	0.21	1.19	-2.50	1.10	1.18	1.34	-0.49	-0.37	-0.20	0.27	1.07
Max ^e	-	-	-	-	-	-	3.51	4.04	3.27	4.84	4.37	4.53	1.13	1.49	1.79	2.13	2.82
UE25P1-210D(1)	210.0	0.0	0.0	2.0	1.0	0.0	0.51	3.56	0.51	1.70	1.78	1.94	0.11	0.96	0.40	0.87	1.67
UE25P1-270D(1)	270.0	0.0	0.0	0.0	0.5	2.0	1.20	3.26	0.86	3.28	2.81	2.97	-0.43	-0.07	0.23	0.57	1.26
UE25P1-290D(1)	290.0	0.0	0.0	0.0	0.5	2.0	1.20	3.26	0.86	3.28	2.81	2.97	-0.43	-0.07	0.23	0.57	1.26
UE25P1-420D(1)	420.0	0.0	0.0	1.0	0.5	3.0	1.36	3.26	1.00	3.46	3.00	3.16	0.08	0.77	0.58	0.97	1.71
UE25P1-580D(1)	580.0	0.0	0.0	0.5	0.5	2.0	1.20	3.26	0.86	3.28	2.82	2.98	-0.16	0.50	0.37	0.75	1.48
UE25P1-820D(1)	820.0	0.0	0.0	0.5	0.5	2.0	1.20	3.26	0.86	3.28	2.82	2.98	-0.16	0.50	0.37	0.75	1.48
UE25P1-910D(1)	910.0	0.0	0.0	0.5	0.5	1.0	0.94	3.26	0.65	2.99	2.53	2.69	-0.29	0.43	0.17	0.57	1.32
UE25P1-1050D(1)	1050.0	0.0	0.0	0.5	0.5	0.0	0.21	3.26	0.21	1.10	1.18	1.34	-0.49	0.36	-0.20	0.27	1.07
UE25P1-1250D(1)	1250.0	0.0	54.0	0.0	0.0	1.0	3.33	3.23	3.10	2.98	2.51	2.67	-0.73	-0.37	-0.07	0.27	0.96
UE25P1-1470S(1)	1470.0	0.0	34.0	0.0	0.0	5.0	3.14	3.05	2.91	3.68	3.21	3.37	-0.03	0.33	0.63	0.97	1.66
UE25P1-1598D(1)	1598.0	0.0	3.0	1.0	0.0	0.0	2.08	1.98	1.85	1.40	1.48	1.64	-0.19	0.66	0.10	0.57	1.37
UE25P1-1650D(1)	1650.0	0.0	0.0	1.0	0.0	5.0	1.55	1.59	1.15	3.68	3.22	3.38	0.20	0.83	0.74	1.11	1.84
UE25P1-1700D(1)	1700.0	0.0	40.0	0.0	0.0	7.0	3.22	3.12	2.98	3.83	3.36	3.52	0.12	0.48	0.78	1.12	1.81
UE25P1-1740D(1)	1740.0	0.0	60.0	0.0	0.0	3.0	3.38	3.28	3.15	3.46	2.99	3.15	-0.25	0.11	0.41	0.75	1.44
UE25P1-1800D(1)	1800.0	0.0	68.0	0.0	0.0	1.0	3.43	3.33	3.20	2.98	2.51	2.67	-0.73	-0.37	-0.07	0.27	0.96
UE25P1-1840D(1)	1840.0	0.0	0.0	1.0	2.0	0.5	1.00	3.86	0.90	2.70	2.28	2.44	-0.13	0.68	0.23	0.67	1.45
UE25P1-1880D(1)	1880.0	0.0	9.0	0.5	0.0	3.0	2.58	2.49	2.34	3.46	2.99	3.15	-0.05	0.55	0.50	0.87	1.59
UE25P1-1930D(1)	1930.0	0.0	0.0	2.0	2.0	5.0	1.62	3.86	1.31	3.68	3.22	3.38	0.35	1.05	0.83	1.22	1.97
UE25P1-1980D(1)	1980.0	0.0	0.0	1.0	1.0	0.5	0.83	3.56	0.67	2.70	2.28	2.44	-0.13	0.68	0.23	0.67	1.45
UE25P1-2000D(1)	2000.0	0.0	0.0	0.5	1.0	1.0	1.01	3.56	0.78	2.99	2.53	2.69	-0.29	0.43	0.17	0.57	1.32
UE25P1-2040D(1)	2040.0	0.0	1.0	0.5	2.0	1.20	3.26	0.86	3.29	2.83	2.99	0.01	0.73	0.47	0.87	1.62	

Table D1. (Continued)

Sample	Depth feet	calcite	zeolite	hematite	mica	smectite	Ca	Cs	Sr	Am	Eu	Sm	Np	U	Pu-5	Pu-10	Pu-15
		Mass %						Log K_d									
UE25P1-2080D(1)	2080.0	0.0	0.0	1.0	0.5	0.5	0.71	3.26	0.48	2.70	2.28	2.44	-0.13	0.68	0.23	0.67	1.45
UE25P1-2130D(1)	2130.0	0.0	0.0	1.0	0.5	0.5	0.71	3.26	0.48	2.70	2.28	2.44	-0.13	0.68	0.23	0.67	1.45
UE25P1-2160D(1)	2160.0	1.0	0.5	1.0	0.5	3.0	1.63	3.27	1.34	3.51	3.09	3.28	0.28	0.77	0.64	1.02	1.76
UE25P1-2220D(1)	2220.0	0.5	28.0	0.0	0.0	3.0	3.06	2.96	2.82	3.48	3.04	3.21	-0.04	0.11	0.45	0.79	1.49
UE25P1-2250D(1)	2250.0	0.0	3.0	0.0	1.0	7.0	2.24	3.58	1.97	3.83	3.36	3.52	0.12	0.48	0.78	1.12	1.81
UE25P1-2290D(1)	2290.0	0.5	31.0	0.0	3.0	6.0	3.11	4.08	2.88	3.77	3.31	3.48	0.17	0.41	0.73	1.07	1.77
UE25P1-2340D(1)	2340.0	0.5	2.0	0.0	1.0	11.0	2.21	3.58	1.91	4.03	3.57	3.73	0.38	0.67	0.98	1.32	2.02
UE25P1-2380D(1)	2380.0	0.0	0.0	1.0	2.0	7.0	1.75	3.86	1.42	3.83	3.36	3.52	0.29	0.88	0.86	1.22	1.94
UE25P1-2420D(1)	2420.0	0.0	0.0	1.0	1.0	0.5	0.83	3.56	0.67	2.70	2.28	2.44	-0.13	0.68	0.23	0.67	1.45
UE25P1-2470D(1)	2470.0	0.0	0.0	1.0	1.0	2.0	1.24	3.56	0.95	3.29	2.83	2.99	0.01	0.73	0.47	0.87	1.62
UE25P1-2520D(1)	2520.0	0.0	0.0	1.0	2.0	0.0	0.81	3.86	0.81	1.40	1.48	1.64	-0.19	0.66	0.10	0.57	1.37
UE25P1-2580D(1)	2580.0	0.0	0.0	1.0	2.0	2.0	1.31	3.86	1.08	3.29	2.83	2.99	0.01	0.73	0.47	0.87	1.62
UE25P1-2640D(1)	2640.0	0.0	0.0	1.0	1.0	7.0	1.72	3.57	1.36	3.83	3.36	3.52	0.29	0.88	0.86	1.22	1.94
UE25P1-2660D(1)	2660.0	1.0	0.0	2.0	1.0	15.0	2.04	3.57	1.66	4.17	3.71	3.88	0.68	1.19	1.20	1.56	2.28
UE25P1-2700D(1)	2700.0	0.5	0.0	1.0	1.0	4.0	1.50	3.56	1.16	3.60	3.16	3.33	0.24	0.80	0.69	1.07	1.80
UE25P1-2760D(1)	2760.0	0.5	13.0	1.0	1.0	13.0	2.79	3.62	2.54	4.10	3.64	3.80	0.53	1.01	1.10	1.46	2.16
UE25P1-2800D(1)	2800.0	0.5	4.0	2.0	1.0	21.0	2.49	3.59	2.19	4.31	3.84	4.01	0.74	1.26	1.31	1.67	2.38
UE25P1-2850D(1)	2850.0	0.0	0.0	2.0	0.5	25.0	2.25	3.30	1.86	4.38	3.91	4.07	0.77	1.30	1.38	1.73	2.44
Avg ^e	-	-	-	-	-	-	1.76	3.35	1.50	3.23	2.83	3.00	0.01	0.59	0.51	0.89	1.63
SD ^{c,e}	-	-	-	-	-	-	0.91	0.47	0.89	0.77	0.64	0.64	0.35	0.39	0.38	0.36	0.35
Median ^e	-	-	-	-	-	-	1.55	3.30	1.16	3.29	2.83	2.99	-0.03	0.68	0.47	0.87	1.62
Min ^e	-	-	-	-	-	-	0.21	1.59	0.21	1.10	1.18	1.34	-0.73	-0.37	-0.20	0.27	0.96
Max ^e	-	-	-	-	-	-	3.43	4.08	3.20	4.38	3.91	4.07	0.77	1.30	1.38	1.73	2.44
USWG1-292(A)	292.0	0.0	0.0	0.5	1.0	0.0	0.51	3.56	0.51	1.10	1.18	1.34	-0.49	0.36	-0.20	0.27	1.07
USWG1-352(A)	352.0	0.0	3.0	1.0	0.5	0.0	2.08	3.28	1.86	1.40	1.48	1.64	-0.19	0.66	0.10	0.57	1.37
USWG1-399(A)	399.0	0.0	0.0	1.0	0.5	0.0	0.21	3.26	0.21	1.40	1.48	1.64	-0.19	0.66	0.10	0.57	1.37
USWG1-450(A)	450.0	0.0	0.0	1.0	0.5	3.0	1.36	3.26	1.00	3.46	3.00	3.16	0.08	0.77	0.58	0.97	1.71
USWG1-553(A)	553.0	0.0	0.0	1.0	0.0	2.0	1.15	1.19	0.75	3.29	2.83	2.99	0.01	0.73	0.47	0.87	1.62
USWG1-619(A)	619.0	0.5	0.0	1.0	0.5	2.0	1.20	3.26	0.86	3.32	2.90	3.08	0.13	0.73	0.51	0.91	1.66
USWG1-673(A)	673.0	0.0	0.0	1.0	0.5	1.0	0.94	3.26	0.65	2.99	2.55	2.71	-0.08	0.70	0.32	0.75	1.51
USWG1-722(A)	722.0	0.0	0.0	0.0	0.5	2.0	1.20	3.26	0.86	3.28	2.81	2.97	-0.43	-0.07	0.23	0.57	1.26

Table D1. (Continued)

Sample	Depth feet	calcite	zeolite	hematite	mica	smectite	Ca	Cs	Sr	Am	Eu	Sm	Np	U	Pu-5	Pu-10	Pu-15
		Mass %					Log K_d										
USWG1-757(A)	757.0	0.0	0.0	1.0	0.5	1.0	0.94	3.26	0.65	2.99	2.55	2.71	-0.08	0.70	0.32	0.75	1.51
USWG1-819(A)	819.0	0.0	0.0	0.5	0.5	2.0	1.20	3.26	0.86	3.28	2.82	2.98	-0.16	0.50	0.37	0.75	1.48
USWG1-874.7(A)	874.7	0.0	0.0	0.5	0.0	2.0	1.15	1.19	0.75	3.28	2.82	2.98	-0.16	0.50	0.37	0.75	1.48
USWG1-936(A)	936.0	35.0	0.0	0.0	0.0	0.0	0.06	log(0)	-1.70	4.03	3.91	4.21	1.38	-2.26	1.25	1.64	2.39
USWG1-995.5(A)	995.5	0.0	0.0	0.5	0.0	3.0	1.33	1.37	0.93	3.46	2.99	3.15	-0.05	0.55	0.50	0.87	1.59
USWG1-1063(A)	1063.0	0.0	0.0	1.0	0.5	2.0	1.20	3.26	0.86	3.29	2.83	2.99	0.01	0.73	0.47	0.87	1.62
USWG1-1104(A)	1104.0	0.0	0.0	1.0	0.0	2.0	1.15	1.19	0.75	3.29	2.83	2.99	0.01	0.73	0.47	0.87	1.62
USWG1-1123(A)	1123.0	0.0	0.0	0.5	0.5	2.0	1.20	3.26	0.86	3.28	2.82	2.98	-0.16	0.50	0.37	0.75	1.48
USWG1-1179(A)	1179.0	0.0	0.0	1.0	0.0	3.0	1.33	1.37	0.93	3.46	3.00	3.16	0.08	0.77	0.58	0.97	1.71
USWG1-1191.9(B)	1191.9	0.0	0.0	1.0	0.0	4.0	1.45	1.49	1.05	3.58	3.12	3.28	0.14	0.80	0.67	1.05	1.78
USWG1-1240.6(C)	1240.6	0.0	0.0	0.5	0.5	2.0	1.20	3.26	0.86	3.28	2.82	2.98	-0.16	0.50	0.37	0.75	1.48
USWG1-1274(A)	1274.0	0.0	0.5	0.5	0.5	2.0	1.55	3.27	1.28	3.28	2.82	2.98	-0.16	0.50	0.37	0.75	1.48
USWG1-1281(A)	1281.0	0.0	0.0	0.5	0.5	2.0	1.20	3.26	0.86	3.28	2.82	2.98	-0.16	0.50	0.37	0.75	1.48
USWG1-1286(B)	1286.0	0.0	10.0	0.0	0.0	33.0	2.80	2.76	2.52	4.50	4.03	4.19	0.79	1.15	1.45	1.79	2.48
USWG1-1319(B)	1319.0	0.0	0.0	0.0	0.0	0.0	log(0)	log(0)	log(0)	log(0)	log(0)	log(0)	log(0)	log(0)	log(0)	log(0)	log(0)
USWG1-1341(B)	1341.0	0.0	2.0	0.0	0.0	0.0	1.90	1.80	1.67	log(0)							
USWG1-1357(B)	1357.0	0.0	0.0	0.0	0.0	1.0	0.85	0.89	0.45	2.98	2.51	2.67	-0.73	-0.37	-0.07	0.27	0.96
USWG1-1392.3(B)	1392.3	0.0	6.0	0.0	0.0	0.5	2.38	2.29	2.15	2.68	2.21	2.37	-1.03	-0.67	-0.37	-0.03	0.66
USWG1-1400(A)	1400.0	0.0	83.0	0.0	0.0	0.5	3.52	3.42	3.29	2.68	2.21	2.37	-1.03	-0.67	-0.37	-0.03	0.66
USWG1-1820.2(B)	1820.2	0.0	54.0	0.0	0.0	1.0	3.33	3.23	3.10	2.98	2.51	2.67	-0.73	-0.37	-0.07	0.27	0.96
USWG1-1942(B)	1942.0	0.0	0.0	0.0	0.0	2.0	1.15	1.19	0.75	3.28	2.81	2.97	-0.43	-0.07	0.23	0.57	1.26
USWG1-2136.3(B)	2136.3	0.0	51.0	0.0	0.0	0.0	3.31	3.21	3.08	log(0)							
USWG1-2173(B)	2173.0	0.0	42.0	0.0	0.5	0.0	3.22	3.50	2.99	log(0)							
USWG1-2190(A)	2190.0	0.0	51.0	0.0	0.5	4.0	3.31	3.54	3.08	3.58	3.11	3.27	-0.13	0.23	0.53	0.87	1.56
USWG1-2198(A)	2198.0	0.0	50.0	0.0	0.5	1.0	3.30	3.53	3.07	2.98	2.51	2.67	-0.73	-0.37	-0.07	0.27	0.96
USWG1-2256(A)	2256.0	0.0	44.5	0.0	0.0	0.0	3.25	3.15	3.02	log(0)							
USWG1-2279(A)	2279.0	0.0	67.0	0.0	0.5	0.5	3.43	3.60	3.20	2.68	2.21	2.37	-1.03	-0.67	-0.37	-0.03	0.66
USWG1-2289(A)	2289.0	0.0	74.0	0.0	0.5	2.0	3.47	3.62	3.24	3.28	2.81	2.97	-0.43	-0.07	0.23	0.57	1.26
USWG1-2316(A)	2316.0	0.0	53.0	0.0	0.5	0.0	3.32	3.54	3.09	log(0)							
USWG1-2401(A)	2401.0	0.0	0.0	1.0	0.5	3.0	1.36	3.26	1.00	3.46	3.00	3.16	0.08	0.77	0.58	0.97	1.71
USWG1-2456(A)	2456.0	0.0	0.0	0.5	0.5	1.0	0.94	3.26	0.65	2.99	2.53	2.69	-0.29	0.43	0.17	0.57	1.32
USWG1-2487(C)	2487.0	0.0	0.0	0.5	1.0	1.0	1.01	3.56	0.78	2.99	2.53	2.69	-0.29	0.43	0.17	0.57	1.32
USWG1-2499(A)	2499.0	0.0	0.0	0.5	0.5	0.5	0.71	3.26	0.48	2.69	2.25	2.41	-0.38	0.40	0.02	0.45	1.21

Table D1. (Continued)

Sample	Depth feet	calcite	zeolite	hematite	mica	smectite	Ca	Cs	Sr	Am	Eu	Sm	Np	U	Pu-5	Pu-10	Pu-15
		Mass %					Log K_d										
USWG1-2506(A)	2506.0	0.0	0.0	0.5	0.5	0.5	0.71	3.26	0.48	2.69	2.25	2.41	-0.38	0.40	0.02	0.45	1.21
USWG1-2544(A)	2544.0	0.0	0.0	0.5	0.5	0.5	0.71	3.26	0.48	2.69	2.25	2.41	-0.38	0.40	0.02	0.45	1.21
USWG1-2564(A)	2564.0	0.0	67.0	0.0	0.5	0.5	3.43	3.60	3.20	2.68	2.21	2.37	-1.03	-0.67	-0.37	-0.03	0.66
USWG1-2600.6(B)	2600.6	0.0	87.0	0.0	0.0	0.0	3.54	3.44	3.31	log(0)							
USWG1-2606(A)	2606.0	0.0	68.0	0.0	0.0	0.5	3.43	3.33	3.20	2.68	2.21	2.37	-1.03	-0.67	-0.37	-0.03	0.66
USWG1-2607(A)	2607.0	0.0	47.0	0.0	0.0	0.0	3.27	3.17	3.04	log(0)							
USWG1-2622(A)	2622.0	0.0	44.0	0.0	0.5	0.5	3.24	3.51	3.01	2.68	2.21	2.37	-1.03	-0.67	-0.37	-0.03	0.66
USWG1-2641.6(B)	2641.6	0.0	36.0	0.0	2.0	2.0	3.16	3.93	2.93	3.28	2.81	2.97	-0.43	-0.07	0.23	0.57	1.26
USWG1-2663(A)	2663.0	0.0	55.0	0.0	2.0	0.5	3.34	3.95	3.11	2.68	2.21	2.37	-1.03	-0.67	-0.37	-0.03	0.66
USWG1-2734(A)	2734.0	0.0	35.0	0.0	2.0	0.5	3.15	3.92	2.92	2.68	2.21	2.37	-1.03	-0.67	-0.37	-0.03	0.66
USWG1-2765(A)	2765.0	0.0	15.5	0.0	1.0	4.0	2.81	3.62	2.58	3.58	3.11	3.27	-0.13	0.23	0.53	0.87	1.56
USWG1-2804(A)	2804.0	0.0	0.0	0.5	1.0	1.0	1.01	3.56	0.78	2.99	2.53	2.69	-0.29	0.43	0.17	0.57	1.32
USWG1-2805(A)	2805.0	0.0	0.0	0.5	0.5	3.0	1.36	3.26	1.00	3.46	2.99	3.15	-0.05	0.55	0.50	0.87	1.59
USWG1-2820(A)	2820.0	0.0	0.0	0.5	1.0	1.0	1.01	3.56	0.78	2.99	2.53	2.69	-0.29	0.43	0.17	0.57	1.32
USWG1-2838(A)	2838.0	0.0	0.0	0.0	0.5	2.0	1.20	3.26	0.86	3.28	2.81	2.97	-0.43	-0.07	0.23	0.57	1.26
USWG1-2869(B)	2869.0	0.0	0.0	0.0	0.5	1.0	0.94	3.26	0.65	2.98	2.51	2.67	-0.73	-0.37	-0.07	0.27	0.96
USWG1-2884(A)	2884.0	0.0	0.0	0.0	1.0	2.0	1.24	3.56	0.95	3.28	2.81	2.97	-0.43	-0.07	0.23	0.57	1.26
USWG1-2915(A)	2915.0	0.0	0.0	0.0	1.0	2.0	1.24	3.56	0.95	3.28	2.81	2.97	-0.43	-0.07	0.23	0.57	1.26
USWG1-2932(A)	2932.0	0.0	0.0	0.0	1.0	1.0	1.01	3.56	0.78	2.98	2.51	2.67	-0.73	-0.37	-0.07	0.27	0.96
USWG1-2938.8(A)	2938.8	0.0	0.0	0.0	2.0	2.0	1.31	3.86	1.08	3.28	2.81	2.97	-0.43	-0.07	0.23	0.57	1.26
USWG1-2948(A)	2948.0	1.0	2.0	0.0	1.0	2.0	1.99	3.57	1.75	3.35	2.95	3.15	0.03	-0.07	0.35	0.70	1.40
USWG1-2966(B)	2966.0	0.0	0.0	0.0	2.0	1.0	1.13	3.86	0.97	2.98	2.51	2.67	-0.73	-0.37	-0.07	0.27	0.96
USWG1-2981(A)	2981.0	0.0	0.0	0.0	1.0	3.0	1.39	3.56	1.07	3.46	2.99	3.15	-0.25	0.11	0.41	0.75	1.44
USWG1-3018(A)	3018.0	0.5	7.0	0.0	1.0	18.0	2.61	3.60	2.34	4.24	3.77	3.94	0.57	0.89	1.19	1.53	2.22
USWG1-3079(A)	3079.0	0.0	13.0	0.0	1.0	11.0	2.78	3.62	2.53	4.02	3.55	3.71	0.31	0.67	0.97	1.31	2.00
USWG1-3167(A)	3167.0	0.0	19.0	0.0	1.0	10.0	2.92	3.63	2.68	3.98	3.51	3.67	0.27	0.63	0.93	1.27	1.96
USWG1-3288(A)	3288.0	0.0	40.0	0.0	0.5	17.0	3.23	3.51	2.99	4.21	3.74	3.90	0.50	0.86	1.16	1.50	2.19
USWG1-3401(A)	3401.0	0.5	10.0	0.0	0.5	4.0	2.63	3.33	2.39	3.60	3.15	3.32	0.04	0.23	0.56	0.91	1.60

Table D1. (Continued)

Sample	Depth feet	calcite	zeolite	hematite	mica	smectite	Ca	Cs	Sr	Am	Eu	Sm	Np	U	Pu-5	Pu-10	Pu-15
		Mass %						Log K_d									
USWG1-3523(A)	3523.0	2.0	13.0	0.0	0.5	7.0	2.75	3.36	2.51	3.86	3.44	3.62	0.43	0.48	0.84	1.19	1.89
Avg ^e	-	-	-	-	-	-	1.92	3.13	1.63	3.16	2.73	2.89	-0.26	0.18	0.28	0.65	1.37
SD ^{c,e}	-	-	-	-	-	-	1.05	0.77	1.12	0.60	0.53	0.54	0.48	0.59	0.42	0.42	0.43
Median ^e	-	-	-	-	-	-	1.36	3.27	1.00	3.28	2.81	2.97	-0.22	0.40	0.23	0.57	1.37
Min ^e	-	-	-	-	-	-	0.06	0.89	-1.70	1.10	1.18	1.34	-1.03	-2.26	-0.37	-0.03	0.66
Max ^e	-	-	-	-	-	-	3.54	3.95	3.31	4.50	4.03	4.21	1.38	1.15	1.45	1.79	2.48
USWG2-10D(1)	10.0	0.0	0.0	0.0	7.0	0.0	1.36	4.41	1.36	log(0)							
USWG2-100D(1)	100.0	0.0	0.0	0.0	3.0	0.0	0.99	4.04	0.99	log(0)							
USWG2-200D(1)	200.0	0.0	0.0	0.0	0.0	0.0	log(0)	log(0)	log(0)	log(0)	log(0)	log(0)	log(0)	log(0)	log(0)	log(0)	log(0)
USWG2-230D(1)	230.0	0.0	0.0	0.0	0.0	0.0	log(0)	log(0)	log(0)	log(0)	log(0)	log(0)	log(0)	log(0)	log(0)	log(0)	log(0)
USWG2-270D(1)	270.0	23.0	0.0	0.0	0.0	6.0	1.64	1.67	1.23	4.11	3.87	4.13	1.23	0.41	1.23	1.60	2.34
USWG2-304(A)	304.0	0.0	0.0	0.0	0.0	0.0	log(0)	log(0)	log(0)	log(0)	log(0)	log(0)	log(0)	log(0)	log(0)	log(0)	log(0)
USWG2-331(A)	331.0	0.0	0.0	0.0	0.0	40.0	2.45	2.49	2.05	4.58	4.11	4.27	0.87	1.23	1.53	1.87	2.56
USWG2-338(A)	338.0	0.0	0.0	0.0	0.0	50.0	2.55	2.59	2.15	4.68	4.21	4.37	0.97	1.33	1.63	1.97	2.66
USWG2-358(A)	358.0	0.0	0.0	0.0	0.0	23.0	2.21	2.25	1.81	4.34	3.87	4.03	0.63	0.99	1.29	1.63	2.32
USWG2-395(A)	395.0	0.0	0.0	0.0	1.0	10.0	1.87	3.57	1.50	3.98	3.51	3.67	0.27	0.63	0.93	1.27	1.96
USWG2-501(A)	501.0	0.0	0.0	0.0	1.5	12.0	1.95	3.74	1.59	4.06	3.59	3.75	0.35	0.71	1.01	1.35	2.04
USWG2-547(B)	547.0	0.0	0.0	0.0	3.0	10.0	1.91	4.04	1.58	3.98	3.51	3.67	0.27	0.63	0.93	1.27	1.96
USWG2-561(A)	561.0	0.0	15.0	0.0	1.5	15.0	2.85	3.78	2.60	4.16	3.69	3.85	0.45	0.81	1.11	1.45	2.14
USWG2-584(A)	584.0	0.0	7.0	0.0	3.0	0.0	2.46	4.05	2.24	log(0)							
USWG2-627(A)	627.0	0.0	15.0	0.0	3.0	10.0	2.83	4.06	2.59	3.98	3.51	3.67	0.27	0.63	0.93	1.27	1.96
USWG2-675(B)	675.0	0.0	23.0	0.0	3.0	40.0	3.08	4.08	2.82	4.58	4.11	4.27	0.87	1.23	1.53	1.87	2.56
USWG2-723(A)	723.0	40.0	0.0	0.0	3.0	10.0	1.91	4.04	1.58	4.34	4.10	4.37	1.47	0.63	1.46	1.84	2.57
USWG2-743(A)	743.0	10.0	3.0	0.0	3.0	35.0	2.58	4.05	2.25	4.56	4.14	4.32	1.13	1.17	1.54	1.89	2.59
USWG2-762(A)	762.0	0.0	75.0	0.0	0.0	3.0	3.48	3.38	3.25	3.46	2.99	3.15	-0.25	0.11	0.41	0.75	1.44
USWG2-770(A)	770.0	0.0	0.0	0.0	7.0	1.0	1.47	4.41	1.41	2.98	2.51	2.67	-0.73	-0.37	-0.07	0.27	0.96
USWG2-822(A)	822.0	0.0	0.0	0.0	3.0	7.0	1.77	4.04	1.47	3.83	3.36	3.52	0.12	0.48	0.78	1.12	1.81
USWG2-855(A)	855.0	0.0	0.0	0.0	3.0	3.0	1.49	4.04	1.26	3.46	2.99	3.15	-0.25	0.11	0.41	0.75	1.44
USWG2-898(A)	898.0	0.0	3.0	0.0	3.0	1.0	2.13	4.04	1.92	2.98	2.51	2.67	-0.73	-0.37	-0.07	0.27	0.96
USWG2-921(D)	921.0	7.0	0.0	0.0	0.0	15.0	2.03	2.07	1.63	4.22	3.81	4.01	0.88	0.81	1.21	1.57	2.27
USWG2-951(A)	951.0	0.0	0.0	0.0	0.0	1.0	0.85	0.89	0.45	2.98	2.51	2.67	-0.73	-0.37	-0.07	0.27	0.96
USWG2-984(A)	984.0	23.0	0.0	0.0	0.0	6.0	1.64	1.67	1.23	4.11	3.87	4.13	1.23	0.41	1.23	1.60	2.34
USWG2-1032(A)	1032.0	0.0	0.0	0.0	1.0	6.0	1.66	3.57	1.30	3.76	3.29	3.45	0.05	0.41	0.71	1.05	1.74

Table D1. (Continued)

Sample	Depth feet	calcite	zeolite	hematite	mica	smectite	Ca	Cs	Sr	Am	Eu	Sm	Np	U	Pu-5	Pu-10	Pu-15
		Mass %					Log K_d										
USWG2-1072(A)	1072.0	0.0	0.0	0.0	1.0	6.0	1.66	3.57	1.30	3.76	3.29	3.45	0.05	0.41	0.71	1.05	1.74
USWG2-1133(A)	1133.0	0.0	0.0	0.0	1.0	10.0	1.87	3.57	1.50	3.98	3.51	3.67	0.27	0.63	0.93	1.27	1.96
USWG2-1178(A)	1178.0	0.0	0.0	0.0	1.0	3.0	1.39	3.56	1.07	3.46	2.99	3.15	-0.25	0.11	0.41	0.75	1.44
USWG2-1234(A)	1234.0	0.0	0.0	0.0	0.0	6.0	1.63	1.67	1.23	3.76	3.29	3.45	0.05	0.41	0.71	1.05	1.74
USWG2-1281(A)	1281.0	0.0	0.0	0.0	0.0	10.0	1.85	1.89	1.45	3.98	3.51	3.67	0.27	0.63	0.93	1.27	1.96
USWG2-1331(A)	1331.0	0.0	0.0	0.0	0.0	10.0	1.85	1.89	1.45	3.98	3.51	3.67	0.27	0.63	0.93	1.27	1.96
USWG2-1382(A)	1382.0	0.0	0.0	0.0	1.0	10.0	1.87	3.57	1.50	3.98	3.51	3.67	0.27	0.63	0.93	1.27	1.96
USWG2-1420(A)	1420.0	0.0	0.0	0.0	0.0	10.0	1.85	1.89	1.45	3.98	3.51	3.67	0.27	0.63	0.93	1.27	1.96
USWG2-1461(A)	1461.0	0.0	0.0	0.0	0.0	10.0	1.85	1.89	1.45	3.98	3.51	3.67	0.27	0.63	0.93	1.27	1.96
USWG2-1536(A)	1536.0	0.0	3.0	0.0	0.0	15.0	2.35	2.32	2.05	4.16	3.69	3.85	0.45	0.81	1.11	1.45	2.14
USWG2-1585(A)	1585.0	0.0	3.0	0.0	0.0	10.0	2.28	2.24	1.99	3.98	3.51	3.67	0.27	0.63	0.93	1.27	1.96
USWG2-1634(A)	1634.0	0.0	40.0	0.0	1.0	40.0	3.27	3.72	3.02	4.58	4.11	4.27	0.87	1.23	1.53	1.87	2.56
USWG2-1664.7(A)	1664.7	0.0	1.0	0.0	0.0	1.0	1.67	1.60	1.42	2.98	2.51	2.67	-0.73	-0.37	-0.07	0.27	0.96
USWG2-1691(B)	1691.0	0.0	57.0	0.0	0.0	10.0	3.37	3.27	3.13	3.98	3.51	3.67	0.27	0.63	0.93	1.27	1.96
USWG2-2744(A)	2744.0	0.0	0.0	0.0	1.0	3.0	1.39	3.56	1.07	3.46	2.99	3.15	-0.25	0.11	0.41	0.75	1.44
USWG2-2820(A)	2820.0	0.0	0.0	0.0	1.0	1.0	1.01	3.56	0.78	2.98	2.51	2.67	-0.73	-0.37	-0.07	0.27	0.96
USWG2-2869(A)	2869.0	0.0	0.0	0.0	3.0	1.0	1.22	4.04	1.10	2.98	2.51	2.67	-0.73	-0.37	-0.07	0.27	0.96
USWG2-2887(A)	2887.0	0.0	0.0	0.0	1.0	3.0	1.39	3.56	1.07	3.46	2.99	3.15	-0.25	0.11	0.41	0.75	1.44
USWG2-2950(A)	2950.0	0.0	0.0	0.0	1.5	6.0	1.68	3.74	1.34	3.76	3.29	3.45	0.05	0.41	0.71	1.05	1.74
USWG2-2970(A)	2970.0	0.0	0.0	0.0	1.5	10.0	1.88	3.74	1.52	3.98	3.51	3.67	0.27	0.63	0.93	1.27	1.96
USWG2-3037(A)	3037.0	0.0	3.0	0.0	1.0	40.0	2.61	3.61	2.27	4.58	4.11	4.27	0.87	1.23	1.53	1.87	2.56
USWG2-3067(A)	3067.0	0.0	37.0	0.0	1.0	0.0	3.17	3.68	2.94	log(0)							
USWG2-3192(A)	3192.0	0.0	40.0	0.0	0.0	7.0	3.22	3.12	2.98	3.83	3.36	3.52	0.12	0.48	0.78	1.12	1.81
USWG2-3228(A)	3228.0	0.0	1.0	0.0	0.0	6.0	1.92	1.89	1.61	3.76	3.29	3.45	0.05	0.41	0.71	1.05	1.74
USWG2-3250(A)	3250.0	0.0	20.0	0.0	1.0	23.0	2.98	3.65	2.73	4.34	3.87	4.03	0.63	0.99	1.29	1.63	2.32
USWG2-3308(A)	3308.0	0.0	0.0	0.0	15.0	3.0	1.84	4.74	1.76	3.46	2.99	3.15	-0.25	0.11	0.41	0.75	1.44
USWG2-3330(A)	3330.0	0.0	0.0	0.0	6.0	0.0	1.29	4.34	1.29	log(0)							
USWG2-3349(A)	3349.0	0.0	0.0	0.0	6.0	1.0	1.42	4.34	1.35	2.98	2.51	2.67	-0.73	-0.37	-0.07	0.27	0.96
USWG2-3366(A)	3366.0	0.0	0.0	0.0	6.0	1.0	1.42	4.34	1.35	2.98	2.51	2.67	-0.73	-0.37	-0.07	0.27	0.96
USWG2-3416(A)	3416.0	0.0	0.0	0.0	6.0	1.0	1.42	4.34	1.35	2.98	2.51	2.67	-0.73	-0.37	-0.07	0.27	0.96

Table D1. (Continued)

Sample	Depth feet	calcite	zeolite	hematite	mica	smectite	Ca	Cs	Sr	Am	Eu	Sm	Np	U	Pu-5	Pu-10	Pu-15
		Mass %					Log K_d										
USWG2-3454(A)	3454.0	0.0	23.0	0.0	3.0	28.0	3.05	4.07	2.80	4.43	3.96	4.12	0.72	1.08	1.38	1.72	2.41
USWG2-3492(A)	3492.0	0.0	23.0	0.0	3.0	18.0	3.02	4.07	2.78	4.24	3.77	3.93	0.53	0.89	1.19	1.53	2.22
USWG2-3512(A)	3512.0	0.0	6.0	0.0	7.0	15.0	2.57	4.41	2.31	4.16	3.69	3.85	0.45	0.81	1.11	1.45	2.14
USWG2-3541(A)	3541.0	0.0	0.0	0.0	7.0	10.0	1.97	4.41	1.71	3.98	3.51	3.67	0.27	0.63	0.93	1.27	1.96
USWG2-3578(A)	3578.0	0.0	23.0	0.0	10.0	23.0	3.05	4.57	2.80	4.34	3.87	4.03	0.63	0.99	1.29	1.63	2.32
USWG2-3627(A)	3627.0	0.0	0.0	0.0	10.0	15.0	2.14	4.56	1.87	4.16	3.69	3.85	0.45	0.81	1.11	1.45	2.14
USWG2-3671(A)	3671.0	7.0	0.0	0.0	7.0	10.0	1.97	4.41	1.71	4.07	3.69	3.90	0.83	0.63	1.08	1.44	2.15
USWG2-3720(A)	3720.0	0.0	0.0	0.0	7.0	10.0	1.97	4.41	1.71	3.98	3.51	3.67	0.27	0.63	0.93	1.27	1.96
USWG2-3724(A)	3724.0	0.0	0.0	0.0	3.0	25.0	2.27	4.04	1.90	4.38	3.91	4.07	0.67	1.03	1.33	1.67	2.36
USWG2-3750(A)	3750.0	0.0	0.0	0.0	10.0	25.0	2.32	4.56	2.01	4.38	3.91	4.07	0.67	1.03	1.33	1.67	2.36
USWG2-3772(A)	3772.0	0.0	0.0	0.0	7.0	23.0	2.27	4.41	1.94	4.34	3.87	4.03	0.63	0.99	1.29	1.63	2.32
USWG2-3795(A)	3795.0	0.0	0.0	0.0	0.0	32.0	2.36	2.40	1.96	4.49	4.02	4.18	0.78	1.14	1.44	1.78	2.47
USWG2-3833(A)	3833.0	0.0	0.0	0.0	6.0	30.0	2.37	4.34	2.02	4.46	3.99	4.15	0.75	1.11	1.41	1.75	2.44
USWG2-3875(A)	3875.0	0.0	0.0	0.0	7.0	25.0	2.30	4.41	1.97	4.38	3.91	4.07	0.67	1.03	1.33	1.67	2.36
USWG2-3908(A)	3908.0	6.0	0.0	0.0	0.0	18.0	2.11	2.15	1.71	4.28	3.86	4.05	0.88	0.89	1.26	1.61	2.32
USWG2-3933(A)	3933.0	7.0	0.0	0.0	0.0	15.0	2.03	2.07	1.63	4.22	3.81	4.01	0.88	0.81	1.21	1.57	2.27
USWG2-3968(A)	3968.0	0.0	0.0	0.0	6.0	18.0	2.17	4.34	1.85	4.24	3.77	3.93	0.53	0.89	1.19	1.53	2.22
Avg ^e	-	-	-	-	-	-	2.08	3.46	1.79	3.93	3.48	3.65	0.29	0.56	0.90	1.24	1.93
SD ^{c,e}	-	-	-	-	-	-	0.61	0.98	0.61	0.49	0.50	0.50	0.56	0.48	0.49	0.50	0.50
Median ^e	-	-	-	-	-	-	0.85	0.89	0.45	2.98	2.51	2.67	-0.73	-0.37	-0.07	0.27	0.96
Min ^e	-	-	-	-	-	-	3.48	4.74	3.25	4.68	4.21	4.37	1.47	1.33	1.63	1.97	2.66
Max ^e	-	-	-	-	-	-	1.97	3.74	1.63	3.98	3.51	3.67	0.27	0.63	0.93	1.27	1.96
ALL DATA																	
Avg ^e	-	-	-	-	-	-	1.89	3.29	1.57	3.41	2.99	3.16	0.00	0.42	0.55	0.91	1.63
SD ^{c,e}	-	-	-	-	-	-	0.88	0.82	0.99	0.78	0.69	0.70	0.53	0.52	0.52	0.51	0.50
Median ^e	-	-	-	-	-	-	1.75	3.50	1.42	3.46	2.99	3.15	-0.04	0.50	0.47	0.87	1.59
Min ^e	-	-	-	-	-	-	0.06	0.89	-2.50	1.10	1.18	1.34	-1.03	-2.26	-0.37	-0.03	0.66
Max ^e	-	-	-	-	-	-	3.54	4.74	3.31	4.84	4.37	4.53	1.47	1.49	1.79	2.13	2.82

^a Uncertainty related to mechanistic model reaction constants and not mineral spatial variability.^b Mass percent calculated from probability and average mineral abundance data reported in Table 13. Mineral abundance data was collected from data in Warren et al. (2000) as described in Section 6.3.1.^c Standard deviation related to variability in mineral abundance for the particular well and not uncertainty in mechanistic model reaction constants.^d Log K_d could not be calculated because K_d was equal to 0.^e Average, standard deviation, minimum, maximum, and median calculated ignoring data for which $K_d=0$ (i.e. log K_d cannot be calculated).

Table D2. Sample stratigraphic units and predicted retardation factors for Tuff Cone hydrostratigraphic unit matrix flow zones.

Sample ^b	Depth feet	Strat. ^d	Ca	Cs	Sr	Am	Eu	Sm	Np	U	Pu-5	Pu-10	Pu-15
Log R													
CHESHIRE ^a	-	-	1.6 (1.6,1.6)	3.4 (2.4,3.4)	1.2 (1.2,1.2)	3.6 (3.4,4.0)	3.2 (2.7,3.6)	3.3 (2.9,3.8)	0.4 (0.2,0.6)	0.8 (0.5,1.2)	0.8 (0.4,1.2)	1.1 (0.7,1.6)	1.8 (1.3,2.3)
TMA ^{a,b}	-	-	3.4 (3.4,3.4)	4.2 (3.2,4.2)	3.2 (3.2,3.2)	4.1 (3.8,4.4)	3.6 (3.1,4.1)	3.8 (3.3,4.3)	0.8 (0.6,1.1)	1.2 (0.9,1.6)	1.2 (0.8,1.6)	1.5 (1.1,2.0)	2.2 (1.7,2.7)
TC ^{a,b}	-	-	3.4 (3.4,3.4)	4.3 (3.3,4.3)	3.1 (3.1,3.1)	4.2 (3.9,4.5)	3.7 (3.3,4.2)	3.9 (3.5,4.4)	0.8 (0.6,1.1)	1.3 (0.9,1.7)	1.3 (0.9,1.7)	1.6 (1.2,2.1)	2.3 (1.8,2.8)
TCB ^{a,b}	-	-	3.6 (3.6,3.6)	4.4 (3.5,4.4)	3.4 (3.4,3.4)	3.5 (3.2,3.8)	3.0 (2.6,3.5)	3.2 (2.8,3.7)	0.6 (0.5,0.9)	1.2 (0.8,1.6)	0.9 (0.6,1.3)	1.2 (0.8,1.7)	2.0 (1.5,2.4)
TBA ^{a,b}	-	-	3.0 (3.0,3.0)	4.4 (3.4,4.4)	2.7 (2.7,2.7)	4.6 (4.4,5.0)	4.2 (3.7,4.7)	4.4 (3.9,4.9)	1.2 (0.9,1.6)	1.5 (1.1,1.9)	1.6 (1.2,2.1)	2.0 (1.5,2.5)	2.7 (2.2,3.2)
BCU ^{a,b}	-	-	2.9 (2.9,2.9)	4.2 (3.3,4.2)	2.7 (2.7,2.7)	4.6 (4.4,5.0)	4.2 (3.7,4.7)	4.4 (3.9,4.9)	1.2 (0.9,1.5)	1.4 (1.1,1.8)	1.6 (1.2,2.1)	2.0 (1.5,2.5)	2.7 (2.2,3.1)
BAQ ^{a,b}	-	-	3.7 (3.7,3.7)	4.7 (3.7,4.7)	3.5 (3.5,3.5)	5.1 (4.8,5.4)	4.7 (4.2,5.1)	4.9 (4.4,5.4)	1.7 (1.4,2.1)	1.9 (1.5,2.3)	2.1 (1.6,2.6)	2.4 (2.0,2.9)	3.1 (2.7,3.6)
J13-130M(1)	130.0	Tpcp	0.00	0.00	0.01	1.89	1.97	2.13	0.47	1.17	0.69	1.09	1.86
J13-150M(1)	150.0	Tpcp	0.00	0.00	0.00	0.00	0.00	0.00	0.00	0.00	0.00	0.00	0.00
J13-180M(1)	180.0	Tpcp	2.34	2.38	1.94	4.46	3.99	4.15	0.82	1.15	1.43	1.76	2.45
J13-185M(1)	185.0	Tptbr	3.50	3.54	3.10	5.63	5.16	5.32	1.92	2.28	2.58	2.92	3.61
J13-210M(1)	210.0	Tptbr	3.14	3.15	2.77	5.18	4.71	4.87	1.51	1.92	2.15	2.49	3.18
J13-244M(1)	244.0	Tptr	1.94	1.98	1.55	4.07	3.61	3.77	0.72	1.30	1.18	1.54	2.26
J13-282M(1)	282.0	Tptp	2.15	4.05	1.80	4.24	3.77	3.93	0.64	0.95	1.22	1.55	2.23
J13-315M(1)	315.0	Tptp	1.73	4.05	1.45	3.77	3.32	3.48	0.61	1.24	1.00	1.37	2.11
J13-336M(1)	336.0	Tptp	1.51	4.05	1.29	3.48	3.03	3.19	0.55	1.21	0.87	1.26	2.00
J13-364M(1)	364.0	Tptp	1.04	4.04	1.04	1.89	1.97	2.13	0.47	1.17	0.69	1.09	1.86
J13-394M(1)	394.0	Tptp	1.04	4.04	1.04	1.89	1.97	2.13	0.47	1.17	0.69	1.09	1.86
J13-395M(1)	395.0	Tptp	0.00	0.00	0.01	1.89	1.97	2.13	0.47	1.17	0.69	1.09	1.86
J13-410M(1)	410.0	Tptp	0.00	0.00	0.00	0.00	0.00	0.00	0.00	0.00	0.00	0.00	0.00
J13-433M(1)	433.0	Tptp	3.83	4.22	3.59	4.24	3.77	3.93	0.64	0.95	1.22	1.55	2.23
J13-444M(1)	444.0	Tptp	4.29	4.19	4.06	4.10	3.67	3.85	0.73	0.79	1.11	1.44	2.13
J13-574M(1)	574.0	Tcp	1.73	4.05	1.45	3.83	3.43	3.63	0.63	0.56	0.89	1.21	1.89
J13-608M(1)	608.0	Tcby	1.94	1.98	1.55	4.07	3.60	3.76	0.51	0.79	1.06	1.38	2.05
J13-610M(1)	610.0	Tcby	1.99	4.05	1.66	4.07	3.60	3.76	0.51	0.79	1.06	1.38	2.05

Table D2. (Continued)

Sample	Depth feet	Strat. ^d	Ca	Cs	Sr	Am	Eu	Sm	Np	U	Pu-5	Pu-10	Pu-15
Log R													
J13-611M(1)	611.0	Tcby	1.99	4.05	1.66	4.07	3.60	3.76	0.51	0.79	1.06	1.38	2.05
J13-650M(1)	650.0	Tcby	1.61	4.65	1.61	1.89	1.97	2.13	0.47	1.17	0.69	1.09	1.86
J13-664M(1)	664.0	Tcby	1.32	4.35	1.32	3.01	2.91	3.19	0.71	1.17	0.81	1.21	1.97
J13-726M(1)	726.0	Tct	2.61	4.83	2.30	4.67	4.20	4.36	1.00	1.34	1.63	1.96	2.65
J13-772M(1)	772.0	Tct	2.10	4.65	1.87	4.07	3.61	3.77	0.72	1.30	1.18	1.54	2.26
J13-817M(1)	817.0	Tct	2.28	4.82	2.05	4.27	3.83	4.01	0.93	1.36	1.34	1.70	2.42
J13-909M(1)	909.0	Tct	2.10	4.65	1.87	4.10	3.68	3.86	0.87	1.30	1.23	1.59	2.31
J13-914M(1)	914.0	Tct	2.29	4.35	1.95	4.43	4.03	4.23	1.15	1.06	1.45	1.79	2.49
Avg	-	-	1.86	3.31	1.65	3.43	3.13	3.29	0.70	1.08	1.07	1.40	2.06
SD^c	-	-	1.12	1.63	1.01	1.45	1.25	1.28	0.40	0.47	0.54	0.59	0.73
Median	-	-	1.96	4.05	1.63	4.07	3.60	3.76	0.64	1.17	1.06	1.38	2.08
Min	-	-	0.00	0.00	0.00	0.00	0.00	0.00	0.00	0.00	0.00	0.00	0.00
Max	-	-	4.29	4.83	4.06	5.63	5.16	5.32	1.92	2.28	2.58	2.92	3.61
UE25P1-210D(1)	210.0	Tpcr	1.32	4.35	1.32	2.49	2.57	2.73	0.95	1.75	1.21	1.67	2.46
UE25P1-270D(1)	270.0	Tpcp	1.99	4.05	1.66	4.07	3.60	3.76	0.51	0.79	1.06	1.38	2.05
UE25P1-290D(1)	290.0	Tpcp	1.99	4.05	1.66	4.07	3.60	3.76	0.51	0.79	1.06	1.38	2.05
UE25P1-420D(1)	420.0	Tptp	2.15	4.05	1.80	4.25	3.79	3.95	0.92	1.56	1.39	1.76	2.49
UE25P1-580D(1)	580.0	Tptp	1.99	4.05	1.66	4.07	3.61	3.77	0.72	1.30	1.18	1.54	2.26
UE25P1-820D(1)	820.0	Tptp	1.99	4.05	1.66	4.07	3.61	3.77	0.72	1.30	1.18	1.54	2.26
UE25P1-910D(1)	910.0	Tptp	1.73	4.05	1.45	3.77	3.32	3.48	0.61	1.24	1.00	1.37	2.11
UE25P1-1050D(1)	1050.0	Tptp	1.04	4.04	1.04	1.89	1.97	2.13	0.47	1.17	0.69	1.09	1.86
UE25P1-1250D(1)	1250.0	Tptp	4.12	4.02	3.89	3.77	3.30	3.46	0.33	0.56	0.79	1.09	1.75
UE25P1-1470S(1)	1470.0	Tcp	3.93	3.83	3.69	4.46	3.99	4.15	0.82	1.15	1.43	1.76	2.45
UE25P1-1598D(1)	1598.0	Tcp	2.86	2.76	2.63	2.19	2.27	2.43	0.69	1.46	0.94	1.37	2.16
UE25P1-1650D(1)	1650.0	Tcp	2.34	2.38	1.94	4.47	4.00	4.16	1.03	1.62	1.54	1.91	2.63
UE25P1-1700D(1)	1700.0	Tcp	4.00	3.91	3.77	4.61	4.14	4.30	0.95	1.28	1.57	1.91	2.59
UE25P1-1740D(1)	1740.0	Tcp	4.17	4.07	3.94	4.24	3.77	3.93	0.64	0.95	1.22	1.55	2.23
UE25P1-1800D(1)	1800.0	Tcp	4.22	4.12	3.99	3.77	3.30	3.46	0.33	0.56	0.79	1.09	1.75
UE25P1-1840D(1)	1840.0	Tcby	1.79	4.65	1.69	3.49	3.07	3.23	0.74	1.48	1.05	1.47	2.24
UE25P1-1880D(1)	1880.0	Tcby	3.37	3.27	3.13	4.24	3.78	3.94	0.80	1.36	1.31	1.67	2.38
UE25P1-1930D(1)	1930.0	Tcby	2.41	4.65	2.10	4.47	4.01	4.17	1.16	1.84	1.63	2.01	2.75
UE25P1-1980D(1)	1980.0	Tcby	1.63	4.35	1.47	3.49	3.07	3.23	0.74	1.48	1.05	1.47	2.24
UE25P1-2000D(1)	2000.0	Tcby	1.81	4.35	1.58	3.77	3.32	3.48	0.61	1.24	1.00	1.37	2.11

Table D2. (Continued)

Sample	Depth feet	Strat. ^d	Ca	Cs	Sr	Am	Eu	Sm	Np	U	Pu-5	Pu-10	Pu-15
Log R													
UE25P1-2040D(1)	2040.0	Tcby	1.99	4.05	1.66	4.07	3.62	3.78	0.86	1.53	1.28	1.67	2.41
UE25P1-2080D(1)	2080.0	Tcby	1.51	4.05	1.29	3.49	3.07	3.23	0.74	1.48	1.05	1.47	2.24
UE25P1-2130D(1)	2130.0	Tcby	1.51	4.05	1.29	3.49	3.07	3.23	0.74	1.48	1.05	1.47	2.24
UE25P1-2160D(1)	2160.0	Tcby	2.42	4.05	2.13	4.29	3.88	4.07	1.10	1.56	1.44	1.82	2.55
UE25P1-2220D(1)	2220.0	Tcby	3.84	3.74	3.61	4.27	3.82	4.00	0.81	0.95	1.26	1.59	2.28
UE25P1-2250D(1)	2250.0	Tcby	3.02	4.36	2.76	4.61	4.14	4.30	0.95	1.28	1.57	1.91	2.59
UE25P1-2290D(1)	2290.0	Tct	3.89	4.86	3.66	4.56	4.10	4.27	1.00	1.22	1.53	1.86	2.55
UE25P1-2340D(1)	2340.0	Tct	2.99	4.36	2.70	4.81	4.35	4.52	1.19	1.47	1.78	2.11	2.80
UE25P1-2380D(1)	2380.0	Tct	2.54	4.65	2.21	4.61	4.15	4.31	1.11	1.67	1.65	2.01	2.73
UE25P1-2420D(1)	2420.0	Tct	1.63	4.35	1.47	3.49	3.07	3.23	0.74	1.48	1.05	1.47	2.24
UE25P1-2470D(1)	2470.0	Tct	2.03	4.35	1.74	4.07	3.62	3.78	0.86	1.53	1.28	1.67	2.41
UE25P1-2520D(1)	2520.0	Tct	1.61	4.65	1.61	2.19	2.27	2.43	0.69	1.46	0.94	1.37	2.16
UE25P1-2580D(1)	2580.0	Tct	2.10	4.65	1.87	4.07	3.62	3.78	0.86	1.53	1.28	1.67	2.41
UE25P1-2640D(1)	2640.0	Tct	2.51	4.35	2.15	4.61	4.15	4.31	1.11	1.67	1.65	2.01	2.73
UE25P1-2660D(1)	2660.0	Tct	2.83	4.36	2.45	4.95	4.50	4.66	1.48	1.98	1.99	2.35	3.07
UE25P1-2700D(1)	2700.0	Tct	2.29	4.35	1.95	4.39	3.94	4.12	1.06	1.59	1.49	1.86	2.59
UE25P1-2760D(1)	2760.0	Tct	3.57	4.40	3.32	4.89	4.42	4.59	1.34	1.80	1.89	2.24	2.95
UE25P1-2800D(1)	2800.0	Tct	3.28	4.38	2.98	5.09	4.63	4.79	1.54	2.05	2.10	2.46	3.17
UE25P1-2850D(1)	2850.0	Tct	3.04	4.09	2.64	5.16	4.70	4.86	1.57	2.09	2.17	2.52	3.22
Avg	-	-	2.55	4.13	2.30	4.02	3.62	3.78	0.87	1.40	1.32	1.69	2.41
SD ^e	-	-	0.91	0.47	0.89	0.77	0.64	0.64	0.30	0.36	0.36	0.35	0.35
Median	-	-	2.34	4.09	1.95	4.07	3.62	3.78	0.82	1.48	1.28	1.67	2.41
Min	-	-	1.04	2.38	1.04	1.89	1.97	2.13	0.33	0.56	0.69	1.09	1.75
Max	-	-	4.22	4.86	3.99	5.16	4.70	4.86	1.57	2.09	2.17	2.52	3.22
USWG1-292(A)	292.0	Tptr	1.32	4.35	1.32	1.89	1.97	2.13	0.47	1.17	0.69	1.09	1.86
USWG1-352(A)	352.0	Tptr	2.87	4.07	2.64	2.19	2.27	2.43	0.69	1.46	0.94	1.37	2.16
USWG1-399(A)	399.0	Tptr	1.04	4.04	1.04	2.19	2.27	2.43	0.69	1.46	0.94	1.37	2.16
USWG1-450(A)	450.0	Tptr	2.15	4.05	1.80	4.25	3.79	3.95	0.92	1.56	1.39	1.76	2.49
USWG1-553(A)	553.0	Tptp	1.94	1.98	1.55	4.07	3.62	3.78	0.86	1.53	1.28	1.67	2.41
USWG1-619(A)	619.0	Tptp	1.99	4.05	1.66	4.11	3.69	3.87	0.97	1.53	1.31	1.70	2.44
USWG1-673(A)	673.0	Tptp	1.73	4.05	1.45	3.78	3.33	3.49	0.78	1.50	1.14	1.54	2.30

Table D2. (Continued)

Sample	Depth feet	Strat. ^d	Ca	Cs	Sr	Am	Eu	Sm	Np	U	Pu-5	Pu-10	Pu-15
			Log R										
USWG1-722(A)	722.0	Tptp	1.99	4.05	1.66	4.07	3.60	3.76	0.51	0.79	1.06	1.38	2.05
USWG1-757(A)	757.0	Tptp	1.73	4.05	1.45	3.78	3.33	3.49	0.78	1.50	1.14	1.54	2.30
USWG1-819(A)	819.0	Tptp	1.99	4.05	1.66	4.07	3.61	3.77	0.72	1.30	1.18	1.54	2.26
USWG1-874.7(A)	874.7	Tptp	1.94	1.98	1.55	4.07	3.61	3.77	0.72	1.30	1.18	1.54	2.26
USWG1-936(A)	936.0	Tptp	0.91	0.00	0.05	4.82	4.70	5.00	2.17	0.01	2.04	2.43	3.18
USWG1-995.5(A)	995.5	Tptp	2.12	2.16	1.72	4.24	3.78	3.94	0.80	1.36	1.31	1.67	2.38
USWG1-1063(A)	1063.0	Tptp	1.99	4.05	1.66	4.07	3.62	3.78	0.86	1.53	1.28	1.67	2.41
USWG1-1104(A)	1104.0	Tptp	1.94	1.98	1.55	4.07	3.62	3.78	0.86	1.53	1.28	1.67	2.41
USWG1-1123(A)	1123.0	Tptp	1.99	4.05	1.66	4.07	3.61	3.77	0.72	1.30	1.18	1.54	2.26
USWG1-1179(A)	1179.0	Tptp	2.12	2.16	1.72	4.25	3.79	3.95	0.92	1.56	1.39	1.76	2.49
USWG1-1191.9(B)	1191.9	Tptp	2.24	2.28	1.84	4.37	3.91	4.07	0.98	1.59	1.47	1.84	2.56
USWG1-1240.6(C)	1240.6	Tptp	1.99	4.05	1.66	4.07	3.61	3.77	0.72	1.30	1.18	1.54	2.26
USWG1-1274(A)	1274.0	Tptp	2.34	4.05	2.07	4.07	3.61	3.77	0.72	1.30	1.18	1.54	2.26
USWG1-1281(A)	1281.0	Tptp	1.99	4.05	1.66	4.07	3.61	3.77	0.72	1.30	1.18	1.54	2.26
USWG1-1286(B)	1286.0	Tptp	3.59	3.54	3.30	5.28	4.81	4.97	1.59	1.94	2.24	2.58	3.26
USWG1-1319(B)	1319.0	Tptp	0.00	0.00	0.00	0.00	0.00	0.00	0.00	0.00	0.00	0.00	0.00
USWG1-1341(B)	1341.0	Tptp	2.69	2.59	2.46	0.00	0.00	0.00	0.00	0.00	0.00	0.00	0.00
USWG1-1357(B)	1357.0	Tptp	1.65	1.68	1.26	3.77	3.30	3.46	0.33	0.56	0.79	1.09	1.75
USWG1-1392.3(B)	1392.3	Tptp	3.17	3.07	2.94	3.46	2.99	3.15	0.20	0.36	0.56	0.82	1.46
USWG1-1400(A)	1400.0	Tptp	4.31	4.21	4.08	3.46	2.99	3.15	0.20	0.36	0.56	0.82	1.46
USWG1-1820.2(B)	1820.2	Tcp	4.12	4.02	3.89	3.77	3.30	3.46	0.33	0.56	0.79	1.09	1.75
USWG1-1942(B)	1942.0	Tcp	1.94	1.98	1.55	4.07	3.60	3.76	0.51	0.79	1.06	1.38	2.05
USWG1-2136.3(B)	2136.3	Tcp	4.09	3.99	3.86	0.00	0.00	0.00	0.00	0.00	0.00	0.00	0.00
USWG1-2173(B)	2173.0	Tcby	4.01	4.28	3.78	0.00	0.00	0.00	0.00	0.00	0.00	0.00	0.00
USWG1-2190(A)	2190.0	Tcby	4.10	4.32	3.87	4.37	3.90	4.06	0.74	1.06	1.34	1.67	2.35
USWG1-2198(A)	2198.0	Tcby	4.09	4.32	3.86	3.77	3.30	3.46	0.33	0.56	0.79	1.09	1.75
USWG1-2256(A)	2256.0	Tcby	4.03	3.93	3.80	0.00	0.00	0.00	0.00	0.00	0.00	0.00	0.00
USWG1-2279(A)	2279.0	Tcby	4.21	4.38	3.98	3.46	2.99	3.15	0.20	0.36	0.56	0.82	1.46
USWG1-2289(A)	2289.0	Tcby	4.26	4.41	4.03	4.07	3.60	3.76	0.51	0.79	1.06	1.38	2.05
USWG1-2316(A)	2316.0	Tcby	4.11	4.33	3.88	0.00	0.00	0.00	0.00	0.00	0.00	0.00	0.00
USWG1-2401(A)	2401.0	Tcby	2.15	4.05	1.80	4.25	3.79	3.95	0.92	1.56	1.39	1.76	2.49
USWG1-2456(A)	2456.0	Tcby	1.73	4.05	1.45	3.77	3.32	3.48	0.61	1.24	1.00	1.37	2.11
USWG1-2487(C)	2487.0	Tcby	1.81	4.35	1.58	3.77	3.32	3.48	0.61	1.24	1.00	1.37	2.11

Table D2. (Continued)

Sample	Depth feet	Strat. ^d	Ca	Cs	Sr	Am	Eu	Sm	Np	U	Pu-5	Pu-10	Pu-15
Log R													
USWG1-2499(A)	2499.0	Tcby	1.51	4.05	1.29	3.48	3.03	3.19	0.55	1.21	0.87	1.26	2.00
USWG1-2506(A)	2506.0	Tcby	1.51	4.05	1.29	3.48	3.03	3.19	0.55	1.21	0.87	1.26	2.00
USWG1-2544(A)	2544.0	Tcby	1.51	4.05	1.29	3.48	3.03	3.19	0.55	1.21	0.87	1.26	2.00
USWG1-2564(A)	2564.0	Tcby	4.21	4.38	3.98	3.46	2.99	3.15	0.20	0.36	0.56	0.82	1.46
USWG1-2600.6(B)	2600.6	Tcby	4.33	4.23	4.10	0.00	0.00	0.00	0.00	0.00	0.00	0.00	0.00
USWG1-2606(A)	2606.0	Tcby	4.22	4.12	3.99	3.46	2.99	3.15	0.20	0.36	0.56	0.82	1.46
USWG1-2607(A)	2607.0	Tcby	4.06	3.96	3.83	0.00	0.00	0.00	0.00	0.00	0.00	0.00	0.00
USWG1-2622(A)	2622.0	Tcby	4.03	4.29	3.80	3.46	2.99	3.15	0.20	0.36	0.56	0.82	1.46
USWG1-2641.6(B)	2641.6	Tct	3.95	4.71	3.72	4.07	3.60	3.76	0.51	0.79	1.06	1.38	2.05
USWG1-2663(A)	2663.0	Tct	4.13	4.74	3.90	3.46	2.99	3.15	0.20	0.36	0.56	0.82	1.46
USWG1-2734(A)	2734.0	Tct	3.93	4.71	3.70	3.46	2.99	3.15	0.20	0.36	0.56	0.82	1.46
USWG1-2765(A)	2765.0	Tct	3.60	4.40	3.36	4.37	3.90	4.06	0.74	1.06	1.34	1.67	2.35
USWG1-2804(A)	2804.0	Tct	1.81	4.35	1.58	3.77	3.32	3.48	0.61	1.24	1.00	1.37	2.11
USWG1-2805(A)	2805.0	Tct	2.15	4.05	1.80	4.24	3.78	3.94	0.80	1.36	1.31	1.67	2.38
USWG1-2820(A)	2820.0	Tct	1.81	4.35	1.58	3.77	3.32	3.48	0.61	1.24	1.00	1.37	2.11
USWG1-2838(A)	2838.0	Tct	1.99	4.05	1.66	4.07	3.60	3.76	0.51	0.79	1.06	1.38	2.05
USWG1-2869(B)	2869.0	Tct	1.73	4.05	1.45	3.77	3.30	3.46	0.33	0.56	0.79	1.09	1.75
USWG1-2884(A)	2884.0	Tct	2.03	4.35	1.74	4.07	3.60	3.76	0.51	0.79	1.06	1.38	2.05
USWG1-2915(A)	2915.0	Tct	2.03	4.35	1.74	4.07	3.60	3.76	0.51	0.79	1.06	1.38	2.05
USWG1-2932(A)	2932.0	Tct	1.81	4.35	1.58	3.77	3.30	3.46	0.33	0.56	0.79	1.09	1.75
USWG1-2938.8(A)	2938.8	Tct	2.10	4.65	1.87	4.07	3.60	3.76	0.51	0.79	1.06	1.38	2.05
USWG1-2948(A)	2948.0	Tct	2.77	4.35	2.53	4.13	3.73	3.93	0.87	0.79	1.16	1.50	2.19
USWG1-2966(B)	2966.0	Tct	1.92	4.65	1.76	3.77	3.30	3.46	0.33	0.56	0.79	1.09	1.75
USWG1-2981(A)	2981.0	Tct	2.18	4.35	1.86	4.24	3.77	3.93	0.64	0.95	1.22	1.55	2.23
USWG1-3018(A)	3018.0	Tct	3.40	4.39	3.12	5.02	4.56	4.72	1.37	1.68	1.98	2.32	3.01
USWG1-3079(A)	3079.0	Tct	3.56	4.40	3.32	4.81	4.34	4.50	1.13	1.47	1.76	2.10	2.79
USWG1-3167(A)	3167.0	Tct	3.70	4.42	3.46	4.77	4.30	4.46	1.09	1.43	1.72	2.06	2.75
USWG1-3288(A)	3288.0	Tct	4.02	4.29	3.78	5.00	4.53	4.69	1.31	1.66	1.95	2.29	2.98
USWG1-3401(A)	3401.0	Tct	3.42	4.12	3.18	4.38	3.94	4.11	0.88	1.06	1.37	1.70	2.39

Table D2. (Continued)

Sample	Depth feet	Strat. ^d	Ca	Cs	Sr	Am	Eu	Sm	Np	U	Pu-5	Pu-10	Pu-15
			Log R										
USWG1-3523(A)	3523.0	Tct	3.54	4.14	3.30	4.65	4.22	4.41	1.24	1.28	1.64	1.98	2.68
Avg	-	-	2.68	3.80	2.40	3.49	3.11	3.26	0.60	0.94	0.99	1.29	1.91
SD ^c	-	-	1.09	1.00	1.11	1.38	1.23	1.28	0.41	0.54	0.51	0.60	0.80
Median	-	-	2.15	4.05	1.80	4.07	3.60	3.76	0.61	1.06	1.06	1.38	2.11
Min	-	-	0.00	0.00	0.00	0.00	0.00	0.00	0.00	0.00	0.00	0.00	0.00
Max	-	-	4.33	4.74	4.10	5.28	4.81	5.00	2.17	1.94	2.24	2.58	3.26
USWG2-10D(1)	10.0	Tpcr	2.14	5.19	2.14	0.00	0.00	0.00	0.00	0.00	0.00	0.00	0.00
USWG2-100D(1)	100.0	Tpcr	1.78	4.82	1.78	0.00	0.00	0.00	0.00	0.00	0.00	0.00	0.00
USWG2-200D(1)	200.0	Tpcp	0.00	0.00	0.00	0.00	0.00	0.00	0.00	0.00	0.00	0.00	0.00
USWG2-230D(1)	230.0	Tpcp	0.00	0.00	0.00	0.00	0.00	0.00	0.00	0.00	0.00	0.00	0.00
USWG2-270D(1)	270.0	Tpy	2.42	2.46	2.02	4.89	4.65	4.92	2.02	1.22	2.02	2.39	3.12
USWG2-304(A)	304.0	Tpy	0.00	0.00	0.00	0.00	0.00	0.00	0.00	0.00	0.00	0.00	0.00
USWG2-331(A)	331.0	Tpy	3.24	3.28	2.84	5.37	4.90	5.06	1.67	2.02	2.32	2.66	3.35
USWG2-338(A)	338.0	Tpy	3.33	3.37	2.94	5.46	4.99	5.15	1.76	2.12	2.42	2.76	3.44
USWG2-358(A)	358.0	Tpg	3.00	3.04	2.60	5.13	4.66	4.82	1.43	1.78	2.08	2.42	3.11
USWG2-395(A)	395.0	Tpg	2.66	4.35	2.29	4.77	4.30	4.46	1.09	1.43	1.72	2.06	2.75
USWG2-501(A)	501.0	Tpp	2.74	4.53	2.37	4.84	4.37	4.53	1.17	1.51	1.80	2.14	2.83
USWG2-547(B)	547.0	Tpp	2.69	4.83	2.37	4.77	4.30	4.46	1.09	1.43	1.72	2.06	2.75
USWG2-561(A)	561.0	Tpp	3.64	4.57	3.39	4.94	4.47	4.63	1.26	1.60	1.90	2.23	2.92
USWG2-584(A)	584.0	Tpp	3.25	4.83	3.03	0.00	0.00	0.00	0.00	0.00	0.00	0.00	0.00
USWG2-627(A)	627.0	Tpp	3.62	4.84	3.38	4.77	4.30	4.46	1.09	1.43	1.72	2.06	2.75
USWG2-675(B)	675.0	Tpp	3.87	4.86	3.61	5.37	4.90	5.06	1.67	2.02	2.32	2.66	3.35
USWG2-723(A)	723.0	Tpp	2.70	4.83	2.37	5.13	4.89	5.15	2.26	1.43	2.25	2.63	3.36
USWG2-743(A)	743.0	Tptbr	3.36	4.84	3.04	5.35	4.92	5.11	1.92	1.96	2.33	2.68	3.38
USWG2-762(A)	762.0	Tptbr	4.26	4.16	4.03	4.24	3.77	3.93	0.64	0.95	1.22	1.55	2.23
USWG2-770(A)	770.0	Tptr	2.26	5.19	2.19	3.77	3.30	3.46	0.33	0.56	0.79	1.09	1.75
USWG2-822(A)	822.0	Tptr	2.56	4.82	2.26	4.61	4.14	4.30	0.95	1.28	1.57	1.91	2.59
USWG2-855(A)	855.0	Tptr	2.28	4.82	2.05	4.24	3.77	3.93	0.64	0.95	1.22	1.55	2.23
USWG2-898(A)	898.0	Tptr	2.92	4.83	2.70	3.77	3.30	3.46	0.33	0.56	0.79	1.09	1.75
USWG2-921(D)	921.0	Tptq	2.81	2.85	2.41	5.00	4.60	4.80	1.68	1.60	2.00	2.35	3.06
USWG2-951(A)	951.0	Tptp	1.65	1.68	1.26	3.77	3.30	3.46	0.33	0.56	0.79	1.09	1.75
USWG2-984(A)	984.0	Tptp	2.42	2.46	2.02	4.89	4.65	4.92	2.02	1.22	2.02	2.39	3.12

Table D2. (Continued)

Sample	Depth feet	Strat. ^d	Ca	Cs	Sr	Am	Eu	Sm	Np	U	Pu-5	Pu-10	Pu-15
Log R													
USWG2-1032(A)	1032.0	Tptp	2.45	4.35	2.09	4.54	4.07	4.23	0.89	1.22	1.51	1.84	2.53
USWG2-1072(A)	1072.0	Tptp	2.45	4.35	2.09	4.54	4.07	4.23	0.89	1.22	1.51	1.84	2.53
USWG2-1133(A)	1133.0	Tptp	2.66	4.35	2.29	4.77	4.30	4.46	1.09	1.43	1.72	2.06	2.75
USWG2-1178(A)	1178.0	Tptp	2.18	4.35	1.86	4.24	3.77	3.93	0.64	0.95	1.22	1.55	2.23
USWG2-1234(A)	1234.0	Tptp	2.42	2.46	2.02	4.54	4.07	4.23	0.89	1.22	1.51	1.84	2.53
USWG2-1281(A)	1281.0	Tptp	2.64	2.68	2.24	4.77	4.30	4.46	1.09	1.43	1.72	2.06	2.75
USWG2-1331(A)	1331.0	Tptp	2.64	2.68	2.24	4.77	4.30	4.46	1.09	1.43	1.72	2.06	2.75
USWG2-1382(A)	1382.0	Tptp	2.66	4.35	2.29	4.77	4.30	4.46	1.09	1.43	1.72	2.06	2.75
USWG2-1420(A)	1420.0	Tptp	2.64	2.68	2.24	4.77	4.30	4.46	1.09	1.43	1.72	2.06	2.75
USWG2-1461(A)	1461.0	Tptp	2.64	2.68	2.24	4.77	4.30	4.46	1.09	1.43	1.72	2.06	2.75
USWG2-1536(A)	1536.0	Tptp	3.14	3.11	2.84	4.94	4.47	4.63	1.26	1.60	1.90	2.23	2.92
USWG2-1585(A)	1585.0	Tptp	3.07	3.02	2.78	4.77	4.30	4.46	1.09	1.43	1.72	2.06	2.75
USWG2-1634(A)	1634.0	Tptp	4.06	4.50	3.81	5.37	4.90	5.06	1.67	2.02	2.32	2.66	3.35
USWG2-1664.7(A)	1664.7	Tptp	2.46	2.38	2.21	3.77	3.30	3.46	0.33	0.56	0.79	1.09	1.75
USWG2-1691(B)	1691.0	Tptp	4.15	4.06	3.92	4.77	4.30	4.46	1.09	1.43	1.72	2.06	2.75
USWG2-2744(A)	2744.0	Tcp	2.18	4.35	1.86	4.24	3.77	3.93	0.64	0.95	1.22	1.55	2.23
USWG2-2820(A)	2820.0	Tcp	1.81	4.35	1.58	3.77	3.30	3.46	0.33	0.56	0.79	1.09	1.75
USWG2-2869(A)	2869.0	Tcp	2.01	4.82	1.89	3.77	3.30	3.46	0.33	0.56	0.79	1.09	1.75
USWG2-2887(A)	2887.0	Tcp	2.18	4.35	1.86	4.24	3.77	3.93	0.64	0.95	1.22	1.55	2.23
USWG2-2950(A)	2950.0	Tcp	2.46	4.53	2.13	4.54	4.07	4.23	0.89	1.22	1.51	1.84	2.53
USWG2-2970(A)	2970.0	Tcp	2.67	4.53	2.31	4.77	4.30	4.46	1.09	1.43	1.72	2.06	2.75
USWG2-3037(A)	3037.0	Tcp	3.39	4.39	3.06	5.37	4.90	5.06	1.67	2.02	2.32	2.66	3.35
USWG2-3067(A)	3067.0	Tcp	3.95	4.47	3.73	0.00	0.00	0.00	0.00	0.00	0.00	0.00	0.00
USWG2-3192(A)	3192.0	Tcp	4.00	3.91	3.77	4.61	4.14	4.30	0.95	1.28	1.57	1.91	2.59
USWG2-3228(A)	3228.0	Tcp	2.70	2.68	2.39	4.54	4.07	4.23	0.89	1.22	1.51	1.84	2.53
USWG2-3250(A)	3250.0	Tcby	3.77	4.43	3.52	5.13	4.66	4.82	1.43	1.78	2.08	2.42	3.11
USWG2-3308(A)	3308.0	Tcby	2.63	5.52	2.54	4.24	3.77	3.93	0.64	0.95	1.22	1.55	2.23
USWG2-3330(A)	3330.0	Tcby	2.08	5.12	2.08	0.00	0.00	0.00	0.00	0.00	0.00	0.00	0.00
USWG2-3349(A)	3349.0	Tcby	2.21	5.12	2.14	3.77	3.30	3.46	0.33	0.56	0.79	1.09	1.75
USWG2-3366(A)	3366.0	Tcby	2.21	5.12	2.14	3.77	3.30	3.46	0.33	0.56	0.79	1.09	1.75
USWG2-3416(A)	3416.0	Tcby	2.21	5.12	2.14	3.77	3.30	3.46	0.33	0.56	0.79	1.09	1.75

Table D2. (Continued)

Sample	Depth feet	Strat. ^d	Ca	Cs	Sr	Am	Eu	Sm	Np	U	Pu-5	Pu-10	Pu-15
Log R													
USWG2-3454(A)	3454.0	Tcby	3.84	4.86	3.58	5.21	4.74	4.90	1.52	1.87	2.17	2.50	3.19
USWG2-3492(A)	3492.0	Tcby	3.81	4.86	3.56	5.02	4.55	4.71	1.33	1.68	1.98	2.31	3.00
USWG2-3512(A)	3512.0	Tct	3.35	5.20	3.10	4.94	4.47	4.63	1.26	1.60	1.90	2.23	2.92
USWG2-3541(A)	3541.0	Tct	2.76	5.19	2.49	4.77	4.30	4.46	1.09	1.43	1.72	2.06	2.75
USWG2-3578(A)	3578.0	Tct	3.83	5.36	3.59	5.13	4.66	4.82	1.43	1.78	2.08	2.42	3.11
USWG2-3627(A)	3627.0	Tct	2.93	5.35	2.66	4.94	4.47	4.63	1.26	1.60	1.90	2.23	2.92
USWG2-3671(A)	3671.0	Tct	2.76	5.19	2.49	4.85	4.47	4.69	1.62	1.43	1.87	2.23	2.93
USWG2-3720(A)	3720.0	Tct	2.76	5.19	2.49	4.77	4.30	4.46	1.09	1.43	1.72	2.06	2.75
USWG2-3724(A)	3724.0	Tct	3.06	4.83	2.69	5.16	4.69	4.85	1.47	1.82	2.12	2.46	3.14
USWG2-3750(A)	3750.0	Tct	3.11	5.35	2.80	5.16	4.69	4.85	1.47	1.82	2.12	2.46	3.14
USWG2-3772(A)	3772.0	Tct	3.05	5.19	2.73	5.13	4.66	4.82	1.43	1.78	2.08	2.42	3.11
USWG2-3795(A)	3795.0	Tct	3.14	3.18	2.74	5.27	4.80	4.96	1.57	1.93	2.22	2.56	3.25
USWG2-3833(A)	3833.0	Tct	3.15	5.13	2.80	5.24	4.77	4.93	1.55	1.90	2.20	2.53	3.22
USWG2-3875(A)	3875.0	Tct	3.09	5.19	2.76	5.16	4.69	4.85	1.47	1.82	2.12	2.46	3.14
USWG2-3908(A)	3908.0	Tct	2.89	2.93	2.49	5.07	4.64	4.84	1.67	1.68	2.05	2.40	3.10
USWG2-3933(A)	3933.0	Tct	2.81	2.85	2.41	5.00	4.60	4.80	1.68	1.60	2.00	2.35	3.06
USWG2-3968(A)	3968.0	Tct	2.95	5.13	2.63	5.02	4.55	4.71	1.33	1.68	1.98	2.31	3.00
Avg	-	-	2.75	4.07	2.48	4.21	3.80	3.95	1.02	1.23	1.52	1.81	2.42
SD ^c	-	-	0.83	1.28	0.78	1.55	1.41	1.47	0.58	0.60	0.69	0.78	0.97
Median	-	-	2.72	4.48	2.40	4.77	4.30	4.46	1.09	1.43	1.72	2.06	2.75
Min	-	-	0.00	0.00	0.00	0.00	0.00	0.00	0.00	0.00	0.00	0.00	0.00
Max	-	-	4.26	5.52	4.03	5.46	4.99	5.15	2.26	2.12	2.42	2.76	3.44
ALL DATA													
Avg	-	-	2.58	3.90	2.32	3.84	3.45	3.60	0.81	1.15	1.25	1.57	2.21
SD ^c	-	-	1.00	1.15	0.98	1.40	1.25	1.29	0.49	0.55	0.61	0.67	0.83
Median	-	-	2.45	4.19	2.14	4.10	3.67	3.85	0.74	1.28	1.22	1.55	2.26
Min	-	-	0.00	0.00	0.00	0.00	0.00	0.00	0.00	0.00	0.00	0.00	0.00
Max	-	-	4.33	5.52	4.10	5.63	5.16	5.32	2.26	2.28	2.58	2.92	3.61

^a Uncertainty related to mechanistic model reaction constants and not mineral spatial variability.^b Mineral abundance data used to calculate Log R are reported in Table D1.^c Standard deviation related to variability in mineral abundance for the particular well and not uncertainty in mechanistic model reaction constants.

^d Stratigraphic names defined in Warren et al. (2000). Tuff Cone hydrostratigraphic unit is a composite of Paintbrush Group (Tp), Volcanics of Area 20 (Ta), and the Crater Flow Group (Tc). Tb_y = Yucca Mountain Lobe; Tcp = Prow Pass Tuff; Tct = Tram Tuff; Tpcp = crystal-poor Tiva Canyon Tuff; tpcr = crystal-rich Tiva Canyon Tuff; Tpg = rhyolite of Black Glass Canyon; Tpp = Pah Canyon Tuff; Tptbr = crystal-rich bedded Topopah Spring Tuff; Tptp = crystal-poor Topopah Spring Tuff; Tptq = quartz-rich Topopah Spring Tuff; Tptr = crystal-rich Topopah Spring Tuff; Tpy = Yucca Mtn. Tuff.

INTENTIONALLY LEFT BLANK

Appendix E. Mineral Abundance and Predicted Radionuclide Retardation Data for Pahute Mesa Fracture Flow Zones

Tables E1 and E2 include all mineralogy/ R / K_d information discussed in this report with regards to fracture flow conditions at Pahute Mesa. These include the mineralogy/ $K_d s / R_s$ based on information in Pawloski et al. (2001) (Section 6.2). It also includes average hydrostratigraphic unit mineralogy/ $R_s / K_d s$ discussed in Section 6.3. Finally, the data in Tables E1 and E2 include the mineralogy/ $R_s / K_d s$ for each fracture lining mineral analysis within the Tuff Cone hydrostratigraphic unit (defined in Drellack (1997) reported in Carlos et al. (1995) and discussed in Section 6.5.2 of this report. Only those sorbing minerals included in our mechanistic sorption model are reported here. We also include manganese oxide mineral abundances (when possible) though they are not used in our radionuclide retardation calculations due to lack of radionuclide sorption data. Predicted radionuclide $K_d s$ are reported alongside the mineral abundance data in Table D1. Table D2 lists the retardation factors for the same samples listed in D1. Table D2 also contains stratigraphic information for each sample. Radionuclide $K_d s$ and R_s were calculated in the same manner as described in Appendix C for porous flow. The methods for calculating K_d for fracture flow conditions were defined in Section 4.2 of this report. For convenience, the following example calculation provides step-by-step instruction of how $K_d s$ (and R_s) were determined.

Predicting radionuclide retardation in a fracture flow environment is significantly more complicated than in the porous flow case. In the fracture flow case, a conceptual model is needed for flow in a fractured medium. The simplest conceptual model is the parallel plate fracture model. The conceptual model introduced in Section 4.2 of this report is based on the parallel plate model but includes two important (but untested) features: the concept of integrating some flow in the matrix alongside the fracture and a rudimentary model for evaluating colloid effects.

The concept of integrating some flow in the matrix was the result of two factors. First, measured effective porosities are not always consistent with the porosities calculated from fracture densities and apertures. As such, it is not clear how best to estimate the quantity of reactive minerals that a flowing fluid contacts. Second, it was found that, depending on the domain size and flow velocities, diffusion into a small volume of matrix at the fracture-matrix interface can be approximately instantaneous. For example, it was estimated that a tracer could diffuse into a few millimeters of mafic-poor Calico Hills lava in less than 24 hours. Based on the CHESHIRE HST flow conditions, diffusion into these few millimeters could be considered instantaneous. Furthermore, flow could be considered to occur within this matrix volume (however, diffusion farther into the matrix must still be accounted for!).

The colloid model described in Section 4.2 was based on the assumption that: colloids are not retarded due to filtration, radionuclide sorption to colloids is an equilibrium process,

and the colloid load in Pahute Mesa waters is constant and uniform. Based on these simplifications, the effect that colloids have on radionuclide transport could be simplified to a retardation factor. However, as stated in Section 4.3, it is likely that this simplification will not adequately describe the behavior of radionuclides in the field, particularly as a result of non-linear and/or kinetically controlled radionuclide sorption to colloids. This concept was introduced primarily to evaluate the effect of colloids and calculate radionuclide retardation at equilibrium. Below, we present an example calculation based on the first entry in Table E1.

Based on the parallel-plate model described in section 4, we can determine the K_d and R under parallel plate fracture flow conditions by the following equations:

$$K_{d,fz} = \frac{1}{\rho_{b,FL}B + \rho_{b,M}C} \sum_{i=1}^n K_{d,i} (\rho_{b,FL}B\phi_{m,i,FL} + \rho_{b,M}C\phi_{m,i,M}) \quad (E1)$$

$$R_{fz} = 1 + \frac{1}{A + \theta_{fl}B + \theta_mC} \sum_{i=1}^n K_{d,i} (\rho_{b,FL}B\phi_{m,i,FL} + \rho_{b,M}C\phi_{m,i,M}) \quad (E2)$$

in the case where colloid effects are ignored and

$$K'_{d,fz} = \frac{1}{(\rho_{b,FL}B + \rho_{b,M}C)R_{col}} \sum_{i=1}^n K_{d,i} (\rho_{b,FL}B\phi_{m,i,FL} + \rho_{b,M}C\phi_{m,i,M}) \quad (E3)$$

$$R'_{fz} = 1 + \frac{1}{(A + \theta_{fl}B + \theta_mC)R_{col}} \sum_{i=1}^n K_{d,i} (\rho_{b,FL}B\phi_{m,i,FL} + \rho_{b,M}C\phi_{m,i,M}) \quad (E4)$$

in the case where the rudimentary colloid model is included. Note that the difference between the two R s and K_d s is simply the addition of parameter R_{col} which accounts for the decrease in K_d or R resulting from radionuclide sorption to colloids. Thus, while Tables E1 and E2 present data that includes the effect of colloids, it is quite simple to convert between the colloid-affected and colloid-unaffected values.

From the equations listed above, it is evident that R s and K_d s can be calculated for the fracture flow system if the bulk density of the matrix ($\rho_{b,M}$), the bulk density of the fracture lining ($\rho_{b,FL}$), the half-aperture (A), the fracture lining thickness (B), the matrix flow zone thickness (C), the porosity of the fracture lining (θ_{fl}), the porosity of the matrix (θ_m), the colloid retardation factor (R_{col}), and the K_d s ($K_{d,i}$) and mass fractions ($\phi_{m,i,FL}$ and $\phi_{m,i,M}$) of individual minerals in the fracture lining and matrix are known.

As an example, we use the mineral abundance information from the first entry in Table E1 (CHESHIRE unclassified HST average fracture mineralogy, Table 9), combined with the first entry in Table D1 (CHESHIRE unclassified HST average matrix mineralogy, Table 9), the individual radionuclide-mineral K_d s of Table 8 (based on Pahute Mesa water chemistry (Table 7) and mechanistic model reaction constants (Appendix A)), the fracture conceptual model parameters listed in Table 10, the fracture lining and matrix

bulk density reported in Table 9, and the predicted colloid K_d s listed in Table 11 to calculate the Cs K_d and R . Using Equation (E1) and ignoring colloid effects, the Cs K_d is calculated by:⁴²

$$K_{d,fz} = \frac{1}{2.16(10^{-4}) + 2.13(2.5 \times 10^{-3})} \left[10^{3.50} (2.16(10^{-4}) 0.082 + 2.13(2.5 \times 10^{-3}) 0.0) + 10^{5.56} (2.16(10^{-4}) 0.0 + 2.13(2.5 \times 10^{-3}) 0.00053) + 10^{2.89} (2.16(10^{-4}) 0.080 + 2.13(2.5 \times 10^{-3}) 0.0025) \right] = 10^{2.30}. \quad (\text{E5})$$

Similarly, Equation (E2) can be used to calculate R (ignoring colloid effects) such that:

$$R_{fz} = 1 + \frac{1}{2.5 \times 10^{-4} + 0.15(10^{-4}) + 0.15(2.5 \times 10^{-3})} \left[10^{3.50} (2.16(10^{-4}) 0.082 + 2.13(2.5 \times 10^{-3}) 0.0) + 10^{5.56} (2.16(10^{-4}) 0.0 + 2.13(2.5 \times 10^{-3}) 0.00053) + 10^{2.89} (2.16(10^{-4}) 0.080 + 2.13(2.5 \times 10^{-3}) 0.0025) \right] = 10^{3.24}. \quad (\text{E6})$$

To account for colloid effects in the rudimentary fashion described in Section 4.3, K_d must simply be divided by the colloid retardation factor, R_{col} :

$$K'_{d,fz} = \frac{K_{d,fz}}{R_{col}} = \frac{K_{d,fz}}{1 + K_{d,col} C_{col}} = \frac{10^{2.30}}{1 + 10^{5.56} (1.17 \times 10^{-4})} = 10^{0.66}. \quad (\text{E7})$$

For this example, the colloid concentration is reported in Table 10 while the colloid K_d s are reported in Table 11.⁴³

Similarly, in the case of R :

⁴² Note that K_d information for Cs is available only for zeolite, mica, and smectite minerals.

⁴³ For Cs, two cases are reported in Table 11. In the first, it is assumed that colloids are dominated by smectite (Cs affinity for these colloids is weak). In the second, it is assumed that colloids are dominated by illite/mica (Cs affinity for these colloids is very strong). In this example, we evaluate the illite/mica colloid case.

$$R'_{fz} = 1 + \frac{R_{fz} - 1}{R_{col}} = 1 + \frac{R_{fz} - 1}{1 + K_{d,col}C_{col}} = 1 + \frac{10^{3.24} - 1}{1 + 10^{5.56}(1.17 \times 10^{-4})} = 10^{1.61} \quad (E8)$$

The various parameters used to calculate fracture flow K_d s and R_s varied depending on the data source. In the case of CHESHIRE unclassified HST model parameters, the location of the various parameters is reported above.

In the case of the average hydrostratigraphic unit radionuclide retardation analysis (Section 6.3), the average matrix and fracture lining mineral abundances are reported in Tables D1 and E1, respectively (these values are also reported in Table 13). Radionuclide-mineral K_d s are taken from Table 8 (based on Pahute Mesa water chemistry (Table 7) and mechanistic model reaction constants (Appendix A)). The fracture conceptual model parameters (A, B, and C) are calculated from information listed in Table 13 or approximated. The parameter A is equal to one half of the reported fracture aperture (Table 13). The parameter B is set to 100 micrometers. The parameter C is calculated from the difference between the average effective porosity (0.0013 for all four fractured hydrostratigraphic units) and the porosity estimated from fracture density, aperture, and fracture lining porosity (all data reported in Table 13). The parameter C for TMA, TC, TBA, and BAQ is equal to 4.6, 0.05, 0.62, and 0.0 mm, respectively. The fracture lining and matrix bulk densities are estimated using an average mineral density of 2.5 g/cm³ and the average matrix porosities of Table 13 (TMA, TC, TBA, and BAQ average porosities are 0.29, 0.285, 0.29, and 0.18, respectively. Calculated bulk densities are 1.78, 1.79, 1.78, and 2.05 g/cm³, respectively).⁴⁴ The predicted colloid K_d s and colloid concentrations are the same as used in the CHESHIRE calculations (Tables 11 and 12).

In the case of heterogeneous fracture lining mineral distribution within the TC hydrostratigraphic unit (Section 6.5.2), the average TC matrix mineral abundances reported in Table D1 are used in combination with the variable fracture lining mineral data reported in Table E1.⁴⁵ Radionuclide-mineral K_d s are taken from Table 8. The fracture conceptual model parameters, fracture lining bulk density, matrix bulk density, fracture lining porosity, and matrix porosity are held constant and equivalent to the average TC values described above. The predicted colloid K_d s and colloid concentrations are the same as used in the CHESHIRE calculations (Tables 11 and 12).

⁴⁴ It was assumed that fracture lining and matrix porosities are equivalent.

⁴⁵ In other words, for the R_s reported in Section 6.5.2 as well as the R_s and K_d s reported in Tables E1 and E2 for wells UE-25, USW-G1, USW-G2, USW-G3, and USW-G4, matrix mineralogy is held constant and equal to the TC hydrostratigraphic unit values reported in Table D1 while fracture lining mineralogy is allowed to vary according to the mineralogy listed in Table E1.

Table E1. Radionuclide sorbing mineral abundances and predicted retardation factors for Tuff Cone hydrostratigraphic unit fracture flow zones.

Sample	Depth feet	Calcite	Zeolite	Hematite	Smectite	MnOx ^f	Ca	Cs ^e	Sr	Am	Eu	Sm	Np	U	Pu -5	Pu -10	Pu -15
		Fracture	Lining	Mass % ^d	-----	Log K _d ^d											
CHESHIRE ^a	-	7.4	8.2	2.7	10.5	-	1.3 (1.3,1.3)	2.3/0.7 (1.3/0.6,2.3/0.7)	1.0 (1.0,1.0)	0.9 (0.9,0.8)	0.9 (0.9,1.0)	1.1 (1.0,1.1)	-0.4 (-0.7,0.1)	0.0 (-0.4,0.4)	-0.1 (-0.5,0.4)	0.3 (-0.2,0.7)	0.8 (0.5,1.0)
TMA ^{a,b}	-	13	7	(5)	15	(5)	2.7 (2.7,2.7)	3.4/1.7 (2.4/1.7,3.4/1.7)	2.4 (2.4,2.4)	1.4 (1.4,1.3)	1.4 (1.3,1.4)	1.5 (1.4,1.5)	0.0 (-0.2,0.4)	0.5 (0.1,0.9)	0.4 (0.0,0.8)	0.7 (0.3,1.1)	1.3 (0.9,1.4)
TC ^{a,b}	-	3	30	(20)	11	(20)	3.0 (3.0,3.0)	3.2/1.6 (2.4/1.7,3.2/1.6)	2.8 (2.8,2.8)	1.9 (2.0,1.9)	2.1 (1.9,2.1)	2.1 (2.1,2.1)	1.5 (0.7,1.5)	2.2 (1.4,2.2)	1.8 (0.9,1.8)	2.1 (1.3,2.1)	2.5 (2.0,2.5)
TBA ^{a,b}	-	0	24	(60)	12	(60)	2.5 (2.5,2.5)	3.6/1.9 (2.6/1.9,3.6/1.9)	2.3 (2.3,2.3)	1.9 (1.9,1.9)	2.0 (1.9,2.0)	2.0 (2.0,2.0)	1.0 (0.6,1.4)	1.7 (1.3,2.1)	1.3 (0.8,1.7)	1.7 (1.2,2.1)	2.3 (1.9,2.5)
BAQ ^{a,b}	-	50	50	(0)	0	(0)	3.3 (3.3,3.3)	3.2/1.6 (2.6/1.9,3.2/1.6)	3.1 (3.1,3.1)	2.2 (2.4,1.9)	2.5 (2.4,2.6)	2.9 (2.9,3.0)	1.5 (1.1,2.0)	-0.3 (-0.3,-0.3)	1.4 (0.9,1.8)	1.7 (1.3,2.1)	2.3 (1.9,2.5)
UE-25	780.8	49.0	2.0	0.0	0.0	0.0	2.26	3.03/1.39	2.02	2.04	2.37	2.51	1.36	-0.05	1.21	1.56	2.11
UE-25	872.7	0.0	68.6	0.0	0.0	0.0	3.29	3.39/1.75	3.06	0.93	0.94	0.94	-0.57	-0.05	-0.09	0.24	0.76
UE-25	967.8	0.0	68.6	0.0	0.0	0.0	3.29	3.39/1.75	3.06	0.93	0.94	0.94	-0.57	-0.05	-0.09	0.24	0.76
UE-25	990.8	0.0	3.6	0.0	3.6	0.0	2.38	3.05/1.41	2.13	1.50	1.50	1.50	-0.15	0.28	0.42	0.73	1.23
UE-25	990.8	0.0	16.7	0.0	2.8	0.0	2.76	3.14/1.50	2.53	1.42	1.42	1.42	-0.21	0.22	0.35	0.66	1.16
UE-25	1049.9	0.0	87.3	0.0	1.8	0.0	3.39	3.46/1.82	3.16	1.30	1.30	1.31	-0.30	0.15	0.24	0.56	1.06
UE-25	1102.4	0.0	14.3	0.0	14.3	0.0	2.76	3.15/1.50	2.51	2.00	2.00	2.00	0.31	0.69	0.91	1.22	1.71
UE-25	1105.6	0.0	82.8	0.0	0.0	0.0	3.37	3.44/1.80	3.14	0.93	0.94	0.94	-0.57	-0.05	-0.09	0.24	0.76
UE-25	1243.4	0.0	74.4	0.0	0.0	0.0	3.32	3.41/1.77	3.09	0.93	0.94	0.94	-0.57	-0.05	-0.09	0.24	0.76
UE-25	1253.3	0.0	64.4	0.0	2.2	0.0	3.27	3.38/1.74	3.04	1.36	1.36	1.36	-0.26	0.18	0.29	0.61	1.11
UE-25	1276.2	0.0	38.5	0.0	36.9	1.5	3.12	3.31/1.66	2.87	2.39	2.39	2.39	0.69	1.06	1.30	1.60	2.09
UE-25	1276.2	0.0	20.0	0.0	48.0	2.0	2.95	3.23/1.59	2.68	2.50	2.50	2.50	0.79	1.16	1.41	1.71	2.20
UE-25	1282.8	0.0	51.0	0.0	49.0	0.0	3.23	3.37/1.73	2.98	2.51	2.50	2.51	0.80	1.17	1.42	1.72	2.21
UE-25	1295.9	0.0	82.8	0.0	17.2	0.0	3.38	3.46/1.81	3.15	2.08	2.07	2.07	0.38	0.76	0.99	1.29	1.78
UE-25	1302.5	0.0	77.4	0.0	16.1	3.2	3.35	3.44/1.79	3.12	2.05	2.05	2.05	0.36	0.74	0.96	1.27	1.76
UE-25	1309.1	0.0	66.7	0.0	13.9	2.8	3.29	3.40/1.76	3.06	1.99	1.99	1.99	0.30	0.68	0.90	1.21	1.70

Table E1. (continued)

Sample	Depth feet	Calcite	Zeolite	Hematite	Smectite	MnOx ^f	Ca	Cs ^e	Sr	Am	Eu	Sm	Np	U	Pu -5	Pu -10	Pu -15
		Fracture	Lining	Mass % ^d	-----	Log K _d ^d											
UE-25	1318.9	0.0	80.6	0.0	2.8	0.0	3.36	3.44/1.79	3.13	1.42	1.42	1.42	-0.21	0.22	0.35	0.66	1.16
UE-25	1322.2	0.0	64.4	0.0	11.1	0.0	3.28	3.39/1.74	3.04	1.90	1.90	1.90	0.22	0.61	0.82	1.12	1.62
UE-25	1338.6	0.0	85.7	0.0	8.9	0.0	3.39	3.46/1.82	3.16	1.82	1.81	1.82	0.14	0.53	0.73	1.04	1.54
UE-25	1361.5	0.0	45.3	0.0	7.8	0.0	3.14	3.31/1.66	2.90	1.77	1.76	1.77	0.09	0.49	0.69	0.99	1.49
UE-25	1417.3	0.0	81.4	0.0	0.0	8.5	3.36	3.44/1.79	3.13	0.93	0.94	0.94	-0.57	-0.05	-0.09	0.24	0.76
UE-25	1420.6	0.0	80.6	0.0	13.9	0.0	3.37	3.45/1.80	3.13	1.99	1.99	1.99	0.30	0.68	0.90	1.21	1.70
UE-25	1420.6	0.0	17.2	0.0	0.0	82.8	2.77	3.14/1.50	2.54	0.93	0.94	0.94	-0.57	-0.05	-0.09	0.24	0.76
UE-25	1643.7	0.0	80.0	0.0	1.7	0.0	3.35	3.43/1.79	3.12	1.28	1.28	1.29	-0.32	0.13	0.22	0.54	1.04
UE-25	1676.5	0.0	67.6	0.0	13.5	0.0	3.30	3.40/1.76	3.06	1.98	1.97	1.98	0.29	0.67	0.89	1.20	1.69
UE-25	2007.9	0.0	0.0	3.3	0.0	0.0	2.10	3.01/1.37	1.87	0.95	1.02	1.03	0.23	1.04	0.53	0.94	1.52
UE-25	2011.2	0.0	0.0	0.0	0.0	45.3	2.10	3.01/1.37	1.87	0.93	0.94	0.94	-0.57	-0.05	-0.09	0.24	0.76
UE-25	2037.4	0.0	80.6	0.0	2.8	0.0	3.36	3.44/1.79	3.13	1.42	1.42	1.42	-0.21	0.22	0.35	0.66	1.16
UE-25	2142.4	0.0	44.6	0.0	1.8	0.0	3.12	3.30/1.65	2.89	1.30	1.30	1.30	-0.31	0.14	0.24	0.55	1.06
UE-25	2142.4	0.0	41.4	0.0	8.6	0.0	3.10	3.29/1.64	2.87	1.81	1.80	1.80	0.13	0.52	0.72	1.03	1.52
UE-25	2165.4	0.0	33.3	0.0	27.6	0.0	3.06	3.27/1.63	2.81	2.27	2.26	2.27	0.57	0.94	1.18	1.48	1.97
UE-25	2165.4	0.0	0.0	0.0	0.0	0.0	2.10	3.01/1.37	1.87	0.93	0.94	0.94	-0.57	-0.05	-0.09	0.24	0.76
UE-25	2181.8	0.0	46.0	0.0	0.0	7.9	3.13	3.30/1.66	2.90	0.93	0.94	0.94	-0.57	-0.05	-0.09	0.24	0.76
UE-25	2211.3	0.0	42.4	0.0	0.0	8.5	3.10	3.28/1.64	2.87	0.93	0.94	0.94	-0.57	-0.05	-0.09	0.24	0.76
UE-25	2234.3	0.0	72.5	0.0	12.5	0.0	3.32	3.42/1.77	3.09	1.95	1.94	1.95	0.26	0.65	0.86	1.17	1.66
UE-25	2237.5	0.0	74.4	0.0	0.0	12.8	3.32	3.41/1.77	3.09	0.93	0.94	0.94	-0.57	-0.05	-0.09	0.24	0.76
UE-25	2362.2	0.0	6.4	1.3	30.8	0.0	2.64	3.12/1.48	2.36	2.31	2.31	2.31	0.67	1.13	1.25	1.56	2.06
UE-25	2372.0	0.0	72.5	0.0	2.5	0.0	3.31	3.41/1.77	3.08	1.39	1.39	1.39	-0.24	0.20	0.32	0.64	1.14
UE-25	2395.0	0.0	42.6	0.0	35.3	0.0	3.15	3.32/1.68	2.91	2.37	2.37	2.37	0.67	1.04	1.28	1.58	2.07
UE-25	3090.6	0.0	0.0	0.0	0.0	49.0	2.10	3.01/1.37	1.87	0.93	0.94	0.94	-0.57	-0.05	-0.09	0.24	0.76
UE-25	3185.7	57.1	0.0	0.0	2.4	14.3	2.14	3.02/1.37	1.89	2.15	2.46	2.59	1.43	0.19	1.30	1.65	2.19
UE-25	3271.0	0.0	72.5	0.0	2.5	0.0	3.31	3.41/1.77	3.08	1.39	1.39	1.39	-0.24	0.20	0.32	0.64	1.14
UE-25	3277.6	75.0	3.1	0.0	3.1	0.0	2.35	3.04/1.40	2.11	2.27	2.57	2.70	1.55	0.25	1.41	1.76	2.31
UE-25	3287.4	0.0	90.6	0.0	3.1	0.0	3.41	3.47/1.83	3.17	1.46	1.45	1.46	-0.18	0.25	0.39	0.70	1.20
UE-25	3290.7	0.0	48.3	0.0	40.0	0.0	3.20	3.35/1.71	2.96	2.42	2.42	2.42	0.72	1.09	1.33	1.63	2.13
UE-25	3290.7	0.0	40.7	0.0	40.7	0.0	3.15	3.32/1.68	2.90	2.43	2.43	2.43	0.73	1.10	1.34	1.64	2.13
UE-25	3349.7	0.0	0.0	0.0	49.0	0.0	2.55	3.11/1.46	2.22	2.51	2.50	2.51	0.80	1.17	1.42	1.72	2.21
UE-25	3526.9	0.0	0.0	0.0	14.7	0.0	2.29	3.04/1.40	2.00	2.01	2.01	2.01	0.32	0.70	0.92	1.23	1.72
UE-25	3671.3	61.5	0.0	0.0	12.8	0.0	2.27	3.04/1.39	1.99	2.34	2.57	2.68	1.48	0.66	1.42	1.76	2.30

Table E1. (continued)

Sample	Depth feet	Calcite	Zeolite	Hematite	Smectite	MnOx ^f	Ca	Cs ^e	Sr	Am	Eu	Sm	Np	U	Pu -5	Pu -10	Pu -15
		Fracture Lining Mass % ^d						Log K _d ^d									
UE-25	3730.3	0.0	0.0	0.0	40.7	10.2	2.50	3.09/1.45	2.18	2.43	2.43	2.43	0.73	1.10	1.34	1.64	2.13
UE-25	3763.1	48.0	0.0	0.0	2.0	0.0	2.14	3.02/1.37	1.89	2.08	2.38	2.51	1.36	0.16	1.22	1.57	2.12
Avg ^e	-	-	-	-	-	-	2.96	3.27/1.63	2.72	1.68	1.71	1.73	0.16	0.44	0.65	0.97	1.47
SD ^{c,e}	-	-	-	-	-	-	0.46	0.16/0.16	0.47	0.57	0.59	0.61	0.63	0.43	0.55	0.55	0.55
Median ^e	-	-	-	-	-	-	3.15	3.32/1.68	2.90	1.81	1.80	1.80	0.14	0.25	0.72	1.03	1.52
Min ^e	-	-	-	-	-	-	2.10	3.01/1.37	1.87	0.93	0.94	0.94	-0.57	-0.05	-0.09	0.24	0.76
Max ^e	-	-	-	-	-	-	3.41	3.47/1.83	3.17	2.51	2.57	2.70	1.55	1.17	1.42	1.76	2.31
USW-G1	337.9	0.0	45.3	0.0	0.0	0.0	3.12	3.30/1.65	2.89	0.93	0.94	0.94	-0.57	-0.05	-0.09	0.24	0.76
USW-G1	426.5	77.4	0.0	3.2	0.0	0.0	2.11	3.01/1.37	1.87	2.23	2.56	2.70	1.57	1.03	1.44	1.80	2.35
USW-G1	626.6	0.0	41.4	0.0	41.4	0.0	3.15	3.32/1.68	2.90	2.44	2.43	2.43	0.73	1.10	1.35	1.65	2.14
USW-G1	685.7	0.0	88.9	0.0	3.7	0.0	3.40	3.47/1.82	3.17	1.51	1.51	1.51	-0.14	0.29	0.44	0.75	1.24
USW-G1	725.1	0.0	96.0	0.0	0.0	0.0	3.43	3.48/1.84	3.20	0.93	0.94	0.94	-0.57	-0.05	-0.09	0.24	0.76
USW-G1	941.6	0.0	96.0	0.0	0.0	0.0	3.43	3.48/1.84	3.20	0.93	0.94	0.94	-0.57	-0.05	-0.09	0.24	0.76
USW-G1	981.0	0.0	96.0	0.0	4.0	0.0	3.43	3.49/1.84	3.20	1.53	1.53	1.53	-0.11	0.31	0.46	0.77	1.27
USW-G1	1105.6	0.0	0.0	2.4	2.4	0.0	2.14	3.02/1.37	1.89	1.39	1.41	1.41	0.21	0.95	0.60	0.97	1.53
USW-G1	1138.5	0.0	0.0	4.7	22.6	0.0	2.37	3.06/1.41	2.06	2.19	2.19	2.19	0.71	1.34	1.21	1.54	2.07
USW-G1	1158.1	0.0	1.4	7.2	34.8	0.0	2.52	3.09/1.45	2.21	2.37	2.37	2.37	0.89	1.52	1.39	1.72	2.25
USW-G1	1164.7	0.0	0.9	4.5	21.4	25.9	2.40	3.06/1.42	2.11	2.17	2.17	2.17	0.69	1.31	1.18	1.52	2.05
USW-G1	1227.0	0.0	42.4	0.0	40.7	0.0	3.16	3.33/1.68	2.91	2.43	2.43	2.43	0.73	1.10	1.34	1.64	2.13
USW-G1	1266.4	92.3	3.8	0.0	0.0	0.0	2.36	3.04/1.40	2.13	2.30	2.64	2.78	1.63	-0.05	1.47	1.82	2.37
USW-G1	1282.8	42.9	42.9	0.0	1.8	0.0	3.10	3.29/1.64	2.87	2.04	2.34	2.47	1.31	0.14	1.18	1.53	2.07
USW-G1	1295.9	0.0	0.0	0.0	40.7	1.7	2.50	3.09/1.45	2.18	2.43	2.43	2.43	0.73	1.10	1.34	1.64	2.13
USW-G1	1338.6	0.0	27.6	0.0	27.6	5.7	2.99	3.24/1.60	2.75	2.27	2.26	2.27	0.57	0.94	1.18	1.48	1.97
USW-G1	1355.0	0.0	40.7	0.0	1.7	0.0	3.08	3.28/1.63	2.85	1.29	1.29	1.29	-0.32	0.13	0.23	0.54	1.05
USW-G1	1922.6	0.0	0.0	0.0	3.3	0.0	2.15	3.02/1.37	1.90	1.48	1.47	1.48	-0.16	0.26	0.40	0.71	1.21
USW-G1	2244.1	0.0	76.3	0.0	0.0	5.3	3.33	3.42/1.78	3.10	0.93	0.94	0.94	-0.57	-0.05	-0.09	0.24	0.76
USW-G1	2283.5	0.0	31.2	0.0	5.4	26.9	2.99	3.23/1.59	2.76	1.63	1.63	1.63	-0.03	0.38	0.56	0.86	1.36
USW-G1	2306.4	0.0	100.0	0.0	0.0	0.0	3.44	3.50/1.85	3.21	0.93	0.94	0.94	-0.57	-0.05	-0.09	0.24	0.76
USW-G1	2506.6	0.0	0.0	0.0	0.0	2.0	2.10	3.01/1.37	1.87	0.93	0.94	0.94	-0.57	-0.05	-0.09	0.24	0.76
USW-G1	2565.6	0.0	3.8	0.0	0.0	0.0	2.36	3.04/1.40	2.13	0.93	0.94	0.94	-0.57	-0.05	-0.09	0.24	0.76
USW-G1	2578.7	0.0	1.6	7.8	7.8	7.8	2.31	3.04/1.40	2.05	1.78	1.80	1.80	0.66	1.43	1.03	1.41	1.98
USW-G1	2792.0	0.0	0.0	0.0	3.2	3.2	2.15	3.02/1.37	1.90	1.47	1.46	1.47	-0.17	0.26	0.39	0.71	1.20
USW-G1	2808.4	0.0	0.0	0.0	3.2	3.2	2.15	3.02/1.37	1.90	1.47	1.46	1.47	-0.17	0.26	0.39	0.71	1.20

Table E1. (continued)

Sample	Depth feet	Calcite	Zeolite	Hematite	Smectite	MnOx ^f	Ca	Cs ^e	Sr	Am	Eu	Sm	Np	U	Pu -5	Pu -10	Pu -15
		Fracture	Lining	Mass % ^d				Log K _d ^d									
USW-G1	2906.8	44.4	0.0	0.0	0.0	1.9	2.10	3.01/1.37	1.87	2.00	2.33	2.46	1.32	-0.05	1.17	1.52	2.06
USW-G1	2919.9	0.0	0.0	0.0	0.0	3.3	2.10	3.01/1.37	1.87	0.93	0.94	0.94	-0.57	-0.05	-0.09	0.24	0.76
USW-G1	2936.4	92.3	0.0	0.0	0.0	0.0	2.11	3.01/1.37	1.87	2.30	2.64	2.78	1.63	-0.05	1.47	1.82	2.37
USW-G1	2936.4	92.3	0.0	0.0	0.0	0.0	2.11	3.01/1.37	1.87	2.30	2.64	2.78	1.63	-0.05	1.47	1.82	2.37
USW-G1	2962.6	2.0	0.0	2.0	0.0	0.0	2.10	3.01/1.37	1.87	1.11	1.28	1.36	0.31	0.84	0.47	0.86	1.43
Avg ^e	-	-	-	-	-	-	2.65	3.17/1.53	2.40	1.66	1.73	1.77	0.31	0.45	0.69	1.02	1.54
SD ^{c,e}	-	-	-	-	-	-	0.53	0.18/0.18	0.54	0.58	0.64	0.67	0.77	0.56	0.60	0.61	0.62
Median ^e	-	-	-	-	-	-	2.40	3.06/1.42	2.13	1.53	1.53	1.53	0.21	0.26	0.56	0.86	1.43
Min ^e	-	-	-	-	-	-	2.10	3.01/1.37	1.87	0.93	0.94	0.94	-0.57	-0.05	-0.09	0.24	0.76
Max ^e	-	-	-	-	-	-	3.44	3.50/1.85	3.21	2.44	2.64	2.78	1.63	1.52	1.47	1.82	2.37
USW-G2	1177.8	0.0	0.0	3.1	3.1	0.0	2.15	3.02/1.37	1.90	1.46	1.48	1.48	0.30	1.05	0.68	1.06	1.62
USW-G2	1282.8	0.0	1.7	8.3	1.7	0.0	2.25	3.03/1.39	2.01	1.31	1.38	1.39	0.61	1.43	0.90	1.32	1.90
USW-G2	1446.9	0.0	6.8	6.8	6.8	0.0	2.53	3.08/1.44	2.29	1.73	1.75	1.75	0.61	1.37	0.98	1.36	1.92
USW-G2	1446.9	21.2	8.8	0.9	4.4	0.0	2.58	3.09/1.45	2.34	1.91	2.13	2.24	1.04	0.68	1.02	1.36	1.90
USW-G2	1450.1	0.0	82.8	0.0	5.7	0.0	3.37	3.45/1.80	3.14	1.66	1.65	1.66	-0.01	0.40	0.58	0.89	1.38
USW-G2	1456.7	0.0	67.6	0.0	2.7	0.0	3.29	3.39/1.75	3.05	1.41	1.41	1.41	-0.22	0.22	0.34	0.66	1.16
USW-G2	1489.5	0.0	2.8	2.8	13.9	0.0	2.42	3.06/1.42	2.16	1.99	1.99	1.99	0.50	1.12	1.00	1.34	1.86
USW-G2	1505.9	0.0	62.0	0.0	6.3	0.0	3.26	3.37/1.73	3.02	1.69	1.69	1.69	0.02	0.43	0.61	0.92	1.41
USW-G2	1515.7	0.0	81.4	0.0	1.7	0.0	3.36	3.44/1.80	3.13	1.29	1.29	1.29	-0.32	0.13	0.23	0.54	1.05
USW-G2	1535.4	0.0	61.9	0.0	2.4	0.0	3.25	3.37/1.73	3.02	1.38	1.38	1.38	-0.25	0.19	0.31	0.62	1.12
USW-G2	1568.2	0.0	88.3	0.0	1.7	0.0	3.39	3.46/1.82	3.16	1.28	1.28	1.29	-0.32	0.13	0.22	0.54	1.04
USW-G2	1568.2	0.0	62.0	0.0	1.3	0.0	3.25	3.37/1.73	3.02	1.22	1.22	1.23	-0.37	0.09	0.17	0.48	0.99
USW-G2	1581.4	0.0	82.8	0.0	1.6	0.0	3.37	3.44/1.80	3.14	1.27	1.27	1.27	-0.33	0.12	0.21	0.53	1.03
USW-G2	1604.3	0.0	57.1	0.0	6.0	29.8	3.22	3.35/1.71	2.99	1.67	1.67	1.67	0.00	0.41	0.59	0.90	1.39
USW-G2	1630.6	0.0	54.5	0.0	11.4	0.0	3.21	3.35/1.71	2.98	1.91	1.91	1.91	0.23	0.61	0.82	1.13	1.62
USW-G2	1630.6	0.0	1.0	0.0	23.3	5.8	2.42	3.07/1.42	2.12	2.20	2.19	2.20	0.50	0.88	1.11	1.41	1.90
USW-G2	1637.1	0.0	16.7	0.0	80.0	0.0	2.98	3.25/1.61	2.69	2.72	2.71	2.71	1.01	1.37	1.62	1.93	2.42
USW-G2	1643.7	0.0	17.2	0.0	82.8	0.0	2.99	3.26/1.62	2.70	2.73	2.73	2.73	1.02	1.39	1.64	1.94	2.43
USW-G2	1643.7	0.0	82.8	0.0	17.2	0.0	3.38	3.46/1.81	3.15	2.08	2.07	2.07	0.38	0.76	0.99	1.29	1.78
USW-G2	1643.7	0.0	50.0	0.0	50.0	0.0	3.23	3.37/1.73	2.98	2.52	2.51	2.51	0.81	1.18	1.43	1.73	2.22
USW-G2	1653.5	0.0	49.0	0.0	47.1	0.0	3.22	3.36/1.72	2.97	2.49	2.49	2.49	0.79	1.15	1.40	1.70	2.19
USW-G2	1656.8	0.0	45.3	0.0	45.3	0.0	3.19	3.35/1.70	2.94	2.48	2.47	2.47	0.77	1.14	1.38	1.69	2.18

Table E1. (continued)

Sample	Depth feet	Calcite	Zeolite	Hematite	Smectite	MnOx ^f	Ca	Cs ^e	Sr	Am	Eu	Sm	Np	U	Pu -5	Pu -10	Pu -15
		Fracture	Lining	Mass % ^d	-----	-----	-----	Log K _d ^d	-----	-----	-----	-----	-----	-----	-----	-----	-----
USW-G2	1669.9	0.0	50.0	0.0	48.0	0.0	3.23	3.37/1.72	2.98	2.50	2.50	2.50	0.79	1.16	1.41	1.71	2.20
USW-G2	1679.8	0.0	68.6	0.0	14.3	2.9	3.30	3.41/1.76	3.07	2.00	2.00	2.00	0.31	0.69	0.91	1.22	1.71
USW-G2	1686.4	0.0	69.4	0.0	13.9	0.0	3.31	3.41/1.77	3.07	1.99	1.99	1.99	0.30	0.68	0.90	1.21	1.70
USW-G2	1758.5	0.0	96.7	0.0	0.0	0.0	3.43	3.49/1.84	3.20	0.93	0.94	0.94	-0.57	-0.05	-0.09	0.24	0.76
USW-G2	1761.8	0.0	3.3	0.0	16.7	0.0	2.47	3.07/1.43	2.20	2.06	2.06	2.06	0.37	0.75	0.97	1.28	1.77
USW-G2	1866.8	0.0	85.3	0.0	0.0	14.7	3.38	3.45/1.81	3.15	0.93	0.94	0.94	-0.57	-0.05	-0.09	0.24	0.76
USW-G2	1866.8	0.0	17.2	0.0	0.0	82.8	2.77	3.14/1.50	2.54	0.93	0.94	0.94	-0.57	-0.05	-0.09	0.24	0.76
USW-G2	2004.6	0.0	37.7	0.0	0.0	0.0	3.05	3.26/1.62	2.82	0.93	0.94	0.94	-0.57	-0.05	-0.09	0.24	0.76
USW-G2	2004.6	0.0	45.3	0.0	1.6	0.0	3.13	3.30/1.66	2.89	1.27	1.27	1.27	-0.33	0.12	0.21	0.53	1.03
USW-G2	2027.6	0.0	70.7	0.0	2.4	0.0	3.30	3.40/1.76	3.07	1.38	1.38	1.39	-0.24	0.20	0.32	0.63	1.13
USW-G2	2066.9	0.0	64.4	0.0	11.1	0.0	3.28	3.39/1.74	3.04	1.90	1.90	1.90	0.22	0.61	0.82	1.12	1.62
USW-G2	2070.2	0.0	49.2	0.0	1.7	0.0	3.16	3.32/1.67	2.93	1.29	1.29	1.29	-0.32	0.13	0.23	0.54	1.05
USW-G2	2086.6	0.0	82.8	0.0	0.0	0.0	3.37	3.44/1.80	3.14	0.93	0.94	0.94	-0.57	-0.05	-0.09	0.24	0.76
USW-G2	2093.2	0.0	52.7	0.0	1.8	0.0	3.19	3.33/1.69	2.95	1.30	1.30	1.31	-0.30	0.15	0.24	0.56	1.06
USW-G2	2122.7	0.0	100.0	0.0	0.0	0.0	3.44	3.50/1.85	3.21	0.93	0.94	0.94	-0.57	-0.05	-0.09	0.24	0.76
USW-G2	2280.2	0.0	80.6	0.0	13.9	0.0	3.37	3.45/1.80	3.13	1.99	1.99	1.99	0.30	0.68	0.90	1.21	1.70
USW-G2	2283.5	0.0	45.5	0.0	1.8	0.0	3.13	3.30/1.66	2.90	1.30	1.30	1.31	-0.30	0.15	0.24	0.56	1.06
USW-G2	2723.1	0.0	0.0	0.0	8.6	50.0	2.22	3.03/1.39	1.95	1.81	1.80	1.80	0.13	0.52	0.72	1.03	1.52
USW-G2	2752.6	0.0	1.9	0.0	44.4	0.0	2.59	3.11/1.47	2.27	2.47	2.46	2.46	0.76	1.13	1.38	1.68	2.17
USW-G2	2762.5	0.0	0.0	0.0	1.4	65.8	2.12	3.01/1.37	1.88	1.24	1.24	1.24	-0.35	0.10	0.18	0.50	1.00
USW-G2	2811.7	0.0	0.0	44.4	1.9	0.0	2.13	3.02/1.37	1.89	1.45	1.67	1.67	1.29	2.14	1.55	1.98	2.58
USW-G2	2854.3	0.0	0.0	8.6	8.6	0.0	2.22	3.03/1.39	1.95	1.82	1.84	1.84	0.70	1.47	1.07	1.45	2.02
USW-G2	2864.2	0.0	0.0	0.0	12.8	74.4	2.27	3.04/1.39	1.99	1.96	1.95	1.96	0.27	0.66	0.87	1.18	1.67
USW-G2	2874.0	0.0	0.0	0.0	1.8	52.7	2.13	3.02/1.37	1.89	1.30	1.30	1.31	-0.30	0.15	0.24	0.56	1.06
USW-G2	2877.3	0.0	0.0	1.3	1.3	64.0	2.12	3.01/1.37	1.88	1.24	1.25	1.26	0.00	0.73	0.40	0.77	1.32
USW-G2	2883.9	0.0	0.0	8.9	42.9	3.6	2.52	3.10/1.45	2.19	2.46	2.46	2.46	0.97	1.61	1.47	1.81	2.34
USW-G2	2893.7	0.0	0.0	0.0	0.0	88.9	2.10	3.01/1.37	1.87	0.93	0.94	0.94	-0.57	-0.05	-0.09	0.24	0.76
USW-G2	2926.5	0.0	0.0	0.0	12.5	25.0	2.27	3.04/1.39	1.99	1.95	1.94	1.95	0.26	0.65	0.86	1.17	1.66
USW-G2	2959.3	0.0	0.0	0.0	80.0	0.0	2.70	3.16/1.51	2.35	2.72	2.71	2.71	1.01	1.37	1.62	1.93	2.42
USW-G2	2959.3	0.0	0.0	0.0	0.0	50.0	2.10	3.01/1.37	1.87	0.93	0.94	0.94	-0.57	-0.05	-0.09	0.24	0.76
USW-G2	3002.0	0.0	0.0	28.9	28.9	7.2	2.42	3.07/1.43	2.11	2.30	2.32	2.32	1.21	1.99	1.58	1.96	2.53
USW-G2	3136.5	0.0	16.7	0.0	0.0	0.0	2.75	3.14/1.50	2.52	0.93	0.94	0.94	-0.57	-0.05	-0.09	0.24	0.76

Table E1. (continued)

Sample	Depth feet	Calcite	Zeolite	Hematite	Smectite	MnOx ^f	Ca	Cs ^e	Sr	Am	Eu	Sm	Np	U	Pu -5	Pu -10	Pu -15
		Fracture	Lining	Mass % ^d													
USW-G2	3169.3	0.0	5.9	23.5	23.5	0.0	2.59	3.10/1.46	2.32	2.21	2.24	2.24	1.12	1.90	1.49	1.87	2.44
USW-G2	3399.0	0.0	0.0	0.0	1.7	49.2	2.13	3.01/1.37	1.88	1.29	1.29	1.29	-0.32	0.13	0.23	0.54	1.05
USW-G2	3408.8	0.0	0.0	32.9	1.4	0.0	2.12	3.01/1.37	1.88	1.36	1.57	1.57	1.16	2.01	1.43	1.85	2.45
USW-G2	3421.9	0.0	0.0	0.0	1.7	81.4	2.13	3.01/1.37	1.88	1.29	1.29	1.29	-0.32	0.13	0.23	0.54	1.05
Avg ^e	-	-	-	-	-	-	2.83	3.23/1.59	2.58	1.66	1.68	1.68	0.17	0.65	0.69	1.01	1.53
SD ^{c,e}	-	-	-	-	-	-	0.49	0.17/0.17	0.50	0.55	0.54	0.54	0.58	0.62	0.56	0.57	0.58
Median ^e	-	-	-	-	-	-	3.02	3.26/1.62	2.76	1.56	1.66	1.66	0.17	0.61	0.70	1.04	1.57
Min ^e	-	-	-	-	-	-	2.10	3.01/1.37	1.87	0.93	0.94	0.94	-0.57	-0.05	-0.09	0.24	0.76
Max ^e	-	-	-	-	-	-	3.44	3.50/1.85	3.21	2.73	2.73	2.73	1.29	2.14	1.64	1.98	2.58
USW-G3/GU3	469.2	100.0	0.0	0.0	0.0	0.0	2.11	3.01/1.37	1.87	2.34	2.67	2.81	1.67	-0.05	1.50	1.86	2.41
USW-G3/GU3	479.0	100.0	0.0	0.0	0.0	0.0	2.11	3.01/1.37	1.87	2.34	2.67	2.81	1.67	-0.05	1.50	1.86	2.41
USW-G3/GU3	498.7	0.0	0.0	0.0	0.0	0.0	2.10	3.01/1.37	1.87	0.93	0.94	0.94	-0.57	-0.05	-0.09	0.24	0.76
USW-G3/GU3	518.4	0.0	0.0	1.8	43.6	0.0	2.52	3.10/1.45	2.19	2.46	2.46	2.46	0.81	1.27	1.39	1.70	2.20
USW-G3/GU3	518.4	0.0	0.0	3.3	0.0	0.0	2.10	3.01/1.37	1.87	0.95	1.02	1.03	0.23	1.04	0.53	0.94	1.52
USW-G3/GU3	521.7	0.0	0.0	0.0	96.0	0.0	2.76	3.18/1.54	2.40	2.80	2.79	2.79	1.09	1.45	1.70	2.00	2.50
USW-G3/GU3	521.7	100.0	0.0	0.0	0.0	0.0	2.11	3.01/1.37	1.87	2.34	2.67	2.81	1.67	-0.05	1.50	1.86	2.41
USW-G3/GU3	521.7	70.6	0.0	0.0	0.0	0.0	2.11	3.01/1.37	1.87	2.19	2.52	2.66	1.52	-0.05	1.36	1.71	2.26
USW-G3/GU3	541.3	0.0	0.0	0.0	82.8	0.0	2.71	3.16/1.52	2.36	2.73	2.73	2.73	1.02	1.39	1.64	1.94	2.43
USW-G3/GU3	541.3	0.0	0.0	0.0	14.7	0.0	2.29	3.04/1.40	2.00	2.01	2.01	2.01	0.32	0.70	0.92	1.23	1.72
USW-G3/GU3	580.7	0.0	0.0	3.1	3.1	0.0	2.15	3.02/1.37	1.90	1.46	1.48	1.48	0.30	1.05	0.68	1.06	1.62
USW-G3/GU3	610.2	0.0	0.0	2.0	0.0	0.0	2.10	3.01/1.37	1.87	0.94	0.99	1.00	0.06	0.85	0.38	0.77	1.35
USW-G3/GU3	689.0	0.0	3.8	0.0	0.0	0.0	2.36	3.04/1.40	2.13	0.93	0.94	0.94	-0.57	-0.05	-0.09	0.24	0.76
USW-G3/GU3	689.0	0.0	0.0	0.0	0.0	0.0	2.10	3.01/1.37	1.87	0.93	0.94	0.94	-0.57	-0.05	-0.09	0.24	0.76
USW-G3/GU3	689.0	0.0	0.0	0.0	41.4	0.0	2.51	3.09/1.45	2.18	2.44	2.43	2.43	0.73	1.10	1.35	1.65	2.14
USW-G3/GU3	689.0	1.5	0.0	0.0	38.5	0.0	2.49	3.09/1.44	2.16	2.41	2.41	2.42	0.76	1.07	1.33	1.63	2.12
USW-G3/GU3	754.6	0.0	0.0	0.0	68.6	14.3	2.65	3.14/1.50	2.31	2.65	2.65	2.65	0.94	1.31	1.56	1.86	2.35
USW-G3/GU3	800.5	0.0	0.0	11.4	11.4	0.0	2.25	3.04/1.39	1.98	1.92	1.94	1.94	0.82	1.59	1.19	1.57	2.13
USW-G3/GU3	803.8	0.0	44.4	0.0	44.4	0.0	3.18	3.34/1.70	2.93	2.47	2.46	2.46	0.76	1.13	1.38	1.68	2.17
USW-G3/GU3	803.8	0.0	0.0	0.0	5.7	27.6	2.19	3.02/1.38	1.93	1.66	1.65	1.66	-0.01	0.40	0.58	0.89	1.38
USW-G3/GU3	810.4	0.0	1.5	1.5	36.9	0.0	2.53	3.10/1.45	2.22	2.39	2.39	2.39	0.74	1.21	1.32	1.63	2.14
USW-G3/GU3	820.2	0.0	0.0	5.7	27.3	28.4	2.41	3.07/1.42	2.10	2.27	2.27	2.27	0.79	1.41	1.28	1.62	2.15
USW-G3/GU3	823.5	0.0	0.0	14.3	0.0	2.29	3.04/1.40	2.00	2.00	2.00	2.00	0.31	0.69	0.91	1.22	1.71	

Table E1. (continued)

Sample	Depth feet	Calcite	Zeolite	Hematite	Smectite	MnOx ^f	Ca	Cs ^e	Sr	Am	Eu	Sm	Np	U	Pu -5	Pu -10	Pu -15
		Fracture	Lining	Mass % ^d				Log K _d									
USW-G3/GU3	823.5	0.0	0.0	0.0	38.1	7.9	2.49	3.09/1.44	2.16	2.40	2.40	2.40	0.70	1.07	1.31	1.61	2.11
USW-G3/GU3	830.1	16.1	0.0	0.0	77.4	0.0	2.69	3.15/1.51	2.34	2.73	2.76	2.78	1.24	1.36	1.66	1.97	2.47
USW-G3/GU3	830.1	66.7	0.0	0.0	2.8	0.0	2.15	3.02/1.37	1.90	2.22	2.52	2.65	1.50	0.23	1.36	1.71	2.26
USW-G3/GU3	846.5	0.0	0.0	3.2	0.0	0.0	2.10	3.01/1.37	1.87	0.95	1.02	1.03	0.22	1.03	0.52	0.92	1.51
USW-G3/GU3	944.9	0.0	0.0	1.8	0.0	1.8	2.10	3.01/1.37	1.87	0.94	0.99	0.99	0.02	0.81	0.34	0.74	1.32
USW-G3/GU3	944.9	0.0	0.0	0.0	0.0	0.0	2.10	3.01/1.37	1.87	0.93	0.94	0.94	-0.57	-0.05	-0.09	0.24	0.76
USW-G3/GU3	951.4	0.0	0.0	0.0	0.0	0.0	2.10	3.01/1.37	1.87	0.93	0.94	0.94	-0.57	-0.05	-0.09	0.24	0.76
USW-G3/GU3	971.1	0.0	7.8	0.0	37.5	9.4	2.71	3.14/1.50	2.42	2.40	2.39	2.39	0.69	1.06	1.30	1.61	2.10
USW-G3/GU3	974.4	0.0	0.0	0.0	0.0	0.0	2.10	3.01/1.37	1.87	0.93	0.94	0.94	-0.57	-0.05	-0.09	0.24	0.76
USW-G3/GU3	977.7	0.0	0.0	2.0	48.0	10.0	2.55	3.11/1.46	2.21	2.50	2.50	2.50	0.85	1.31	1.43	1.74	2.24
USW-G3/GU3	981.0	0.0	0.0	0.0	28.9	7.2	2.42	3.07/1.43	2.11	2.29	2.28	2.29	0.59	0.96	1.20	1.50	1.99
USW-G3/GU3	987.5	0.0	0.0	5.4	5.4	5.4	2.18	3.02/1.38	1.92	1.65	1.67	1.67	0.52	1.28	0.89	1.27	1.83
USW-G3/GU3	1007.2	0.0	0.0	0.0	0.0	0.0	2.10	3.01/1.37	1.87	0.93	0.94	0.94	-0.57	-0.05	-0.09	0.24	0.76
USW-G3/GU3	1072.8	44.4	0.0	0.0	0.0	0.0	2.10	3.01/1.37	1.87	2.00	2.33	2.46	1.32	-0.05	1.17	1.52	2.06
USW-G3/GU3	1072.8	3.3	0.0	0.0	0.0	0.0	2.10	3.01/1.37	1.87	1.19	1.38	1.48	0.26	-0.05	0.27	0.61	1.15
USW-G3/GU3	1164.7	0.0	11.9	2.4	57.1	2.4	2.85	3.20/1.55	2.56	2.58	2.57	2.57	0.92	1.39	1.51	1.82	2.32
USW-G3/GU3	1184.4	0.0	68.6	0.0	14.3	0.0	3.30	3.41/1.76	3.07	2.00	2.00	2.00	0.31	0.69	0.91	1.22	1.71
USW-G3/GU3	1190.9	0.0	40.0	0.0	8.3	1.7	3.09	3.28/1.64	2.85	1.79	1.79	1.79	0.12	0.51	0.71	1.02	1.51
USW-G3/GU3	1190.9	0.0	44.4	0.0	9.3	0.0	3.13	3.30/1.66	2.90	1.83	1.83	1.83	0.15	0.55	0.75	1.05	1.55
USW-G3/GU3	1190.9	0.0	44.4	0.0	0.0	0.0	3.12	3.29/1.65	2.89	0.93	0.94	0.94	-0.57	-0.05	-0.09	0.24	0.76
USW-G3/GU3	1200.8	0.0	50.0	0.0	50.0	0.0	3.23	3.37/1.73	2.98	2.52	2.51	2.51	0.81	1.18	1.43	1.73	2.22
USW-G3/GU3	1200.8	0.0	33.3	0.0	33.3	0.0	3.07	3.28/1.64	2.82	2.35	2.34	2.34	0.64	1.02	1.26	1.56	2.05
USW-G3/GU3	1210.6	0.0	1.5	0.0	36.9	1.5	2.53	3.10/1.45	2.22	2.39	2.39	2.39	0.69	1.06	1.30	1.60	2.09
USW-G3/GU3	1210.6	0.0	0.0	0.0	17.2	0.0	2.32	3.05/1.40	2.02	2.08	2.07	2.07	0.38	0.76	0.99	1.29	1.78
USW-G3/GU3	1233.6	0.0	0.0	0.0	43.6	1.8	2.52	3.10/1.45	2.19	2.46	2.46	2.46	0.76	1.12	1.37	1.67	2.16
USW-G3/GU3	1715.9	43.6	0.0	1.8	1.8	0.0	2.13	3.02/1.37	1.89	2.05	2.35	2.48	1.33	0.84	1.22	1.58	2.13
USW-G3/GU3	1715.9	7.2	34.8	0.0	1.4	0.0	3.02	3.25/1.60	2.79	1.52	1.71	1.81	0.58	0.11	0.58	0.92	1.45
USW-G3/GU3	1735.6	0.7	1.7	1.7	8.3	0.0	2.32	3.04/1.40	2.06	1.80	1.81	1.82	0.37	0.92	0.82	1.15	1.68
USW-G3/GU3	1935.7	0.0	80.0	0.0	0.0	0.0	3.35	3.43/1.79	3.12	0.93	0.94	0.94	-0.57	-0.05	-0.09	0.24	0.76
USW-G3/GU3	2014.4	0.0	59.0	0.0	28.9	0.0	3.26	3.38/1.74	3.02	2.29	2.28	2.29	0.59	0.96	1.20	1.50	1.99
USW-G3/GU3	2014.4	0.0	61.5	0.0	12.8	0.0	3.26	3.38/1.73	3.02	1.96	1.95	1.96	0.27	0.66	0.87	1.18	1.67
USW-G3/GU3	2096.5	0.0	3.2	3.2	0.0	2.15	3.02/1.37	1.90	1.47	1.49	1.49	0.31	1.07	0.69	1.07	1.63	

Table E1. (continued)

Sample	Depth feet	Calcite	Zeolite	Hematite	Smectite	MnOx ^f	Ca	Cs ^e	Sr	Am	Eu	Sm	Np	U	Pu -5	Pu -10	Pu -15
		Fracture	Lining	Mass % ^d										Log K _d ^d			
USW-G3/GU3	2155.5	0.0	3.2	0.0	3.2	0.0	2.36	3.05/1.40	2.11	1.47	1.46	1.47	-0.17	0.26	0.39	0.71	1.20
USW-G3/GU3	2198.2	0.0	41.4	0.0	41.4	0.0	3.15	3.32/1.68	2.90	2.44	2.43	2.43	0.73	1.10	1.35	1.65	2.14
USW-G3/GU3	2208.0	0.0	96.0	0.0	0.0	0.0	3.43	3.48/1.84	3.20	0.93	0.94	0.94	-0.57	-0.05	-0.09	0.24	0.76
USW-G3/GU3	2290.0	0.0	60.0	0.0	12.5	0.0	3.25	3.37/1.73	3.01	1.95	1.94	1.95	0.26	0.65	0.86	1.17	1.66
USW-G3/GU3	2326.1	0.0	61.5	0.0	12.8	0.0	3.26	3.38/1.73	3.02	1.96	1.95	1.96	0.27	0.66	0.87	1.18	1.67
USW-G3/GU3	2378.6	0.0	12.8	0.0	12.8	0.0	2.72	3.13/1.49	2.47	1.96	1.95	1.96	0.27	0.66	0.87	1.18	1.67
USW-G3/GU3	2385.2	0.0	1.9	0.0	44.4	0.0	2.59	3.11/1.47	2.27	2.47	2.46	2.46	0.76	1.13	1.38	1.68	2.17
USW-G3/GU3	2431.1	0.0	60.0	0.0	2.5	0.0	3.24	3.36/1.72	3.01	1.39	1.39	1.39	-0.24	0.20	0.32	0.64	1.14
USW-G3/GU3	2503.3	0.0	68.6	0.0	14.3	0.0	3.30	3.41/1.76	3.07	2.00	2.00	2.00	0.31	0.69	0.91	1.22	1.71
USW-G3/GU3	2559.1	0.0	9.8	0.0	0.3	0.0	2.59	3.09/1.45	2.36	1.03	1.03	1.04	-0.50	-0.01	0.00	0.32	0.83
USW-G3/GU3	2634.5	0.0	14.6	0.0	7.3	7.3	2.74	3.14/1.49	2.50	1.74	1.74	1.74	0.07	0.47	0.66	0.97	1.46
USW-G3/GU3	2654.2	0.0	62.3	0.0	31.2	0.0	3.29	3.40/1.75	3.04	2.32	2.31	2.32	0.62	0.99	1.23	1.53	2.02
USW-G3/GU3	2831.4	0.0	40.7	0.0	8.5	0.0	3.10	3.28/1.64	2.86	1.80	1.80	1.80	0.12	0.52	0.72	1.02	1.52
USW-G3/GU3	2910.1	66.7	2.8	0.0	13.9	0.0	2.43	3.06/1.42	2.16	2.37	2.61	2.72	1.52	0.68	1.46	1.80	2.33
USW-G3/GU3	2956.0	77.4	3.2	0.0	0.0	0.0	2.33	3.04/1.40	2.09	2.23	2.56	2.70	1.56	-0.05	1.40	1.75	2.30
USW-G3/GU3	2972.4	0.0	16.1	0.0	3.2	0.0	2.76	3.14/1.50	2.52	1.47	1.46	1.47	-0.17	0.26	0.39	0.71	1.20
USW-G3/GU3	3038.1	0.0	80.0	0.0	3.3	0.0	3.36	3.44/1.79	3.12	1.48	1.47	1.48	-0.16	0.26	0.40	0.71	1.21
USW-G3/GU3	3195.5	0.0	43.6	0.0	1.8	0.0	3.11	3.29/1.65	2.88	1.30	1.30	1.31	-0.30	0.15	0.24	0.56	1.06
USW-G3/GU3	3238.2	0.0	1.8	0.0	1.8	43.6	2.26	3.03/1.39	2.02	1.30	1.30	1.31	-0.30	0.15	0.24	0.56	1.06
USW-G3/GU3	3264.4	0.0	48.6	0.0	48.6	0.0	3.22	3.36/1.72	2.97	2.51	2.50	2.50	0.80	1.17	1.41	1.72	2.21
USW-G3/GU3	3264.4	0.0	43.6	0.0	43.6	0.0	3.17	3.34/1.69	2.92	2.46	2.46	2.46	0.76	1.12	1.37	1.67	2.16
USW-G3/GU3	3290.7	0.0	60.0	0.0	2.5	12.5	3.24	3.36/1.72	3.01	1.39	1.39	1.39	-0.24	0.20	0.32	0.64	1.14
USW-G3/GU3	3294.0	0.0	66.7	0.0	2.8	0.0	3.28	3.39/1.74	3.05	1.42	1.42	1.42	-0.21	0.22	0.35	0.66	1.16
Avg ^e	-	-	-	-	-	-	2.63	3.16/1.51	2.37	1.86	1.90	1.92	0.42	0.64	0.86	1.19	1.70
SD ^{c,e}	-	-	-	-	-	-	0.45	0.15/0.15	0.46	0.59	0.61	0.62	0.63	0.52	0.55	0.55	0.54
Median ^e	-	-	-	-	-	-	2.53	3.10/1.45	2.20	1.98	1.98	1.98	0.34	0.69	0.91	1.22	1.71
Min ^e	-	-	-	-	-	-	2.10	3.01/1.37	1.87	0.93	0.94	0.94	-0.57	-0.05	-0.09	0.24	0.76
Max ^e	-	-	-	-	-	-	3.43	3.48/1.84	3.20	2.80	2.79	2.81	1.67	1.59	1.70	2.00	2.50
USW-G4	351.0	0.0	37.5	1.6	7.8	0.0	3.06	3.27/1.63	2.83	1.77	1.77	1.77	0.28	0.90	0.78	1.12	1.64
USW-G4	593.8	0.0	0.0	0.0	3.2	0.0	2.15	3.02/1.37	1.90	1.47	1.46	1.47	-0.17	0.26	0.39	0.71	1.20
USW-G4	669.3	85.7	0.0	0.0	3.6	0.0	2.16	3.02/1.38	1.90	2.32	2.63	2.76	1.60	0.28	1.47	1.82	2.36
USW-G4	685.7	0.0	96.0	0.0	0.0	0.0	3.43	3.48/1.84	3.20	0.93	0.94	0.94	-0.57	-0.05	-0.09	0.24	0.76

Table E1. (continued)

Sample	Depth feet	Calcite	Zeolite	Hematite	Smectite	MnOx ^f	Ca	Cs ^e	Sr	Am	Eu	Sm	Np	U	Pu -5	Pu -10	Pu -15
		Fracture	Lining	Mass % ^d	Log K _d												
USW-G4	698.8	0.0	6.1	0.0	29.3	0.0	2.63	3.12/1.47	2.35	2.29	2.29	2.29	0.59	0.96	1.20	1.51	2.00
USW-G4	698.8	2.8	0.0	0.0	66.7	0.0	2.64	3.14/1.49	2.30	2.65	2.65	2.65	0.99	1.30	1.56	1.86	2.35
USW-G4	777.6	0.0	0.0	1.8	1.8	0.0	2.13	3.02/1.37	1.89	1.31	1.33	1.33	0.11	0.84	0.50	0.87	1.42
USW-G4	810.4	0.0	44.4	0.0	44.4	0.0	3.18	3.34/1.70	2.93	2.47	2.46	2.46	0.76	1.13	1.38	1.68	2.17
USW-G4	889.1	0.0	0.0	1.7	8.5	0.0	2.22	3.03/1.39	1.95	1.80	1.80	1.80	0.31	0.93	0.81	1.15	1.67
USW-G4	984.3	0.0	0.0	2.8	2.8	0.0	2.14	3.02/1.37	1.90	1.43	1.45	1.45	0.26	1.01	0.64	1.01	1.57
USW-G4	1000.7	0.0	0.0	7.8	7.8	0.0	2.21	3.03/1.38	1.95	1.78	1.80	1.80	0.66	1.43	1.03	1.41	1.98
USW-G4	1007.2	0.0	7.8	7.8	1.6	0.0	2.53	3.08/1.44	2.30	1.30	1.36	1.37	0.58	1.40	0.88	1.29	1.87
USW-G4	1040.0	0.0	1.0	1.0	23.3	0.0	2.42	3.07/1.42	2.12	2.20	2.20	2.20	0.55	1.02	1.13	1.44	1.95
USW-G4	1072.8	0.0	0.0	2.9	0.0	0.0	2.10	3.01/1.37	1.87	0.95	1.01	1.02	0.18	0.98	0.48	0.88	1.47
USW-G4	1072.8	0.0	7.2	1.4	7.2	0.0	2.55	3.09/1.44	2.30	1.74	1.74	1.75	0.25	0.87	0.75	1.09	1.61
USW-G4	1082.7	0.0	0.0	1.0	23.5	0.0	2.37	3.06/1.42	2.07	2.20	2.20	2.20	0.56	1.02	1.14	1.45	1.95
USW-G4	1148.3	0.0	0.0	0.0	31.2	0.0	2.44	3.07/1.43	2.12	2.32	2.31	2.32	0.62	0.99	1.23	1.53	2.02
USW-G4	1161.4	0.0	0.0	0.0	1.8	0.0	2.13	3.02/1.37	1.89	1.30	1.30	1.31	-0.30	0.15	0.24	0.56	1.06
USW-G4	1174.5	0.0	40.7	0.0	1.7	0.0	3.08	3.28/1.63	2.85	1.29	1.29	1.29	-0.32	0.13	0.23	0.54	1.05
USW-G4	1200.8	0.0	0.0	1.7	1.7	8.3	2.13	3.01/1.37	1.88	1.29	1.30	1.31	0.08	0.81	0.47	0.84	1.39
USW-G4	1243.4	0.0	0.0	1.7	8.5	0.0	2.22	3.03/1.39	1.95	1.80	1.80	1.80	0.31	0.93	0.81	1.15	1.67
USW-G4	1253.3	0.0	45.3	0.0	1.6	0.0	3.13	3.30/1.66	2.89	1.27	1.27	1.27	-0.33	0.12	0.21	0.53	1.03
USW-G4	1253.3	0.0	39.1	0.0	0.0	7.8	3.07	3.27/1.62	2.83	0.93	0.94	0.94	-0.57	-0.05	-0.09	0.24	0.76
USW-G4	1259.8	0.0	48.0	0.0	10.0	12.0	3.16	3.32/1.68	2.93	1.86	1.86	1.86	0.18	0.57	0.78	1.08	1.58
USW-G4	1305.8	0.0	100.0	0.0	0.0	0.0	3.44	3.50/1.85	3.21	0.93	0.94	0.94	-0.57	-0.05	-0.09	0.24	0.76
USW-G4	1309.1	0.0	100.0	0.0	0.0	0.0	3.44	3.50/1.85	3.21	0.93	0.94	0.94	-0.57	-0.05	-0.09	0.24	0.76
USW-G4	1315.6	0.0	40.7	0.0	40.7	1.7	3.15	3.32/1.68	2.90	2.43	2.43	2.43	0.73	1.10	1.34	1.64	2.13
USW-G4	1325.5	0.0	70.6	0.0	0.0	0.0	3.30	3.40/1.76	3.07	0.93	0.94	0.94	-0.57	-0.05	-0.09	0.24	0.76
USW-G4	1325.5	0.0	45.3	0.0	45.3	0.0	3.19	3.35/1.70	2.94	2.48	2.47	2.47	0.77	1.14	1.38	1.69	2.18
USW-G4	1341.9	0.0	71.4	0.0	14.3	0.0	3.32	3.42/1.77	3.09	2.00	2.00	2.00	0.31	0.69	0.91	1.22	1.71
USW-G4	1341.9	0.0	70.6	0.0	14.7	0.0	3.32	3.41/1.77	3.08	2.01	2.01	2.01	0.32	0.70	0.92	1.23	1.72
USW-G4	1341.9	0.0	14.7	0.0	70.6	0.0	2.93	3.23/1.59	2.64	2.67	2.66	2.66	0.96	1.32	1.57	1.87	2.36
USW-G4	1351.7	0.0	48.1	0.0	46.2	1.9	3.21	3.36/1.71	2.96	2.48	2.48	2.48	0.78	1.15	1.39	1.69	2.19
USW-G4	1361.5	0.0	16.7	0.0	66.7	0.0	2.95	3.24/1.59	2.66	2.64	2.64	2.64	0.93	1.30	1.55	1.85	2.34
USW-G4	1381.2	0.0	50.0	0.0	0.0	0.0	3.16	3.32/1.67	2.93	0.93	0.94	0.94	-0.57	-0.05	-0.09	0.24	0.76
USW-G4	1437.0	0.0	100.0	0.0	0.0	0.0	3.44	3.50/1.85	3.21	0.93	0.94	0.94	-0.57	-0.05	-0.09	0.24	0.76

Table E1. (continued)

Sample	Depth feet	Calcite	Zeolite	Hematite	Smectite	MnOx ^f	Ca	Cs ^e	Sr	Am	Eu	Sm	Np	U	Pu -5	Pu -10	Pu -15
		Fracture	Lining	Mass % ^d	-----	-----	-----	-----	-----	-----	-----	Log K _d ^d	-----	-----	-----	-----	
USW-G4	1512.5	0.0	65.9	0.0	0.0	0.0	3.27	3.38/1.74	3.04	0.93	0.94	0.94	-0.57	-0.05	-0.09	0.24	0.76
USW-G4	1542.0	0.0	80.6	0.0	2.8	0.0	3.36	3.44/1.79	3.13	1.42	1.42	1.42	-0.21	0.22	0.35	0.66	1.16
USW-G4	1643.7	0.0	100.0	0.0	0.0	0.0	3.44	3.50/1.85	3.21	0.93	0.94	0.94	-0.57	-0.05	-0.09	0.24	0.76
USW-G4	1669.9	0.0	22.2	0.0	0.0	64.4	2.85	3.17/1.53	2.62	0.93	0.94	0.94	-0.57	-0.05	-0.09	0.24	0.76
USW-G4	1692.9	0.0	70.7	0.0	2.4	0.0	3.30	3.40/1.76	3.07	1.38	1.38	1.39	-0.24	0.20	0.32	0.63	1.13
USW-G4	1706.0	0.0	100.0	0.0	0.0	0.0	3.44	3.50/1.85	3.21	0.93	0.94	0.94	-0.57	-0.05	-0.09	0.24	0.76
USW-G4	1715.9	0.0	70.7	0.0	12.2	0.0	3.31	3.41/1.77	3.08	1.94	1.93	1.94	0.25	0.64	0.85	1.16	1.65
USW-G4	1761.8	0.0	16.7	0.0	80.0	0.0	2.98	3.25/1.61	2.69	2.72	2.71	2.71	1.01	1.37	1.62	1.93	2.42
USW-G4	1761.8	0.0	18.8	0.0	75.0	0.0	2.99	3.26/1.61	2.71	2.69	2.69	2.69	0.98	1.35	1.60	1.90	2.39
USW-G4	1788.1	0.0	100.0	0.0	0.0	0.0	3.44	3.50/1.85	3.21	0.93	0.94	0.94	-0.57	-0.05	-0.09	0.24	0.76
USW-G4	1971.8	0.0	85.3	0.0	0.0	0.0	3.38	3.45/1.81	3.15	0.93	0.94	0.94	-0.57	-0.05	-0.09	0.24	0.76
USW-G4	1991.5	0.0	48.3	0.0	1.7	0.0	3.15	3.31/1.67	2.92	1.28	1.28	1.29	-0.32	0.13	0.22	0.54	1.04
USW-G4	1994.8	0.0	31.4	0.0	26.0	31.4	3.03	3.26/1.62	2.79	2.24	2.24	2.24	0.54	0.92	1.15	1.46	1.95
USW-G4	2063.6	0.0	96.7	0.0	0.0	0.0	3.43	3.49/1.84	3.20	0.93	0.94	0.94	-0.57	-0.05	-0.09	0.24	0.76
USW-G4	2070.2	0.0	85.3	0.0	0.0	0.0	3.38	3.45/1.81	3.15	0.93	0.94	0.94	-0.57	-0.05	-0.09	0.24	0.76
USW-G4	2099.7	0.0	45.3	0.0	0.0	45.3	3.12	3.30/1.65	2.89	0.93	0.94	0.94	-0.57	-0.05	-0.09	0.24	0.76
USW-G4	2099.7	0.0	50.0	0.0	0.0	0.0	3.16	3.32/1.67	2.93	0.93	0.94	0.94	-0.57	-0.05	-0.09	0.24	0.76
USW-G4	2100.1	0.0	82.8	0.0	0.0	0.0	3.37	3.44/1.80	3.14	0.93	0.94	0.94	-0.57	-0.05	-0.09	0.24	0.76
USW-G4	2100.1	0.0	96.2	0.0	0.0	0.0	3.43	3.48/1.84	3.20	0.93	0.94	0.94	-0.57	-0.05	-0.09	0.24	0.76
USW-G4	2100.4	0.0	96.0	0.0	4.0	0.0	3.43	3.49/1.84	3.20	1.53	1.53	1.53	-0.11	0.31	0.46	0.77	1.27
USW-G4	2101.0	0.0	96.7	0.0	0.0	0.0	3.43	3.49/1.84	3.20	0.93	0.94	0.94	-0.57	-0.05	-0.09	0.24	0.76
USW-G4	2101.0	0.0	82.9	0.0	0.0	0.0	3.37	3.44/1.80	3.14	0.93	0.94	0.94	-0.57	-0.05	-0.09	0.24	0.76
USW-G4	2135.8	0.0	0.0	0.0	0.0	0.0	2.10	3.01/1.37	1.87	0.93	0.94	0.94	-0.57	-0.05	-0.09	0.24	0.76
USW-G4	2145.7	0.0	98.0	0.0	0.0	0.0	3.44	3.49/1.85	3.21	0.93	0.94	0.94	-0.57	-0.05	-0.09	0.24	0.76
USW-G4	2145.7	0.0	93.5	0.0	0.0	0.0	3.42	3.48/1.83	3.19	0.93	0.94	0.94	-0.57	-0.05	-0.09	0.24	0.76
USW-G4	2247.4	0.0	88.9	0.0	0.0	0.0	3.40	3.46/1.82	3.17	0.93	0.94	0.94	-0.57	-0.05	-0.09	0.24	0.76
USW-G4	2345.8	0.0	0.0	0.0	0.0	0.0	2.10	3.01/1.37	1.87	0.93	0.94	0.94	-0.57	-0.05	-0.09	0.24	0.76
USW-G4	2578.7	44.4	0.0	0.0	0.0	0.0	2.10	3.01/1.37	1.87	2.00	2.33	2.46	1.32	-0.05	1.17	1.52	2.06
USW-G4	2614.8	0.0	0.0	0.0	1.4	32.9	2.12	3.01/1.37	1.88	1.24	1.24	1.24	-0.35	0.10	0.18	0.50	1.00
USW-G4	2690.3	0.0	0.0	0.0	45.3	0.0	2.53	3.10/1.46	2.20	2.48	2.47	2.47	0.77	1.14	1.38	1.69	2.18
USW-G4	2696.9	0.0	90.6	0.0	0.0	0.0	3.40	3.47/1.82	3.17	0.93	0.94	0.94	-0.57	-0.05	-0.09	0.24	0.76
USW-G4	2729.7	0.0	96.2	0.0	0.0	0.0	3.43	3.48/1.84	3.20	0.93	0.94	0.94	-0.57	-0.05	-0.09	0.24	0.76
USW-G4	2792.0	0.0	100.0	0.0	0.0	0.0	3.44	3.50/1.85	3.21	0.93	0.94	0.94	-0.57	-0.05	-0.09	0.24	0.76

Table E1. (continued)

Sample	Depth feet	Calcite	Zeolite	Hematite	Smectite	MnOx ^f	Ca	Cs ^e	Sr	Am	Eu	Sm	Np	U	Pu -5	Pu -10	Pu -15
		Fracture	Lining	Mass % ^d										Log K _d ^d			
USW-G4	2824.8	0.0	80.6	0.0	3.2	0.0	3.36	3.44/1.79	3.13	1.47	1.46	1.47	-0.17	0.26	0.39	0.71	1.20
USW-G4	2831.4	0.0	74.4	0.0	12.8	0.0	3.33	3.42/1.78	3.10	1.96	1.95	1.96	0.27	0.66	0.87	1.18	1.67
USW-G4	2854.3	0.0	0.0	8.5	1.7	8.5	2.13	3.01/1.37	1.88	1.32	1.39	1.39	0.62	1.43	0.91	1.32	1.91
USW-G4	2887.1	0.0	0.0	9.3	1.9	0.0	2.13	3.02/1.37	1.89	1.34	1.41	1.42	0.65	1.47	0.95	1.36	1.94
USW-G4	2903.5	0.0	0.0	2.0	0.0	0.0	2.10	3.01/1.37	1.87	0.94	0.99	1.00	0.06	0.85	0.38	0.77	1.35
USW-G4	2916.7	0.0	0.0	1.4	1.4	32.4	2.12	3.01/1.37	1.88	1.24	1.26	1.26	0.01	0.73	0.41	0.77	1.33
USW-G4	2918.3	1.9	0.0	0.0	0.0	44.4	2.10	3.01/1.37	1.87	1.09	1.23	1.31	0.05	-0.05	0.14	0.48	1.01
USW-G4	2919.9	0.0	0.0	8.6	8.6	0.0	2.22	3.03/1.39	1.95	1.82	1.84	1.84	0.70	1.47	1.07	1.45	2.02
USW-G4	2923.2	0.0	0.0	0.0	0.0	45.3	2.10	3.01/1.37	1.87	0.93	0.94	0.94	-0.57	-0.05	-0.09	0.24	0.76
USW-G4	2929.8	0.0	9.4	0.0	45.3	0.0	2.77	3.16/1.52	2.49	2.48	2.47	2.47	0.77	1.14	1.38	1.69	2.18
USW-G4	2946.2	0.0	0.0	0.0	1.9	44.4	2.13	3.02/1.37	1.89	1.31	1.31	1.31	-0.30	0.15	0.25	0.56	1.07
USW-G4	2952.8	0.0	0.0	0.0	0.0	70.6	2.10	3.01/1.37	1.87	0.93	0.94	0.94	-0.57	-0.05	-0.09	0.24	0.76
USW-G4	2956.0	0.0	0.0	0.0	8.6	41.4	2.22	3.03/1.39	1.95	1.81	1.80	1.80	0.13	0.52	0.72	1.03	1.52
USW-G4	2969.2	0.0	0.0	0.0	1.9	44.4	2.13	3.02/1.37	1.89	1.31	1.31	1.31	-0.30	0.15	0.25	0.56	1.07
USW-G4	2970.8	0.0	14.7	0.0	70.6	0.0	2.93	3.23/1.59	2.64	2.67	2.66	2.66	0.96	1.32	1.57	1.87	2.36
USW-G4	2970.8	1.9	0.0	0.0	0.0	44.4	2.10	3.01/1.37	1.87	1.09	1.23	1.31	0.05	-0.05	0.14	0.48	1.01
USW-G4	2982.3	0.0	0.0	0.0	0.0	14.7	2.10	3.01/1.37	1.87	0.93	0.94	0.94	-0.57	-0.05	-0.09	0.24	0.76
USW-G4	2985.6	0.0	0.0	2.5	12.5	12.5	2.27	3.04/1.39	1.99	1.95	1.95	1.95	0.46	1.08	0.96	1.30	1.82
USW-G4	2986.9	0.0	0.0	9.4	0.0	0.0	2.10	3.01/1.37	1.87	1.00	1.15	1.16	0.64	1.47	0.90	1.33	1.92
USW-G4	2986.9	0.0	0.0	0.0	0.0	45.3	2.10	3.01/1.37	1.87	0.93	0.94	0.94	-0.57	-0.05	-0.09	0.24	0.76
Avg ^e	-	-	-	-	-	-	2.81	3.23/1.59	2.56	1.48	1.50	1.51	0.02	0.48	0.50	0.83	1.35
SD ^{c,e}	-	-	-	-	-	-	0.54	0.19/0.19	0.55	0.60	0.60	0.61	0.58	0.56	0.58	0.58	0.58
Median ^e	-	-	-	-	-	-	2.99	3.26/1.61	2.71	1.30	1.30	1.31	-0.11	0.22	0.38	0.71	1.20
Min ^e	-	-	-	-	-	-	2.10	3.01/1.37	1.87	0.93	0.94	0.94	-0.57	-0.05	-0.09	0.24	0.76
Max ^e	-	-	-	-	-	-	3.44	3.50/1.85	3.21	2.72	2.71	2.76	1.60	1.47	1.62	1.93	2.42
ALL DATA																	
Avg ^e	-	-	-	-	-	-	2.78	3.21/1.57	2.53	1.66	1.69	1.71	0.20	0.54	0.67	1.00	1.51
SD ^{c,e}	-	-	-	-	-	-	0.51	0.18/0.18	0.52	0.59	0.61	0.62	0.64	0.55	0.58	0.58	0.58
Median ^e	-	-	-	-	-	-	2.10	3.18/1.37	1.87	0.93	0.94	0.94	-0.57	-0.05	-0.09	0.24	0.76
Min ^e	-	-	-	-	-	-	3.44	3.01/1.85	3.21	2.80	2.79	2.81	1.67	2.14	1.70	2.00	2.58
Max ^e	-	-	-	-	-	-	2.85	3.50/1.54	2.56	1.63	1.65	1.66	0.22	0.49	0.71	1.03	1.53

^a Uncertainty (in parentheses) related to mechanistic model reaction constants and not mineral spatial variability.

^b Mass percent for fracture lining minerals also reported in Table 13. Iron oxide and manganese oxide fracture lining mineral abundances were not distinguished by Drellack et al. (1997) and reported as Fe/MnOx. Thus, two K_d s are provided for each radionuclide that sorbs to iron oxides. In the first, we assume that most of the Fe/MnOx is iron oxide and calculate K_d from this iron oxide abundance. In the second, we assume that most of the Fe/MnOx is manganese oxide. However, since radionuclide sorption to manganese oxides is not included in our model, this is equivalent to ignoring radionuclide sorption to Fe/MnOx minerals.

^c Standard deviation (in parentheses) related to variability in mineral abundance for the particular drill hole and not uncertainty in mechanistic model reaction constants.

^d To calculate the fracture flow zone R or K_d , fracture lining and matrix mineralogy must be known. Matrix mineralogy is listed in Table D1. In the case of CHESHIRE, we use the average matrix mineralogy at CHESHIRE. In the case of the hydrostratigraphic units, we use the average matrix mineralogy for each hydrostratigraphic unit. In the case of individual samples reported for specific wells and depths, the TC hydrostratigraphic matrix mineralogy was assumed. All specific drill hole samples reported here are part of the TC hydrostratigraphic unit as defined in Drellack et al. (1997).

^e Two values are reported for Cs. First, it is assumed that colloids are dominated by smectites. The colloid load is not high enough for smectite colloids to affect Cs transport. Second, it is assumed that colloids are dominated by illite/mica. Since Cs sorbs very strongly to this mineral, colloids are predicted to significantly increase the transport of Cs. These two cases provide the extreme cases for colloid facilitated Cs transport.

^f Manganese oxide mineral abundances are reported here but are not included in our K_d predictions. Radionuclide sorption to manganese oxides was not included in our model.

Table E2. Radionuclide sorbing mineral abundances and predicted retardation factors for Tuff Cone hydrostratigraphic unit fracture flow zones.

Sample	Depth feet	Strat. ^a	Ca	Cs	Sr	Am	Eu	Sm	Np	U	Pu -5	Pu -10	Pu -15
Log R ^b													
CHESHIRE ^a	-	-	2.2 (2.2,2.2)	1.6/1.6 (2.3/1.6,3.2/1.6)	1.9 (1.9,1.9)	1.8 (1.9,1.8)	1.9 (1.8,1.9)	2.0 (2.0,2.0)	1.0 (0.4,1.0)	1.3 (0.6,1.3)	1.3 (0.6,1.3)	1.6 (0.8,1.6)	1.9 (1.4,1.9)
TMA ^a	-	-	3.3 (3.3,3.3)	4.0/2.4 (3.1/2.4,4.0/2.4)	3.1 (3.1,3.1)	2.0 (2.1,2.0)	2.1 (2.0,2.1)	2.1 (2.1,2.2)	0.8 (0.6,1.1)	1.2 (0.9,1.5)	1.1 (0.7,1.5)	1.4 (1.0,1.8)	1.9 (1.6,2.1)
TC ^a	-	-	3.0 (3.0,3.0)	3.2/1.6 (2.4/1.7,3.2/1.6)	2.7 (2.7,2.7)	1.9 (1.9,1.9)	2.0 (1.9,2.0)	2.1 (2.0,2.1)	1.1 (0.7,1.5)	1.8 (1.4,2.2)	1.4 (0.9,1.8)	1.7 (1.3,2.1)	2.3 (2.0,2.5)
TBA ^a	-	-	3.2 (3.2,3.2)	4.3/2.7 (3.3/2.6,4.3/2.7)	3.0 (3.0,3.0)	2.6 (2.7,2.6)	2.7 (2.6,2.7)	2.7 (2.7,2.8)	1.7 (1.3,2.1)	2.5 (2.0,2.9)	2.0 (1.6,2.5)	2.4 (2.0,2.8)	3.0 (2.7,3.2)
BAQ ^a	-	-	3.4 (3.4,3.4)	3.3/1.6 (2.7/1.9,3.3/1.6)	3.1 (3.1,3.1)	2.3 (2.5,1.9)	2.6 (2.5,2.7)	3.0 (2.9,3.0)	1.6 (1.2,2.1)	0.2 (0.2,0.2)	1.5 (1.0,1.9)	1.8 (1.4,2.2)	2.3 (2.0,2.5)
UE-25	780.8	Tpt	2.22	2.99/1.37	1.99	2.01	2.33	2.47	1.34	0.26	1.20	1.53	2.07
UE-25	872.7	Tpt	3.25	3.36/1.72	3.02	0.94	0.95	0.96	0.10	0.26	0.24	0.41	0.80
UE-25	967.8	Tpt	3.25	3.36/1.72	3.02	0.94	0.95	0.96	0.10	0.26	0.24	0.41	0.80
UE-25	990.8	Tpt	2.34	3.01/1.39	2.10	1.48	1.47	1.48	0.22	0.44	0.54	0.78	1.22
UE-25	990.8	Tpt	2.73	3.11/1.48	2.49	1.40	1.40	1.40	0.19	0.40	0.49	0.72	1.16
UE-25	1049.9	Tpt	3.35	3.42/1.79	3.12	1.29	1.29	1.29	0.16	0.36	0.42	0.64	1.06
UE-25	1102.4	Tpt	2.72	3.11/1.48	2.47	1.97	1.96	1.97	0.46	0.74	0.93	1.21	1.68
UE-25	1105.6	Tpt	3.33	3.41/1.77	3.10	0.94	0.95	0.96	0.10	0.26	0.24	0.41	0.80
UE-25	1243.4	Tpt	3.29	3.38/1.74	3.06	0.94	0.95	0.96	0.10	0.26	0.24	0.41	0.80
UE-25	1253.3	Tpt	3.23	3.34/1.71	3.00	1.34	1.34	1.34	0.18	0.38	0.45	0.67	1.11
UE-25	1276.2	Tpt	3.08	3.27/1.64	2.84	2.36	2.35	2.35	0.74	1.06	1.28	1.58	2.06
UE-25	1276.2	Tpt	2.91	3.19/1.56	2.64	2.47	2.46	2.46	0.83	1.16	1.39	1.68	2.17
UE-25	1282.8	Tpt	3.20	3.34/1.70	2.95	2.47	2.47	2.47	0.83	1.16	1.40	1.69	2.18
UE-25	1295.9	Tpt	3.34	3.42/1.78	3.11	2.04	2.04	2.04	0.51	0.80	1.00	1.28	1.76

Table E2. (continued)

Sample	Depth feet	Strat. ^d	Ca	Cs	Sr	Am	Eu	Sm	Np	U	Pu -5	Pu -10	Pu -15
							Log R ^b						
UE-25	1302.5	Tpt	3.32	3.40/1.77	3.08	2.02	2.01	2.01	0.49	0.78	0.97	1.25	1.73
UE-25	1309.1	Tpt	3.26	3.36/1.73	3.02	1.96	1.95	1.96	0.45	0.74	0.92	1.20	1.67
UE-25	1318.9	Tpt	3.32	3.40/1.76	3.09	1.40	1.40	1.40	0.19	0.40	0.49	0.72	1.16
UE-25	1322.2	Tpt	3.24	3.35/1.72	3.01	1.87	1.87	1.87	0.40	0.67	0.85	1.12	1.59
UE-25	1338.6	Tpt	3.35	3.42/1.79	3.12	1.79	1.79	1.79	0.36	0.62	0.78	1.04	1.51
UE-25	1361.5	Tpt	3.10	3.27/1.64	2.86	1.74	1.74	1.74	0.33	0.59	0.74	1.00	1.47
UE-25	1417.3	Th	3.32	3.40/1.77	3.09	0.94	0.95	0.96	0.10	0.26	0.24	0.41	0.80
UE-25	1420.6	Th	3.33	3.41/1.77	3.10	1.96	1.95	1.96	0.45	0.74	0.92	1.20	1.67
UE-25	1420.6	Th	2.73	3.11/1.48	2.50	0.94	0.95	0.96	0.10	0.26	0.24	0.41	0.80
UE-25	1643.7	Th	3.32	3.40/1.76	3.09	1.27	1.27	1.27	0.16	0.35	0.40	0.62	1.05
UE-25	1676.5	Th	3.26	3.36/1.73	3.03	1.95	1.94	1.94	0.45	0.73	0.91	1.19	1.66
UE-25	2007.9	Th	2.07	2.97/1.35	1.84	0.97	1.03	1.04	0.41	1.05	0.61	0.95	1.50
UE-25	2011.2	Tcp	2.07	2.97/1.35	1.84	0.94	0.95	0.96	0.10	0.26	0.24	0.41	0.80
UE-25	2037.4	Tcp	3.32	3.40/1.76	3.09	1.40	1.40	1.40	0.19	0.40	0.49	0.72	1.16
UE-25	2142.4	Tcp	3.08	3.26/1.63	2.85	1.29	1.29	1.29	0.16	0.36	0.41	0.63	1.06
UE-25	2142.4	Tcp	3.07	3.25/1.62	2.83	1.78	1.77	1.77	0.35	0.61	0.77	1.03	1.50
UE-25	2165.4	Tcp	3.02	3.24/1.60	2.77	2.23	2.23	2.23	0.64	0.96	1.17	1.46	1.94
UE-25	2165.4	Tcp	2.07	2.97/1.35	1.84	0.94	0.95	0.96	0.10	0.26	0.24	0.41	0.80
UE-25	2181.8	Tcp	3.09	3.26/1.63	2.86	0.94	0.95	0.96	0.10	0.26	0.24	0.41	0.80
UE-25	2211.3	Tcp	3.06	3.25/1.61	2.83	0.94	0.95	0.96	0.10	0.26	0.24	0.41	0.80
UE-25	2234.3	Tcp	3.29	3.38/1.75	3.05	1.92	1.91	1.91	0.43	0.71	0.89	1.16	1.63
UE-25	2237.5	Tcp	3.29	3.38/1.74	3.06	0.94	0.95	0.96	0.10	0.26	0.24	0.41	0.80
UE-25	2362.2	Tcb	2.61	3.08/1.46	2.33	2.28	2.28	2.28	0.72	1.13	1.24	1.53	2.03
UE-25	2372.0	Tcb	3.28	3.37/1.74	3.05	1.37	1.37	1.37	0.19	0.39	0.47	0.70	1.13
UE-25	2395.0	Tcb	3.12	3.29/1.65	2.87	2.34	2.33	2.33	0.72	1.04	1.27	1.56	2.04
UE-25	3090.6	Tct	2.07	2.97/1.35	1.84	0.94	0.95	0.96	0.10	0.26	0.24	0.41	0.80
UE-25	3185.7	Tct	2.11	2.98/1.36	1.86	2.12	2.42	2.55	1.41	0.39	1.28	1.62	2.16
UE-25	3271.0	Tct	3.28	3.37/1.74	3.05	1.37	1.37	1.37	0.19	0.39	0.47	0.70	1.13
UE-25	3277.6	Tct	2.32	3.01/1.38	2.07	2.23	2.54	2.67	1.52	0.42	1.39	1.73	2.27
UE-25	3287.4	Tct	3.37	3.43/1.80	3.14	1.43	1.43	1.44	0.21	0.42	0.51	0.75	1.19
UE-25	3290.7	Tct	3.17	3.32/1.68	2.92	2.39	2.38	2.39	0.76	1.09	1.32	1.61	2.09
UE-25	3290.7	Tct	3.11	3.28/1.65	2.86	2.40	2.39	2.39	0.77	1.09	1.32	1.62	2.10
UE-25	3349.7	Tct	2.52	3.07/1.44	2.18	2.47	2.47	2.47	0.83	1.16	1.40	1.69	2.18

Table E2. (continued)

Sample	Depth feet	Strat. ^d	Ca	Cs	Sr	Am	Eu	Sm	Np	U	Pu -5	Pu -10	Pu -15
							Log R ^b						
UE-25	3526.9	Tct	2.26	3.01/1.38	1.97	1.98	1.98	1.98	0.47	0.75	0.94	1.22	1.69
UE-25	3671.3	Tct	2.24	3.00/1.38	1.96	2.31	2.54	2.65	1.46	0.71	1.40	1.74	2.27
UE-25	3730.3	Tct	2.47	3.06/1.43	2.14	2.40	2.39	2.39	0.77	1.09	1.32	1.62	2.10
UE-25	3763.1	Tct	2.10	2.98/1.35	1.86	2.05	2.35	2.48	1.34	0.37	1.22	1.55	2.09
Avg	-	-	2.93	3.24/1.61	2.68	1.66	1.69	1.71	0.46	0.59	0.76	1.01	1.47
SD ^c	-	-	0.46	0.16/0.16	0.47	0.55	0.57	0.59	0.40	0.32	0.42	0.48	0.52
Median	-	-	3.11	3.28/1.65	2.86	1.78	1.77	1.77	0.36	0.42	0.77	1.03	1.50
Min	-	-	2.07	2.97/1.35	1.84	0.94	0.95	0.96	0.10	0.26	0.24	0.41	0.80
Max	-	-	3.37	3.43/1.80	3.14	2.47	2.54	2.67	1.52	1.16	1.40	1.74	2.27
USW-G1	337.9	Tpt	3.09	3.26/1.63	2.86	0.94	0.95	0.96	0.10	0.26	0.24	0.41	0.80
USW-G1	426.5	Tpt	2.07	2.97/1.35	1.84	2.20	2.53	2.67	1.55	1.04	1.42	1.77	2.32
USW-G1	626.6	Tpt	3.12	3.29/1.65	2.87	2.40	2.40	2.40	0.78	1.10	1.33	1.62	2.11
USW-G1	685.7	Tpt	3.36	3.43/1.79	3.13	1.49	1.48	1.49	0.22	0.44	0.54	0.79	1.23
USW-G1	725.1	Tpt	3.39	3.45/1.81	3.16	0.94	0.95	0.96	0.10	0.26	0.24	0.41	0.80
USW-G1	941.6	Tpt	3.39	3.45/1.81	3.16	0.94	0.95	0.96	0.10	0.26	0.24	0.41	0.80
USW-G1	981.0	Tpt	3.39	3.45/1.81	3.16	1.51	1.51	1.51	0.23	0.46	0.56	0.81	1.26
USW-G1	1105.6	Tpt	2.11	2.98/1.36	1.86	1.37	1.39	1.39	0.40	0.97	0.66	0.98	1.50
USW-G1	1138.5	Tpt	2.33	3.02/1.40	2.03	2.16	2.16	2.16	0.76	1.32	1.20	1.52	2.04
USW-G1	1158.1	Tpt	2.48	3.06/1.43	2.17	2.33	2.33	2.34	0.91	1.49	1.37	1.69	2.21
USW-G1	1164.7	Tpt	2.36	3.03/1.40	2.07	2.13	2.13	2.14	0.74	1.30	1.18	1.50	2.01
USW-G1	1227.0	Tpt	3.12	3.29/1.66	2.87	2.40	2.39	2.39	0.77	1.09	1.32	1.62	2.10
USW-G1	1266.4	Tpt	2.33	3.01/1.38	2.09	2.27	2.60	2.74	1.61	0.26	1.45	1.79	2.34
USW-G1	1282.8	Tpt	3.07	3.25/1.62	2.84	2.01	2.30	2.43	1.29	0.36	1.17	1.50	2.04
USW-G1	1295.9	Tpt	2.47	3.06/1.43	2.14	2.40	2.39	2.39	0.77	1.09	1.32	1.62	2.10
USW-G1	1338.6	Tpt	2.96	3.21/1.57	2.71	2.23	2.23	2.23	0.64	0.96	1.17	1.46	1.94
USW-G1	1355.0	Tpt	3.05	3.24/1.61	2.82	1.27	1.27	1.28	0.16	0.35	0.41	0.62	1.05
USW-G1	1922.6	Tcp	2.12	2.98/1.36	1.87	1.45	1.45	1.46	0.21	0.43	0.52	0.76	1.21
USW-G1	2244.1	Tcb	3.30	3.38/1.75	3.07	0.94	0.95	0.96	0.10	0.26	0.24	0.41	0.80
USW-G1	2283.5	Tcb	2.95	3.20/1.57	2.72	1.61	1.60	1.61	0.27	0.51	0.63	0.89	1.34
USW-G1	2306.4	Tcb	3.41	3.46/1.82	3.18	0.94	0.95	0.96	0.10	0.26	0.24	0.41	0.80
USW-G1	2506.6	Tcb	2.07	2.97/1.35	1.84	0.94	0.95	0.96	0.10	0.26	0.24	0.41	0.80
USW-G1	2565.6	Tcb	2.32	3.01/1.38	2.09	0.94	0.95	0.96	0.10	0.26	0.24	0.41	0.80
USW-G1	2578.7	Tcb	2.28	3.00/1.38	2.02	1.75	1.77	1.77	0.72	1.41	1.04	1.40	1.95

Table E2. (continued)

Sample	Depth feet	Strat. ^d	Ca	Cs	Sr	Am	Eu	Sm	Np	U	Pu -5	Pu -10	Pu -15
Log R ^b													
USW-G1	2792.0	Tct	2.12	2.98/1.36	1.87	1.44	1.44	1.45	0.21	0.42	0.52	0.75	1.20
USW-G1	2808.4	Tct	2.12	2.98/1.36	1.87	1.44	1.44	1.45	0.21	0.42	0.52	0.75	1.20
USW-G1	2906.8	Tct	2.07	2.97/1.35	1.84	1.97	2.29	2.43	1.30	0.26	1.16	1.49	2.03
USW-G1	2919.9	Tct	2.07	2.97/1.35	1.84	0.94	0.95	0.96	0.10	0.26	0.24	0.41	0.80
USW-G1	2936.4	Tct	2.07	2.97/1.35	1.84	2.27	2.60	2.74	1.61	0.26	1.45	1.79	2.34
USW-G1	2936.4	Tct	2.07	2.97/1.35	1.84	2.27	2.60	2.74	1.61	0.26	1.45	1.79	2.34
USW-G1	2962.6	Tct	2.07	2.97/1.35	1.84	1.11	1.27	1.34	0.46	0.87	0.57	0.88	1.41
Avg	-	-	2.62	3.14/1.51	2.37	1.65	1.72	1.75	0.59	0.62	0.80	1.07	1.54
SD ^c	-	-	0.53	0.18/0.18	0.53	0.56	0.62	0.65	0.53	0.42	0.47	0.53	0.59
Median	-	-	2.36	3.03/1.40	2.09	1.51	1.51	1.51	0.40	0.42	0.63	0.89	1.41
Min	-	-	2.07	2.97/1.35	1.84	0.94	0.95	0.96	0.10	0.26	0.24	0.41	0.80
Max	-	-	3.41	3.46/1.82	3.18	2.40	2.60	2.74	1.61	1.49	1.45	1.79	2.34
USW-G2	1177.8	Tpt	2.12	2.98/1.36	1.87	1.44	1.46	1.46	0.45	1.06	0.73	1.06	1.59
USW-G2	1282.8	Tpt	2.22	2.99/1.37	1.98	1.30	1.36	1.37	0.68	1.41	0.92	1.30	1.87
USW-G2	1446.9	Tpt	2.50	3.04/1.42	2.25	1.70	1.72	1.72	0.68	1.36	0.99	1.34	1.89
USW-G2	1446.9	Tpt	2.55	3.06/1.43	2.31	1.88	2.10	2.20	1.05	0.74	1.02	1.34	1.87
USW-G2	1450.1	Tpt	3.33	3.41/1.77	3.10	1.63	1.63	1.63	0.28	0.52	0.65	0.91	1.36
USW-G2	1456.7	Tpt	3.25	3.36/1.72	3.02	1.39	1.39	1.40	0.19	0.40	0.48	0.71	1.15
USW-G2	1489.5	Tpt	2.39	3.03/1.40	2.12	1.96	1.96	1.96	0.59	1.12	1.01	1.32	1.83
USW-G2	1505.9	Tpt	3.22	3.34/1.70	2.99	1.66	1.66	1.66	0.29	0.54	0.68	0.94	1.40
USW-G2	1515.7	Tpt	3.32	3.40/1.77	3.09	1.27	1.27	1.28	0.16	0.35	0.41	0.62	1.05
USW-G2	1535.4	Tpt	3.21	3.33/1.70	2.98	1.36	1.36	1.36	0.18	0.39	0.46	0.69	1.12
USW-G2	1568.2	Tpt	3.36	3.43/1.79	3.13	1.27	1.27	1.27	0.16	0.35	0.40	0.62	1.05
USW-G2	1568.2	Tpt	3.21	3.33/1.70	2.98	1.21	1.21	1.22	0.14	0.33	0.37	0.58	1.00
USW-G2	1581.4	Tpt	3.33	3.41/1.77	3.10	1.25	1.26	1.26	0.15	0.35	0.40	0.61	1.04
USW-G2	1604.3	Tpt	3.19	3.32/1.68	2.95	1.64	1.64	1.64	0.29	0.53	0.66	0.92	1.38
USW-G2	1630.6	Tpt	3.18	3.31/1.68	2.94	1.88	1.88	1.88	0.41	0.68	0.85	1.13	1.60
USW-G2	1630.6	Tpt	2.38	3.03/1.40	2.09	2.17	2.16	2.16	0.59	0.90	1.11	1.39	1.87
USW-G2	1637.1	Tpt	2.94	3.22/1.58	2.65	2.68	2.68	2.68	1.02	1.36	1.60	1.90	2.38
USW-G2	1643.7	Tpt	2.95	3.22/1.59	2.66	2.70	2.69	2.69	1.03	1.37	1.61	1.91	2.40
USW-G2	1643.7	Tpt	3.34	3.42/1.78	3.11	2.04	2.04	2.04	0.51	0.80	1.00	1.28	1.76

Table E2. (continued)

Sample	Depth feet	Strat. ^d	Ca	Cs	Sr	Am	Eu	Sm	Np	U	Pu -5	Pu -10	Pu -15
							Log R ^b						
USW-G2	1643.7	Tpt	3.19	3.33/1.70	2.94	2.48	2.48	2.48	0.84	1.17	1.41	1.70	2.19
USW-G2	1653.5	Tpt	3.18	3.33/1.69	2.93	2.46	2.45	2.45	0.82	1.15	1.38	1.68	2.16
USW-G2	1656.8	Tpt	3.15	3.31/1.67	2.90	2.44	2.44	2.44	0.81	1.13	1.37	1.66	2.14
USW-G2	1669.9	Tpt	3.19	3.33/1.70	2.94	2.47	2.46	2.46	0.83	1.16	1.39	1.68	2.17
USW-G2	1679.8	Tpt	3.27	3.37/1.73	3.03	1.97	1.96	1.97	0.46	0.74	0.93	1.21	1.68
USW-G2	1686.4	Tpt	3.27	3.37/1.74	3.04	1.96	1.95	1.96	0.45	0.74	0.92	1.20	1.67
USW-G2	1758.5	Th	3.39	3.45/1.81	3.16	0.94	0.95	0.96	0.10	0.26	0.24	0.41	0.80
USW-G2	1761.8	Th	2.43	3.04/1.41	2.16	2.03	2.03	2.03	0.50	0.79	0.98	1.27	1.74
USW-G2	1866.8	Th	3.34	3.41/1.78	3.11	0.94	0.95	0.96	0.10	0.26	0.24	0.41	0.80
USW-G2	1866.8	Th	2.73	3.11/1.48	2.50	0.94	0.95	0.96	0.10	0.26	0.24	0.41	0.80
USW-G2	2004.6	Th	3.02	3.22/1.59	2.78	0.94	0.95	0.96	0.10	0.26	0.24	0.41	0.80
USW-G2	2004.6	Th	3.09	3.26/1.63	2.86	1.25	1.26	1.26	0.15	0.35	0.40	0.61	1.04
USW-G2	2027.6	Th	3.27	3.37/1.73	3.04	1.36	1.36	1.37	0.18	0.39	0.46	0.69	1.13
USW-G2	2066.9	Th	3.24	3.35/1.72	3.01	1.87	1.87	1.87	0.40	0.67	0.85	1.12	1.59
USW-G2	2070.2	Th	3.12	3.28/1.65	2.89	1.27	1.27	1.28	0.16	0.35	0.41	0.62	1.05
USW-G2	2086.6	Th	3.33	3.41/1.77	3.10	0.94	0.95	0.96	0.10	0.26	0.24	0.41	0.80
USW-G2	2093.2	Th	3.15	3.30/1.66	2.92	1.29	1.29	1.29	0.16	0.36	0.42	0.64	1.06
USW-G2	2122.7	Th	3.41	3.46/1.82	3.18	0.94	0.95	0.96	0.10	0.26	0.24	0.41	0.80
USW-G2	2280.2	Th	3.33	3.41/1.77	3.10	1.96	1.95	1.96	0.45	0.74	0.92	1.20	1.67
USW-G2	2283.5	Th	3.09	3.26/1.63	2.86	1.29	1.29	1.29	0.16	0.36	0.42	0.64	1.06
USW-G2	2723.1	Tcp	2.19	2.99/1.37	1.92	1.78	1.77	1.77	0.35	0.61	0.77	1.03	1.50
USW-G2	2752.6	Tcp	2.55	3.08/1.45	2.23	2.43	2.43	2.43	0.80	1.13	1.36	1.65	2.14
USW-G2	2762.5	Tcp	2.09	2.98/1.35	1.85	1.23	1.23	1.23	0.15	0.34	0.38	0.59	1.01
USW-G2	2811.7	Tcp	2.10	2.98/1.35	1.86	1.42	1.64	1.65	1.28	2.10	1.53	1.95	2.54
USW-G2	2854.3	Tcp	2.19	2.99/1.37	1.92	1.79	1.81	1.81	0.75	1.45	1.07	1.43	1.99
USW-G2	2864.2	Tcp	2.24	3.00/1.38	1.96	1.93	1.92	1.92	0.43	0.71	0.89	1.17	1.64
USW-G2	2874.0	Tcp	2.10	2.98/1.35	1.85	1.29	1.29	1.29	0.16	0.36	0.42	0.64	1.06
USW-G2	2877.3	Tcp	2.09	2.98/1.35	1.85	1.23	1.24	1.25	0.29	0.77	0.52	0.81	1.31
USW-G2	2883.9	Tcp	2.48	3.06/1.43	2.15	2.42	2.42	2.42	0.99	1.58	1.45	1.78	2.30
USW-G2	2893.7	Tcp	2.07	2.97/1.35	1.84	0.94	0.95	0.96	0.10	0.26	0.24	0.41	0.80
USW-G2	2926.5	Tcp	2.23	3.00/1.38	1.95	1.92	1.91	1.91	0.43	0.71	0.89	1.16	1.63
USW-G2	2959.3	Tcp	2.67	3.12/1.49	2.32	2.68	2.68	2.68	1.02	1.36	1.60	1.90	2.38

Table E2. (continued)

Sample	Depth feet	Strat. ^d	Ca	Cs	Sr	Am	Eu	Sm	Np	U	Pu -5	Pu -10	Pu -15
								Log R ^b					
USW-G2	2959.3	Tcp	2.07	2.97/1.35	1.84	0.94	0.95	0.96	0.10	0.26	0.24	0.41	0.80
USW-G2	3002.0	Tcp	2.38	3.03/1.41	2.07	2.27	2.29	2.29	1.20	1.96	1.55	1.93	2.49
USW-G2	3136.5	Tcp	2.72	3.10/1.47	2.49	0.94	0.95	0.96	0.10	0.26	0.24	0.41	0.80
USW-G2	3169.3	Tcp	2.56	3.07/1.44	2.29	2.18	2.20	2.20	1.12	1.87	1.47	1.84	2.40
USW-G2	3399.0	Tcp	2.09	2.98/1.35	1.85	1.27	1.27	1.28	0.16	0.35	0.41	0.62	1.05
USW-G2	3408.8	Tcp	2.09	2.98/1.35	1.85	1.34	1.54	1.54	1.16	1.97	1.41	1.82	2.41
USW-G2	3421.9	Tcp	2.09	2.98/1.35	1.85	1.27	1.27	1.28	0.16	0.35	0.41	0.62	1.05
Avg	-	-	2.80	3.19/1.56	2.55	1.65	1.66	1.67	0.46	0.77	0.79	1.05	1.52
SD ^c	-	-	0.49	0.17/0.17	0.50	0.53	0.53	0.53	0.36	0.51	0.45	0.51	0.55
Median	-	-	2.98	3.22/1.59	2.72	1.54	1.63	1.64	0.37	0.68	0.75	1.05	1.54
Min	-	-	2.07	2.97/1.35	1.84	0.94	0.95	0.96	0.10	0.26	0.24	0.41	0.80
Max	-	-	3.41	3.46/1.82	3.18	2.70	2.69	2.69	1.28	2.10	1.61	1.95	2.54
USW-G3/GU3	469.2	Tpt	2.07	2.97/1.35	1.84	2.30	2.63	2.77	1.64	0.26	1.48	1.83	2.37
USW-G3/GU3	479.0	Tpt	2.07	2.97/1.35	1.84	2.30	2.63	2.77	1.64	0.26	1.48	1.83	2.37
USW-G3/GU3	498.7	Tpt	2.07	2.97/1.35	1.84	0.94	0.95	0.96	0.10	0.26	0.24	0.41	0.80
USW-G3/GU3	518.4	Tpt	2.49	3.06/1.43	2.16	2.43	2.42	2.42	0.84	1.26	1.37	1.68	2.17
USW-G3/GU3	518.4	Tpt	2.07	2.97/1.35	1.84	0.97	1.03	1.04	0.41	1.05	0.61	0.95	1.50
USW-G3/GU3	521.7	Tpt	2.73	3.15/1.52	2.37	2.76	2.75	2.76	1.09	1.43	1.67	1.97	2.46
USW-G3/GU3	521.7	Tpt	2.07	2.97/1.35	1.84	2.30	2.63	2.77	1.64	0.26	1.48	1.83	2.37
USW-G3/GU3	521.7	Tpt	2.07	2.97/1.35	1.84	2.16	2.49	2.63	1.49	0.26	1.34	1.68	2.22
USW-G3/GU3	541.3	Tpt	2.68	3.13/1.50	2.32	2.70	2.69	2.69	1.03	1.37	1.61	1.91	2.40
USW-G3/GU3	541.3	Tpt	2.26	3.01/1.38	1.97	1.98	1.98	1.98	0.47	0.75	0.94	1.22	1.69
USW-G3/GU3	580.7	Tpt	2.12	2.98/1.36	1.87	1.44	1.46	1.46	0.45	1.06	0.73	1.06	1.59
USW-G3/GU3	610.2	Tpt	2.07	2.97/1.35	1.84	0.96	1.00	1.01	0.31	0.88	0.50	0.81	1.34
USW-G3/GU3	689.0	Tpt	2.32	3.01/1.38	2.09	0.94	0.95	0.96	0.10	0.26	0.24	0.41	0.80
USW-G3/GU3	689.0	Tpt	2.07	2.97/1.35	1.84	0.94	0.95	0.96	0.10	0.26	0.24	0.41	0.80
USW-G3/GU3	689.0	Tpt	2.47	3.06/1.43	2.15	2.40	2.40	2.40	0.78	1.10	1.33	1.62	2.11
USW-G3/GU3	689.0	Tpt	2.45	3.05/1.42	2.13	2.38	2.38	2.39	0.80	1.07	1.31	1.60	2.09
USW-G3/GU3	754.6	Tpt	2.62	3.10/1.47	2.27	2.62	2.61	2.61	0.96	1.30	1.53	1.83	2.32
USW-G3/GU3	800.5	Tpt	2.22	3.00/1.37	1.95	1.89	1.91	1.91	0.85	1.56	1.18	1.54	2.10
USW-G3/GU3	803.8	Tpt	3.14	3.30/1.67	2.89	2.43	2.43	2.43	0.80	1.13	1.36	1.65	2.14
USW-G3/GU3	803.8	Tpt	2.15	2.99/1.36	1.89	1.63	1.63	1.63	0.28	0.52	0.65	0.91	1.36

Table E2. (continued)

Sample	Depth feet	Strat. ^d	Ca	Cs	Sr	Am	Eu	Sm	Np	U	Pu -5	Pu -10	Pu -15
											Log R ^b		
USW-G3/GU3	810.4	Tpt	2.50	3.06/1.43	2.19	2.36	2.35	2.35	0.78	1.20	1.31	1.61	2.10
USW-G3/GU3	820.2	Tpt	2.37	3.03/1.40	2.06	2.23	2.23	2.23	0.82	1.40	1.27	1.59	2.11
USW-G3/GU3	823.5	Tpt	2.25	3.01/1.38	1.97	1.97	1.96	1.97	0.46	0.74	0.93	1.21	1.68
USW-G3/GU3	823.5	Tpt	2.45	3.05/1.42	2.13	2.37	2.36	2.37	0.75	1.07	1.30	1.59	2.07
USW-G3/GU3	830.1	Tpt	2.66	3.12/1.49	2.31	2.70	2.72	2.75	1.23	1.34	1.63	1.94	2.43
USW-G3/GU3	830.1	Tpt	2.11	2.98/1.36	1.86	2.18	2.49	2.62	1.47	0.41	1.34	1.68	2.22
USW-G3/GU3	846.5	Tpt	2.07	2.97/1.35	1.84	0.97	1.03	1.04	0.40	1.04	0.60	0.94	1.49
USW-G3/GU3	944.9	Tpt	2.07	2.97/1.35	1.84	0.96	1.00	1.00	0.29	0.84	0.48	0.78	1.30
USW-G3/GU3	944.9	Tpt	2.07	2.97/1.35	1.84	0.94	0.95	0.96	0.10	0.26	0.24	0.41	0.80
USW-G3/GU3	951.4	Tpt	2.07	2.97/1.35	1.84	0.94	0.95	0.96	0.10	0.26	0.24	0.41	0.80
USW-G3/GU3	971.1	Tpt	2.67	3.10/1.48	2.39	2.36	2.36	2.36	0.74	1.06	1.29	1.58	2.07
USW-G3/GU3	974.4	Tpt	2.07	2.97/1.35	1.84	0.94	0.95	0.96	0.10	0.26	0.24	0.41	0.80
USW-G3/GU3	977.7	Tpt	2.51	3.07/1.44	2.18	2.47	2.46	2.46	0.88	1.30	1.41	1.72	2.21
USW-G3/GU3	981.0	Tpt	2.38	3.03/1.41	2.07	2.25	2.25	2.25	0.66	0.97	1.19	1.48	1.96
USW-G3/GU3	987.5	Tpt	2.15	2.99/1.36	1.89	1.62	1.64	1.64	0.60	1.27	0.91	1.26	1.80
USW-G3/GU3	1007.2	Tpt	2.07	2.97/1.35	1.84	0.94	0.95	0.96	0.10	0.26	0.24	0.41	0.80
USW-G3/GU3	1072.8	Tpt	2.07	2.97/1.35	1.84	1.97	2.29	2.43	1.30	0.26	1.16	1.49	2.03
USW-G3/GU3	1072.8	Tpt	2.07	2.97/1.35	1.84	1.18	1.36	1.46	0.43	0.26	0.43	0.68	1.14
USW-G3/GU3	1164.7	Tpt	2.82	3.16/1.53	2.53	2.54	2.54	2.54	0.94	1.37	1.48	1.79	2.28
USW-G3/GU3	1184.4	Tpt	3.27	3.37/1.73	3.03	1.97	1.96	1.97	0.46	0.74	0.93	1.21	1.68
USW-G3/GU3	1190.9	Tpt	3.05	3.25/1.61	2.82	1.76	1.76	1.76	0.34	0.60	0.76	1.02	1.49
USW-G3/GU3	1190.9	Tpt	3.09	3.27/1.63	2.86	1.80	1.80	1.80	0.36	0.63	0.79	1.06	1.52
USW-G3/GU3	1190.9	Tpt	3.08	3.26/1.62	2.85	0.94	0.95	0.96	0.10	0.26	0.24	0.41	0.80
USW-G3/GU3	1200.8	Tpt	3.19	3.33/1.70	2.94	2.48	2.48	2.48	0.84	1.17	1.41	1.70	2.19
USW-G3/GU3	1200.8	Tpt	3.03	3.24/1.61	2.78	2.31	2.31	2.31	0.70	1.02	1.24	1.54	2.02
USW-G3/GU3	1210.6	Tpt	2.50	3.06/1.43	2.19	2.36	2.35	2.35	0.74	1.06	1.28	1.58	2.06
USW-G3/GU3	1210.6	Tpt	2.28	3.01/1.39	1.99	2.04	2.04	2.04	0.51	0.80	1.00	1.28	1.76
USW-G3/GU3	1233.6	Tpt	2.49	3.06/1.43	2.16	2.43	2.42	2.42	0.79	1.12	1.35	1.64	2.13
USW-G3/GU3	1715.9	Tcb	2.10	2.98/1.35	1.85	2.01	2.31	2.44	1.32	0.87	1.21	1.55	2.10
USW-G3/GU3	1715.9	Tcb	2.99	3.21/1.58	2.76	1.49	1.68	1.78	0.65	0.34	0.65	0.94	1.43
USW-G3/GU3	1735.6	Tcb	2.29	3.01/1.38	2.03	1.77	1.78	1.79	0.50	0.94	0.85	1.15	1.65
USW-G3/GU3	1935.7	Tcb	3.32	3.40/1.76	3.09	0.94	0.95	0.96	0.10	0.26	0.24	0.41	0.80

Table E2. (continued)

Sample	Depth feet	Strat. ^d	Ca	Cs	Sr	Am	Eu	Sm	Np	U	Pu -5	Pu -10	Pu -15
								Log R ^b					
USW-G3/GU3	2014.4	Tcb	3.23	3.35/1.71	2.99	2.25	2.25	2.25	0.66	0.97	1.19	1.48	1.96
USW-G3/GU3	2014.4	Tcb	3.22	3.34/1.71	2.99	1.93	1.92	1.92	0.43	0.71	0.89	1.17	1.64
USW-G3/GU3	2096.5	Tcb	2.12	2.98/1.36	1.87	1.45	1.47	1.47	0.46	1.07	0.74	1.07	1.60
USW-G3/GU3	2155.5	Tcb	2.32	3.01/1.38	2.08	1.44	1.44	1.45	0.21	0.42	0.52	0.75	1.20
USW-G3/GU3	2198.2	Tcb	3.12	3.29/1.65	2.87	2.40	2.40	2.40	0.78	1.10	1.33	1.62	2.11
USW-G3/GU3	2208.0	Tcb	3.39	3.45/1.81	3.16	0.94	0.95	0.96	0.10	0.26	0.24	0.41	0.80
USW-G3/GU3	2290.0	Tcb	3.21	3.34/1.70	2.98	1.92	1.91	1.91	0.43	0.71	0.89	1.16	1.63
USW-G3/GU3	2326.1	Tcb	3.22	3.34/1.71	2.99	1.93	1.92	1.92	0.43	0.71	0.89	1.17	1.64
USW-G3/GU3	2378.6	Tcb	2.69	3.10/1.47	2.44	1.93	1.92	1.92	0.43	0.71	0.89	1.17	1.64
USW-G3/GU3	2385.2	Tcb	2.55	3.08/1.45	2.23	2.43	2.43	2.43	0.80	1.13	1.36	1.65	2.14
USW-G3/GU3	2431.1	Tcb	3.20	3.33/1.69	2.97	1.37	1.37	1.37	0.19	0.39	0.47	0.70	1.13
USW-G3/GU3	2503.3	Tcb	3.27	3.37/1.73	3.03	1.97	1.96	1.97	0.46	0.74	0.93	1.21	1.68
USW-G3/GU3	2559.1	Tcb	2.55	3.06/1.43	2.32	1.03	1.04	1.04	0.11	0.28	0.28	0.46	0.86
USW-G3/GU3	2634.5	Tct	2.70	3.10/1.47	2.46	1.72	1.71	1.71	0.32	0.57	0.72	0.98	1.44
USW-G3/GU3	2654.2	Tct	3.25	3.36/1.73	3.01	2.29	2.28	2.28	0.68	1.00	1.22	1.51	1.99
USW-G3/GU3	2831.4	Tct	3.06	3.25/1.62	2.82	1.77	1.77	1.77	0.35	0.60	0.76	1.03	1.49
USW-G3/GU3	2910.1	Tct	2.39	3.03/1.40	2.12	2.34	2.57	2.68	1.49	0.74	1.44	1.77	2.30
USW-G3/GU3	2956.0	Tct	2.29	3.00/1.38	2.06	2.20	2.53	2.66	1.53	0.26	1.38	1.72	2.26
USW-G3/GU3	2972.4	Tct	2.72	3.10/1.48	2.49	1.44	1.44	1.45	0.21	0.42	0.52	0.75	1.20
USW-G3/GU3	3038.1	Tct	3.32	3.40/1.76	3.09	1.45	1.45	1.46	0.21	0.43	0.52	0.76	1.21
USW-G3/GU3	3195.5	Tct	3.08	3.25/1.62	2.84	1.29	1.29	1.29	0.16	0.36	0.42	0.64	1.06
USW-G3/GU3	3238.2	Tct	2.23	2.99/1.37	1.99	1.29	1.29	1.29	0.16	0.36	0.42	0.64	1.06
USW-G3/GU3	3264.4	Tct	3.18	3.33/1.69	2.93	2.47	2.47	2.47	0.83	1.16	1.39	1.69	2.17
USW-G3/GU3	3264.4	Tct	3.14	3.30/1.67	2.89	2.43	2.42	2.42	0.79	1.12	1.35	1.64	2.13
USW-G3/GU3	3290.7	Tct	3.20	3.33/1.69	2.97	1.37	1.37	1.37	0.19	0.39	0.47	0.70	1.13
USW-G3/GU3	3294.0	Tct	3.24	3.35/1.72	3.01	1.40	1.40	1.40	0.19	0.40	0.49	0.72	1.16
Avg	-	-	2.59	3.12/1.49	2.33	1.84	1.88	1.90	0.61	0.75	0.93	1.21	1.68
SD ^c	-	-	0.45	0.15/0.14	0.46	0.57	0.59	0.61	0.43	0.39	0.44	0.49	0.52
Median	-	-	2.49	3.06/1.43	2.17	1.95	1.94	1.95	0.48	0.74	0.93	1.21	1.68
Min	-	-	2.07	2.97/1.35	1.84	0.94	0.95	0.96	0.10	0.26	0.24	0.41	0.80
Max	-	-	3.39	3.45/1.81	3.16	2.76	2.75	2.77	1.64	1.56	1.67	1.97	2.46
USW-G4	351.0		3.03	3.23/1.60	2.79	1.74	1.74	1.75	0.44	0.92	0.82	1.11	1.61
USW-G4	593.8		2.12	2.98/1.36	1.87	1.44	1.44	1.45	0.21	0.42	0.52	0.75	1.20

Table E2. (continued)

Sample	Depth feet	Strat. ^d	Ca	Cs	Sr	Am	Eu	Sm	Np	U	Log R ^b		
											Pu -5	Pu -10	Pu -15
USW-G4	669.3		2.13	2.98/1.36	1.87	2.29	2.59	2.73	1.58	0.44	1.45	1.79	2.33
USW-G4	685.7		3.39	3.45/1.81	3.16	0.94	0.95	0.96	0.10	0.26	0.24	0.41	0.80
USW-G4	698.8		2.59	3.08/1.45	2.32	2.26	2.25	2.26	0.66	0.98	1.19	1.48	1.97
USW-G4	698.8		2.61	3.10/1.47	2.26	2.61	2.61	2.62	1.00	1.28	1.53	1.83	2.32
USW-G4	777.6		2.10	2.98/1.35	1.85	1.30	1.31	1.32	0.34	0.87	0.59	0.89	1.40
USW-G4	810.4		3.14	3.30/1.67	2.89	2.43	2.43	2.43	0.80	1.13	1.36	1.65	2.14
USW-G4	889.1		2.19	2.99/1.37	1.92	1.77	1.77	1.77	0.46	0.94	0.84	1.14	1.64
USW-G4	984.3		2.11	2.98/1.36	1.86	1.41	1.43	1.43	0.43	1.01	0.70	1.02	1.55
USW-G4	1000.7		2.18	2.99/1.37	1.91	1.75	1.77	1.77	0.72	1.41	1.04	1.40	1.95
USW-G4	1007.2		2.50	3.04/1.42	2.26	1.28	1.35	1.35	0.65	1.38	0.90	1.28	1.84
USW-G4	1040.0		2.38	3.03/1.40	2.09	2.17	2.16	2.16	0.63	1.03	1.13	1.42	1.91
USW-G4	1072.8	Tpt	2.07	2.97/1.35	1.84	0.96	1.02	1.03	0.38	0.99	0.57	0.90	1.44
USW-G4	1072.8	Tpt	2.51	3.05/1.42	2.27	1.71	1.72	1.72	0.42	0.89	0.79	1.09	1.59
USW-G4	1082.7	Tpt	2.34	3.02/1.40	2.04	2.17	2.17	2.17	0.64	1.03	1.13	1.43	1.92
USW-G4	1148.3	Tpt	2.40	3.04/1.41	2.09	2.29	2.28	2.28	0.68	1.00	1.22	1.51	1.99
USW-G4	1161.4	Tpt	2.10	2.98/1.35	1.85	1.29	1.29	1.29	0.16	0.36	0.42	0.64	1.06
USW-G4	1174.5	Tpt	3.05	3.24/1.61	2.82	1.27	1.27	1.28	0.16	0.35	0.41	0.62	1.05
USW-G4	1200.8	Tpt	2.09	2.98/1.35	1.85	1.28	1.29	1.30	0.32	0.84	0.57	0.87	1.38
USW-G4	1243.4	Tpt	2.19	2.99/1.37	1.92	1.77	1.77	1.77	0.46	0.94	0.84	1.14	1.64
USW-G4	1253.3	Tpt	3.09	3.26/1.63	2.86	1.25	1.26	1.26	0.15	0.35	0.40	0.61	1.04
USW-G4	1253.3	Tpt	3.03	3.23/1.60	2.80	0.94	0.95	0.96	0.10	0.26	0.24	0.41	0.80
USW-G4	1259.8	Tpt	3.12	3.28/1.65	2.89	1.83	1.83	1.83	0.38	0.65	0.81	1.08	1.55
USW-G4	1305.8	Tpt	3.41	3.46/1.82	3.18	0.94	0.95	0.96	0.10	0.26	0.24	0.41	0.80
USW-G4	1309.1	Tpt	3.41	3.46/1.82	3.18	0.94	0.95	0.96	0.10	0.26	0.24	0.41	0.80
USW-G4	1315.6	Tpt	3.11	3.28/1.65	2.86	2.40	2.39	2.39	0.77	1.09	1.32	1.62	2.10
USW-G4	1325.5	Tpt	3.26	3.36/1.73	3.03	0.94	0.95	0.96	0.10	0.26	0.24	0.41	0.80
USW-G4	1325.5	Tpt	3.15	3.31/1.67	2.90	2.44	2.44	2.44	0.81	1.13	1.37	1.66	2.14
USW-G4	1341.9	Tpt	3.28	3.38/1.74	3.05	1.97	1.96	1.97	0.46	0.74	0.93	1.21	1.68
USW-G4	1341.9	Tpt	3.28	3.38/1.74	3.04	1.98	1.98	1.98	0.47	0.75	0.94	1.22	1.69
USW-G4	1341.9	Tpt	2.89	3.19/1.56	2.60	2.63	2.62	2.63	0.97	1.31	1.55	1.84	2.33
USW-G4	1351.7	Tpt	3.17	3.32/1.69	2.92	2.45	2.44	2.45	0.81	1.14	1.37	1.67	2.15
USW-G4	1361.5	Tpt	2.91	3.20/1.57	2.63	2.61	2.60	2.60	0.95	1.28	1.52	1.82	2.31
USW-G4	1381.2	Tpt	3.13	3.28/1.65	2.90	0.94	0.95	0.96	0.10	0.26	0.24	0.41	0.80

Table E2. (continued)

Sample	Depth feet	Strat. ^d	Ca	Cs	Sr	Am	Eu	Sm	Np	U	Pu -5	Pu -10	Pu -15
Log R ^b													
USW-G4	1437.0	Th	3.41	3.46/1.82	3.18	0.94	0.95	0.96	0.10	0.26	0.24	0.41	0.80
USW-G4	1512.5	Th	3.24	3.35/1.71	3.01	0.94	0.95	0.96	0.10	0.26	0.24	0.41	0.80
USW-G4	1542.0	Th	3.32	3.40/1.76	3.09	1.40	1.40	1.40	0.19	0.40	0.49	0.72	1.16
USW-G4	1643.7	Th	3.41	3.46/1.82	3.18	0.94	0.95	0.96	0.10	0.26	0.24	0.41	0.80
USW-G4	1669.9	Th	2.82	3.14/1.51	2.59	0.94	0.95	0.96	0.10	0.26	0.24	0.41	0.80
USW-G4	1692.9	Th	3.27	3.37/1.73	3.04	1.36	1.36	1.37	0.18	0.39	0.46	0.69	1.13
USW-G4	1706.0	Th	3.41	3.46/1.82	3.18	0.94	0.95	0.96	0.10	0.26	0.24	0.41	0.80
USW-G4	1715.9	Th	3.28	3.38/1.74	3.04	1.91	1.90	1.91	0.42	0.70	0.88	1.15	1.62
USW-G4	1761.8	Tcp	2.94	3.22/1.58	2.65	2.68	2.68	2.68	1.02	1.36	1.60	1.90	2.38
USW-G4	1761.8	Tcp	2.95	3.22/1.59	2.67	2.66	2.65	2.65	0.99	1.33	1.57	1.87	2.36
USW-G4	1788.1	Tcp	3.41	3.46/1.82	3.18	0.94	0.95	0.96	0.10	0.26	0.24	0.41	0.80
USW-G4	1971.8	Tcp	3.34	3.41/1.78	3.11	0.94	0.95	0.96	0.10	0.26	0.24	0.41	0.80
USW-G4	1991.5	Tcp	3.11	3.28/1.64	2.88	1.27	1.27	1.27	0.16	0.35	0.40	0.62	1.05
USW-G4	1994.8	Tcp	3.00	3.22/1.59	2.75	2.21	2.21	2.21	0.62	0.93	1.15	1.44	1.92
USW-G4	2063.6	Tcp	3.39	3.45/1.81	3.16	0.94	0.95	0.96	0.10	0.26	0.24	0.41	0.80
USW-G4	2070.2	Tcp	3.34	3.41/1.78	3.11	0.94	0.95	0.96	0.10	0.26	0.24	0.41	0.80
USW-G4	2099.7	Tcp	3.09	3.26/1.63	2.86	0.94	0.95	0.96	0.10	0.26	0.24	0.41	0.80
USW-G4	2099.7	Tcp	3.13	3.28/1.65	2.90	0.94	0.95	0.96	0.10	0.26	0.24	0.41	0.80
USW-G4	2100.1	Tcp	3.33	3.41/1.77	3.10	0.94	0.95	0.96	0.10	0.26	0.24	0.41	0.80
USW-G4	2100.1	Tcp	3.39	3.45/1.81	3.16	0.94	0.95	0.96	0.10	0.26	0.24	0.41	0.80
USW-G4	2100.4	Tcp	3.39	3.45/1.81	3.16	1.51	1.51	1.51	0.23	0.46	0.56	0.81	1.26
USW-G4	2101.0	Tcp	3.39	3.45/1.81	3.16	0.94	0.95	0.96	0.10	0.26	0.24	0.41	0.80
USW-G4	2101.0	Tcp	3.33	3.41/1.77	3.10	0.94	0.95	0.96	0.10	0.26	0.24	0.41	0.80
USW-G4	2135.8	Tcp	2.07	2.97/1.35	1.84	0.94	0.95	0.96	0.10	0.26	0.24	0.41	0.80
USW-G4	2145.7	Tcp	3.40	3.45/1.82	3.17	0.94	0.95	0.96	0.10	0.26	0.24	0.41	0.80
USW-G4	2145.7	Tcp	3.38	3.44/1.80	3.15	0.94	0.95	0.96	0.10	0.26	0.24	0.41	0.80
USW-G4	2247.4	Tcb	3.36	3.43/1.79	3.13	0.94	0.95	0.96	0.10	0.26	0.24	0.41	0.80
USW-G4	2345.8	Tcb	2.07	2.97/1.35	1.84	0.94	0.95	0.96	0.10	0.26	0.24	0.41	0.80
USW-G4	2578.7	Tcb	2.07	2.97/1.35	1.84	1.97	2.29	2.43	1.30	0.26	1.16	1.49	2.03
USW-G4	2614.8	Tcb	2.09	2.98/1.35	1.85	1.23	1.23	1.23	0.15	0.34	0.38	0.59	1.01
USW-G4	2690.3	Tcb	2.50	3.06/1.44	2.17	2.44	2.44	2.44	0.81	1.13	1.37	1.66	2.14
USW-G4	2696.9	Tcb	3.37	3.43/1.79	3.14	0.94	0.95	0.96	0.10	0.26	0.24	0.41	0.80
USW-G4	2729.7	Tcb	3.39	3.45/1.81	3.16	0.94	0.95	0.96	0.10	0.26	0.24	0.41	0.80

Table E2. (continued)

Sample	Depth feet	Strat. ^d	Ca	Cs	Sr	Am	Eu	Sm	Np	U	Pu -5	Pu -10	Pu -15
Log R ^b													
USW-G4	2792.0	Tct	3.41	3.46/1.82	3.18	0.94	0.95	0.96	0.10	0.26	0.24	0.41	0.80
USW-G4	2824.8	Tct	3.32	3.40/1.77	3.09	1.44	1.44	1.45	0.21	0.42	0.52	0.75	1.20
USW-G4	2831.4	Tct	3.30	3.39/1.75	3.06	1.93	1.92	1.92	0.43	0.71	0.89	1.17	1.64
USW-G4	2854.3	Tct	2.09	2.98/1.35	1.85	1.30	1.37	1.37	0.68	1.41	0.93	1.31	1.88
USW-G4	2887.1	Tct	2.10	2.98/1.35	1.86	1.33	1.39	1.40	0.71	1.45	0.96	1.34	1.91
USW-G4	2903.5	Tct	2.07	2.97/1.35	1.84	0.96	1.00	1.01	0.31	0.88	0.50	0.81	1.34
USW-G4	2916.7	Tct	2.09	2.98/1.35	1.85	1.23	1.24	1.25	0.29	0.77	0.52	0.81	1.31
USW-G4	2918.3	Tct	2.07	2.97/1.35	1.84	1.09	1.22	1.30	0.31	0.26	0.36	0.58	1.02
USW-G4	2919.9	Tct	2.19	2.99/1.37	1.92	1.79	1.81	1.81	0.75	1.45	1.07	1.43	1.99
USW-G4	2923.2	Tct	2.07	2.97/1.35	1.84	0.94	0.95	0.96	0.10	0.26	0.24	0.41	0.80
USW-G4	2929.8	Tct	2.74	3.13/1.50	2.45	2.44	2.44	2.44	0.81	1.13	1.37	1.66	2.14
USW-G4	2946.2	Tct	2.10	2.98/1.35	1.86	1.29	1.29	1.30	0.16	0.36	0.42	0.64	1.07
USW-G4	2952.8	Tct	2.07	2.97/1.35	1.84	0.94	0.95	0.96	0.10	0.26	0.24	0.41	0.80
USW-G4	2956.0	Tct	2.19	2.99/1.37	1.92	1.78	1.77	1.77	0.35	0.61	0.77	1.03	1.50
USW-G4	2969.2	Tct	2.10	2.98/1.35	1.86	1.29	1.29	1.30	0.16	0.36	0.42	0.64	1.07
USW-G4	2970.8	Tct	2.89	3.19/1.56	2.60	2.63	2.62	2.63	0.97	1.31	1.55	1.84	2.33
USW-G4	2970.8	Tct	2.07	2.97/1.35	1.84	1.09	1.22	1.30	0.31	0.26	0.36	0.58	1.02
USW-G4	2982.3	Tct	2.07	2.97/1.35	1.84	0.94	0.95	0.96	0.10	0.26	0.24	0.41	0.80
USW-G4	2985.6	Tct	2.23	3.00/1.38	1.95	1.92	1.92	1.92	0.56	1.08	0.97	1.28	1.79
USW-G4	2986.9	Tct	2.07	2.97/1.35	1.84	1.01	1.15	1.15	0.70	1.45	0.92	1.31	1.89
USW-G4	2986.9	Tct	2.07	2.97/1.35	1.84	0.94	0.95	0.96	0.10	0.26	0.24	0.41	0.80
Avg	-	-	2.78	3.20/1.57	2.53	1.47	1.49	1.50	0.38	0.64	0.66	0.90	1.35
SD ^c	-	-	0.54	0.19/0.19	0.55	0.58	0.59	0.59	0.33	0.42	0.45	0.50	0.55
Median	-	-	2.95	3.22/1.59	2.67	1.28	1.29	1.30	0.23	0.40	0.50	0.75	1.20
Min	-	-	2.07	2.97/1.35	1.84	0.94	0.95	0.96	0.10	0.26	0.24	0.41	0.80
Max	-	-	3.41	3.46/1.82	3.18	2.68	2.68	2.73	1.58	1.45	1.60	1.90	2.38
ALL DATA													
Avg	-	-	2.74	3.18/1.55	2.49	1.65	1.68	1.69	0.49	0.68	0.79	1.04	1.51
SD ^c	-	-	0.51	0.18/0.17	0.52	0.57	0.59	0.60	0.41	0.42	0.45	0.51	0.55
Median	-	-	2.82	3.15/1.52	2.53	1.61	1.63	1.63	0.40	0.59	0.76	1.03	1.50
Min	-	-	2.07	2.97/1.35	1.84	0.94	0.95	0.96	0.10	0.26	0.24	0.41	0.80
Max	-	-	3.41	3.46/1.82	3.18	2.76	2.75	2.77	1.64	2.10	1.67	1.97	2.54

^a Uncertainty (in parentheses) related to mechanistic model reaction constants and not mineral spatial variability.

^b Mass percent for fracture lining minerals reported in Table E1.

^c Standard deviation (in parentheses) related to variability in mineral abundance for the particular drill hole and not uncertainty in mechanistic model reaction constants.

^d Stratigraphic names defined in Warren et al. (2000). However, the units were identified by Carlos et al. (1995). Tuff Cone hydrostratigraphic unit is a composite of Paintbrush Group (Tp), Volcanics of Area 20 (Ta), and the Crater Flow Group (Tc). Tcb = Bullfrog Tuff; Tcp = Prow Pass Tuff; Tct = Tram Tuff; Th = Calico Hills Formation; Tpt = Topopah Spring Tuff.

^e Two values are reported for Cs. First, it is assumed that colloids are dominated by smectites. The colloid load is not high enough for smectite colloids to affect Cs transport. Second, it is assumed that colloids are dominated by illite/mica. Since Cs sorbs very strongly to this mineral, colloids are predicted to significantly increase the transport of Cs. These two cases provide the extreme cases for colloid facilitated Cs transport.

University of California
Lawrence Livermore National Laboratory
Technical Information Department
Livermore, CA 94551

